Environmental Measurements in the Beaufort Sea, Spring 1990

by
T. Wen
F.W. Karig
W.J. Felton
J.C. Luby
K.L. Williams

Technical Report
APL-UW TR 9105
December 1990

Applied Physics Laboratory, University of Washington
Seattle, Washington 98105-6698

Contract N00039-88-C-0054

Acknowledgments

The research presented in this report was sponsored by the organizations participating in the ICEX APLIS 90 ice camp. Funding was provided by the Naval Sea Systems Command and the Office of Naval Technology.

The purpose of this report is simply to present the environmental data obtained during the camp. The data analysis is very limited. All the data presented here are stored in digital format and are available for further analysis. Requests for data should be forwarded to

Director
Applied Physics Laboratory
1013 NE 40th St.
Seattle, WA 98105.

ABSTRACT

This report summarizes environmental data obtained in March and April 1990 at an ice camp in the Beaufort Sea 375 km north of Prudhoe Bay, Alaska. The measurements include weather, floe drift, CTD profiles, ice properties, currents, and underwater noise.

TABLE OF CONTENTS

LIST OF FIGURES

EXECUTIVE SUMMARY

This report presents environmental and ambient noise data obtained by the Applied Physics Laboratory of the University of Washington (APL-UW) at APLIS 90, an ice camp established in the Beaufort Sea in spring 1990 to support Navy-sponsored tests and research during ICEX 1-90. Participants in ICEX 1-90 included the Arctic Submarine Laboratory at the Naval Ocean Systems Center, the David Taylor Research Center, the Naval Air Development Center, the Naval Research Laboratory, the Naval Surface Weapons Center, the Naval Underwater Systems Center, the University of Texas Applied Research Laboratories, and the Applied Physics Laboratory, University of Washington. The camp was established and operated by APL-UW and lasted from 3 March until 11 April, when all major objectives were completed.

The purpose of this report is to provide field data to ice camp participants; thus data analysis is limited. The data were collected to document the meteorological and oceanographic conditions that existed during camp activities, and to furnish insight into the underwater sound-speed structure and ambient noise during acoustic experiments. The main data sets are weather, floe drift, CTD profiles, ice properties, and ambient noise.

I. INTRODUCTION

This report presents environmental data taken by the Applied Physics Laboratory, University of Washington, in the spring of 1990 at ice camp APLIS in the Beaufort Sea. The camp was established and maintained by APL-UW personnel to support Navy-sponsored tests and research conducted by the many organizations participating in ICEX 1-90. The environmental data described here—weather, floe drift, CTD profiles, ice properties, and underwater noise—were gathered primarily to support analysis of acoustic data obtained by camp participants. Also documented is some logistic information for future reference.

The camp was established on a multiyear floe approximately 375 km north of Prudhoe Bay, Alaska (Figure 1). The floe was chosen on 28 February after a 2-day search. Over the next few days, planes flew the first loads of equipment to the site, and personnel commuted to the floe to build the camp. On 3 March four people spent the first night at the camp, which was subsequently occupied for 5-1/2 weeks and evacuated on

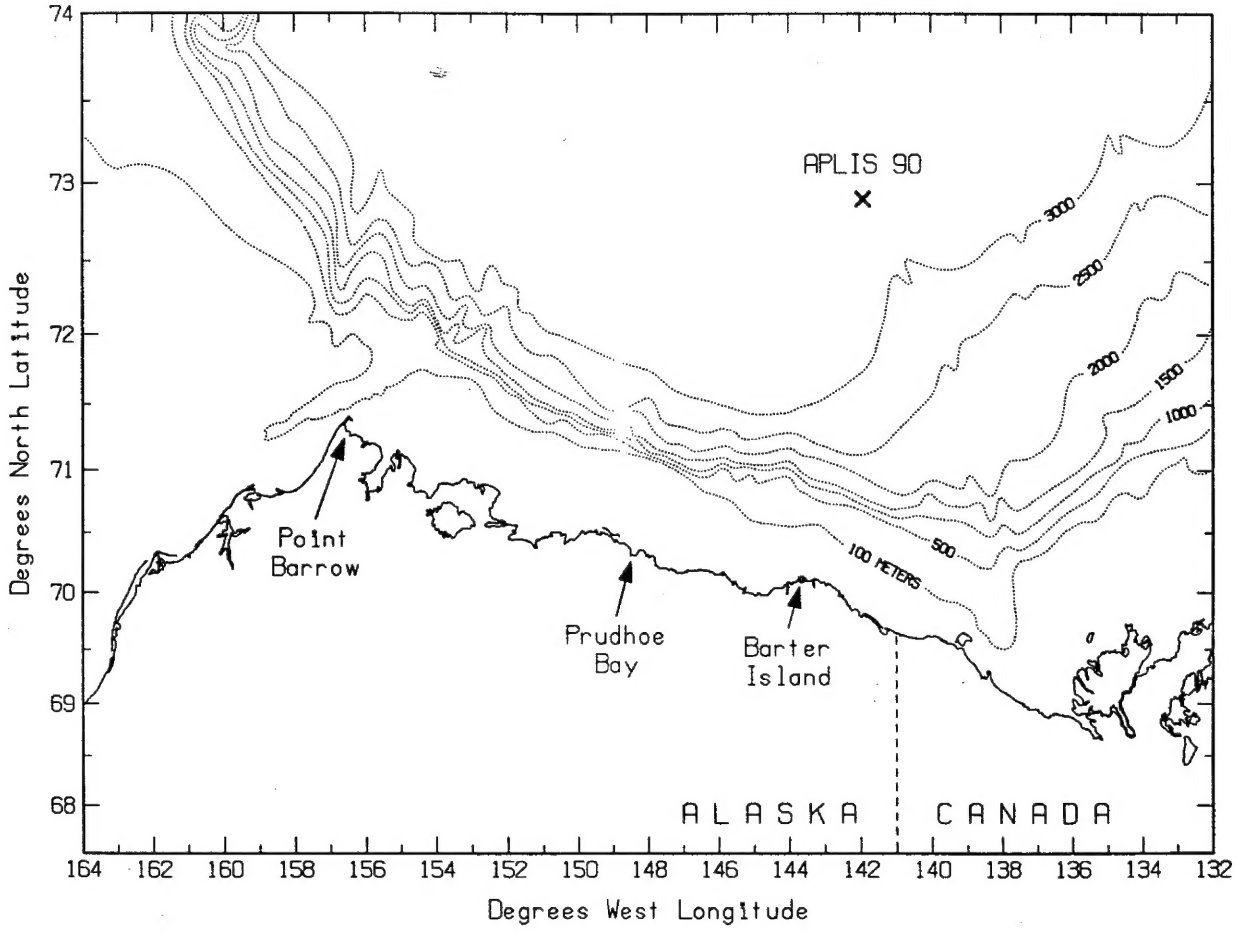

Figure. 1. Position of APLIS 90 ice camp (bathymetric contours in meters).

11 April upon successful completion of the test and research objectives. During this period, the floe drifted circuitously and ended up 22 km southeast of its position at first sighting.

The camp was established at the edge of a refrozen lead, which was essential for building a runway for aircraft, the only means of transportation to and from the camp. The finished runway was used almost daily by a Twin Otter and a CASA 212-200 and was long enough to handle a commercial C-130 Hercules, which delivered fuel on two occasions. Multiyear pressure ridges and rubble fields surrounded the lead and the camp. All parts of the floe were accessible by snowmobile with only moderate detouring.

Air temperature, air pressure, wind direction, and wind speed were recorded automatically at 10-min intervals. In general, the weather was benign, with low winds and temperatures above −30°C. Only near the end of the camp did the wind speed reach 15 m/s.

Conductivity-temperature-depth (CTD) casts were made, usually early in the day, to determine the properties of the water column down to 400 m. Sound speed profiles were then derived from the measured temperature and salinity and used to preduct the performance of acoustic equipment.

Ambient noise was recorded whenever resources allowed. Sources of ambient noise included thermal cracking of the ice, ridging, wind-generated waves at open leads, and bioorganisms. These data are useful for interpreting the acoustic test data.

II. THE CAMP

Selection of the ice floe used for the camp was based on several criteria. First, the floe had to be at least 3×4 km to support the planned tests. Second, it had to have a refrozen lead long enough and thick enough (at least 1.2 m) to serve as a runway, since transportation to and from the camp depended entirely on aircraft. Third, the floe needed to be over water with good acoustic-propagation characteristics, i.e., a minimal shadow zone and the longest possible propagation range. The third stipulation required that the camp be located north of 72° latitude, where the warm subsurface intrusion (a remnant of the summertime Alaskan Coastal Current) which produces complex sound-speed structure is less pronounced and the deeper water helps reduce acoustic interference from the bottom. The fourth criterion was that the site had to be far enough east to allow for the westerly drift that historically occurs in this area during the spring. A 3×5 km floe fulfilling these requirements was found at a latitude of 72°52.4′N on the second day of search.

The camp was established near the edge of the floe, next to a refrozen lead (Figure 2) chosen for its relatively smooth surface. The thickness of the ice ranged from 2.0–2.4 m, more than adequate to support the camp structures but not too thick for drilling hydroholes. A sketch of the camp layout and a corresponding photograph are shown in Figure 3.

An X-Y coordinate system for tracking underwater vehicles and surveying hydroholes was set up as shown in Figure 2. The origin of the system was a hydrohole in the control building, and the X-axis extended parallel to the long axis of the floe. An array of tracking hydrophones was centered at the camp, and a second array was located about 5000 m away on the negative X-axis. Signals from both arrays were cabled back to the control building. Both arrays used the same coordinate system, established during an initial survey with the camp array. The farther array was first surveyed in its own coordinate system and then mapped into the camp coordinate system by using both arrays to survey two points located about midway between the two arrays and 4000 yd from each other. Knowledge of the coordinates of the two points in each of the arrays allowed use of a simple transformation to map the farther array into the coordinate system of the camp array. This method was more accurate than surveying the farther array directly from the camp array because of the shorter survey range.

Often a point on the ice had to be located in range coordinates. For this task, a combination infrared ranging device/surveying transit was set up on the roof of the control building over the (0,0) hydrohole. The range and bearing from (0,0) to a hand-held optical reflector at the desired survey point were measured and converted to X-Y range coordinates.

A transit was used in celestial sightings to determine the floe's orientation (the bearing of the +Y axis relative to true north). The bearing of the +Y axis thus determined was 307.5° with only minor changes during the camp period. Details of the celestial sighting will be described further in a later section.

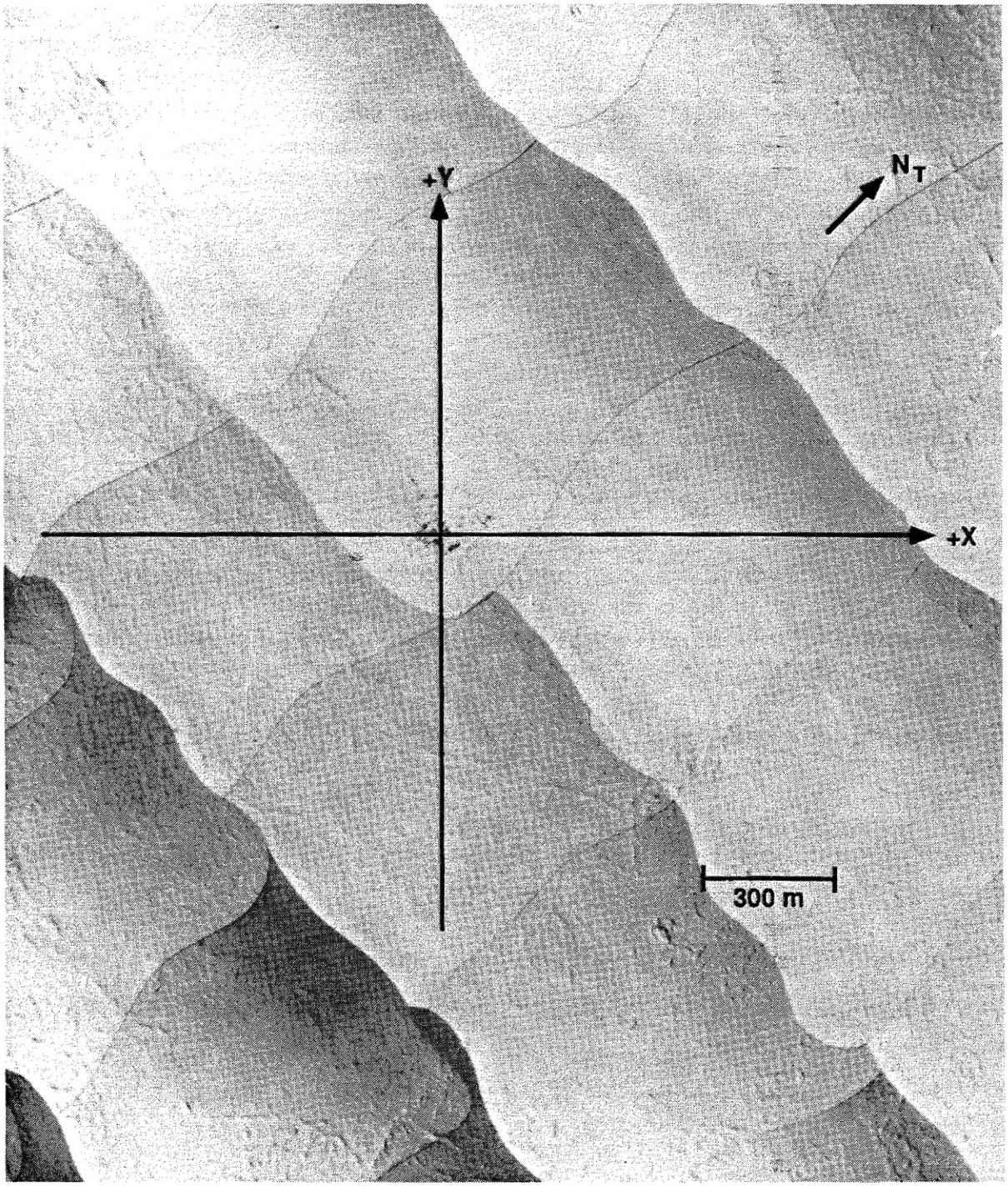

Figure 2. A photo-mosaic of the floe with X-Y axes of tracking system superposed; scale = 300 m per inch (photograph taken from Canadian Forces CP-140 in support of Maritime Patrol aircraft operations during ICEX 90).

III. WEATHER

Weather data were collected throughout the camp's occupancy, using a Weatherpak 100 weather station manufactured by Coastal Climate Co. in Seattle. The Weatherpak was mounted at a height of 10 m on a telescoping mast supported by guy wires. Air temperature, atmospheric pressure, and wind speed and direction were recorded at regular intervals. Wind direction was automatically converted into the direction relative to magnetic north using the Weatherpak's internal compass reading. To control the weather station and display meteorological data in real time, a laptop personal computer in the control building was connected to the station via an RS-232C link. The Weatherpak was programmed to average the weather parameters for 5 s at 10-min intervals. The weather parameters could also be read at any time by pressing a programmed menu key on the laptop PC. The sampled data were stored in the Weatherpak's internal memory and also downloaded to the PC for real-time monitoring. Once a day, the data collected during the previous 24 hours were downloaded to the PC and stored on a floppy disk. The accuracy of the meteorological measurements is 0.5 m/s for wind speed, 2° for wind direction, 0.5 mbar for atmospheric pressure, and 0.2°C for temperature.

The meteorological data are shown in Figure 4. The two sharp spikes in the temperature record (on 26 March and 3 April) correspond to brief periods of almost calm winds. The diurnal pattern in the air temperature is absent whenever the wind speed exceeds ~5 m/s. During these periods, however, there was also either partial or complete cloud cover. Figure 5 shows a histogram of the wind direction. Southwesterly winds predominated during the camp period. This is diametrically opposite the usual wind direction we have observed in this region in previous years.

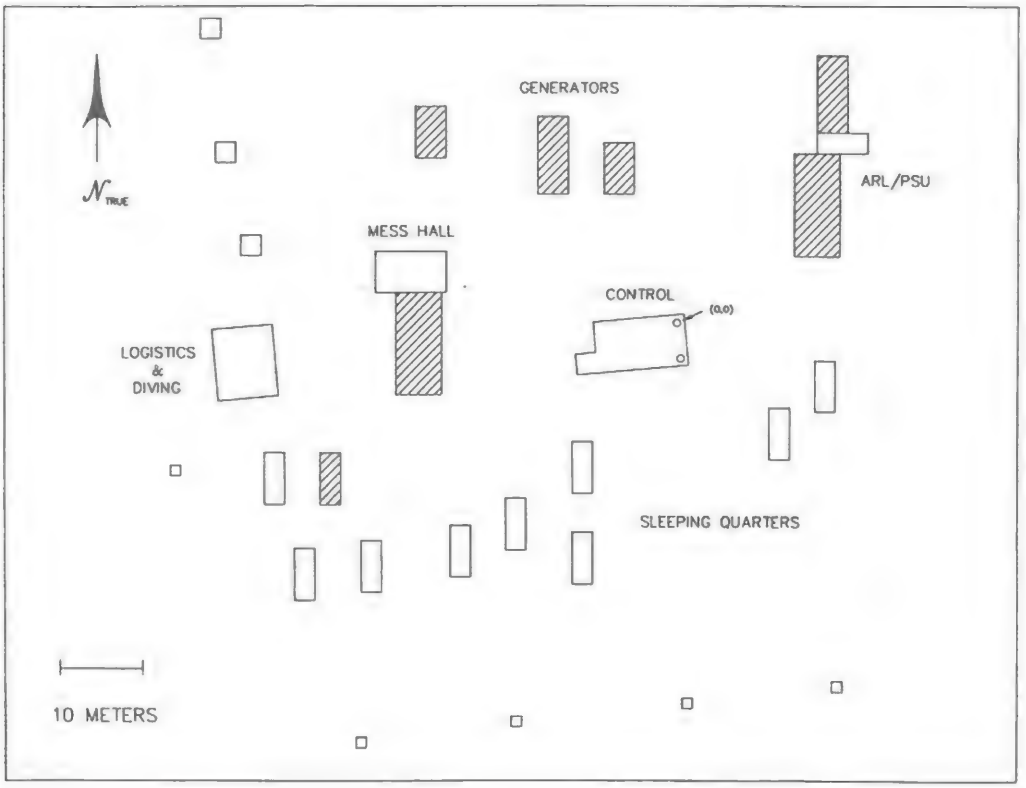

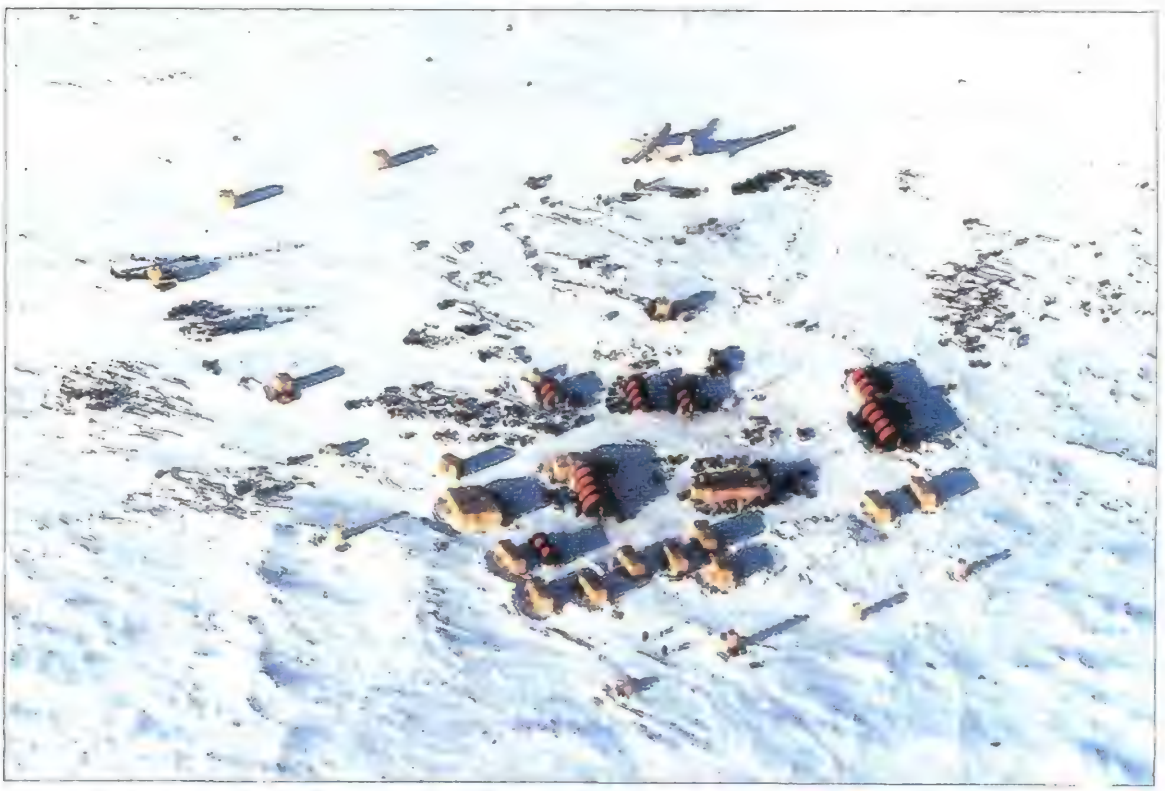

Figure 3. Top: Sketch showing layout of the camp structures. Cross hatching denotes tents; other structures are made of plywood. Small circles on the control hut indicate 0.91-m-diameter hydroholes, and (0,0) indicates the origin Bottom: Photograph of camp layout.

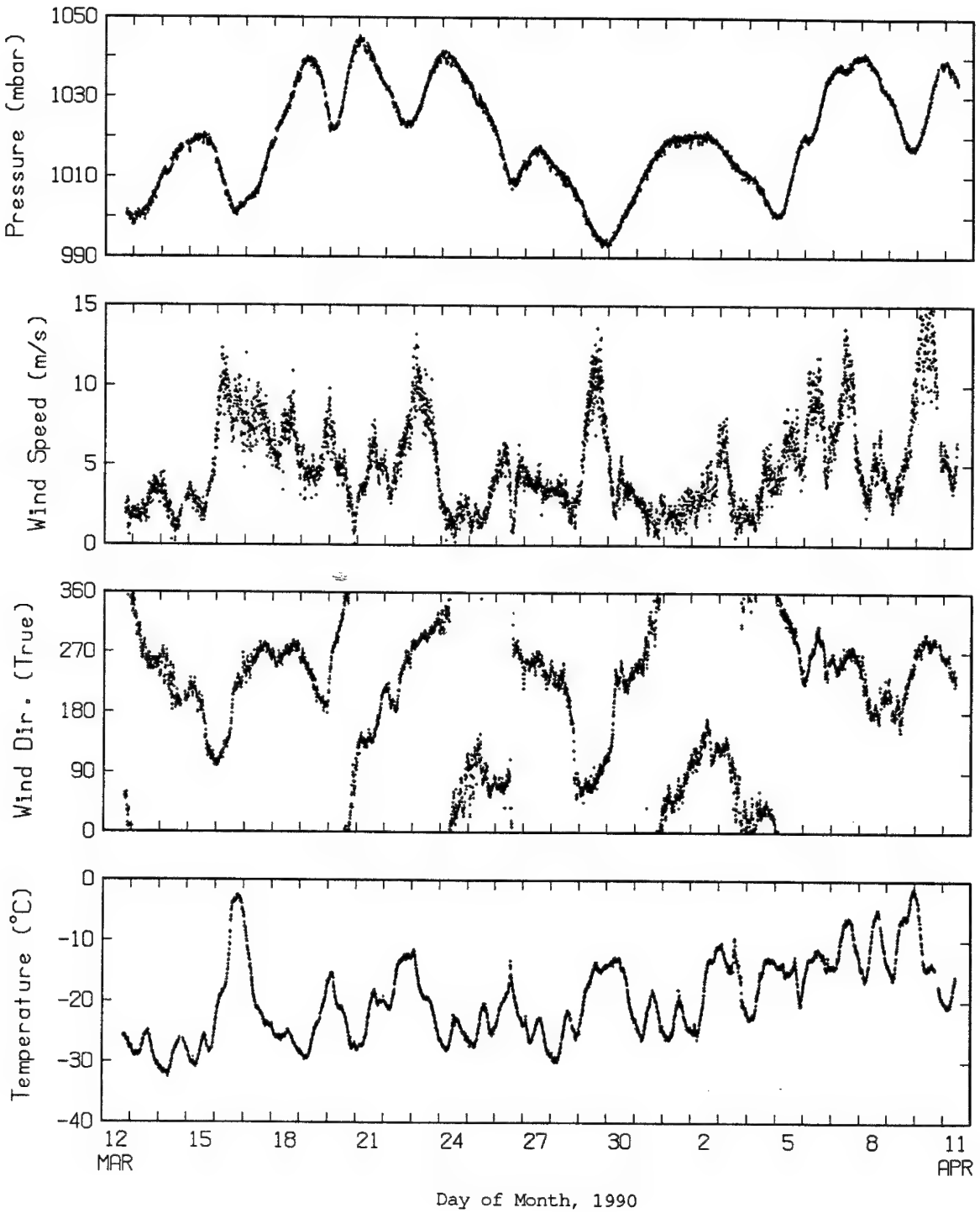

Figure 4. Weather measurements at APLIS 90.

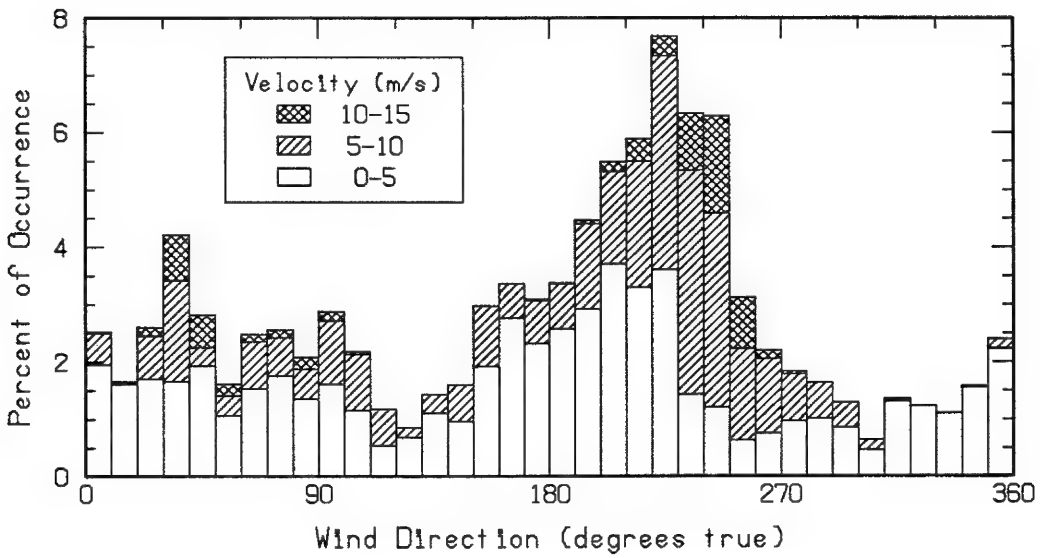

Figure 5. Histogram of the wind vectors.

IV. FLOE MOVEMENT

The camp's position was determined initially with an Omega navigation system aboard the Twin Otter aircraft. On 3 March a Transit Satellite Navigation System (NAVSAT) receiver (Furuno FSN-80) was set up, and on 12 March a Global Positioning System (GPS) receiver/clock (Kinemetrics/Truetime GPS-DC).

The NAVSAT fixes were stored automatically in the receiver for all satellite passes, which occurred at an average interval of 20 minutes. Every few hours, all accumulated sets of time, position, and elevation-angle data were recalled manually and recorded in a logbook.

An HP85 computer was connected to the GPS receiver via a GPIB interface and used as a data logger. The GPS fixes were read from the receiver every 10 min and stored on a tape cartridge. Because of problems with the receiver, gaps occurred in the GPS position data and were filled in with the NAVSAT data.

The positions were smoothed using a five-point, unweighted, running-average filter. Positions obtained from NAVSAT satellites with elevation angles greater than 60° were discarded because they were previously found[1] to be offset in longitude compared with those from satellites with lower elevation angles. Figure 6 shows a plot of the smoothed drift track of the floe. A list of floe position, drift speed, and direction is given in Appendix A. The NAVSAT and GPS data are reported in Coordinated Universal Time (UTC); other data (such as weather, CTD, etc.) are logged in local time, which was set to the time in Prudhoe Bay to facilitate logistic coordination. To correlate the drift data with data logged in local time, use a time offset of 9 hours (e.g., 1200 UTC = 0300 local) through 6 April, and an offset of 8 hours after Daylight Saving Time went into effect on 7 April.

The drift speed and direction of the floe are shown in Figure 7. Wind speed and direction are superposed for comparison (note that wind direction here is defined as the direction "to" which the wind is blowing). The speeds and directions are highly correlated, suggesting that the floe drift was mainly wind driven. The drift direction was generally to the right of the wind owing to the Coriolis effect.

The amount of rotation as the floe drifted was determined by measuring the true bearing of the +Y axis of the X-Y coordinate system. To do this, we first read the grid bearing of the sun or the moon with the transit positioned atop the control building over the (0,0) hydrohole while the 0° reference mark of the transit was oriented toward the +Y direction of the range. Then the true bearing of the sun or the moon at the time of the transit sighting was calculated using information from a nautical almanac. The difference between the true and grid bearings of the sun or the moon was the true bearing of the +Y axis. The celestial sightings showed very little rotation during the period of the camp, contrary to experiences at previous camps where rotations of up to 5° were measured. The +Y axis of the system remained at a true bearing of 307.5° ± 0.5° for the camp's duration. The small amount of rotation is probably due to the sparseness of open leads in the general vicinity and the small net drift during the camp.

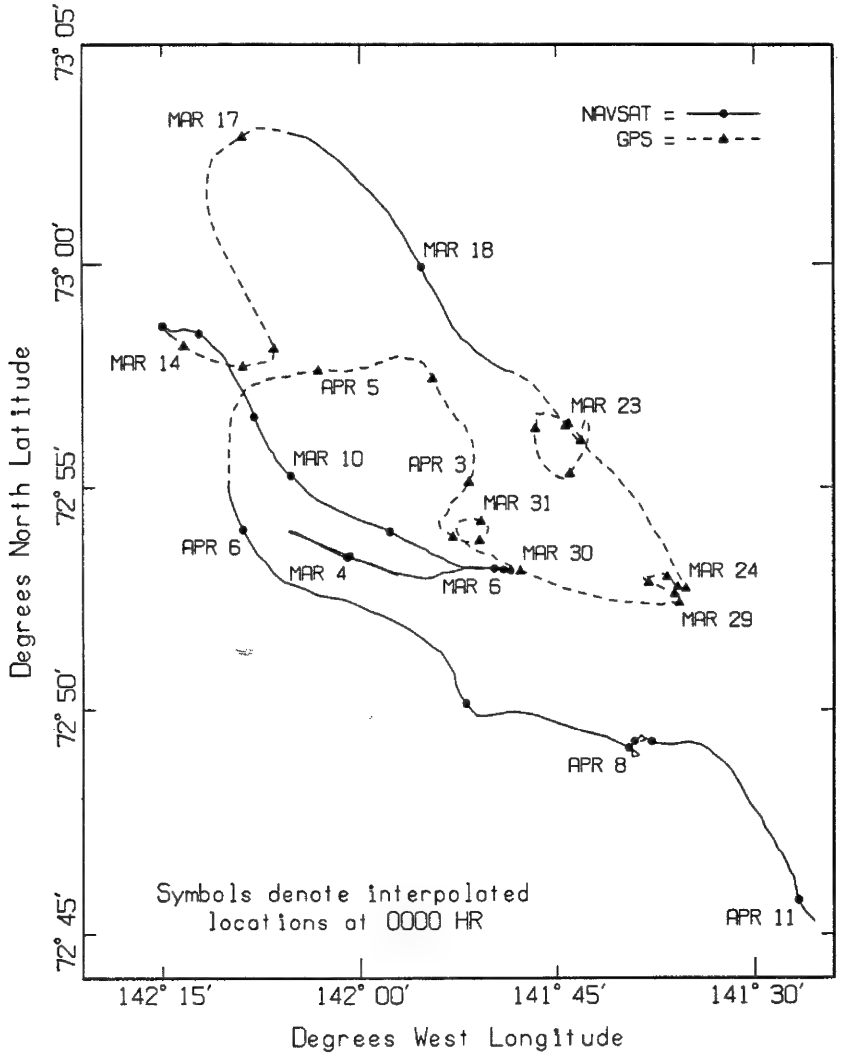

Figure 6. Drift track of APLIS 90, based on satellite fixes.

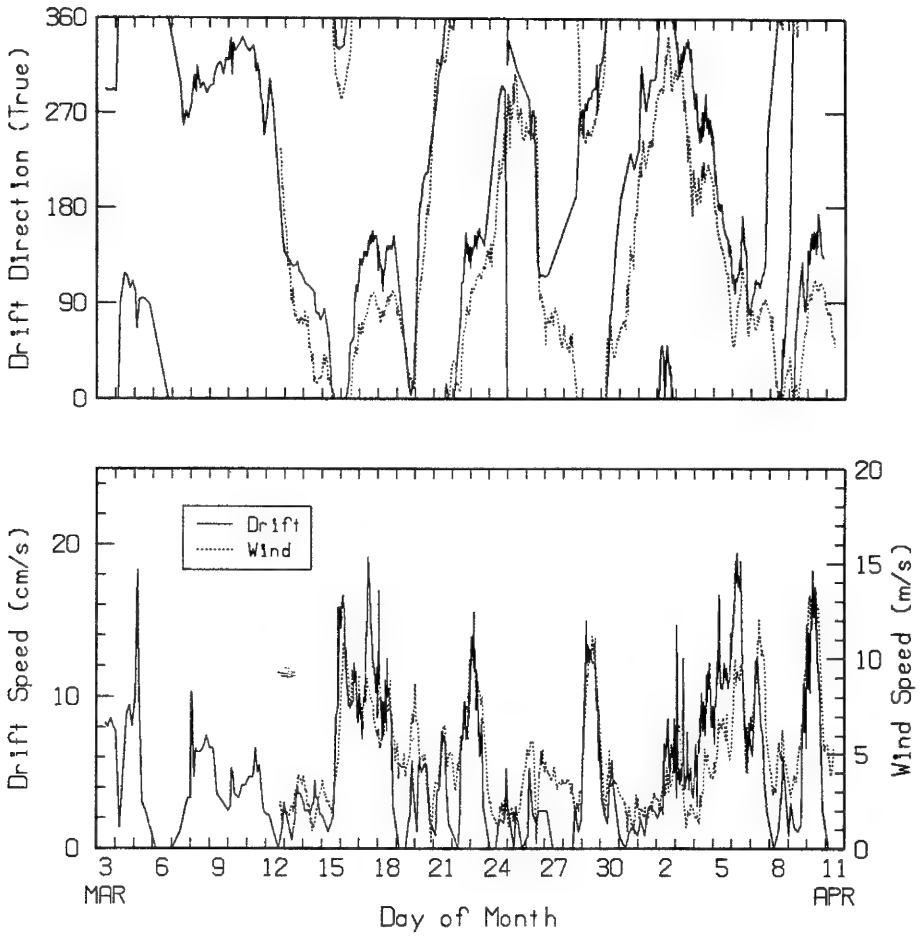

Figure 7. Drift speed and direction of APLIS 90.

V. CTD MEASUREMENTS

CTD casts were made at least once each day to obtain temperature and salinity profiles of the water column. From these casts, sound speed profiles were derived to furnish insight into the sound speed structure and dynamics of the water below the camp.

The CTD profiler comprised a solid-state data logger (Sea-Bird), a thermistor (Sea-Bird), a conductivity cell (Sea-Bird), and a pressure sensor (Paroscientific Digiquartz). The profiler was attached to the end of a 6.4-mm-diameter nylon line and deployed with a motor-powered winch mounted on the wall next to a hydrohole in the control building. To ensure adequate flushing of seawater through the conductivity cell, the profiler was lowered at a rate of ~1.3 m/s, the maximum speed of the dc winch motor. Because the sampling rate of the logger is 8 Hz, the water column was sampled at ~16 cm intervals, resulting in high-resolution temperature and salinity profiles. Casts were generally made only to ~400 m because water properties at greater depths do not vary significantly from day to day. One cast was made to 700 m to obtain the water properties at greater depths. After each cast, the raw data were read out of the logger via an RS-232C link to an HP Integral Personal Computer for processing and plotting. The raw data were first converted to temperature, conductivity, and depth using sensor calibration constants. UNESCO '83 algorithms[2] were then used to compute salinity, sound speed, and σ_t (the density of the *in situ* water with the pressure reduced to atmospheric). Before the trip, the sensors were calibrated at the Northwest Regional Calibration Center in Bellevue, Washington. The accuracy of the measurements is 0.002° C for temperature, 0.002 ppt for salinity, 0.005 m/s for sound speed, and 0.002 kg/m^3 for σ_t.

Table I lists the casts made at the camp. The CTD plots for all the casts are given in Appendix B. As an example, the CTD profiles for the 700-m cast (14) are shown in Figure 8 and the corresponding temperature–salinity (T–S) diagram in Figure 9. For this particular profile, the well-mixed upper layer is only 20 m thick, although it has been previously observed to extend as thick as 60 m. A warmer intrusion from the Bering Sea lies under the mixed layer, creating a thermocline and a halocine (and therefore a pycnocline) between the two layers. The intrusion extends to a depth of 80 m, and below that lies colder Chukchi Sea bottom water. Below ~200 m is Atlantic water with a temperature maximum of 0.5°C. Figure 10 is an expansion of Figure 8 showing a staircase-like structure in the temperature profile between 290 and 350 m. This phenomenon was observed in other casts as well. The layers are 1–2 m thick with temperature steps of up to 0.015°C and can be attributed to double diffusion.[3] The temperature staircase effect has been observed in the Arctic Ocean (at higher latitudes) by Padman and Dillon[3] (74°N), by Neshyba et al.[4] (84 °N), and by Judd[5] (88°N).

Whenever ray tracing was needed in the field to help interpret the results of acoustic tests, abbreviated (sparsely sampled) SSPs were used instead of the original SSP to reduce the computation time. The points in the abbreviated profiles were selected at

Table I. List of CTD casts.

Date	Local Time	Cast No.	Location	
03-13-90	2029	1	72°58.0´N	142°12.3´W
03-14-90	0719	2	72°57.8´N	142°10.4´W
03-14-90	1839	3	72°57.8´N	142°08.0´W
03-14-90	2039	4	72°57.8´N	142°07.8´W
03-15-90	0645	5	72°57.9´N	142°06.7´W
03-15-90	2045	6	72°58.9´N	142°07.9´W
03-16-90	0705	7	73°01.7´N	142°11.5´W
03-16-90	2149	8	73°02.8´N	142°04.2´W
03-17-90	0650	9	73°01.9´N	141°59.9´W
03-18-90	0647	10	72°57.5´N	141°47.9´W
03-19-90	0727	11	72°55.9´N	141°43.1´W
03-19-90	1031	12	72°55.9´N	141°43.1´W
03-19-90	1156	13	72°56.0´N	141°43.2´W
03-20-90	0645	14	72°56.1´N	141°42.6´W
03-21-90	0915	15	72°55.6´N	141°46.1´W
03-22-90	0635	16	72°56.6´N	141°46.5´W
03-23-90	0647	17	72°53.8´N	141°37.1´W
03-24-90	0627	18	72°52.7´N	141°35.1´W
03-25-90	1117	19	72°52.9´N	141°36.5´W
03-26-90	0720	20	72°53.0´N	141°38.2´W
03-27-90	1123	21	72°56.6´N	141°36.1´W
03-28-90	0624	22	72°52.5´N	141°35.6´W
03-29-90	0606	23	72°52.4´N	141°40.6´W
03-29-90	2131	24	72°53.7´N	141°51.8´W
03-30-90	1038	25	72°54.2´N	141°52.0´W
03-30-90	1430	26	72°54.4´N	141°51.0´W
03-30-90	2117	27	72°54.3´N	141°51.0´W
03-31-90	1540	28	72°53.8´N	141°50.8´W
04-01-90	0807	29	72°53.8´N	141°52.3´W
04-01-90	2254	30	72°54.1´N	141°53.9´W
04-02-90	1046	31	72°54.7´N	141°52.9´W
04-03-90	0632	32	72°56.7´N	141°53.0´W
04-03-90	2203	33	72°57.9´N	141°55.6´W
04-04-90	1927	34	72°57.5´N	142°06.5´W
04-05-90	1409	36	72°54.7´N	142°10.0´W
04-05-90	2120	37	72°52.9´N	142°06.3´W
04-06-90	0819	38	72°51.8´N	141°56.1´W
04-08-90	1222	39	72°49.0´N	141°39.7´W
04-09-90	1156	41	72°49.4´N	141°38.4´W

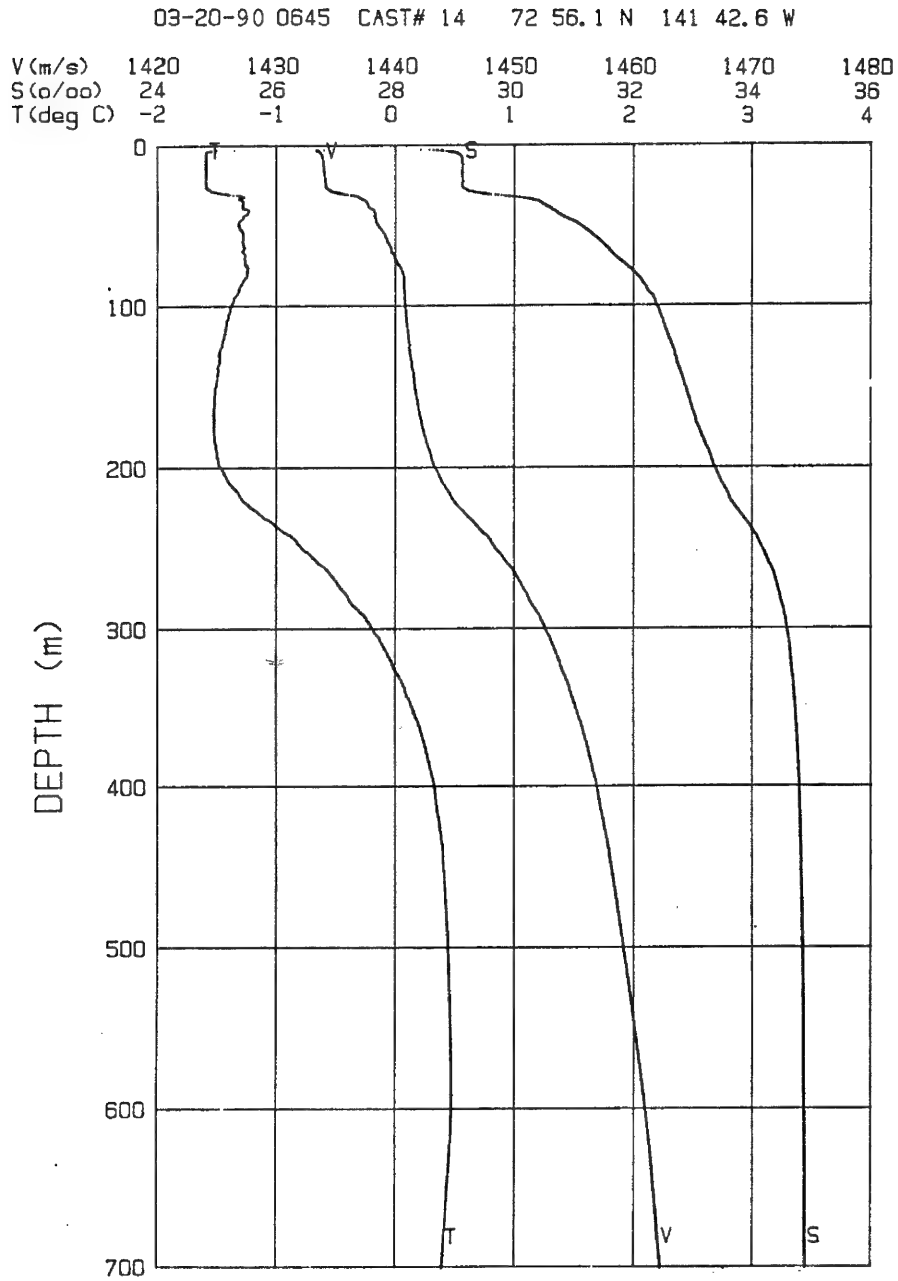

Figure 8. Example of CTD profiles made during APLIS 90 casts (cast 14 to 700 m).

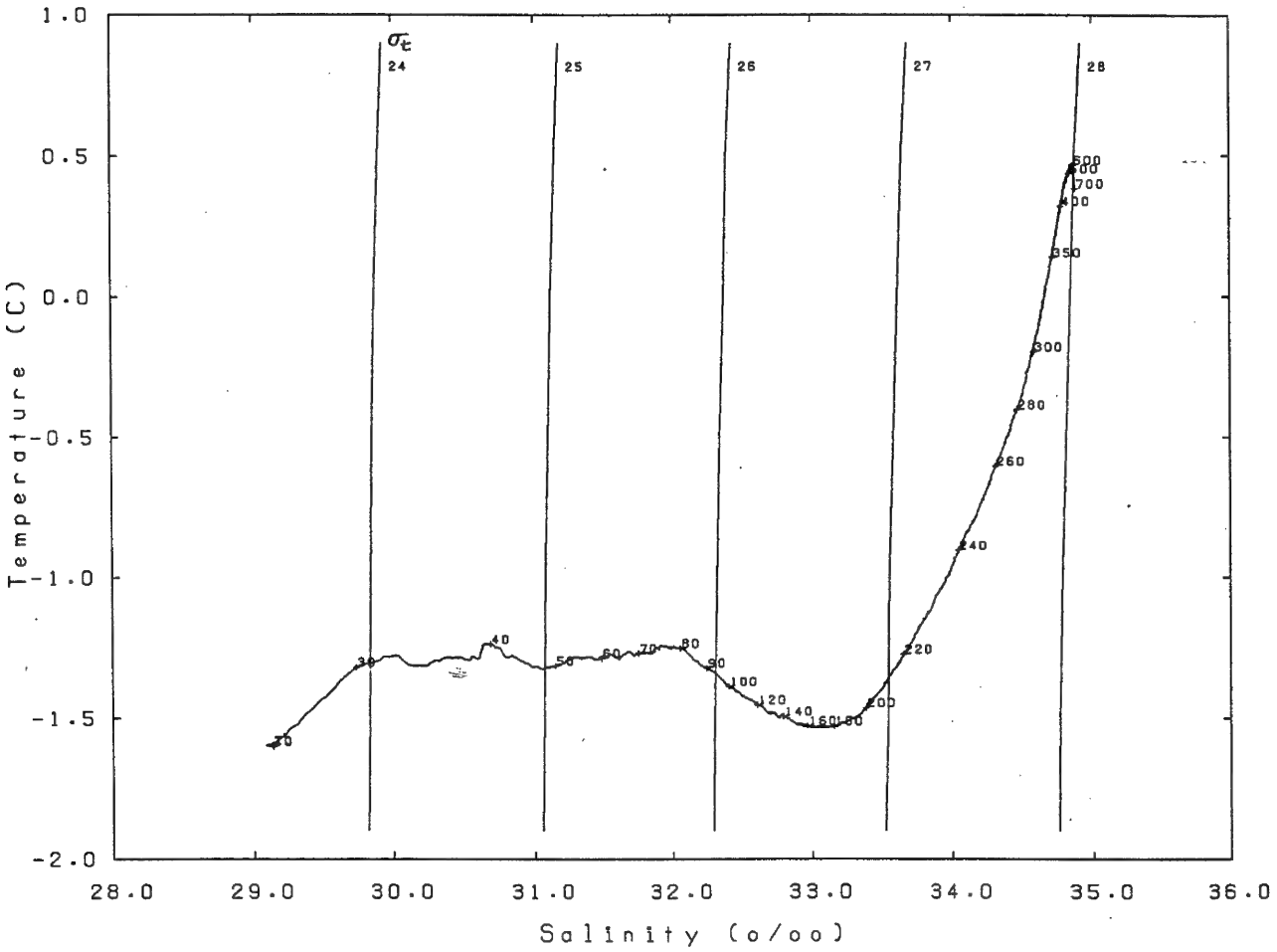

Figure 9. Temperature–salinity diagram computed for CTD cast shown in Figure 8.

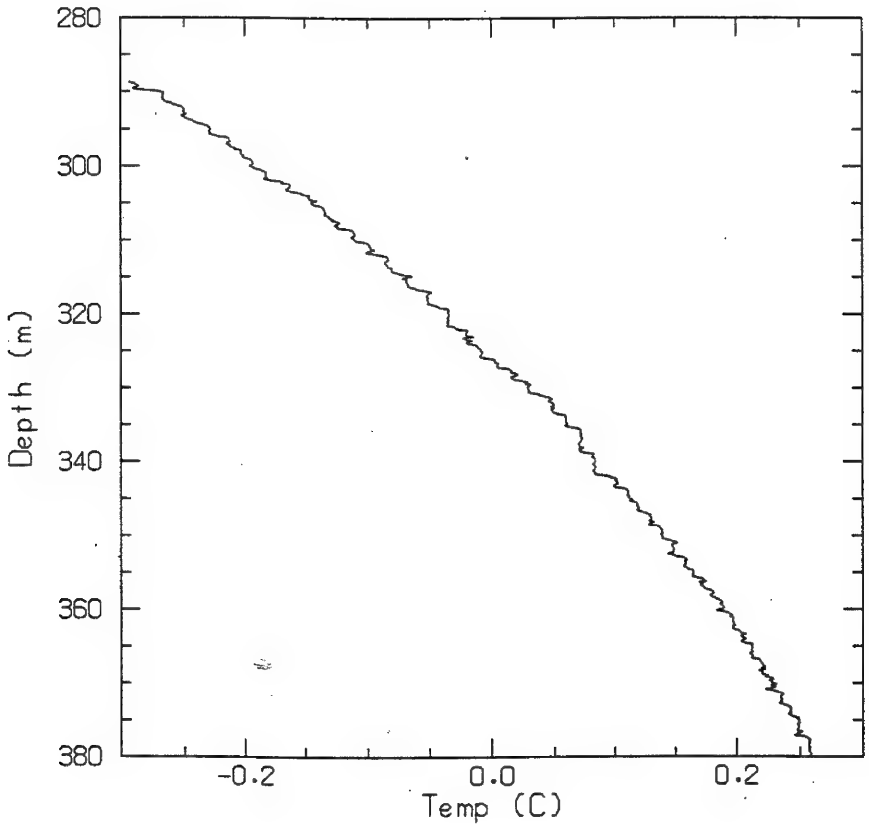

Figure 10. Temperature staircase in cast 14. Temperature steps are about 0.015°C.

small intervals when the change in the speed gradient was large and at larger intervals when the change was small. The abbreviated SSP for cast 14 is shown in Figure 11. It is a typical sound speed profile for Beaufort Sea. There is a large change in the sound speed gradient near the surface caused by the sharp transition in temperature and salinity at the base of the mixed surface layer and another, less pronounced, change in gradient at ~200 m. The effect of these two features on sound propagation is shown by the ray traces in Figure 11. The trace in Figure 11a is for a source at a depth of 30.5 m, the depth of the tracking hydrophones. Because of the closeness of the source to the large sound-speed gradient near the surface, near-horizontal rays are strongly refracted upward. The pausity of rays in the area around 100 m depth and 4000 m range would produce lower signal levels for tracking. The more gradual change in gradient at ~200 m produces a region of multipath interference at a range of about 4000 m. In Figure 11b, the source is at 60.9 m, the depth of one of the acoustic scanners used in the experiments. In this case, the rays are refracted upward to a lesser extent because the source is farther away from the sharp sound-speed gradient. The effect of the change in gradient at 200 m, however, remains about the same as in Figure 11a.

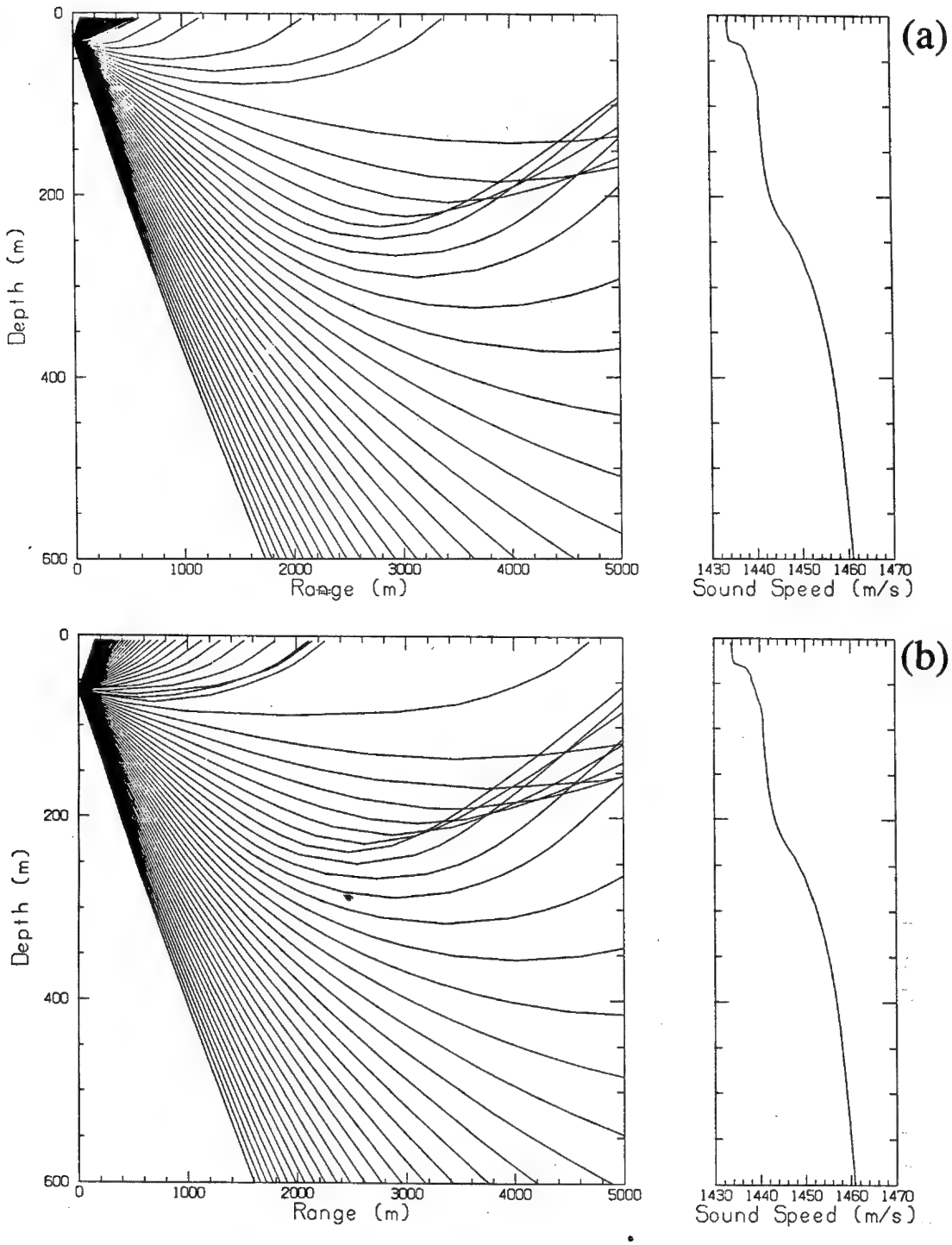

Figure 11. Ray trace using SSP of cast 14 with ray angles from –20° to +20° at 5° increments: (a) source at 30.5 m, (b) source at 60.9 m.

The depth of the thermocline (the sharp transition in the temperature profile) is of great interest for two reasons: first, because the sound speed is largely a function of the temperature and, second, because the change in sound speed gradient can have a major effect on sound propagation, as shown above, Figure 12 shows the depth of the thermocline, which stayed above 31 m during the camp's occupancy. The depths were estimated from the CTD profiles shown in Appendix B.

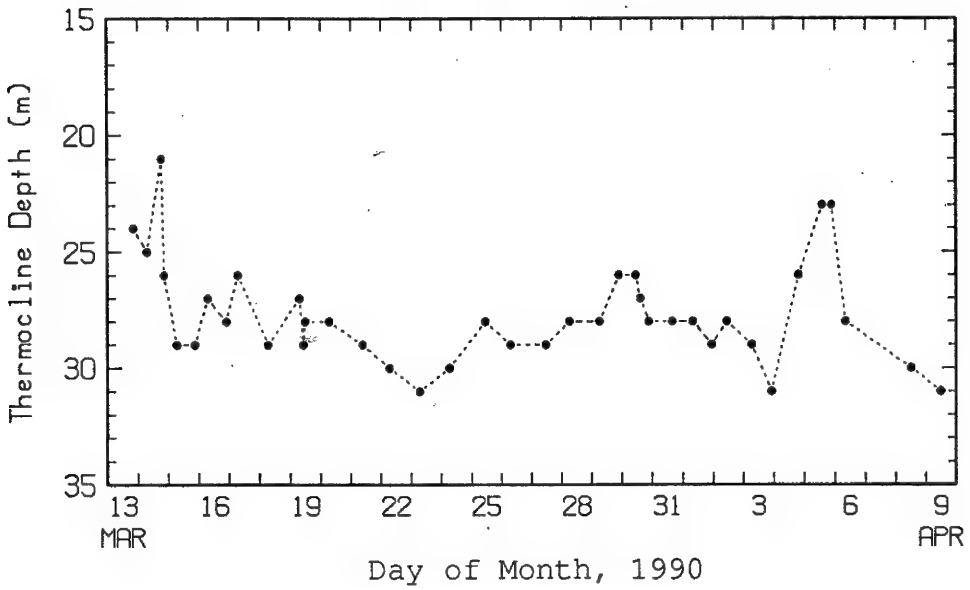

Figure 12. Daily variation in thermocline depth.

VI. CURRENTS

The angle of the winch line during a CTD cast was used to estimate the direction and magnitude of the current relative to the moving floe. Usually the angle was small, implying a low current, and no casts were made to measure the current. However, on four occasions when the wind was relatively high, the angle was large, and a separate cast was made to determine the current's magnitude and the direction.

For the current casts, the CTD unit was replaced with an InterOcean S4 current meter; a 4.5 kg lead weight was attached 1 m below the meter to keep it vertical. Once enabled, the current meter sampled continuously at 0.5 s intervals. To obtain stable current measurements, we lowered the meter in ~5 m depth increments and stopped for 30 s at each depth. We then calculated the mean and standard deviation for each stop. The results of the four casts are shown in Figure 13 along with the corresponding absolute current relative to the earth, which was obtained by vector summing the relative current and the floe's motion. Much of the fluctuation in the direction of the absolute current is because there was almost no water movement relative to the earth, and therefore the direction resulting from the vector addition was subject to measurement error.

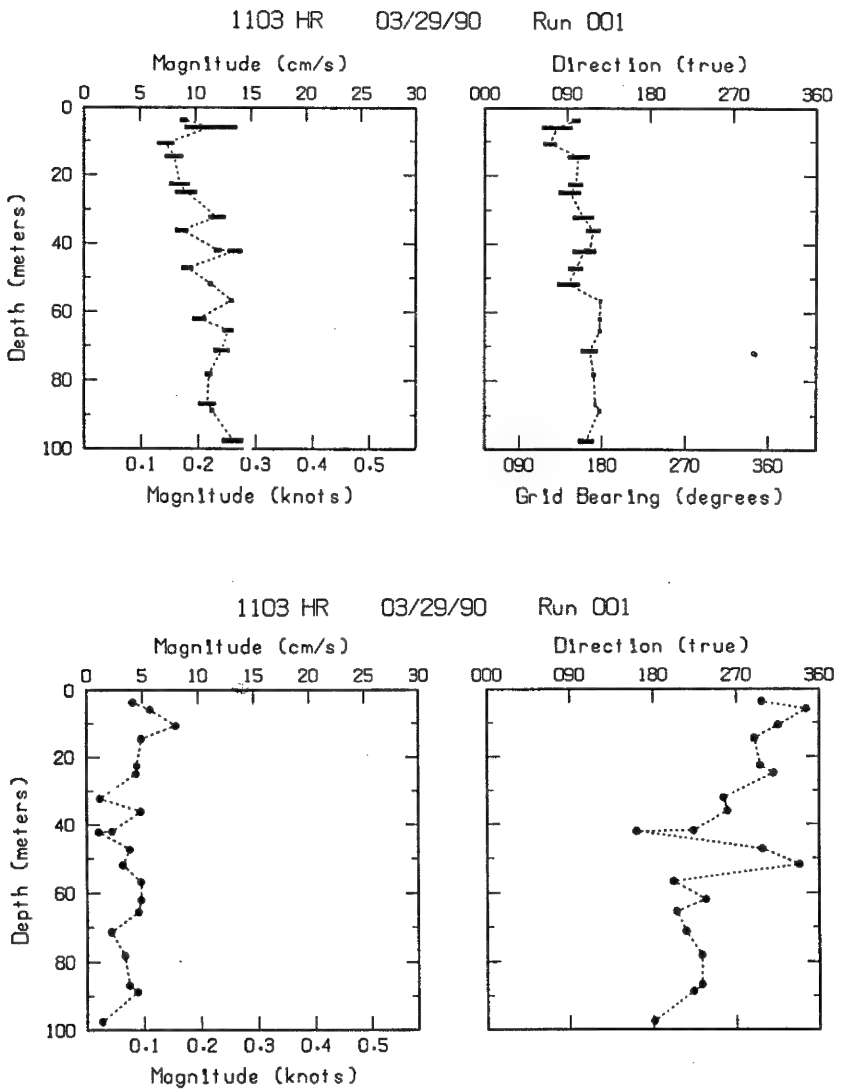

Figure 13a. Current magnitude and direction relative to (top) the floe and (bottom) the earth as a function of depth for run 001 (horizontal bars indicate the standard deviation).

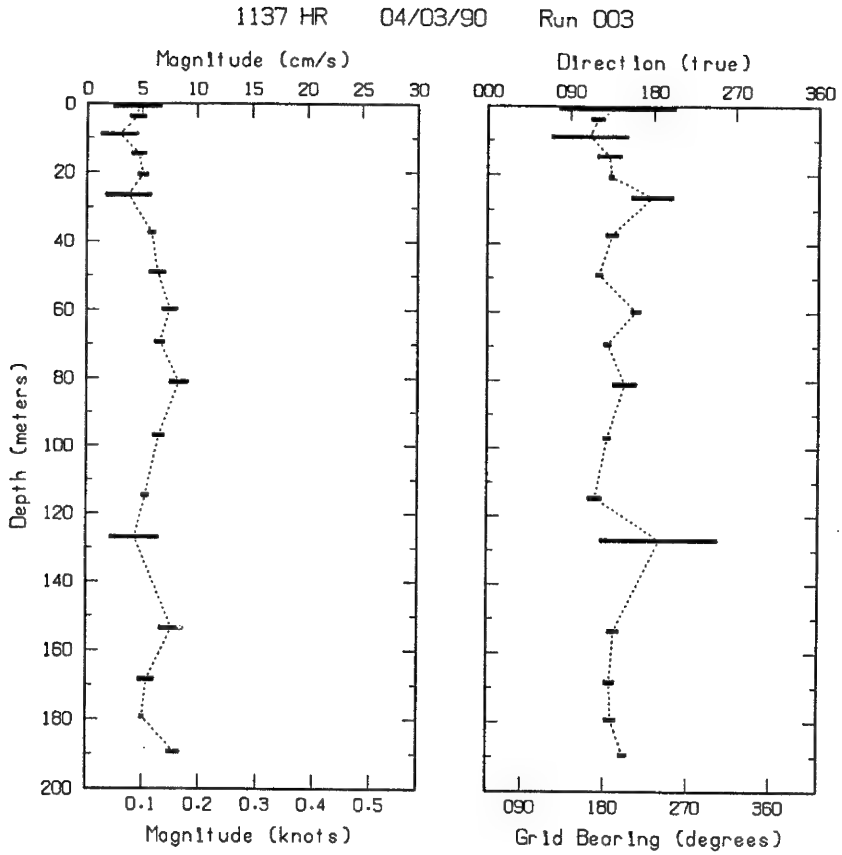

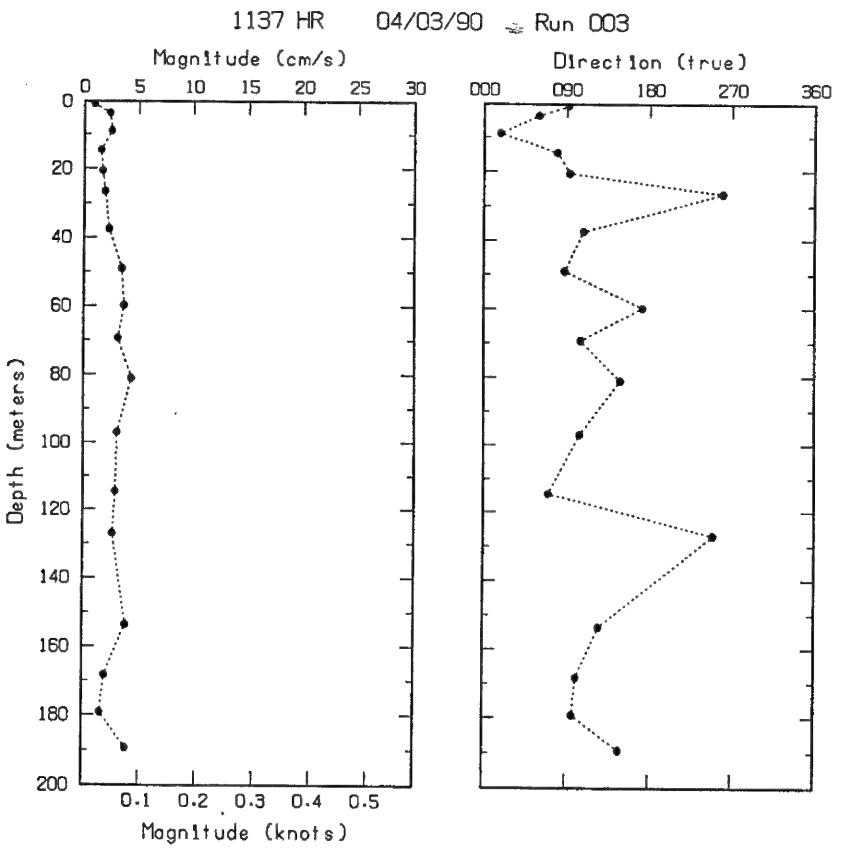

Magnetic bearing + 37 degrees = True bearing
True bearing of +Y axis = 307.5 degrees
Floe drift speed = 4.0 cm/s
Floe drift direction = 330 degrees true

Figure 13b. Current magnitude and direction relative to (top) the floe and (bottom) the earth as a function of depth for run 003 (horizontal bars indicate the standard deviation).

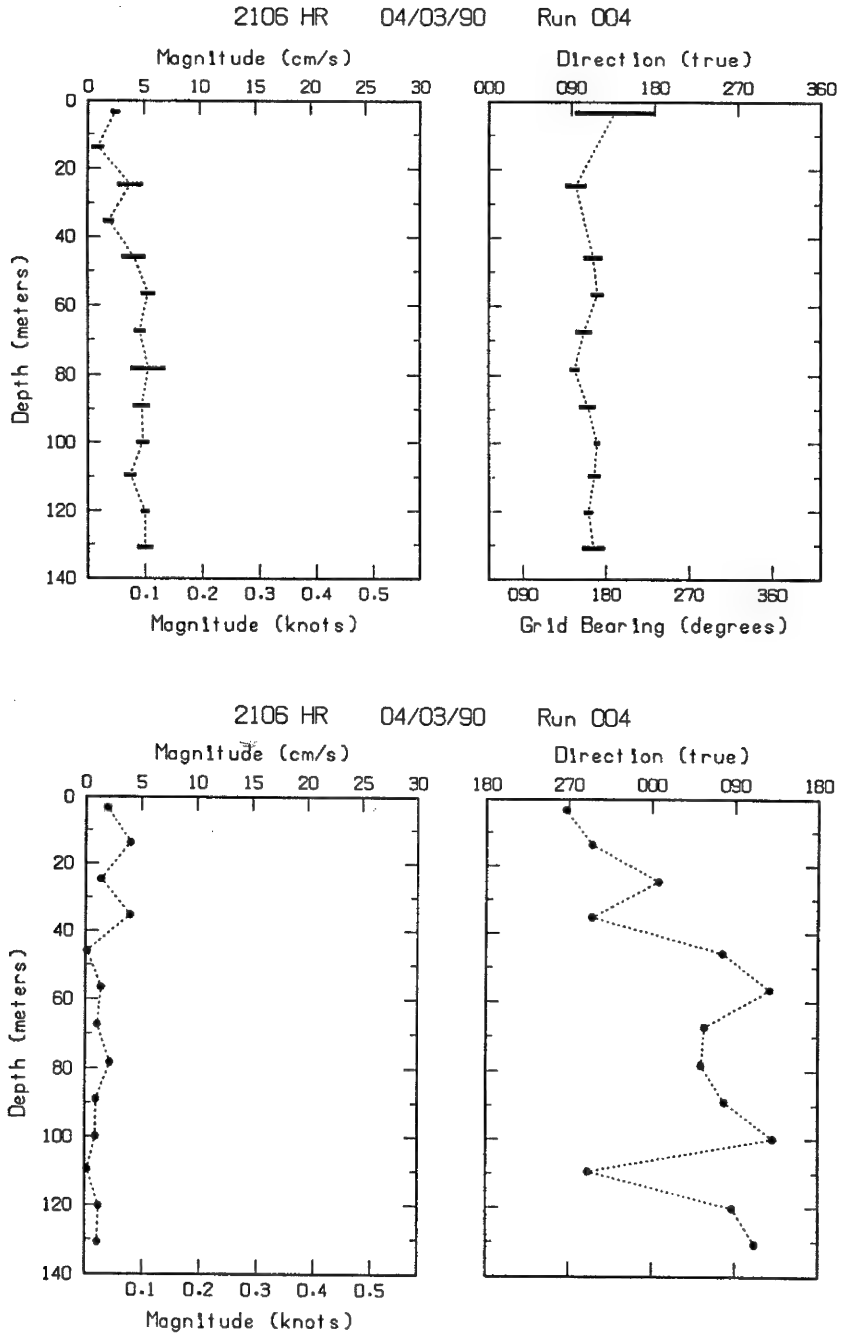

Magnetic bearing + 37 degrees = True bearing
True bearing of +Y axis = 307.5 degrees
Floe drift speed = 4.0 cm/s
Floe drift direction = 295 degrees true

Figure 13c. Current magnitude and direction relative to (top) the floe and (bottom) the earth as a function of depth for run 004 (horizontal bars indicate the standard deviation).

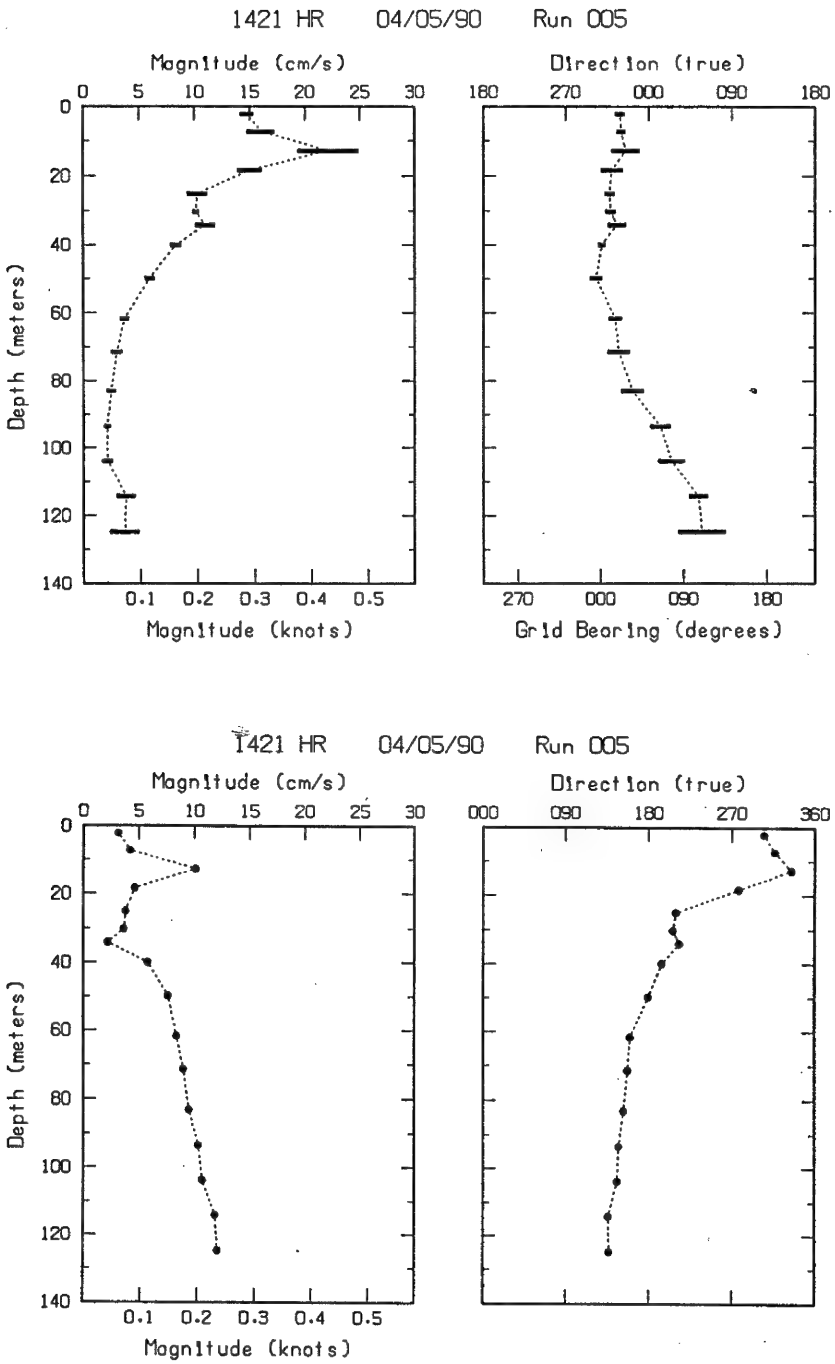

Figure 13d. Current magnitude and direction relative to (top) the floe and (bottom) the earth as a function of depth for run 005 (horizontal bars indicate the standard deviation).

VII. ICE CORES

Two sets of ice cores were obtained during the camp. The first was taken to determine the mechanical properties of the ice and the second to determine the acoustic properties.

The first set consisted of four cores taken in a large refrozen lead of first-year ice approximately 5500 m from the camp. The lead was about 117 cm thick and at least 3 km × 1 km in size. The cores were obtained on 4 April from different sites, 8 days after tests conducted in the same area by one of the ICEX participants. The second set consisted of two cores taken from multiyear ice at the edge of the camp. The relatively level surface suggested that the area had been a melt pond during the previous summer.

Because the temperature and salinity of the ice affect its mechanical and acoustic properties, both parameters were measured. The procedure for sampling the ice is described below.

A. Cores from First-Year Ice

The four cores (designated DT-1 through DT-4) were removed from undisturbed ice ~3 m away from the broken ice generated by the other tests. For each core, ~30 cm long segments were removed one at a time, using a 7.6 cm (inside diameter) SIPRE corer. The short segments reduced the time the core was exposed to the ambient air during handling and therefore limited temperature changes. Upon removal, each segment was also wrapped in 0.32 cm-thick closed-cell foam for insulation. The segments were then placed in a miter box and sawed into 7.6-cm-long sections. After each section was sawed off, a 0.32-cm-diameter hole was drilled to a depth of 3.8 cm at the midpoint, and a digital thermometer was inserted to read the temperature of the ice. The section was then sealed in a jar, and the depth of the section and the corresponding temperature were recorded. This procedure was repeated until the whole segment, and subsequently the whole ice column, was sampled. Near the bottom of the ice, the holes were partially filled with brine/seawater. The last segment of each core except DT-1 was saturated with seawater/brine. (The lowest 20 cm of DT-1 was pushed beneath the neighboring ice and could not be recovered.)

The last portion of each segment was usually less than 7 cm long and was discarded; so was the top portion of any segment that had broken off unevenly. After the temperature measurements, some sections of cores DT-2, DT-3, and DT-4 were deliberately discarded because of a shortage of storage jars. This should pose no problem since, based on past measurements,[6–8] the temperature and salinity profiles in first-year ice are fairly smooth and predictable and can be interpolated accurately.

The air temperature at the time of core sampling was −13.8°C. The temperature of the seawater was −1.76°C, and the salinity was 29.4 ppt.

The samples were taken back to the camp, melted, and analyzed for salinity using the thermistor and conductivity cell of the CTD profiler. Tygon tubing was attached to both ends of the 1 cm × 18 cm cylindrical cell, and the thermistor was inserted into the tubing near the cell. When the melted sample was poured into the tubing and the cell, both the conductivity and the temperature were measured simultaneously, and the salinity was computed. The sample water remained stationary in the cell, which was mounted off-horizontal to avoid trapping air.

Tables C1a–C1d in Appendix C show the measured and the computed properties of the ice cores. Because of brine drainage and the irregular diameters of the hand-drilled cores, the density of the ice was not measured by dividing the core weight by its volume. Instead, density and brine volume were calculated from the measured temperature and salinity using the relationships derived by Cox and Weeks.[9] Young's modulus (E) was computed from the computed brine volume using the empirical formula of Langleben and Pounder.[10] Strength factor, the last column in the tables, is a function of brine volume and is an indicator of the tensile strength as given by Weeks and Assur.[11] The properties listed in Table C1 are plotted in Figure 14.

The temperature and salinity profiles of the four cores are plotted together in Figure 15 for comparison. Above 65 cm, the temperature profiles of the four cores are similar and are almost linear. The deviation from linearity for cores DT-2, DT-3, and DT-4 was most interesting. According to field notes, this deviation occurred in the last segment of each core. (The last segment of DT-1 was not recovered). We believe that the lower portion of the ice was porous enough to allow seawater (at a temperature of −1.8°C) to seep in under hydrostatic pressure when the ice above it was removed and thereby warm up the ice. This explanation is plausible if the seepage rate is inversely proportional to the thickness of the remaining ice. The length of the last core segment was 20 cm, 43 cm, and 52 cm for cores DT-2, D-3, and D-4, respectively. The deviation from a linear temperature profile appears to be more for the shorter segments. In Figure 15, the temperature readings of the lowest two sections of core DT-2, which has the shortest last segment, have a nearly constant value of −1.8°C. Another possible explanation for the temperature nonlinearity is that the ice near the bottom has a different thermal conductivity than that above. If this were the case, however, the deviation should be the same for all the cores: therefore, this explanation is unlikely.

The salinity profiles in Figure 15b are typical of first-year ice. The salinity is high near the surface owing to a faster freezing rate and decreases as the ice becomes thicker and grows more slowly, allowing a longer time for brine expulsion. Near the bottom, the salinity should increase again because the brine has less time to drain out. However, the measurements show relatively low salinities near the bottom. This could be explained, again, by seawater seepage and dilution or displacement of brine, which has a higher salinity (37.6 ppt at −2°C and 70.6 ppt at −4°C)[9] than seawater (~29–30 ppt).

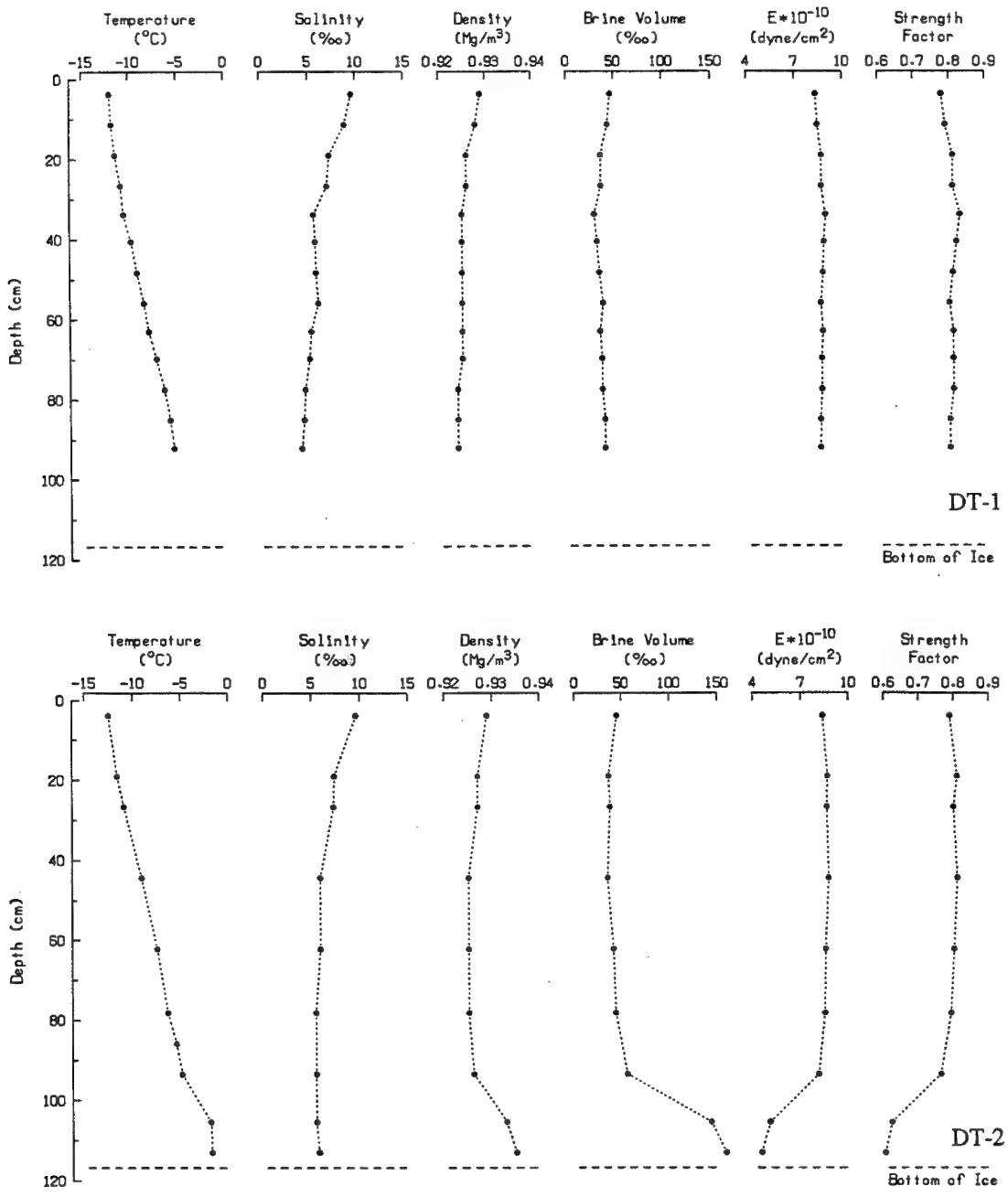

Figure 14. Measured and computed properties of ice cores DT-1, DT-2, DT-3, and DT-4.

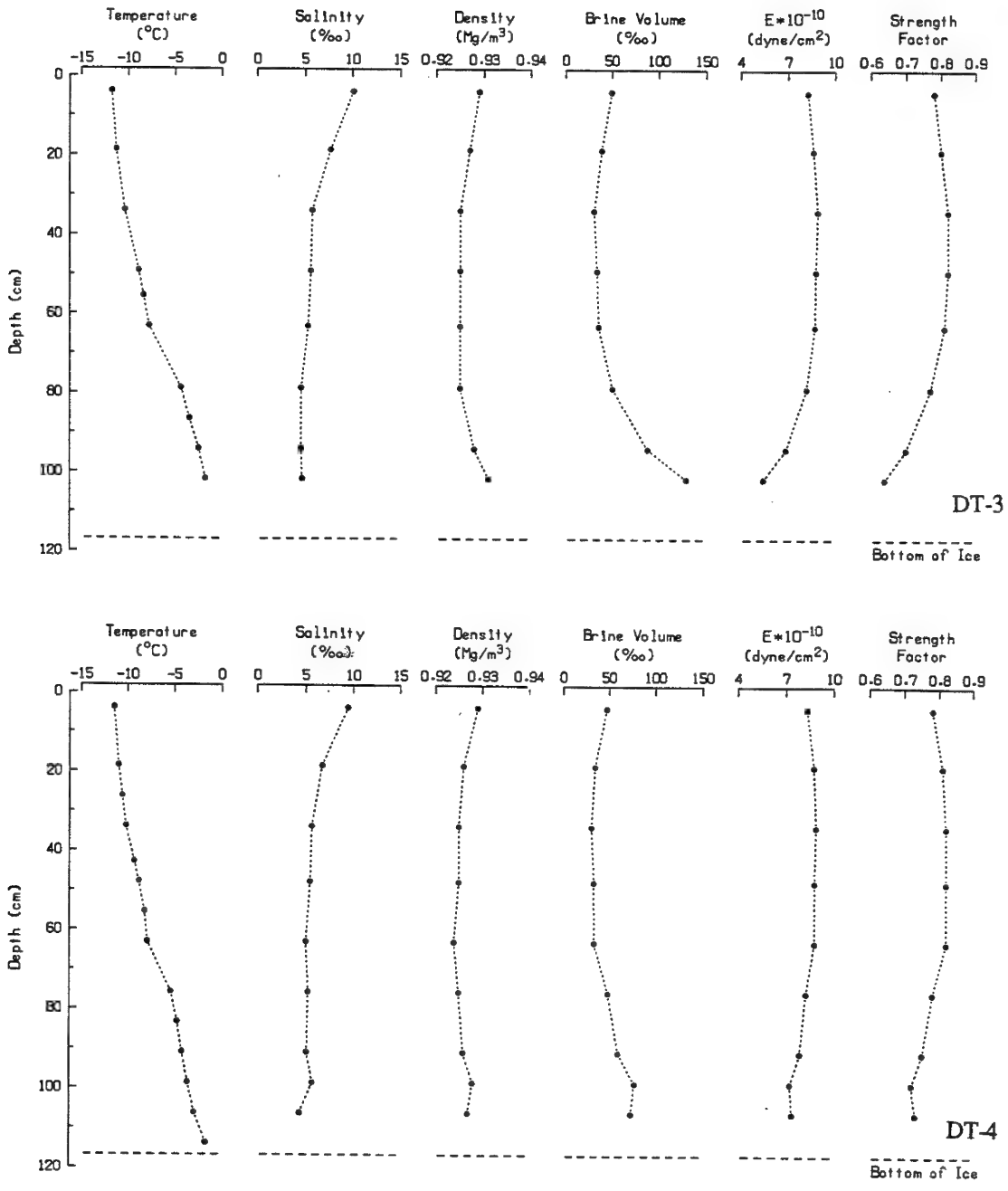

Figure 14, cont.

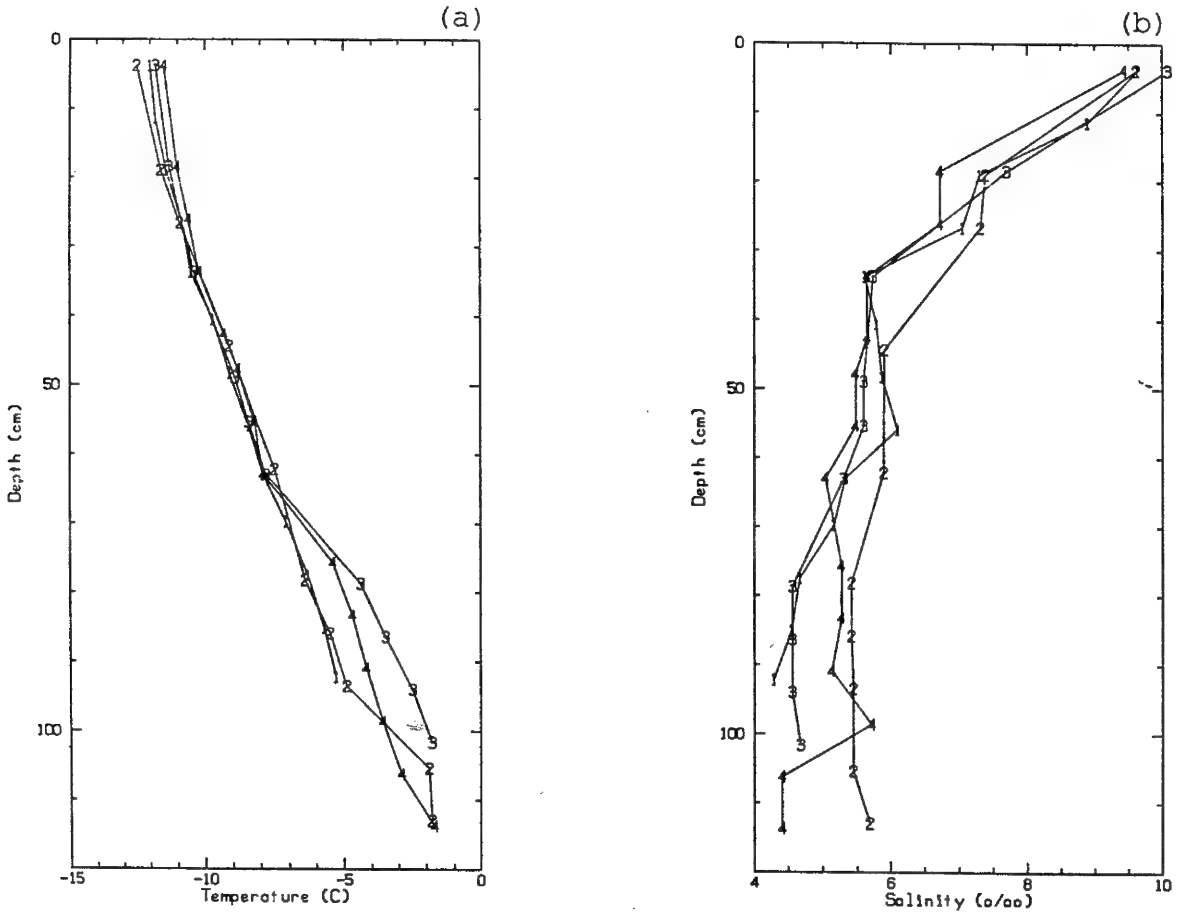

Figure 15. Comparison of temperature and salinity in ice cores DT-1, DT-2, DT-3, and DT-4.

B. Cores From Multiyear Ice

The two cores taken near the camp edge were analyzed to determine, in addition to temperature and salinity, the longitudinal and shear sound speeds of the ice for modeling sound speeds in porous material and for comparison with profiles obtained during acoustic tests conducted in the same general area. The procedure for obtaining the cores and measuring their temperature and salinity was the same as described previously, except that the depths of the core segments were not as carefully determined since rough estimates were adequate for the purpose of the study. To determine the sound speeds in the cores, we used a velocimeter[12] to measure the time-of-flight of a high-frequency acoustic pulse from one end of the core to the other.

Figure 16 shows the temperature and the salinity profiles of the two cores, designated APL-1 and APL-2. The measured and the computed properties are also given in Tables C2a and C2b. The general shape of the salinity profile is quite different from that of the first-year ice, particularly in the upper 50 cm. Although the surface of the floe in this area was relatively level and resembled first-year ice, the low salinity near the surface suggests that the ice was multiyear and the area had been a melt pond previously.

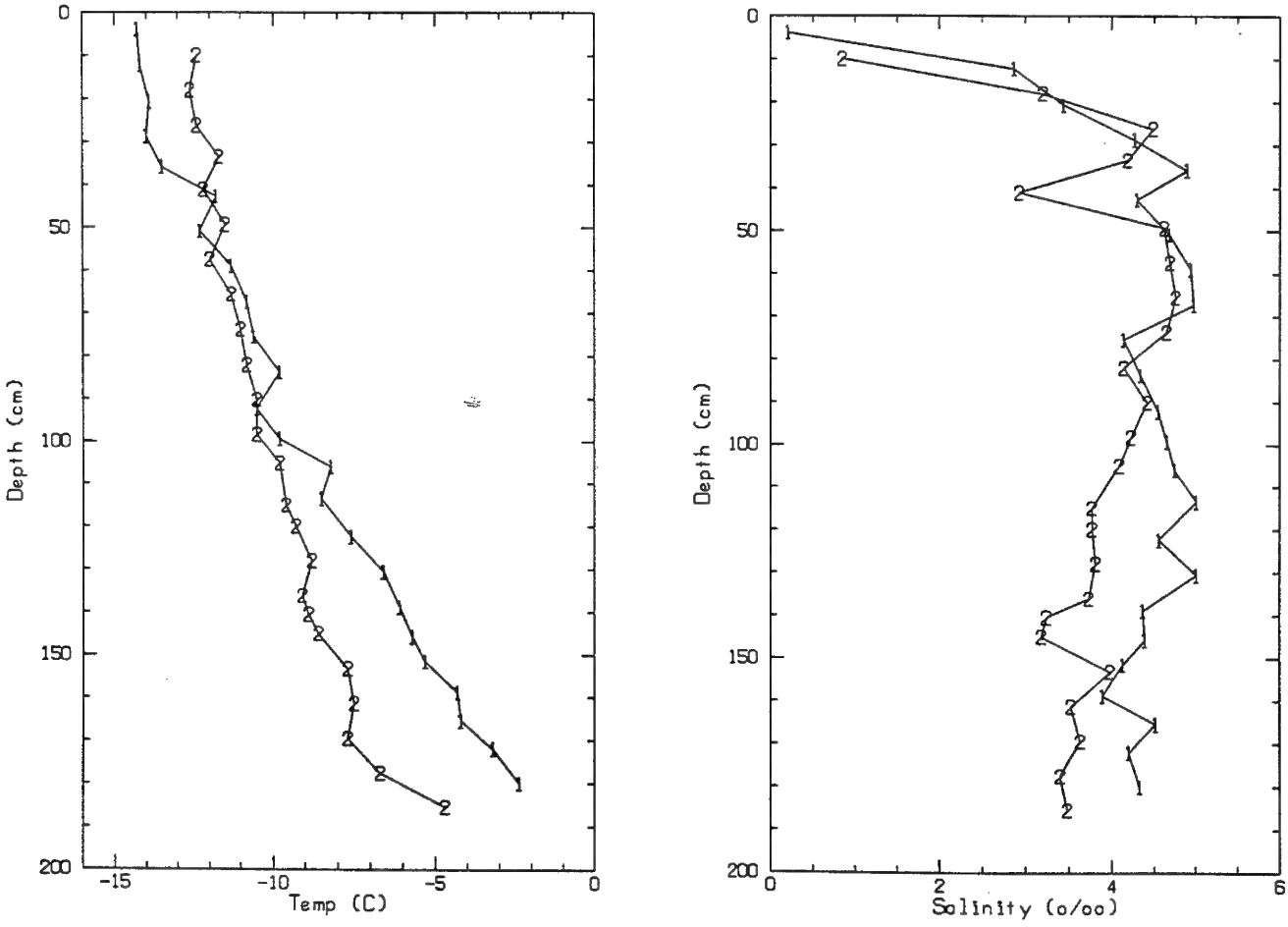

Figure 16. Comparison of temperature and salinity in ice cores APL-1 and APL-2.

Figure 17 shows the sound speeds measured in the cores. Monostatic measurements were made of the longitudinal sound speed in the same area by transmitting acoustic pulses from a source in the water below the ice upward into the ice column and recording the reflections from the air–ice interface. The longitudinal sound speed in the ice was then calculated from the thickness of the ice and the difference in travel time between the reflections from the ice–water interface and the ice–air interface interface. These calculations yielded an average longitudinal sound speed of 3834 ± 43 m/s, somewhat higher than the eyeball average of ~3650 m/s given by the velocimeter measurements. Using the measured sound speeds, temperature, and salinity of cores APL-1 and APL-2 and four cores obtained in new ice grown for an acoustic experiment,[13] we derived a set of seven elastic moduli for a simplified Biot model[14] modified to represent ice as a closed-pore, isotropic, air-free solid. Then using the moduli, we computed the sound speed as a function of the measured temperature and salinity. The model results are also shown in Figure 17. The modeled sound speeds agree well with the measured ones because the former are based on the latter. A truer verification of the model would be to apply the moduli to a new set of core samples and then compare the measured and the derived sound speeds.

The last two columns in Tables C2a and C2b give the sound speeds predicted by a model[7] that treats the ice as a solid, homogeneous, elastic material whose sound speed depends on the bulk values of modulus of elasticity, density, and Poisson's ratio. The predicted values are higher than the measured one by about 8%. Thus the homogeneous solid model is not as good at predicting the sound speeds in sea ice as the Biot model.

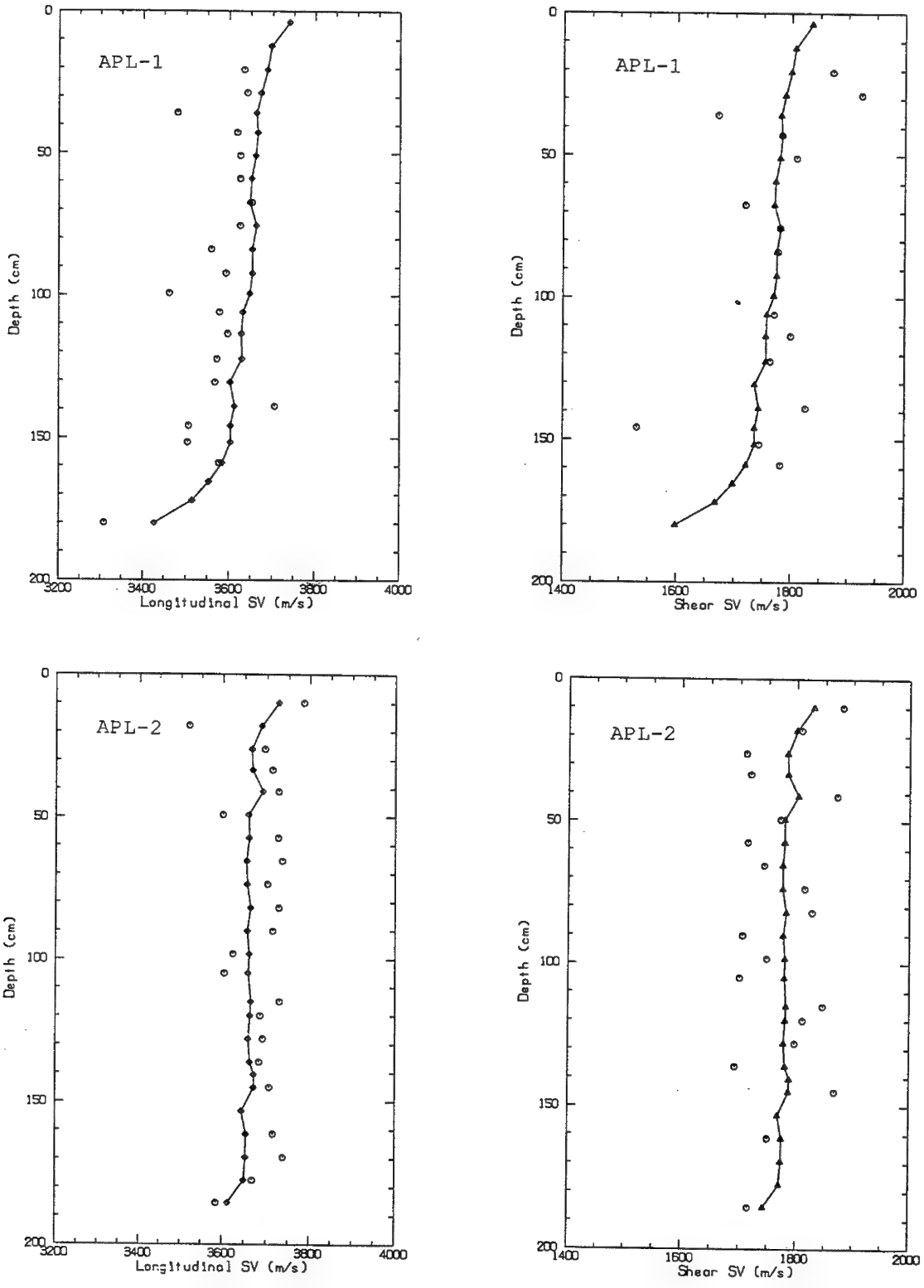

Figure 17. Comparison of measured sound speed (circles) and derived (solid line) in ice cores APL-1 and APL-2.

VIII. UNDER-ICE AMBIENT NOISE

To measure ambient noise, an array of four low-noise (equivalent to an in-water level of ~17 dBs), omnidirectional hydrophones (ITC 6050C) was deployed ~700 m from the camp to minimize interference from noise generated by camp activities. The hydrophones were configured in an orthogonal system with one (30.5 m deep) serving as the origin and the other three arranged along X,Y,Z axes, each 15.2 m from the origin. With this layout, a noise burst received at the spatially separated hydrophones could be cross correlated to estimate the direction and range of the source.

The ambient noise signals were cabled back to the camp, amplified by 20 dB, and recorded on a VCR data recorder with a 20 kHz bandwidth. The recorder had two digital channels with a dynamic range of 88 dB and two HF channels with a dynamic range of 75 dB. An HP41CX hand-held calculator was used to control the recorder, turning it on at hourly intervals and shutting it off after a programmed recording period of 5 min. Unfortunately, because of the failure of one of the two VCR recording systems at the camp, the remaining one had to be time-shared by several projects, and only a few periods of ambient noise were recorded.

During processing back in the laboratory, the data tapes were played back, and the signal from the hydrophone at the origin of the orthogonal array was fed into an HP3561 spectrum analyzer operating in narrowband mode with a Hanning data window and, at the same time, into an amplifier/speaker for audio monitoring. Thirty-two consecutive spectra were ensemble averaged to obtain a smoothed spectrum. Plots of the spectra are given in Appendix D. The first two spectra in Appendix D, with a bandwidth >20 kHz, are additional spectra obtained in real time and stored in the HP3561's memory. All sound levels have been corrected for overall hydrophone and system sensitivity (−138 dB // μPa) and calibration loss (2 dB) to yield spectral units, i.e., decibels re 1 μPa // 1 Hz. When the ambient noise was low, the high frequencies were masked by the self-noise of the hydrophones. The measured level is the incoherent sum of the ambient noise and the hydrophone self-noise. Therefore the measured level is always higher than the actual level. If the ambient level were the same as the self-noise of 17 dBs, for example, the measured level would be 20 dBs. The difference between the two is significant only when the measured noise level is a few decibels above the self-noise limit of the hydrophone. When the measured level is 17 dBs, the actual ambient noise level cannot be determined. Therefore no attempts have been made to correct for the incoherent noise summing in the results presented here.

The spectral lines at higher frequencies in Appendix D are caused by either electronic equipment or man-made waterborne acoustic signals. Higher harmonics of 60 Hz dominate in many cases. For comparison, the noise level at Sea State 0 (SS0) for the open ocean is also shown. At times, the noise level is more than 10 dB below that at SS0. In previous measurements in the Arctic,[15] the ambient noise level was lower than that at SS0 50% of the time.

To illustrate the effect of wind speed on the under-ice ambient noise, noise level and wind speed were plotted against time using levels at arbitrarily selected frequencies of 1, 2, 5, 10, and 20 kHz from the spectra in Appendix D. Figure 18a is for a period with low wind and Figure 18b for one with generally higher wind. In Figure 18a, the ambient noise is highly correlated with wind speed except for one measurement on 27 March at 0500 hours. In Figure 18b, only the higher frequency noise is correlated. The levels of high-frequency noise from 1800–2100 on 6 April (Figure 18b) are about 10 dB lower than those in Figure 18a, although the wind was about the same. This suggests that other environmental factors are contributing to the ambient noise besides the wind.

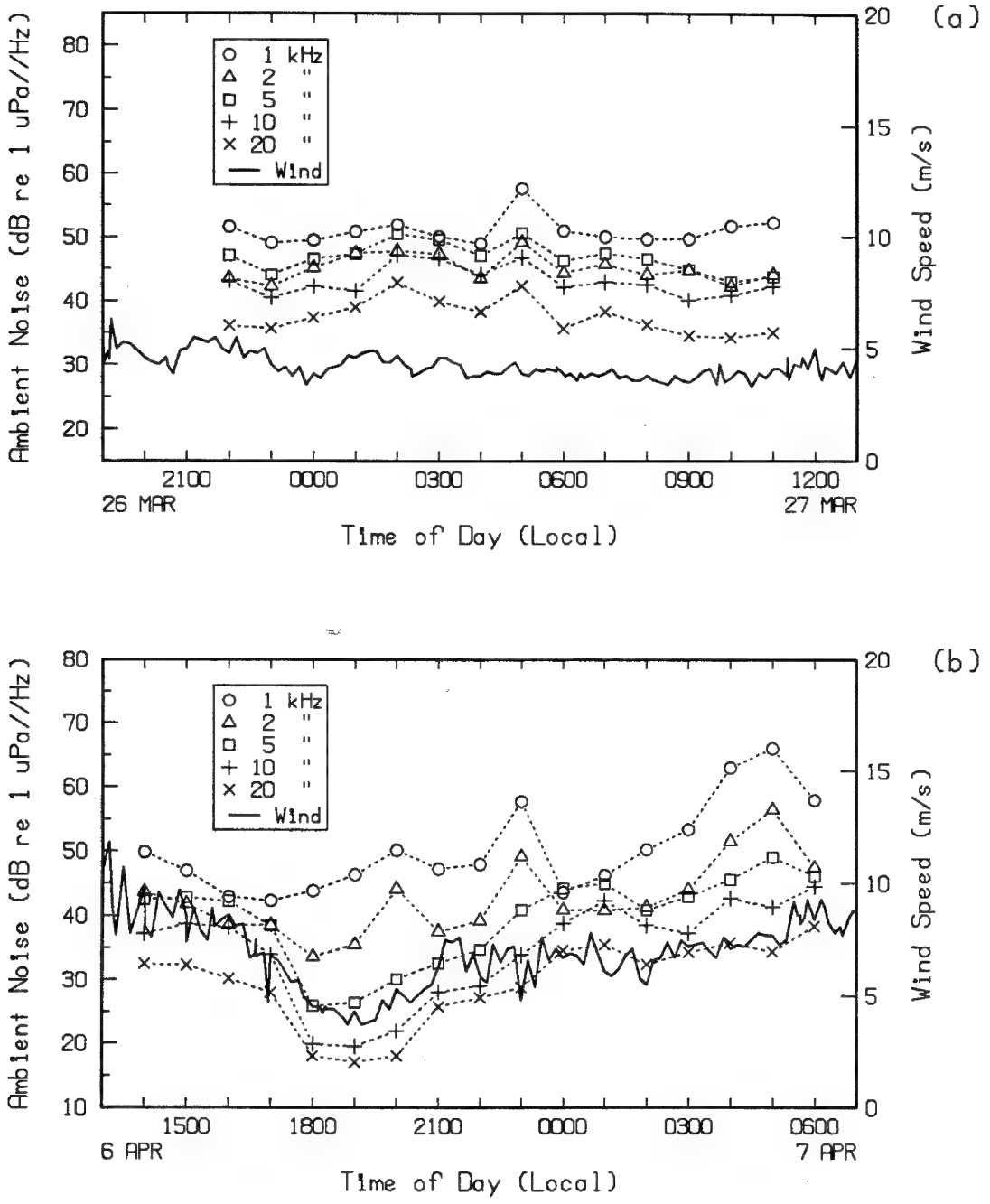

Figure 18. Wind speed and ambient noise at 1, 2, 5, 10, and 20 kHz; (a) from 1900L on 3/26/90 to 1300L on 3/27/90, (b) from 1300L on 4/6 to 0700L on 4/7/90.

IX. REFERENCES

1. G.R. Garrison, T. Wen, and M.L. Welch, "Environmental Measurements in the Beaufort Sea, Autumn 1984," APL-UW 3-85, Applied Physics Laboratory, University of Washington, Seattle, Washington, March 1985.

2. N.P. Fofonoff and R.C. Millard, Jr., "Algorithms for computation of fundamental properties of seawater," UNESCO Technical Papers in Marine Science, #44, 1983.

3. L. Padman and T. Dillon, "Vertical heat fluxes through the Beaufort Sea thermohaline staircase," *J. Geophys. Res.*, **92**, 10,799–10,806 (1987).

4. S. Neshyba, V.R. Neal, and W. Denner, "Temperature and conductivity measurements under Ice Island T-3," *J. Geophys. Res.*, **76**, 8107–8120 (1971).

5. R.R. Judd, "Oceanographic and Weather Data for Ice Camp Crystal during the AREA 88 Experiment," TR 1343, Naval Ocean Systems Center, San Diego, CA, 1990.

6. G.R. Garrison, T. Wen, R.E. Francois, W.J. Felton, and M.L. Welch, "Environmental Measurements in the Beaufort Sea, Spring 1986," APL-UW 4-86, Applied Physics Laboratory, University of Washington, Seattle, Washington, January 1987.

7. T. Wen, W.J. Felton, J.C. Luby, W.L.J. Fox, and K.L. Kientz, "Environmental Measurements in the Beaufort Sea, Spring 1988," APL-UW TR 8822, Applied Physics Laboratory, University of Washington, Seattle, Washington, March 1989.

8. T. Wen, F. Karig, R. Stein, and W. Fox, "Environmental and Acoustic Measurements in Kane Basin, off Greenland, Spring 1989," APL-UW TM 10-89, Applied Physics Laboratory, University of Washington, Seattle, Washington, December 1989.

9. G.F.N. Cox and W. F. Weeks, "Equations for determining the gas and brine volumes in sea-ice samples," *J. Glaciology*, **29**, 306–316 (1983).

10. M.P. Langleben and E.R. Pounder, "Elastic parameters of sea ice," in *Ice and Snow - Properties, Processes, and Applications*, W.D. Kingery, ed., MIT press, 1963.

11. W.F. Weeks and A. Assur, "The mechanical properties of sea ice," in *Cold Regions Science and Engineering, Part II: Physical Science*, Section C: Physics and Mechanics of Ice, U.S. Army Cold Regions Research and Engineering Laboratory, Hanover, New Hampshire, 1967.

12. K. L. Williams, R. Stein, T. Wen, and R.E. Francois, "Determination of elastic moduli of sea ice," *Oceans '89 Proceedings*, **4**, 1231–1235 (1989).

13. APL-UW 9108, "Analysis of Acoustic Measurements in the Beaufort Sea, 1990," Applied Physics Laboratory, University of Washington, Seattle, Washington (in preparation).

14. K.L. Williams, R.E. Francois, R. Stein, and T. Wen, "Biot elastic moduli of sea ice," *J. Acoust. Soc. Am.*, **87**, Suppl. S1, s56 (1990).

15. T. Wen, "Ambient Noise in the Beaufort Sea, Spring 1988," APL-UW TM 2-90, Applied Physics Laboratory, University of Washington, Seattle, Washington, February 1990.

APPENDIX A

List of Floe Position, Drift Speed, and Direction

Data points have been smoothed with a five-point, running-average filter. Times are given in Coordinated Universal Time. To obtain local time, subtract 9 hours for days up to and including 7 April and 8 hours afterward. Drift speed and direction are not given if the drift is less than 0.2 km in an 8-hour period.

List of CTD casts

Date	Local Time	Cast #	Location	
03-13-90	2029	1	72-58.0 N	142-12.3 W
03-14-90	0719	2	72 57.8 N	142 10.4 W
03-14-90	1839	3	72-57.8 N	142-08.0 W
03-14-90	2039	4	72-57.8 N	142-07.8 W
03-15-90	0645	5	72-57.9 N	142-06.7 W
03-15-90	2045	6	72-58.9 N	142-07.9 W
03-16-90	0705	7	73-01.7 N	142-11.5 W
03-16-90	2149	8	73-02.8 N	142-04.2 W
03-17-90	0650	9	73-01.9 N	141-59.9 W
03-18-90	0647	10	72-57.5 N	141-47.9 W
03-19-90	0727	11	72-55.9 N	141-43.1 W
03-19-90	1031	12	72-55.9 N	141-43.1 W
03-19-90	1156	13	72-56.0 N	141-43.2 W
03-20-90	0645	14	72-56.1 N	141-42.6 W
03-21-90	0915	15	72-55.6 N	141-46.1 W
03-22-90	0635	16	72-56.6 N	141-46.5 W
03-23-90	0647	17	72 53.8 N	141 37.1 W
03-24-90	0627	18	72 52.7 N	141 35.1 W
03-25-90	1117	19	72 52.9 N	141 36.5 W
03-26-90	0720	20	72 53.0 N	141 38.2 W
03-27-90	1123	21	72-56.6 N	141-36.1 W
03-28-90	0624	22	72-52.5 N	141-35.6 W
03-29-90	0606	23	72-52.4 N	141-40.6 W
03-29-90	2131	24	72-53.7 N	141-51.8 W
03-30-90	1038	25	72-54.2 N	141-52.0 W
03-30-90	1430	26	72-54.4 N	141-51.0 W
03-30-90	2117	27	72-54.3 N	141-51.0 W
03-31-90	1540	28	72-53.8 N	141-50.8 W
04-01-90	0807	29	72-53.8 N	141-52.3 W
04-01-90	2254	30	72-54.1 N	141-53.9 W
04-02-90	1046	31	72-54.7 N	141-52.9 W
04-03-90	0632	32	72-56.7 N	141-53.0 W
04-03-90	2203	33	72-57.9 N	141-55.6 W
04-04-90	1927	34	72-57.5 N	142-06.5 W
04-05-90	1409	36	72-54.7 N	142-10.0 W
04-05-90	2120	37	72-52.9 N	142-06.3 W
04-06-90	0819	38	72-51.8 N	141-56.1 W
04-08-90	1222	39	72-49.0 N	141-39.7 W
04-09-90	1156	41	72-49.4 N	141-38.4 W

Coordinated Universal Time Date mm dd	Time hhmm	North Latitude dd mm.ss	West Longitude ddd mm.ss	Drift Speed km/h	Drift Dir true
MAR 3	1646	72 53.03	141 57.14		
MAR 3	2013	72 53.25	141 58.91	0.30	293
MAR 3	2335	72 53.44	142 0.55	0.29	291
MAR 4	0257	72 53.65	142 2.32	0.31	291
MAR 4	0613	72 53.85	142 3.88	0.29	293
MAR 4	0925	72 54.02	142 5.43	0.28	290
MAR 4	1443	72 54.02	142 4.98	0.05	089
MAR 4	2011	72 53.71	142 3.04	0.22	118
MAR 4	2335	72 53.45	142 1.22	0.32	116
MAR 5	0304	72 53.29	141 59.16	0.34	104
MAR 5	0635	72 53.09	141 57.42	0.29	111
MAR 5	1017	72 52.95	141 55.03	0.36	100
MAR 5	1104	72 52.98	141 54.43	0.42	079
MAR 5	1155	72 53.08	141 53.64	0.55	066
MAR 5	1237	72 53.11	141 52.88	0.60	082
MAR 5	1345	72 53.21	141 51.55	0.66	075
MAR 5	1455	72 53.19	141 50.68	0.41	093
MAR 5	1924	72 53.17	141 49.81	0.11	095
MAR 5	2348	72 53.16	141 49.06	0.09	093
MAR 6	0410	72 53.16	141 48.59	0.06	089
MAR 6	1314	72 53.18	141 48.65	0.00	
MAR 6	2233	72 53.13	141 48.49	0.00	
MAR 7	0939	72 53.10	141 48.45	0.00	
MAR 7	1924	72 53.21	141 49.11	0.04	299
MAR 7	2311	72 53.18	141 49.57	0.07	257
MAR 8	0223	72 53.19	141 50.14	0.10	272
MAR 8	0537	72 53.17	141 50.83	0.12	264
MAR 8	0843	72 53.19	141 51.49	0.12	277
MAR 8	0949	72 53.21	141 52.23	0.37	275
MAR 8	1047	72 53.28	141 52.84	0.37	291
MAR 8	1129	72 53.32	141 53.20	0.30	290
MAR 8	1325	72 53.43	141 53.69	0.17	306
MAR 8	1543	72 53.53	141 54.62	0.24	289
MAR 8	1637	72 53.61	141 54.89	0.23	315
MAR 8	2055	72 53.82	141 56.52	0.23	293
MAR 9	0106	72 54.09	141 58.16	0.24	299
MAR 9	0523	72 54.28	142 0.16	0.27	288
MAR 9	0929	72 54.51	142 1.76	0.24	295
MAR 9	1328	72 54.74	142 3.32	0.24	296
MAR 9	1516	72 54.86	142 3.90	0.22	306

Date	Time	Latitude	Longitude	Speed	Dir
MAR 9	1851	72 55.05	142 4.51	0.13	315
MAR 9	2231	72 55.22	142 5.03	0.12	318
MAR 10	0215	72 55.36	142 5.65	0.11	306
MAR 10	0549	72 55.50	142 6.05	0.10	321
MAR 10	0928	72 55.65	142 6.45	0.09	320
MAR 10	1205	72 55.78	142 6.60	0.10	341
MAR 10	1310	72 55.85	142 6.90	0.19	306
MAR 10	1506	72 56.03	142 7.15	0.18	337
MAR 10	1700	72 56.14	142 7.40	0.13	328
MAR 10	2245	72 56.49	142 7.93	0.12	335
MAR 11	0253	72 56.82	142 8.29	0.15	342
MAR 11	0715	72 57.13	142 8.83	0.15	333
MAR 11	1147	72 57.49	142 9.57	0.17	328
MAR 11	1625	72 57.88	142 10.19	0.17	334
MAR 11	1813	72 58.03	142 10.57	0.20	325
MAR 11	1951	72 58.17	142 11.12	0.24	309
MAR 11	2140	72 58.31	142 11.57	0.20	317
MAR 11	2313	72 58.41	142 11.94	0.18	313
MAR 12	0057	72 58.50	142 12.49	0.20	299
MAR 12	0211	72 58.54	142 12.88	0.18	284
MAR 12	0413	72 58.56	142 13.36	0.13	281
MAR 12	0636	72 58.52	142 13.75	0.09	248
MAR 12	1023	72 58.52	142 14.33	0.08	270
MAR 12	1350	72 58.60	142 14.76	0.08	302
MAR 12	1747	72 58.61	142 15.13	0.05	274
MAR 13	0150	72 58.63	142 14.88	0.00	
MAR 13	0635	72 58.53	142 14.67	0.05	148
MAR 13	0846	72 58.43	142 14.39	0.11	138
MAR 13	1843	72 58.36	142 14.05	0.02	125
MAR 13	2235	72 58.27	142 13.64	0.07	125
MAR 14	0059	72 58.15	142 13.11	0.15	129
MAR 14	0323	72 58.06	142 12.61	0.13	120
MAR 14	0549	72 57.98	142 12.11	0.13	118
MAR 14	0919	72 57.90	142 11.47	0.11	112
MAR 14	1139	72 57.86	142 11.10	0.09	108
MAR 14	1553	72 57.80	142 10.45	0.09	106
MAR 14	1819	72 57.78	142 10.09	0.08	104
MAR 14	2029	72 57.75	142 9.70	0.10	102
MAR 14	2251	72 57.73	142 9.22	0.11	100
MAR 15	0013	72 57.74	142 8.81	0.16	083
MAR 15	0159	72 57.76	142 8.43	0.12	080
MAR 15	0349	72 57.77	142 8.04	0.12	081
MAR 15	0621	72 57.80	142 7.68	0.08	074

Date	Time	Latitude	Longitude	Speed	Dir
MAR 15	0849	72 57.82	142 7.31	0.08	078
MAR 15	1151	72 57.83	142 6.93	0.07	085
MAR 15	1729	72 57.89	142 6.61	0.04	057
MAR 15	2109	72 58.01	142 6.54	0.06	010
MAR 16	0011	72 58.14	142 6.51	0.08	003
MAR 16	0213	72 58.37	142 6.87	0.23	335
MAR 16	0307	72 58.51	142 7.11	0.31	332
MAR 16	0401	72 58.64	142 7.35	0.32	332
MAR 16	0455	72 58.78	142 7.60	0.33	332
MAR 16	0549	72 58.93	142 7.86	0.34	332
MAR 16	0612	72 59.03	142 8.06	0.57	330
MAR 16	0640	72 59.12	142 8.24	0.43	331
MAR 16	0748	72 59.43	142 8.78	0.57	332
MAR 16	0856	72 59.74	142 9.33	0.57	332
MAR 16	1011	73 0.06	142 9.87	0.52	333
MAR 16	1115	73 0.36	142 10.39	0.59	333
MAR 16	1219	73 0.67	142 10.90	0.60	334
MAR 16	1249	73 0.82	142 11.07	0.58	341
MAR 16	1319	73 0.97	142 11.22	0.58	343
MAR 16	1341	73 1.08	142 11.32	0.56	344
MAR 16	1405	73 1.19	142 11.42	0.54	346
MAR 16	1429	73 1.30	142 11.48	0.51	349
MAR 16	1459	73 1.43	142 11.53	0.48	353
MAR 16	1529	73 1.55	142 11.55	0.47	358
MAR 16	1559	73 1.67	142 11.53	0.44	002
MAR 16	1629	73 1.78	142 11.51	0.41	003
MAR 16	1659	73 1.89	142 11.48	0.40	004
MAR 16	1739	73 2.03	142 11.42	0.38	007
MAR 16	1815	73 2.14	142 11.32	0.38	013
MAR 16	1859	73 2.28	142 11.21	0.35	014
MAR 16	1939	73 2.39	142 11.08	0.34	017
MAR 16	2055	73 2.54	142 10.46	0.34	050
MAR 16	2211	73 2.68	142 9.83	0.34	053
MAR 16	2327	73 2.82	142 9.17	0.34	054
MAR 17	0043	73 2.95	142 8.49	0.35	056
MAR 17	0159	73 3.07	142 7.79	0.35	059
MAR 17	0229	73 3.06	142 7.39	0.44	094
MAR 17	0303	73 3.06	142 6.95	0.42	091
MAR 17	0345	73 3.03	142 6.41	0.42	098
MAR 17	0419	73 3.00	142 6.00	0.40	103
MAR 17	0449	73 2.97	142 5.65	0.40	107
MAR 17	0525	73 2.94	142 5.20	0.42	105
MAR 17	0623	73 2.90	142 4.61	0.34	100

Date	Time	Latitude	Longitude	Speed	Dir
MAR 17	0736	73 2.84	142 3.97	0.30	107
MAR 17	0845	73 2.73	142 3.32	0.36	121
MAR 17	0923	73 2.64	142 2.99	0.37	131
MAR 17	1102	73 2.47	142 2.26	0.31	129
MAR 17	1207	73 2.36	142 1.75	0.31	125
MAR 17	1329	73 2.23	142 1.24	0.26	130
MAR 17	1445	73 2.05	142 0.69	0.36	138
MAR 17	1612	73 1.85	142 0.07	0.35	138
MAR 17	1729	73 1.61	141 59.21	0.50	133
MAR 17	1840	73 1.38	141 58.45	0.50	136
MAR 17	1940	73 1.16	141 57.78	0.55	138
MAR 17	2025	73 0.92	141 57.27	0.69	148
MAR 17	2125	73 0.64	141 56.61	0.64	145
MAR 17	2229	73 0.32	141 56.06	0.62	153
MAR 17	2349	72 59.99	141 55.32	0.54	146
MAR 18	0104	72 59.68	141 54.91	0.50	158
MAR 18	0245	72 59.35	141 54.18	0.43	147
MAR 18	0411	72 59.04	141 53.66	0.44	153
MAR 18	0519	72 58.83	141 53.28	0.40	152
MAR 18	0624	72 58.63	141 52.95	0.37	153
MAR 18	0725	72 58.45	141 52.45	0.43	141
MAR 18	0813	72 58.34	141 52.19	0.31	145
MAR 18	0848	72 58.27	141 51.80	0.42	120
MAR 18	0930	72 58.19	141 51.50	0.32	133
MAR 18	1002	72 58.06	141 51.12	0.61	138
MAR 18	1044	72 57.96	141 50.62	0.46	124
MAR 18	1141	72 57.84	141 50.06	0.41	126
MAR 18	1249	72 57.72	141 49.47	0.33	124
MAR 18	1351	72 57.63	141 48.86	0.36	115
MAR 18	1446	72 57.61	141 48.44	0.26	101
MAR 18	1537	72 57.54	141 47.93	0.35	113
MAR 18	1629	72 57.47	141 47.57	0.27	122
MAR 18	1709	72 57.41	141 47.21	0.35	122
MAR 18	1759	72 57.33	141 46.83	0.30	123
MAR 18	1839	72 57.22	141 46.51	0.40	138
MAR 18	1919	72 57.12	141 46.21	0.37	138
MAR 18	2019	72 57.00	141 45.91	0.28	144
MAR 18	2101	72 56.87	141 45.55	0.45	140
MAR 18	2133	72 56.78	141 45.31	0.39	141
MAR 18	2207	72 56.70	141 45.08	0.36	141
MAR 18	2241	72 56.61	141 44.84	0.38	142
MAR 18	2315	72 56.52	141 44.61	0.37	143
MAR 18	2349	72 56.42	141 44.38	0.38	143

Date	Time	Latitude	Longitude	Speed	Dir
MAR 19	0029	72 56.32	141 44.10	0.36	142
MAR 19	0109	72 56.22	141 43.84	0.34	140
MAR 19	0149	72 56.13	141 43.60	0.32	143
MAR 19	0229	72 56.04	141 43.34	0.33	140
MAR 19	0439	72 55.94	141 43.18	0.10	153
MAR 19	1249	72 55.95	141 43.12	0.00	
MAR 19	2059	72 55.98	141 43.22	0.00	
MAR 20	0029	72 56.09	141 43.12	0.06	013
MAR 20	0309	72 56.20	141 43.10	0.08	003
MAR 20	0429	72 56.32	141 43.04	0.17	007
MAR 20	0529	72 56.43	141 42.93	0.21	016
MAR 20	0659	72 56.54	141 42.84	0.14	014
MAR 20	1149	72 56.46	141 42.59	0.04	138
MAR 20	1309	72 56.34	141 42.55	0.16	173
MAR 20	1409	72 56.23	141 42.56	0.21	182
MAR 20	1509	72 56.12	141 42.60	0.21	185
MAR 20	1619	72 56.00	141 42.65	0.19	187
MAR 20	1739	72 55.88	141 42.81	0.18	201
MAR 20	1935	72 55.70	141 43.13	0.19	207
MAR 20	2051	72 55.59	141 43.37	0.20	211
MAR 20	2207	72 55.48	141 43.61	0.20	211
MAR 20	2323	72 55.37	141 43.86	0.19	213
MAR 21	0039	72 55.25	141 44.10	0.20	213
MAR 21	0339	72 55.19	141 44.44	0.07	237
MAR 21	1149	72 55.22	141 44.82	0.03	283
MAR 21	1329	72 55.28	141 45.17	0.13	299
MAR 21	1459	72 55.35	141 45.47	0.14	308
MAR 21	1639	72 55.43	141 45.78	0.14	313
MAR 21	1749	72 55.52	141 46.01	0.18	322
MAR 21	1849	72 55.62	141 46.22	0.22	328
MAR 21	1939	72 55.74	141 46.42	0.28	332
MAR 21	2051	72 55.90	141 46.58	0.26	343
MAR 21	2157	72 56.05	141 46.65	0.27	352
MAR 21	2305	72 56.22	141 46.68	0.27	356
MAR 21	2359	72 56.34	141 46.58	0.25	014
MAR 22	0119	72 56.44	141 46.50	0.15	012
MAR 22	0449	72 56.55	141 46.54	0.06	354
MAR 22	0925	72 56.66	141 46.61	0.04	349
MAR 22	1729	72 56.65	141 46.25	0.00	
MAR 22	1949	72 56.67	141 45.88	0.09	079
MAR 22	2043	72 56.63	141 45.51	0.23	109
MAR 22	2153	72 56.57	141 44.98	0.26	109
MAR 22	2305	72 56.52	141 44.45	0.26	110

Date	Time	Latitude	Longitude	Speed	Dir
MAR 22	2359	72 56.44	141 44.08	0.27	124
MAR 23	0039	72 56.36	141 43.78	0.33	131
MAR 23	0119	72 56.27	141 43.53	0.33	140
MAR 23	0159	72 56.17	141 43.30	0.35	149
MAR 23	0235	72 56.06	141 43.15	0.35	156
MAR 23	0323	72 55.98	141 42.89	0.26	137
MAR 23	0409	72 55.88	141 42.66	0.29	146
MAR 23	0459	72 55.77	141 42.40	0.29	144
MAR 23	0549	72 55.69	141 42.10	0.26	130
MAR 23	0629	72 55.61	141 41.74	0.37	129
MAR 23	0709	72 55.51	141 41.50	0.33	143
MAR 23	0749	72 55.45	141 41.19	0.31	122
MAR 23	0835	72 55.35	141 40.79	0.38	130
MAR 23	0915	72 55.24	141 40.46	0.42	140
MAR 23	1007	72 55.07	141 40.02	0.45	142
MAR 23	1033	72 54.99	141 39.74	0.50	135
MAR 23	1117	72 54.83	141 39.31	0.50	140
MAR 23	1149	72 54.72	141 38.99	0.49	139
MAR 23	1219	72 54.62	141 38.73	0.48	143
MAR 23	1249	72 54.52	141 38.51	0.43	145
MAR 23	1319	72 54.41	141 38.31	0.46	151
MAR 23	1349	72 54.28	141 38.07	0.56	153
MAR 23	1419	72 54.18	141 37.90	0.42	153
MAR 23	1449	72 54.07	141 37.71	0.46	152
MAR 23	1519	72 53.96	141 37.47	0.47	146
MAR 23	1559	72 53.86	141 37.18	0.38	140
MAR 23	1639	72 53.76	141 36.95	0.33	145
MAR 23	1719	72 53.64	141 36.73	0.37	151
MAR 23	1749	72 53.54	141 36.58	0.42	157
MAR 23	1829	72 53.41	141 36.39	0.39	155
MAR 23	1919	72 53.30	141 36.25	0.27	160
MAR 23	1959	72 53.20	141 36.09	0.30	153
MAR 23	2123	72 53.06	141 35.82	0.22	152
MAR 23	2247	72 52.89	141 35.51	0.25	150
MAR 23	2349	72 52.74	141 35.21	0.31	149
MAR 24	0209	72 52.64	141 34.95	0.10	143
MAR 24	1029	72 52.69	141 35.12	0.00	
MAR 24	1829	72 52.70	141 35.20	0.00	
MAR 24	2147	72 52.73	141 35.57	0.06	286
MAR 25	0049	72 52.78	141 35.90	0.07	296
MAR 25	0419	72 52.82	141 36.25	0.06	292
MAR 25	0643	72 52.77	141 35.91	0.09	119
MAR 25	0749	72 52.85	141 36.18	0.19	316
MAR 25	0957	72 52.96	141 36.32	0.10	339
MAR 25	1759	72 52.90	141 36.30	0.00	

Date	Time	Latitude	Longitude	Speed	Dir
MAR 25	1959	72 52.97	141 36.58	0.10	311
MAR 26	0409	72 53.02	141 36.67	0.00	
MAR 26	1139	72 53.05	141 37.05	0.03	282
MAR 26	1249	72 53.02	141 37.42	0.18	256
MAR 26	1359	72 52.97	141 37.80	0.19	244
MAR 26	1539	72 52.97	141 38.19	0.13	272
MAR 26	1809	72 52.98	141 38.57	0.08	272
MAR 26	2213	72 52.90	141 38.24	0.06	127
MAR 27	0137	72 52.83	141 37.74	0.09	115
MAR 27	0501	72 52.76	141 37.24	0.09	116
MAR 27	0825	72 52.69	141 36.71	0.09	114
MAR 27	1149	72 52.61	141 36.20	0.09	116
MAR 27	1949	72 52.61	141 36.15	0.00	
MAR 28	0513	72 52.60	141 35.92	0.00	
MAR 28	1401	72 52.59	141 35.68	0.00	
MAR 28	2201	72 52.51	141 35.61	0.00	
MAR 29	0003	72 52.41	141 35.69	0.10	191
MAR 29	0449	72 52.40	141 36.07	0.04	264
MAR 29	0837	72 52.40	141 36.57	0.07	273
MAR 29	0949	72 52.35	141 37.02	0.22	247
MAR 29	1049	72 52.35	141 37.45	0.23	272
MAR 29	1129	72 52.36	141 37.88	0.35	273
MAR 29	1209	72 52.38	141 38.25	0.31	279
MAR 29	1249	72 52.39	141 38.72	0.38	276
MAR 29	1319	72 52.40	141 39.10	0.41	275
MAR 29	1357	72 52.41	141 39.65	0.47	273
MAR 29	1433	72 52.43	141 40.24	0.54	273
MAR 29	1509	72 52.44	141 40.78	0.50	276
MAR 29	1619	72 52.51	141 41.69	0.44	284
MAR 29	1709	72 52.57	141 42.39	0.48	284
MAR 29	1759	72 52.62	141 43.09	0.47	284
MAR 29	1849	72 52.67	141 43.79	0.47	284
MAR 29	1939	72 52.73	141 44.48	0.47	284
MAR 29	2101	72 52.86	141 45.52	0.45	292
MAR 29	2223	72 52.98	141 46.55	0.44	292
MAR 29	2345	72 53.11	141 47.57	0.44	293
MAR 30	0107	72 53.25	141 48.57	0.44	294
MAR 30	0229	72 53.39	141 49.57	0.44	295
MAR 30	0309	72 53.48	141 49.88	0.37	316
MAR 30	0349	72 53.48	141 50.32	0.37	270
MAR 30	0429	72 53.54	141 50.67	0.33	299
MAR 30	0509	72 53.58	141 51.07	0.35	287
MAR 30	0549	72 53.65	141 51.47	0.38	303
MAR 30	0649	72 53.72	141 51.78	0.21	306

Date	Time	Latitude	Longitude	Speed	Dir
MAR 30	0739	72 53.81	141 52.06	0.27	317
MAR 30	0841	72 53.90	141 52.33	0.21	316
MAR 30	1033	72 53.99	141 52.58	0.12	321
MAR 30	1445	72 54.16	141 52.67	0.08	351
MAR 30	1819	72 54.25	141 52.45	0.06	035
MAR 30	2007	72 54.28	141 51.95	0.15	078
MAR 30	2139	72 54.30	141 51.52	0.16	079
MAR 30	2259	72 54.29	141 51.11	0.17	094
MAR 30	2359	72 54.26	141 50.75	0.21	106
MAR 31	0119	72 54.20	141 50.41	0.16	120
MAR 31	0259	72 54.11	141 50.19	0.12	143
MAR 31	0915	72 54.00	141 50.25	0.03	188
MAR 31	1719	72 53.93	141 50.45	0.00	
MAR 31	2213	72 53.86	141 50.74	0.04	231
APR 1	0249	72 53.77	141 50.97	0.05	216
APR 1	0915	72 53.71	141 51.30	0.03	236
APR 1	1159	72 53.79	141 51.56	0.07	315
APR 1	1759	72 53.79	141 51.93	0.03	272
APR 1	2147	72 53.85	141 52.54	0.09	288
APR 2	0005	72 53.92	141 52.89	0.10	302
APR 2	0223	72 53.98	141 53.23	0.10	302
APR 2	0441	72 54.04	141 53.56	0.09	302
APR 2	0659	72 54.11	141 53.88	0.09	303
APR 2	1037	72 54.23	141 54.00	0.07	344
APR 2	1259	72 54.31	141 53.72	0.09	044
APR 2	1459	72 54.39	141 53.43	0.10	050
APR 2	1749	72 54.48	141 53.20	0.08	034
APR 2	1839	72 54.59	141 53.25	0.25	352
APR 2	2001	72 54.70	141 52.90	0.21	042
APR 2	2107	72 54.80	141 52.52	0.24	050
APR 2	2215	72 54.90	141 52.14	0.25	046
APR 2	2259	72 55.00	141 51.93	0.30	031
APR 2	2339	72 55.09	141 51.73	0.31	032
APR 3	0029	72 55.19	141 51.58	0.24	023
APR 3	0139	72 55.29	141 51.37	0.18	031
APR 3	0249	72 55.41	141 51.35	0.19	003
APR 3	0339	72 55.53	141 51.36	0.25	358
APR 3	0439	72 55.64	141 51.28	0.22	010
APR 3	0539	72 55.77	141 51.35	0.24	351
APR 3	0657	72 55.90	141 51.34	0.18	000
APR 3	0745	72 56.03	141 51.44	0.31	347
APR 3	0845	72 56.15	141 51.59	0.24	339
APR 3	1029	72 56.25	141 51.80	0.12	327
APR 3	1059	72 56.38	141 51.97	0.53	339

Date	Time	Latitude	Longitude	Speed	Dir
APR 3	1149	72 56.47	141 52.26	0.26	313
APR 3	1309	72 56.54	141 52.59	0.17	306
APR 3	1439	72 56.64	141 52.82	0.15	325
APR 3	1555	72 56.75	141 53.06	0.19	327
APR 3	1709	72 56.82	141 53.32	0.16	314
APR 3	1819	72 56.94	141 53.51	0.21	334
APR 3	1849	72 57.04	141 53.76	0.45	321
APR 3	2023	72 57.14	141 53.95	0.14	329
APR 3	2203	72 57.26	141 54.12	0.15	338
APR 3	2319	72 57.37	141 54.31	0.18	333
APR 4	0009	72 57.49	141 54.45	0.28	341
APR 4	0159	72 57.61	141 54.67	0.14	331
APR 4	0319	72 57.70	141 54.94	0.17	320
APR 4	0419	72 57.80	141 55.11	0.20	332
APR 4	0549	72 57.85	141 55.45	0.14	297
APR 4	0737	72 57.89	141 55.83	0.12	288
APR 4	0905	72 57.90	141 56.24	0.15	275
APR 4	1009	72 57.92	141 56.69	0.23	279
APR 4	1059	72 57.96	141 57.06	0.25	289
APR 4	1309	72 57.93	141 57.45	0.10	255
APR 4	1359	72 57.89	141 57.83	0.26	252
APR 4	1449	72 57.84	141 58.19	0.26	242
APR 4	1549	72 57.81	141 58.60	0.23	257
APR 4	1639	72 57.76	141 59.01	0.30	245
APR 4	1719	72 57.71	141 59.36	0.32	243
APR 4	1759	72 57.69	141 59.73	0.31	261
APR 4	1839	72 57.69	142 0.18	0.37	271
APR 4	1951	72 57.63	142 0.77	0.28	248
APR 4	2057	72 57.62	142 1.48	0.35	268
APR 4	2205	72 57.64	142 2.17	0.33	274
APR 4	2249	72 57.67	142 2.52	0.27	288
APR 4	2339	72 57.66	142 2.95	0.28	265
APR 5	0019	72 57.63	142 3.36	0.35	256
APR 5	0049	72 57.62	142 3.74	0.41	263
APR 5	0129	72 57.59	142 4.19	0.38	256
APR 5	0209	72 57.58	142 4.62	0.35	266
APR 5	0243	72 57.53	142 5.04	0.42	250
APR 5	0319	72 57.50	142 5.44	0.38	253
APR 5	0359	72 57.49	142 5.91	0.39	264
APR 5	0429	72 57.47	142 6.32	0.44	263
APR 5	0509	72 57.45	142 6.79	0.39	261
APR 5	0549	72 57.42	142 7.24	0.37	256
APR 5	0629	72 57.36	142 7.57	0.32	240
APR 5	0719	72 57.33	142 8.00	0.29	254

Date	Time	Latitude	Longitude	Speed	Dir
APR 5	0815	72 57.26	142 8.43	0.29	240
APR 5	0855	72 57.18	142 8.74	0.34	229
APR 5	0943	72 57.06	142 9.02	0.33	214
APR 5	1049	72 56.92	142 9.21	0.25	202
APR 5	1129	72 56.83	142 9.44	0.32	215
APR 5	1209	72 56.71	142 9.64	0.36	206
APR 5	1249	72 56.59	142 9.76	0.34	196
APR 5	1329	72 56.46	142 9.85	0.38	190
APR 5	1359	72 56.34	142 9.88	0.43	184
APR 5	1429	72 56.23	142 9.90	0.44	183
APR 5	1509	72 56.08	142 9.89	0.39	178
APR 5	1539	72 55.97	142 9.90	0.42	181
APR 5	1609	72 55.83	142 9.94	0.52	184
APR 5	1639	72 55.67	142 9.96	0.60	182
APR 5	1709	72 55.51	142 9.96	0.58	179
APR 5	1739	72 55.38	142 9.94	0.48	177
APR 5	1822	72 55.21	142 9.95	0.44	180
APR 5	1855	72 55.10	142 9.97	0.40	182
APR 5	1929	72 54.98	142 9.99	0.38	183
APR 5	2015	72 54.83	142 9.89	0.38	169
APR 5	2119	72 54.62	142 9.68	0.38	163
APR 5	2207	72 54.46	142 9.50	0.38	160
APR 5	2254	72 54.29	142 9.25	0.44	156
APR 6	0001	72 54.06	142 8.86	0.44	154
APR 6	0133	72 53.76	142 8.32	0.40	151
APR 6	0250	72 53.50	142 7.80	0.43	149
APR 6	0410	72 53.31	142 7.16	0.38	134
APR 6	0534	72 53.07	142 6.58	0.39	144
APR 6	0651	72 52.89	142 5.86	0.41	130
APR 6	0751	72 52.80	142 4.97	0.51	109
APR 6	0852	72 52.72	142 4.19	0.45	109
APR 6	0959	72 52.58	142 3.24	0.52	116
APR 6	1102	72 52.52	142 2.23	0.53	099
APR 6	1158	72 52.48	142 1.26	0.58	099
APR 6	1247	72 52.39	142 0.48	0.56	111
APR 6	1352	72 52.23	141 59.24	0.68	113
APR 6	1447	72 52.12	141 58.25	0.63	110
APR 6	1549	72 51.94	141 57.06	0.70	116
APR 6	1649	72 51.78	141 56.05	0.63	119
APR 6	1749	72 51.58	141 55.13	0.62	126
APR 6	1832	72 51.42	141 54.53	0.62	131
APR 6	1914	72 51.30	141 53.84	0.62	121
APR 6	1949	72 51.14	141 53.49	0.61	147
APR 6	2027	72 50.94	141 53.06	0.68	147

Date	Time	Latitude	Longitude	Speed	Dir
APR 6	2053	72 50.80	141 52.82	0.67	152
APR 6	2137	72 50.59	141 52.72	0.55	172
APR 6	2253	72 50.32	141 52.34	0.43	157
APR 7	0008	72 50.14	141 51.83	0.35	140
APR 7	0119	72 49.99	141 51.46	0.29	142
APR 7	0227	72 49.88	141 51.06	0.26	133
APR 7	0333	72 49.87	141 50.48	0.29	091
APR 7	0449	72 49.89	141 50.08	0.18	080
APR 7	0549	72 49.90	141 49.67	0.23	084
APR 7	0651	72 49.92	141 49.17	0.26	082
APR 7	0757	72 49.96	141 48.58	0.30	078
APR 7	0912	72 49.96	141 48.02	0.25	090
APR 7	1029	72 49.94	141 47.47	0.23	097
APR 7	1136	72 49.92	141 47.04	0.22	098
APR 7	1247	72 49.88	141 46.45	0.28	101
APR 7	1353	72 49.81	141 45.85	0.32	112
APR 7	1525	72 49.70	141 44.68	0.44	108
APR 7	1734	72 49.52	141 43.02	0.45	109
APR 7	2004	72 49.40	141 41.31	0.38	103
APR 7	2230	72 49.24	141 40.17	0.29	115
APR 8	0054	72 49.07	141 39.13	0.27	118
APR 8	0243	72 48.97	141 38.72	0.16	129
APR 8	0603	72 48.92	141 39.21	0.09	250
APR 8	1445	72 48.98	141 39.30	0.00	
APR 8	2018	72 49.11	141 39.24	0.04	007
APR 8	2301	72 49.25	141 39.28	0.10	355
APR 9	0101	72 49.33	141 38.85	0.14	056
APR 9	0206	72 49.43	141 38.56	0.22	040
APR 9	1016	72 49.31	141 38.27	0.03	142
APR 9	1222	72 49.28	141 38.67	0.11	251
APR 9	1649	72 49.35	141 38.31	0.05	056
APR 9	2202	72 49.32	141 37.94	0.04	100
APR 10	0146	72 49.25	141 37.63	0.06	128
APR 10	0303	72 49.23	141 36.93	0.30	097
APR 10	0432	72 49.22	141 36.19	0.28	091
APR 10	0516	72 49.24	141 35.66	0.39	082
APR 10	0639	72 49.27	141 34.95	0.28	082
APR 10	0718	72 49.24	141 34.51	0.38	100
APR 10	0823	72 49.21	141 34.05	0.24	104
APR 10	0909	72 49.09	141 33.42	0.53	122
APR 10	0946	72 48.99	141 33.14	0.39	139
APR 10	1113	72 48.81	141 32.33	0.38	126
APR 10	1202	72 48.65	141 31.79	0.51	135
APR 10	1318	72 48.43	141 31.38	0.37	151

Date	Time	Latitude	Longitude	Speed	Dir
APR 10	1355	72 48.29	141 31.07	0.51	146
APR 10	1422	72 48.18	141 30.85	0.53	149
APR 10	1454	72 48.04	141 30.63	0.53	155
APR 10	1529	72 47.89	141 30.37	0.52	151
APR 10	1601	72 47.77	141 30.06	0.53	142
APR 10	1645	72 47.56	141 29.51	0.66	141
APR 10	1730	72 47.35	141 29.22	0.57	157
APR 10	1806	72 47.21	141 28.86	0.55	144
APR 10	1841	72 47.06	141 28.55	0.55	148
APR 10	1920	72 46.88	141 28.26	0.56	153
APR 10	1946	72 46.78	141 27.93	0.62	136
APR 10	2011	72 46.66	141 27.77	0.54	157
APR 10	2041	72 46.54	141 27.55	0.52	153
APR 10	2111	72 46.39	141 27.35	0.61	157
APR 10	2145	72 46.26	141 27.02	0.53	143
APR 10	2219	72 46.12	141 26.98	0.46	174
APR 10	2300	72 45.97	141 26.86	0.42	167
APR 10	2334	72 45.84	141 26.76	0.44	167
APR 11	0031	72 45.65	141 26.52	0.38	158
APR 11	0128	72 45.49	141 26.16	0.38	145
APR 11	0240	72 45.37	141 25.75	0.27	136
APR 11	0452	72 45.29	141 25.48	0.09	132
APR 11	1301	72 45.31	141 25.59	0.00	

APPENDIX B

CTD Profiles at APLIS 90

All times are local

S = Salinity

T = Temperature

V = Sound speed

There is no plot of cast 40 because of operator error.
On casts 12 and 13, σ_t is shown instead of *V*.
Plots for casts 10, 12, 13, 16, 20, and 29 include whole or partial upcasts.

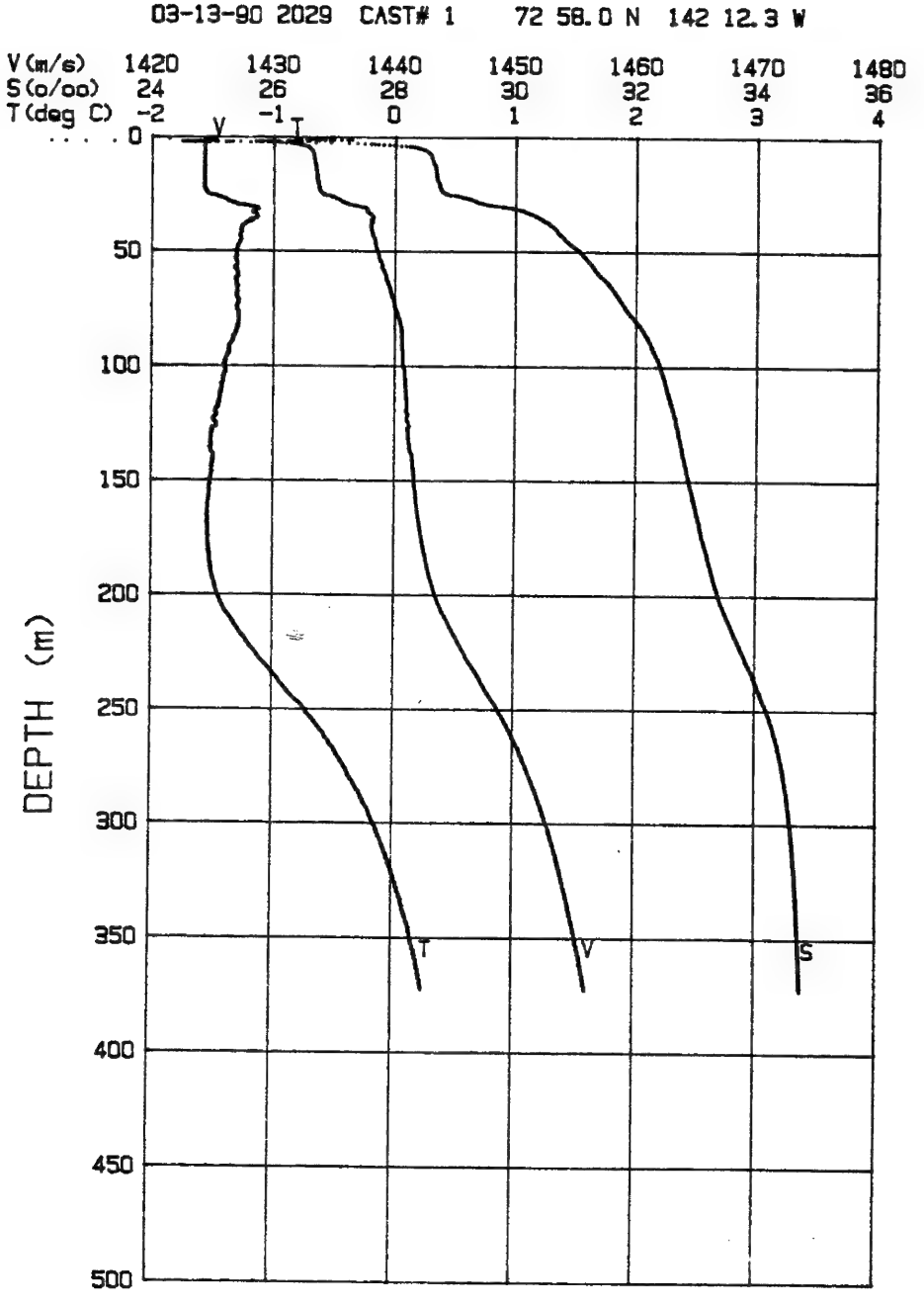
03-13-90 2029 CAST# 1 72 58.0 N 142 12.3 W
V(m/s) 1420 1430 1440 1450 1460 1470 1480
S(o/oo) 24 26 28 30 32 34 36
T(deg C) -2 -1 0 1 2 3 4
DEPTH (m)
0
50
100
150
200
250
300
350
400
450
500
V
T
T
V
S

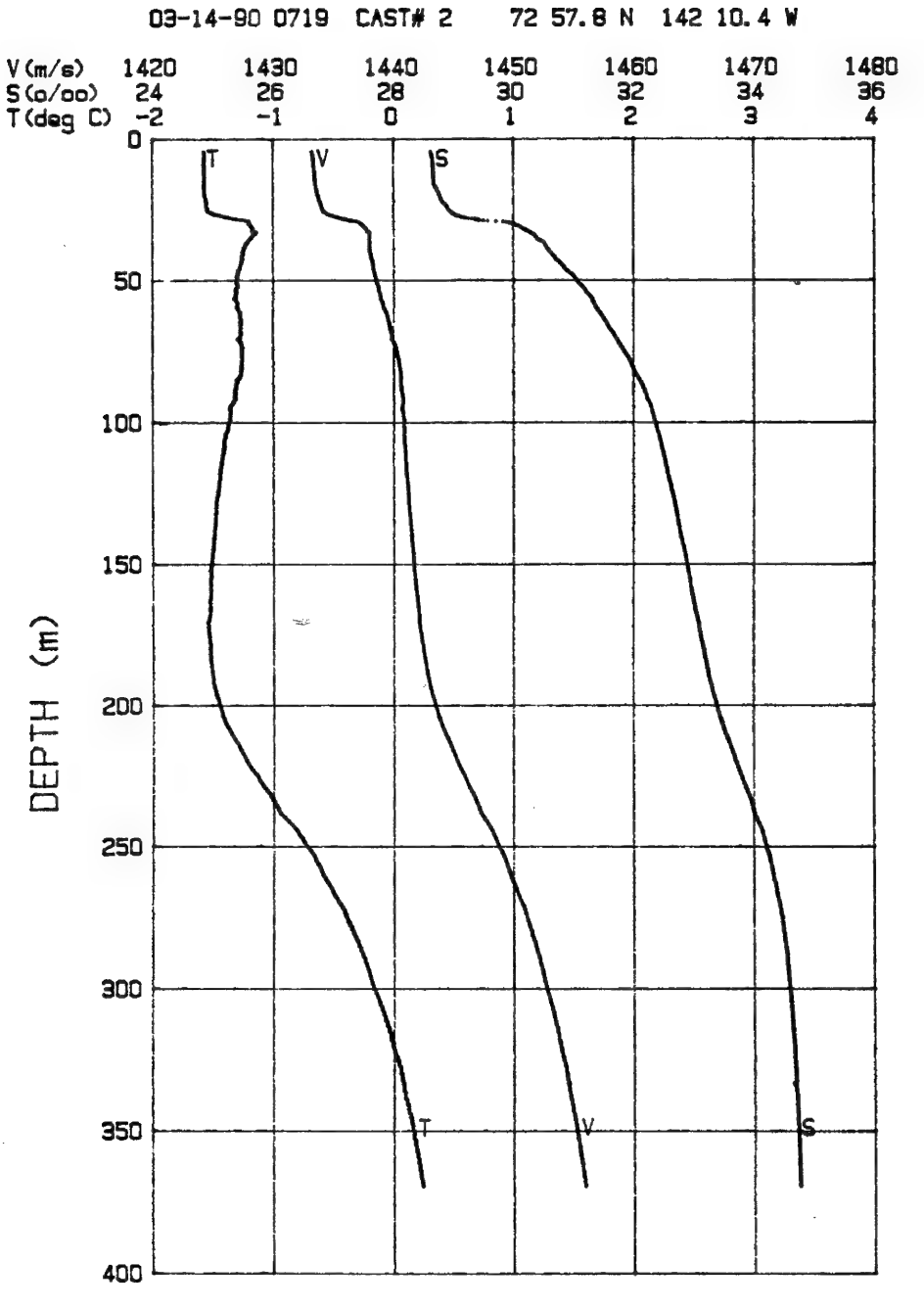
03-14-90 0719 CAST# 2 72 57.8 N 142 10.4 W
V(m/s) 1420 1430 1440 1450 1460 1470 1480
S(o/oo) 24 26 28 30 32 34 36
T(deg C) -2 -1 0 1 2 3 4
DEPTH (m)
0
50
100
150
200
250
300
350
400
T
V
S

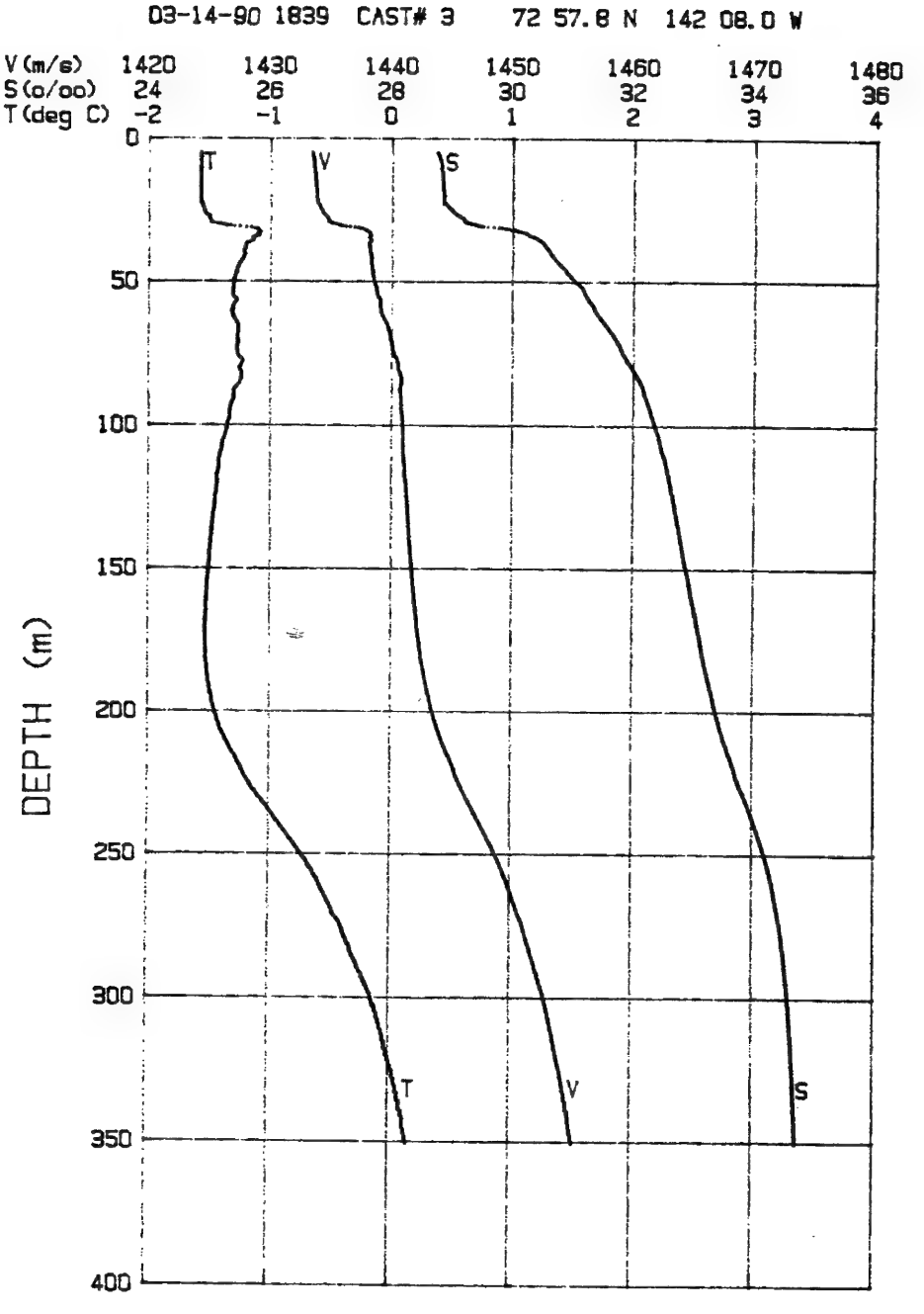
03-14-90 1839 CAST# 3 72 57.8 N 142 08.0 W
V(m/s) 1420 1430 1440 1450 1460 1470 1480
S(o/oo) 24 26 28 30 32 34 36
T(deg C) -2 -1 0 1 2 3 4
DEPTH (m)
0
50
100
150
200
250
300
350
400
T
V
S

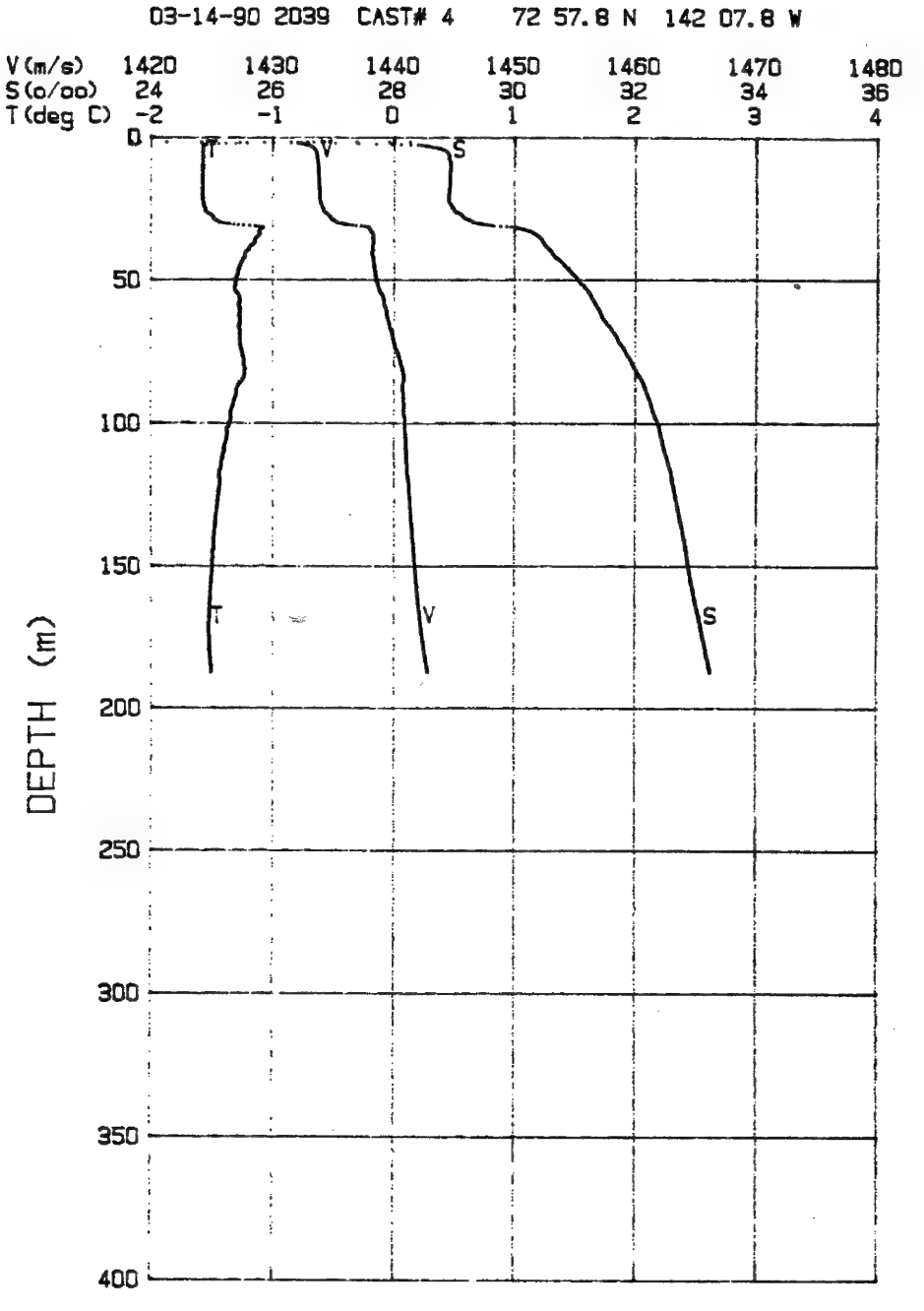
03-14-90 2039 CAST# 4 72 57.8 N 142 07.8 W
V(m/s) 1420 1430 1440 1450 1460 1470 1480
S(o/oo) 24 26 28 30 32 34 36
T(deg C) -2 -1 0 1 2 3 4
0
50
100
150
200
250
300
350
400
DEPTH (m)
T
V
S

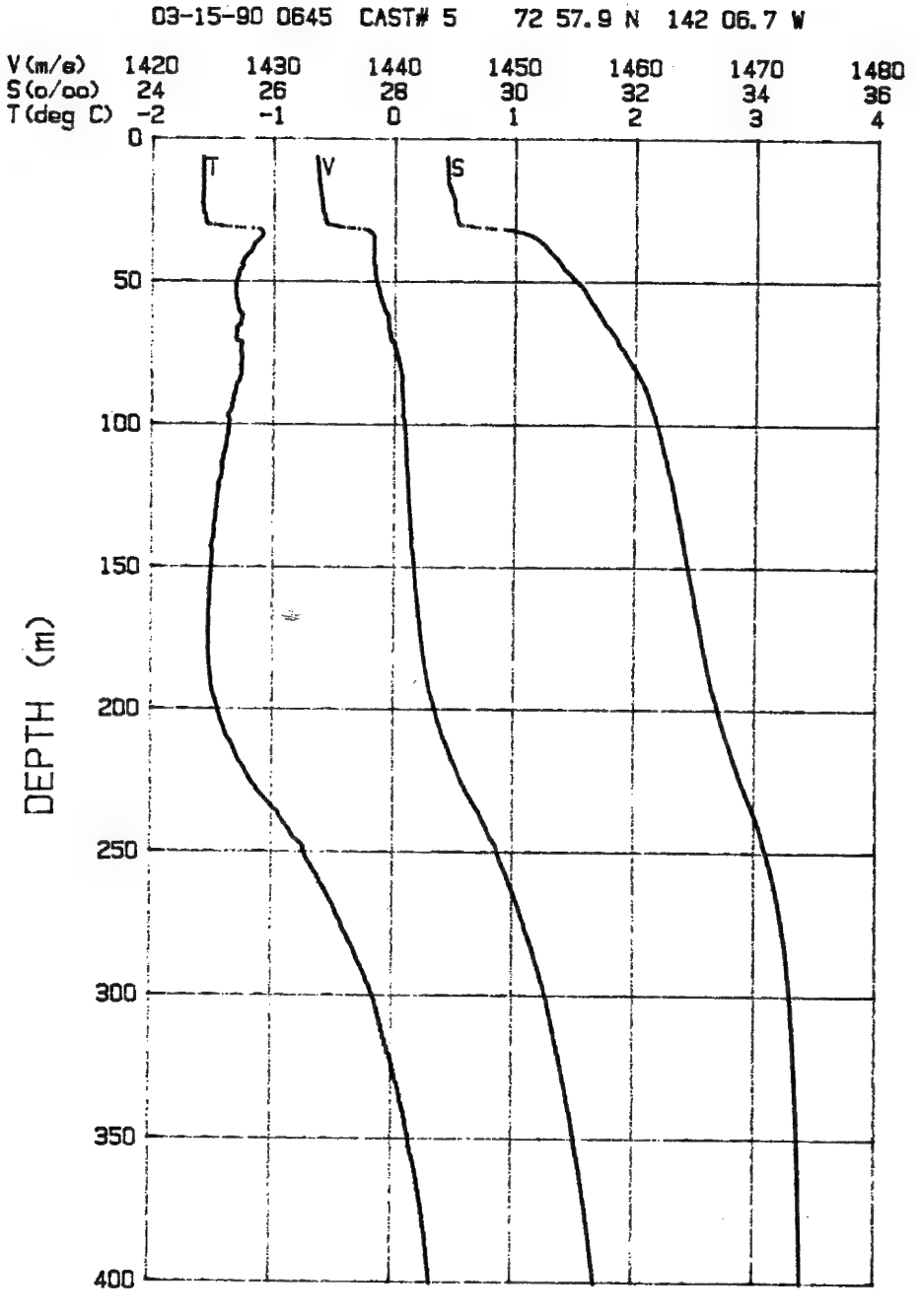
03-15-90 0645 CAST# 5 72 57.9 N 142 06.7 W
V(m/s) 1420 1430 1440 1450 1460 1470 1480
S(o/oo) 24 26 28 30 32 34 36
T(deg C) -2 -1 0 1 2 3 4
T
V
S
DEPTH (m)
0
50
100
150
200
250
300
350
400

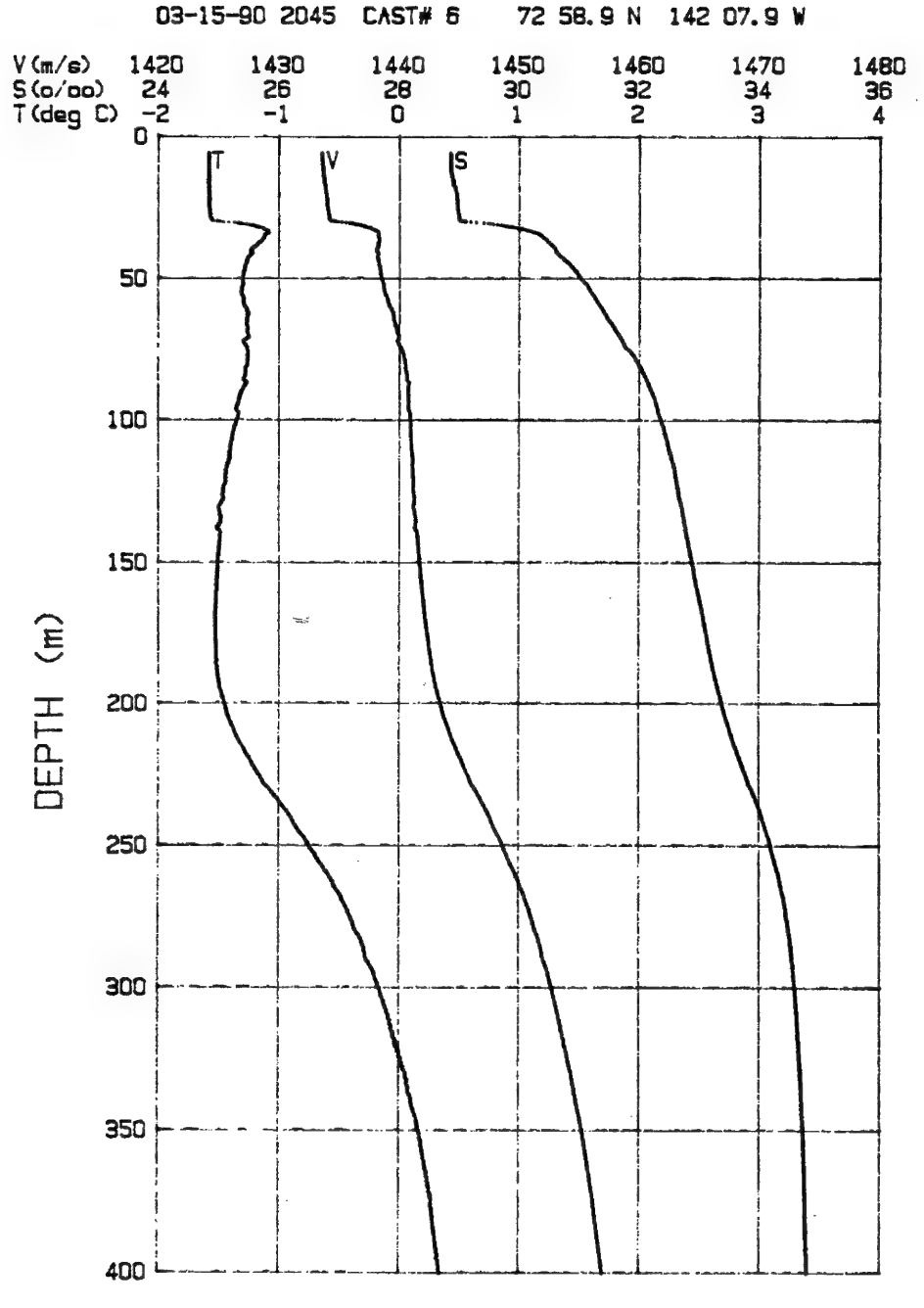
03-15-90 2045 CAST# 6 72 58.9 N 142 07.9 W
V(m/s) 1420 1430 1440 1450 1460 1470 1480
S(o/oo) 24 26 28 30 32 34 36
T(deg C) -2 -1 0 1 2 3 4
T
V
S
DEPTH (m)
0
50
100
150
200
250
300
350
400

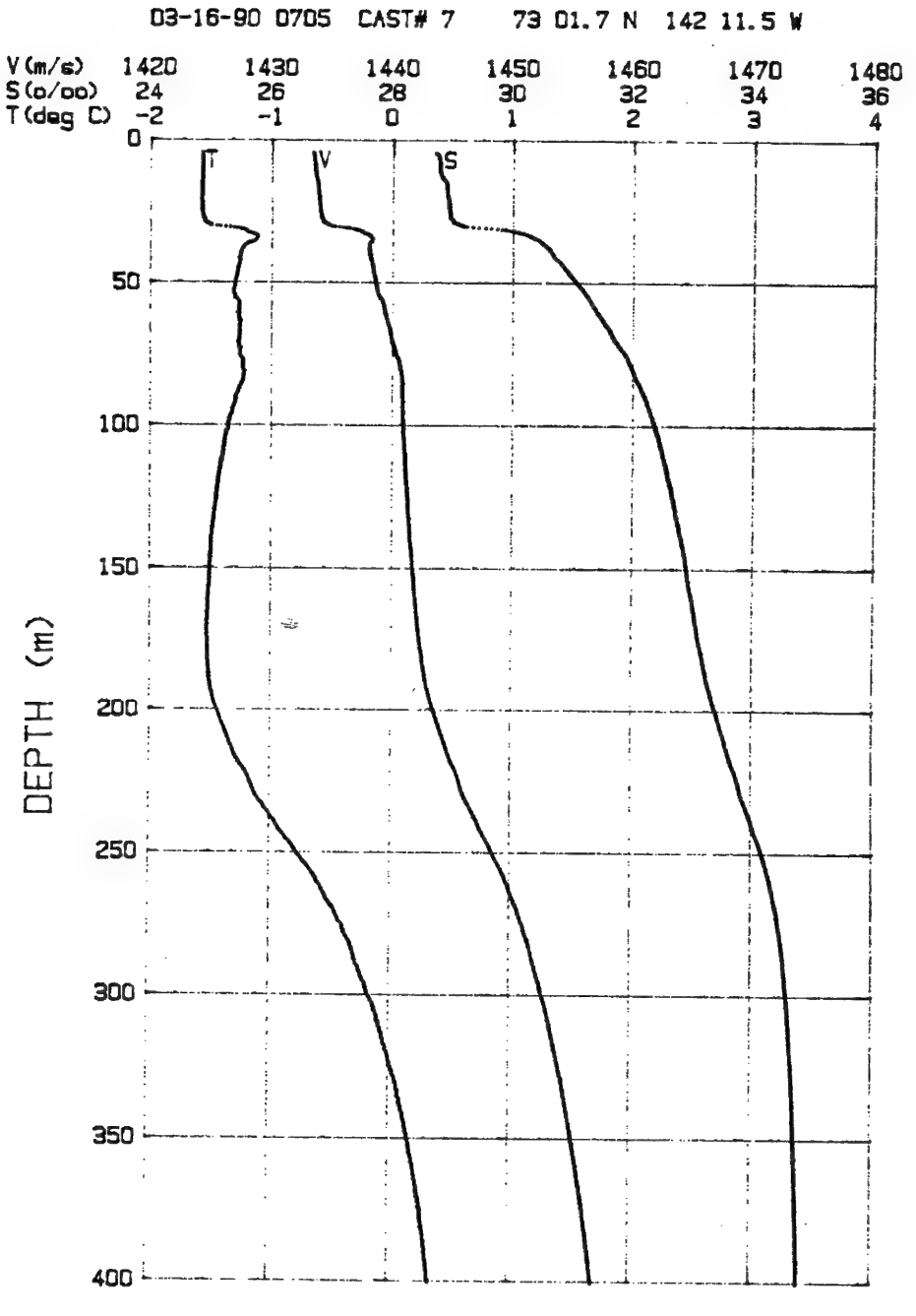
03-16-90 0705 CAST# 7 73 01.7 N 142 11.5 W
V(m/s) 1420 1430 1440 1450 1460 1470 1480
S(o/oo) 24 26 28 30 32 34 36
T(deg C) -2 -1 0 1 2 3 4
T
V
S
DEPTH (m)
0
50
100
150
200
250
300
350
400

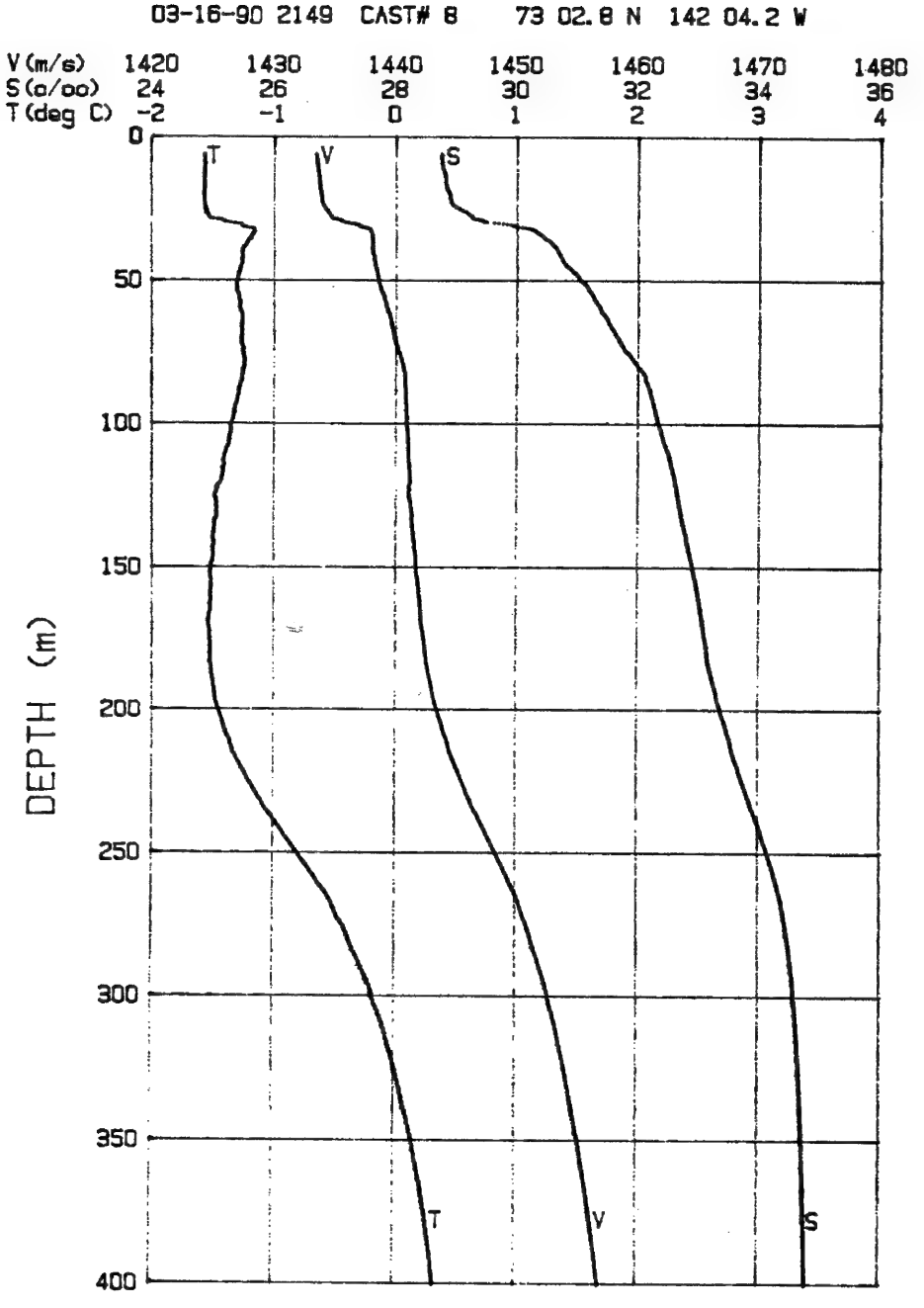
03-16-90 2149 CAST# 8 73 02.8 N 142 04.2 W
V(m/s) 1420 1430 1440 1450 1460 1470 1480
S(o/oo) 24 26 28 30 32 34 36
T(deg C) -2 -1 0 1 2 3 4
DEPTH (m)
0
50
100
150
200
250
300
350
400
T
V
S

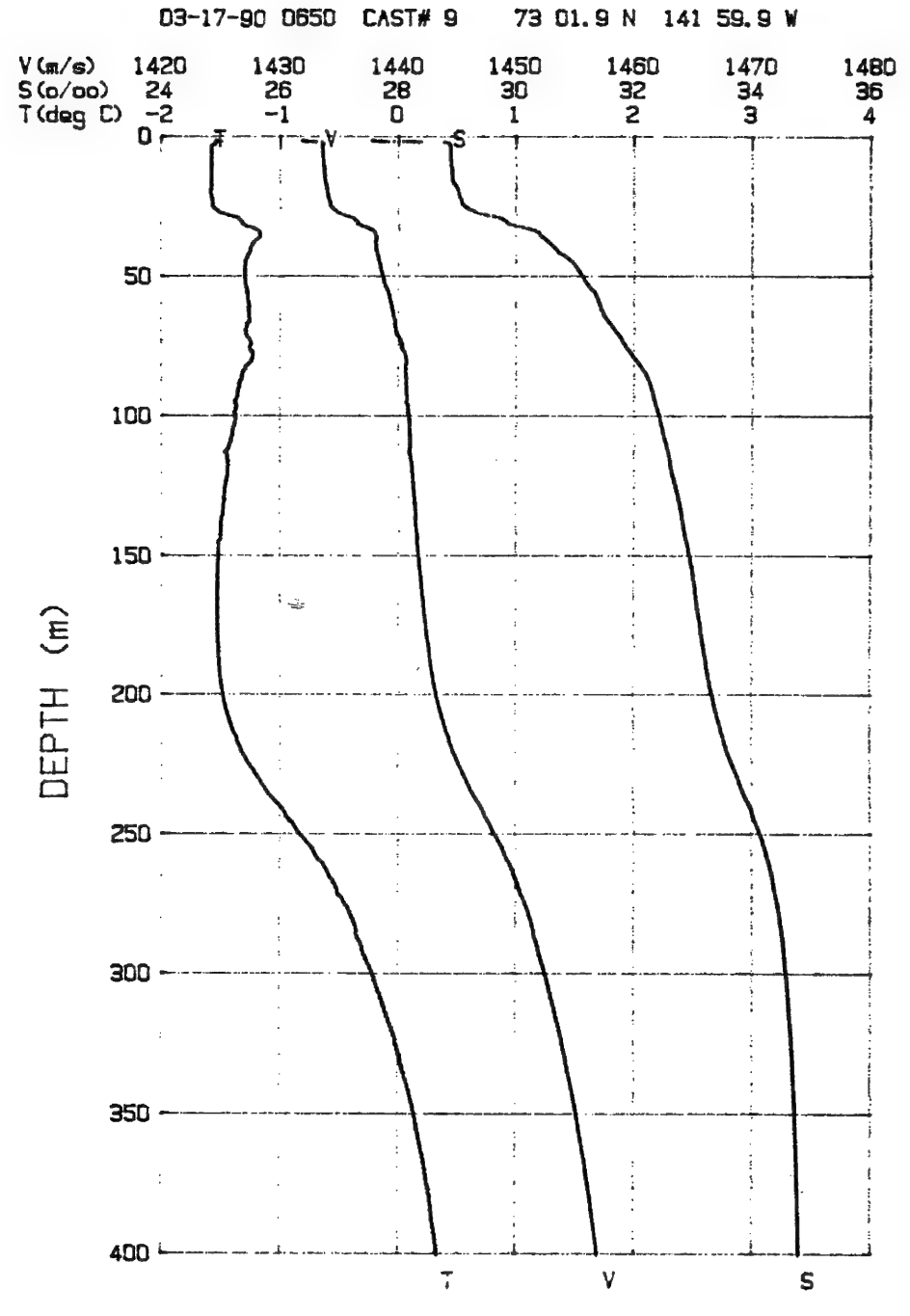
03-17-90 0650 CAST# 9 73 01.9 N 141 59.9 W
V(m/s) 1420 1430 1440 1450 1460 1470 1480
S(o/oo) 24 26 28 30 32 34 36
T(deg C) -2 -1 0 1 2 3 4
T
V
S
0
50
100
150
200
250
300
350
400
DEPTH (m)
T
V
S

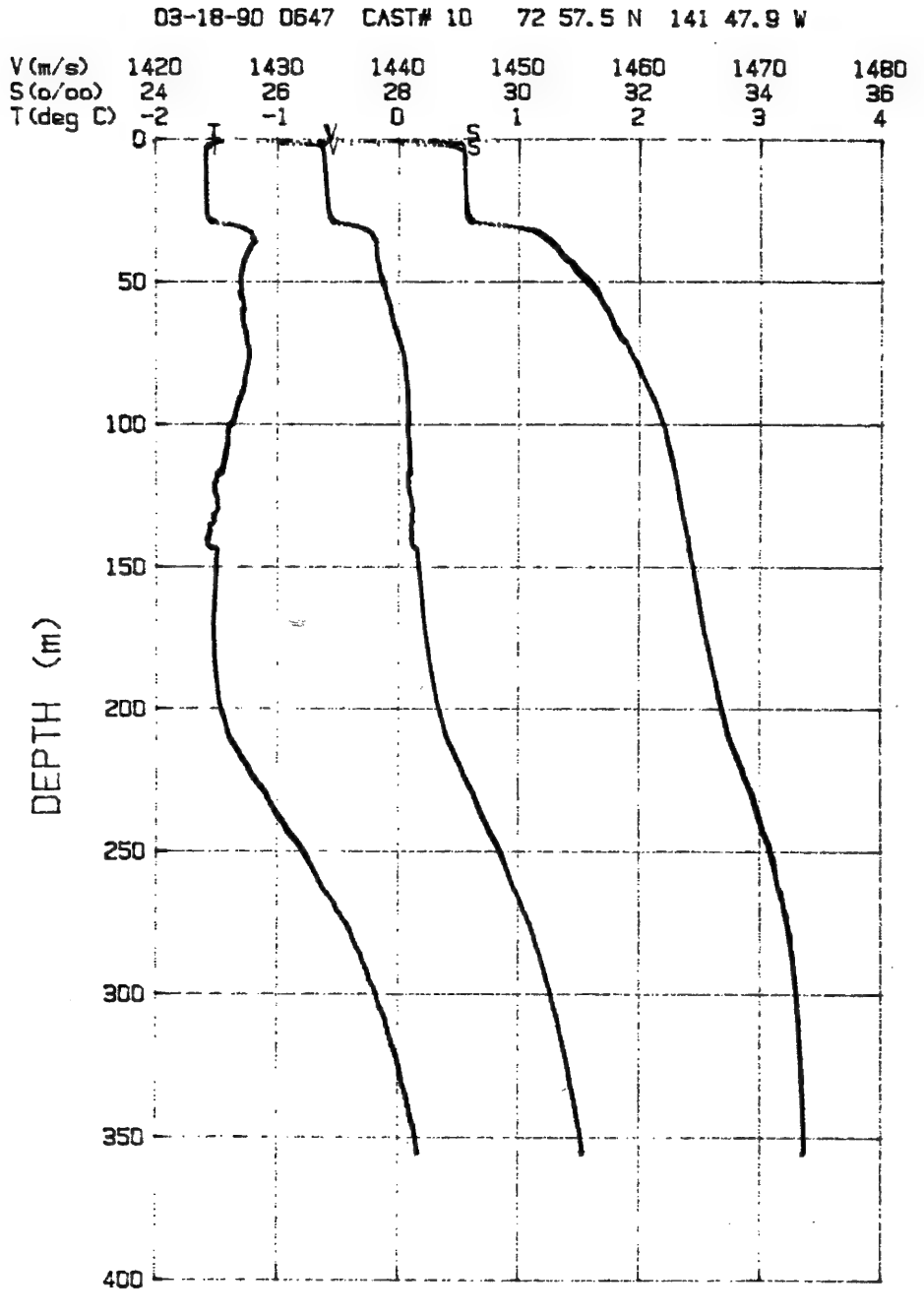
03-18-90 0647 CAST# 10 72 57.5 N 141 47.9 W
V(m/s) 1420 1430 1440 1450 1460 1470 1480
S(o/oo) 24 26 28 30 32 34 36
T(deg C) -2 -1 0 1 2 3 4
T
V
S
DEPTH (m)
0
50
100
150
200
250
300
350
400

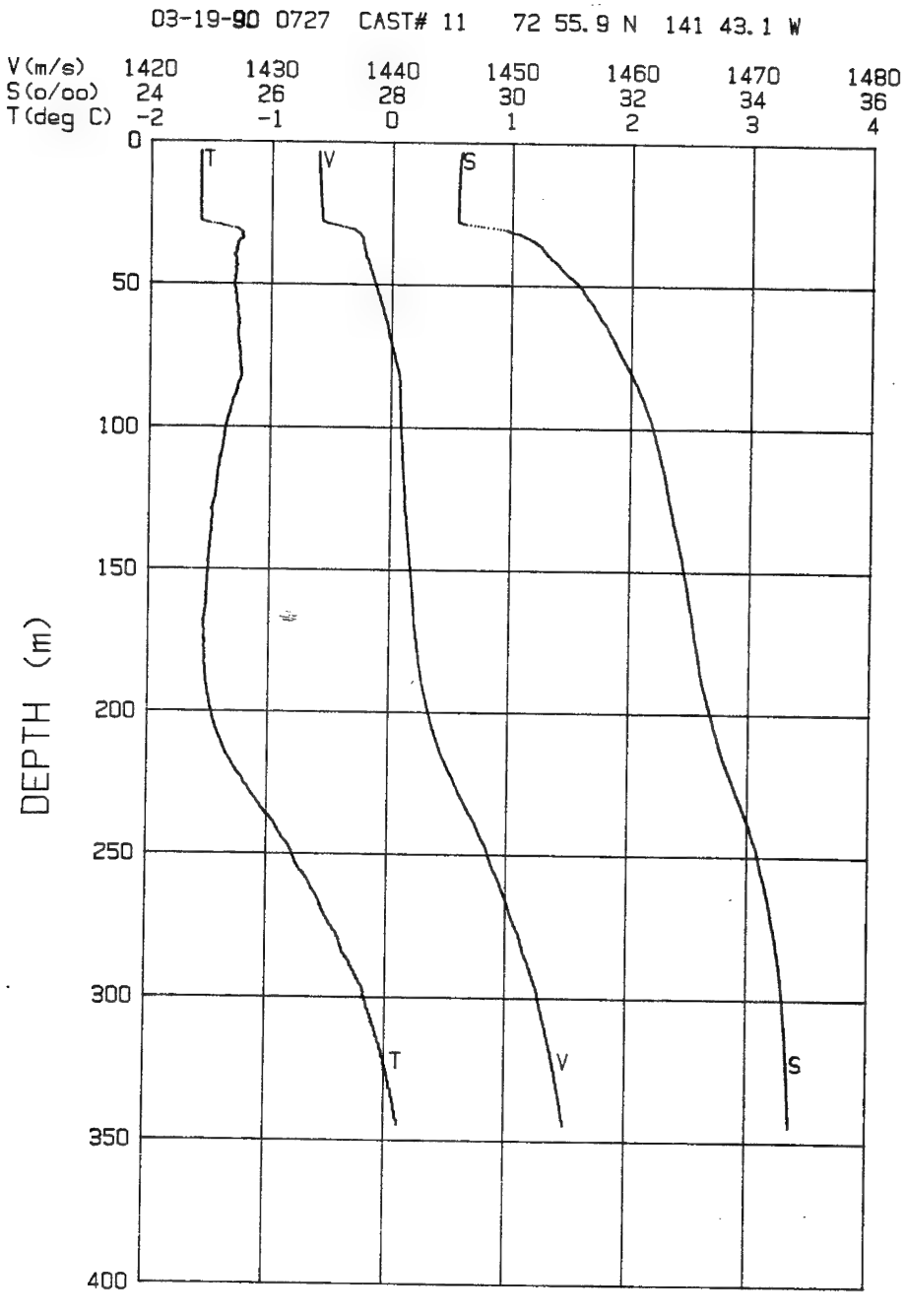
03-19-90 0727 CAST# 11 72 55.9 N 141 43.1 W
V(m/s) 1420 1430 1440 1450 1460 1470 1480
S(o/oo) 24 26 28 30 32 34 36
T(deg C) -2 -1 0 1 2 3 4
DEPTH (m)
0
50
100
150
200
250
300
350
400
T
V
S

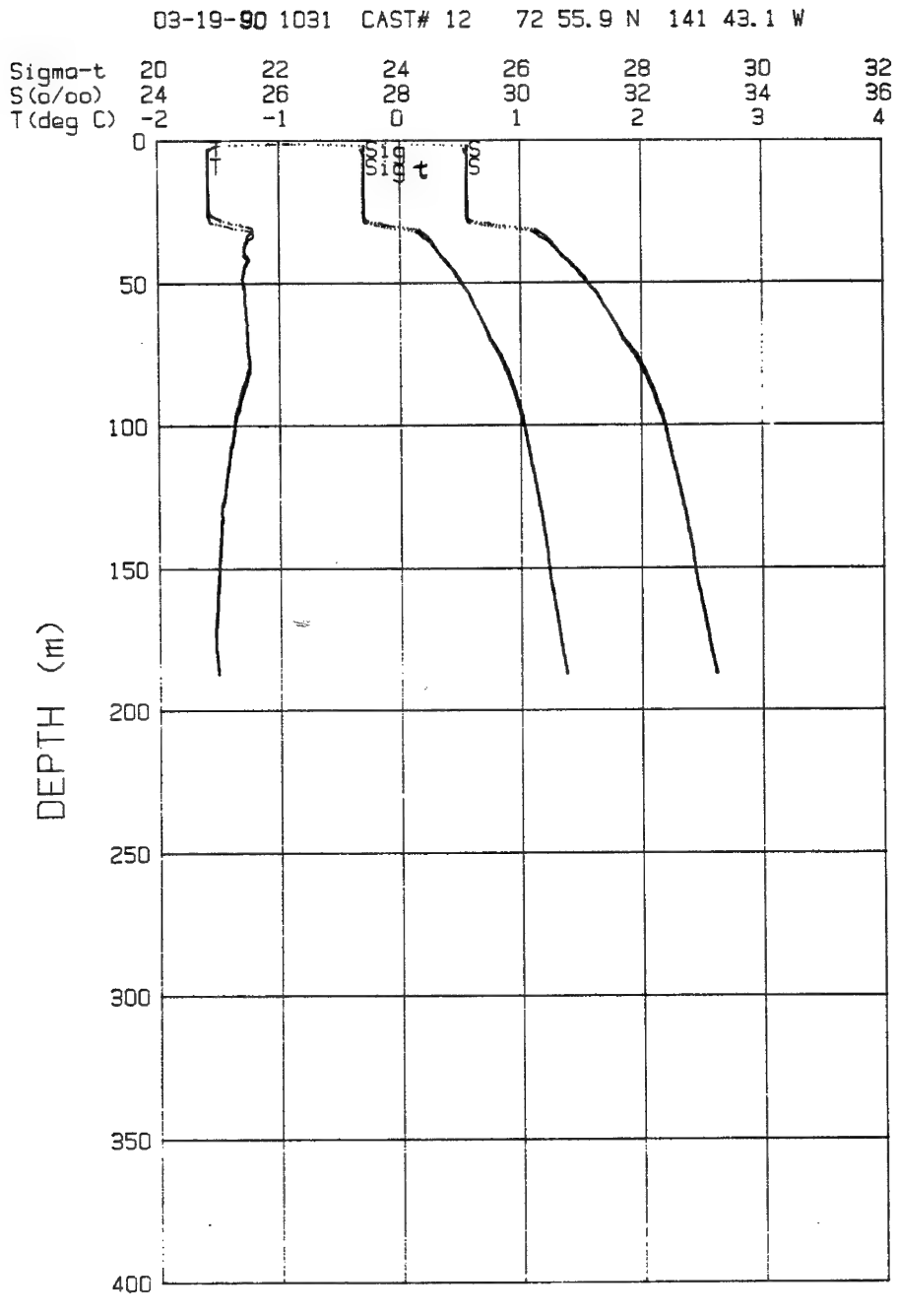
03-19-90 1031 CAST# 12 72 55.9 N 141 43.1 W
Sigma-t 20 22 24 26 28 30 32
S(o/oo) 24 26 28 30 32 34 36
T(deg C) -2 -1 0 1 2 3 4
0
50
100
150
200
250
300
350
400
DEPTH (m)
T
t

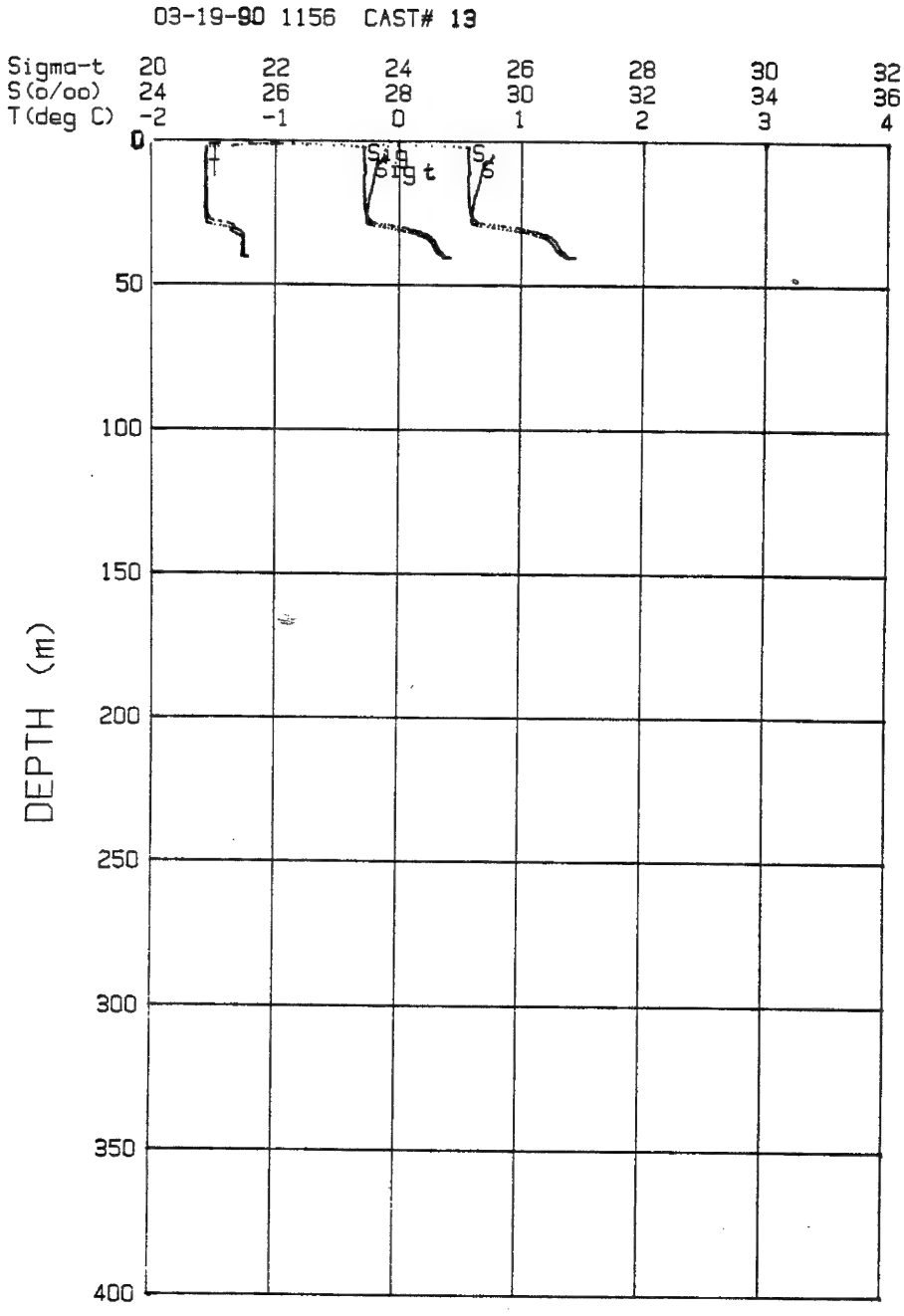
03-19-90 1156 CAST# 13
Sigma-t 20 22 24 26 28 30 32
S(o/oo) 24 26 28 30 32 34 36
T(deg C) -2 -1 0 1 2 3 4
Sig t
S
0
50
100
150
200
250
300
350
400
DEPTH (m)

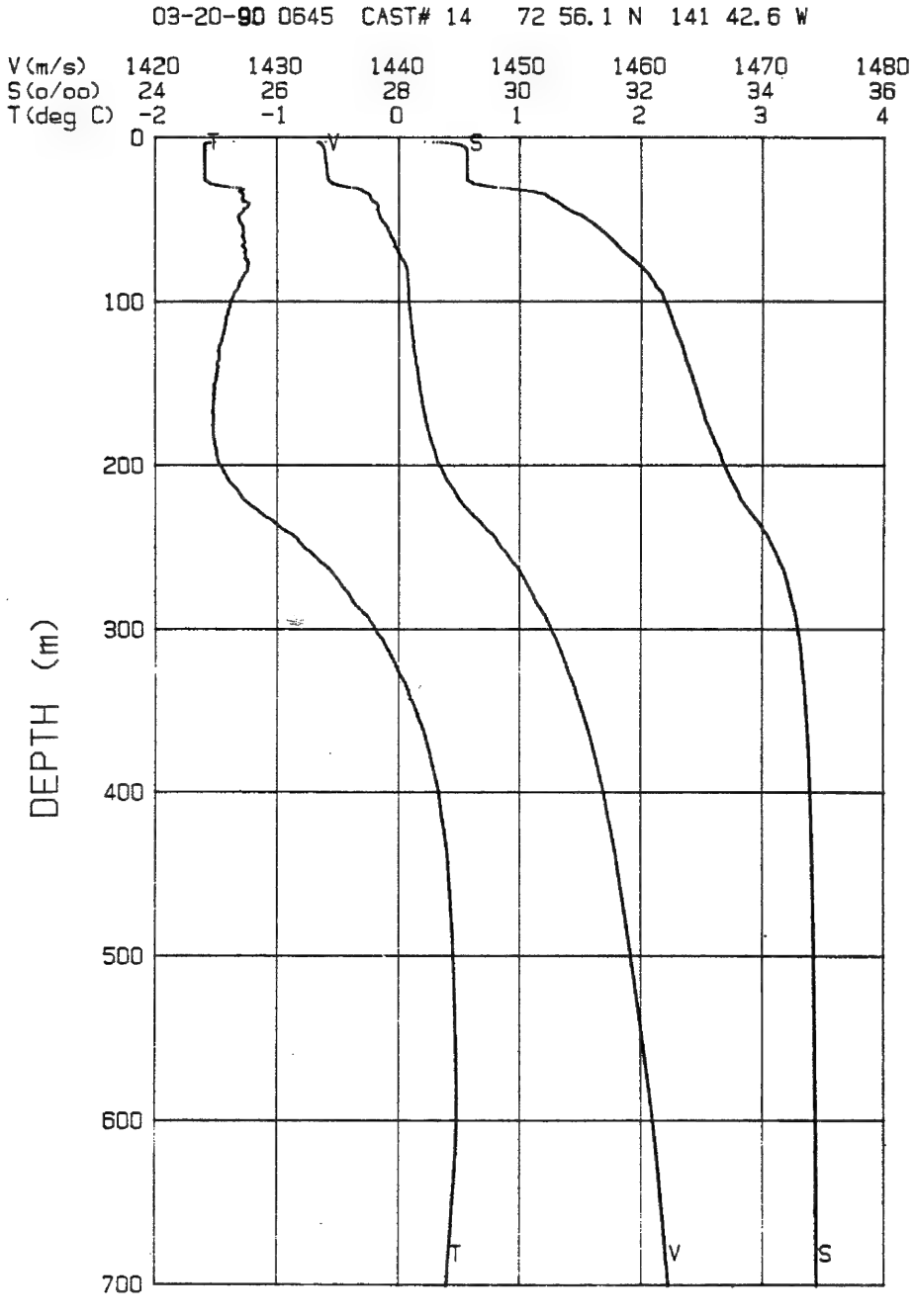
03-20-90 0645 CAST# 14 72 56.1 N 141 42.6 W
V(m/s) 1420 1430 1440 1450 1460 1470 1480
S(o/oo) 24 26 28 30 32 34 36
T(deg C) -2 -1 0 1 2 3 4
DEPTH (m)
0
100
200
300
400
500
600
700
T
V
S

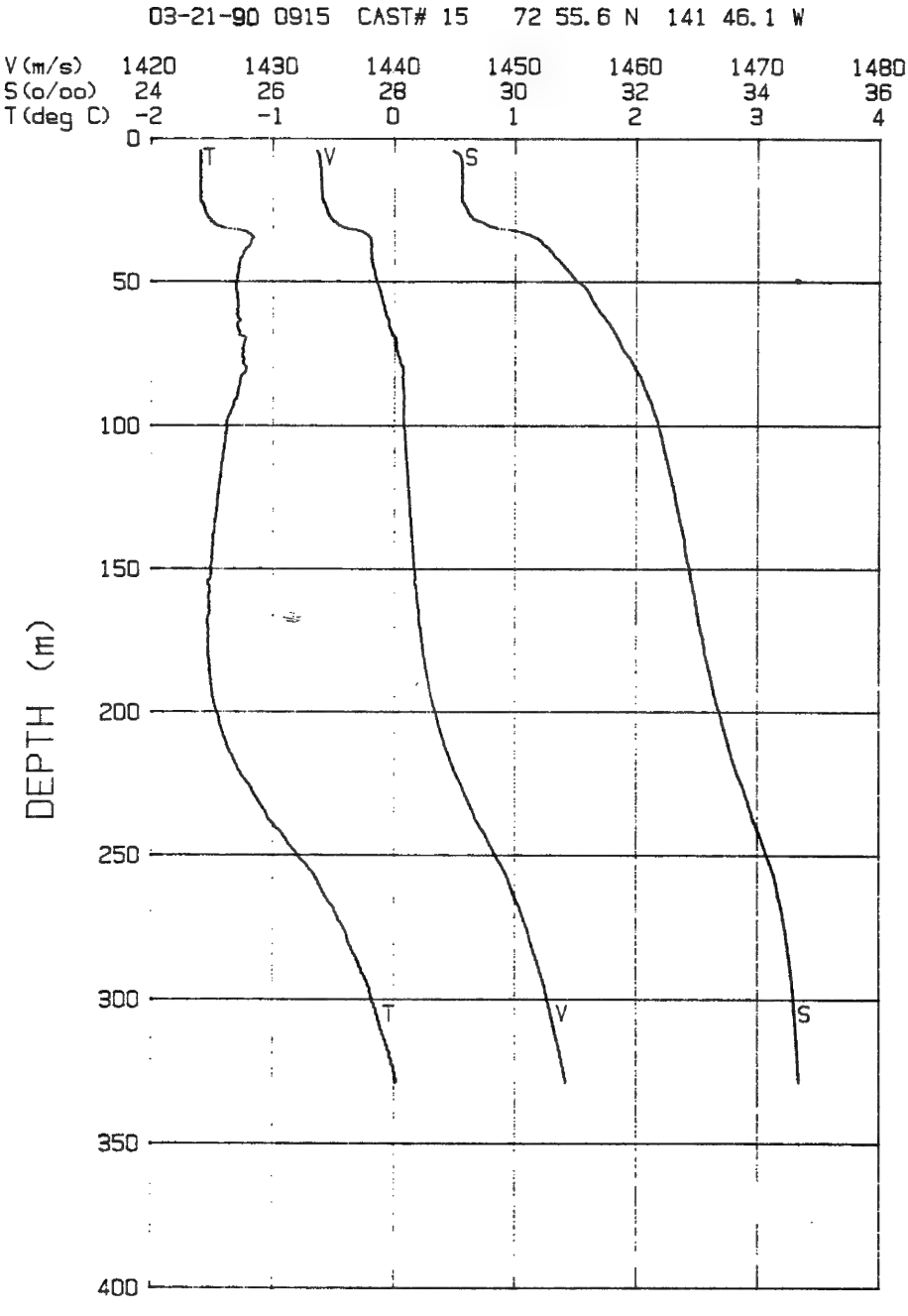
03-21-90 0915 CAST# 15 72 55.6 N 141 46.1 W
V(m/s) 1420 1430 1440 1450 1460 1470 1480
S(o/oo) 24 26 28 30 32 34 36
T(deg C) -2 -1 0 1 2 3 4
DEPTH (m)
0
50
100
150
200
250
300
350
400
T
V
S

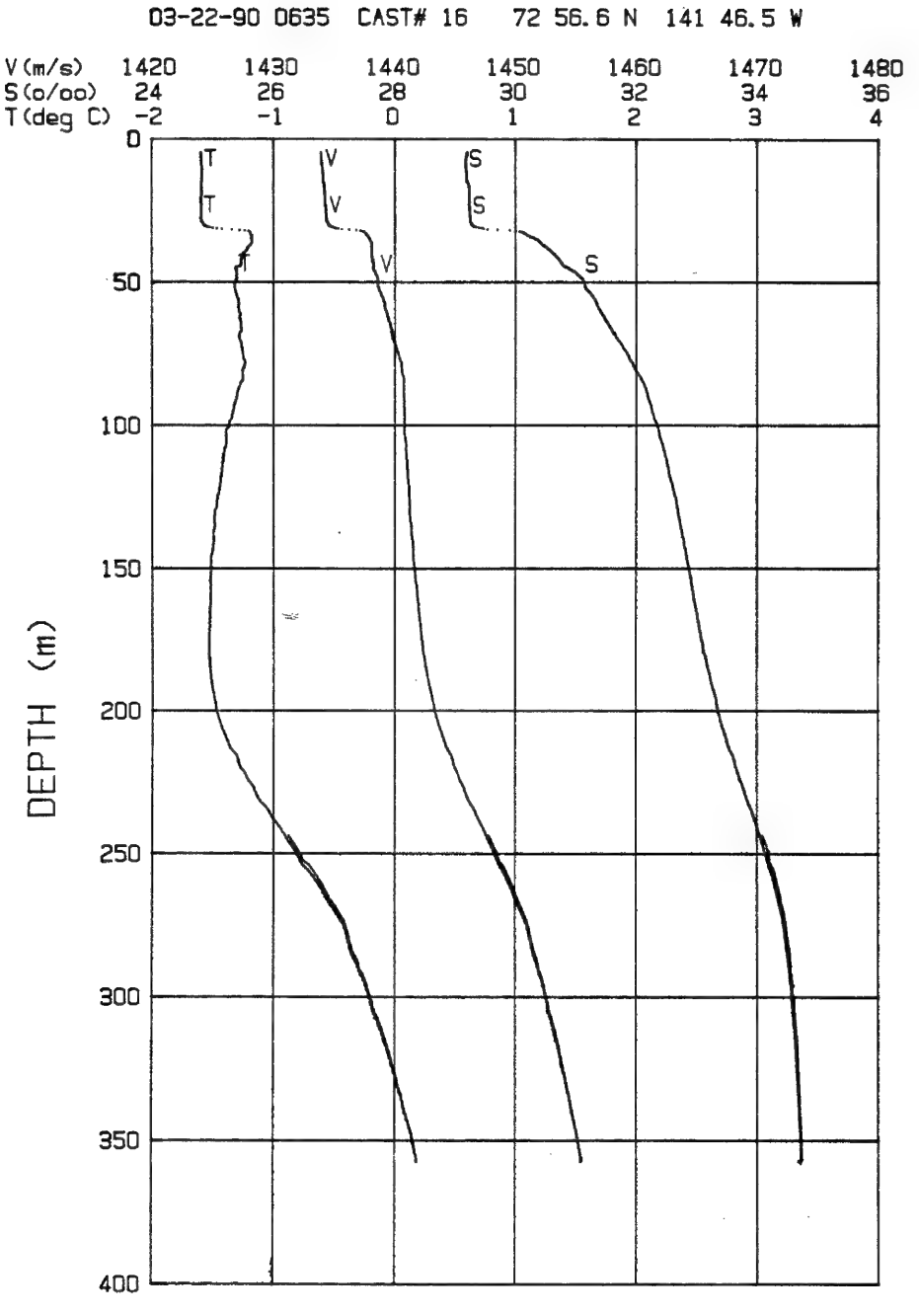
03-22-90 0635 CAST# 16 72 56.6 N 141 46.5 W
V(m/s) 1420 1430 1440 1450 1460 1470 1480
S(o/oo) 24 26 28 30 32 34 36
T(deg C) -2 -1 0 1 2 3 4
DEPTH (m)
0
50
100
150
200
250
300
350
400
T
V
S

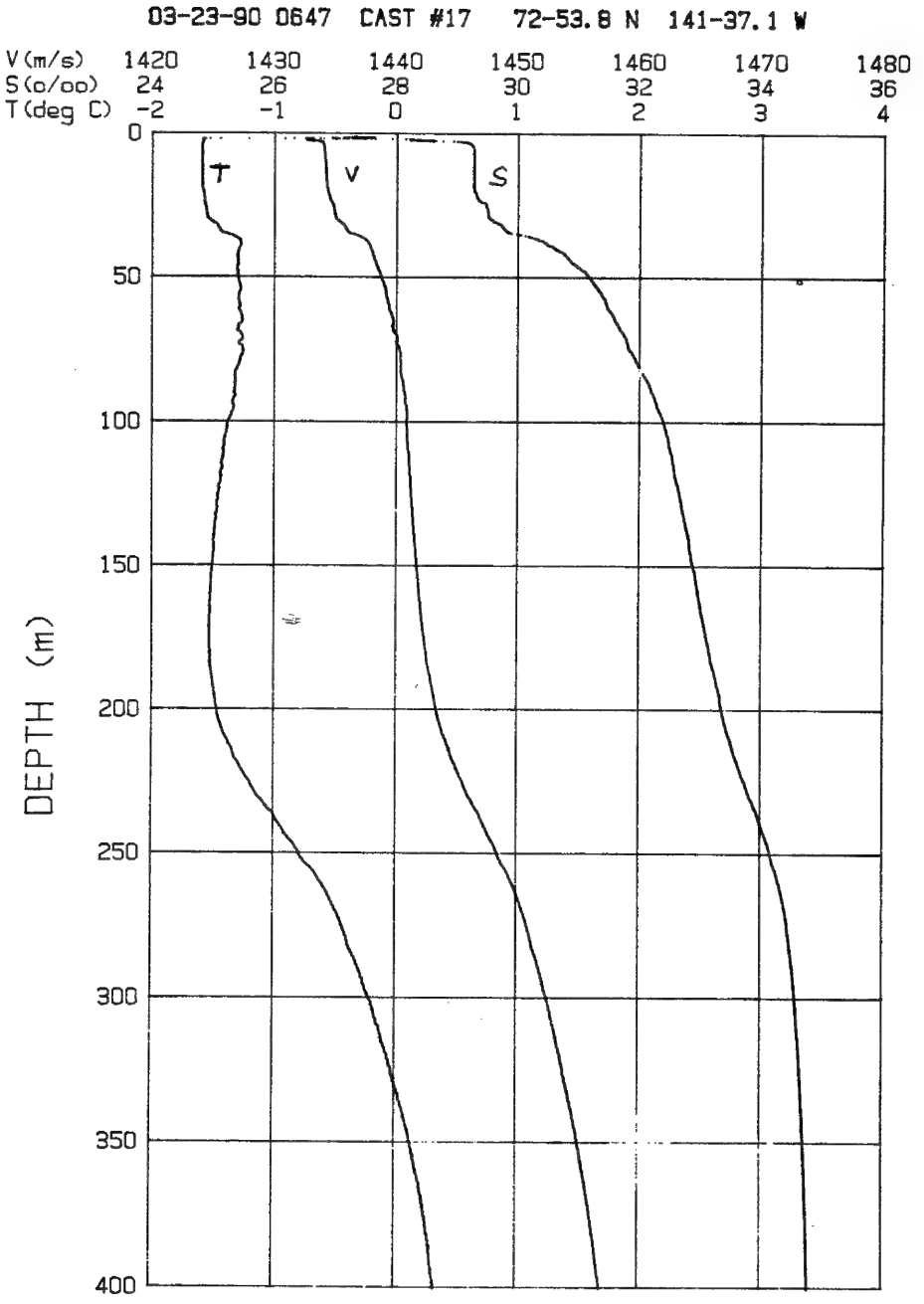
03-23-90 0647 CAST #17 72-53.8 N 141-37.1 W
V(m/s) 1420 1430 1440 1450 1460 1470 1480
S(o/oo) 24 26 28 30 32 34 36
T(deg C) -2 -1 0 1 2 3 4
T
V
S
DEPTH (m)
0
50
100
150
200
250
300
350
400

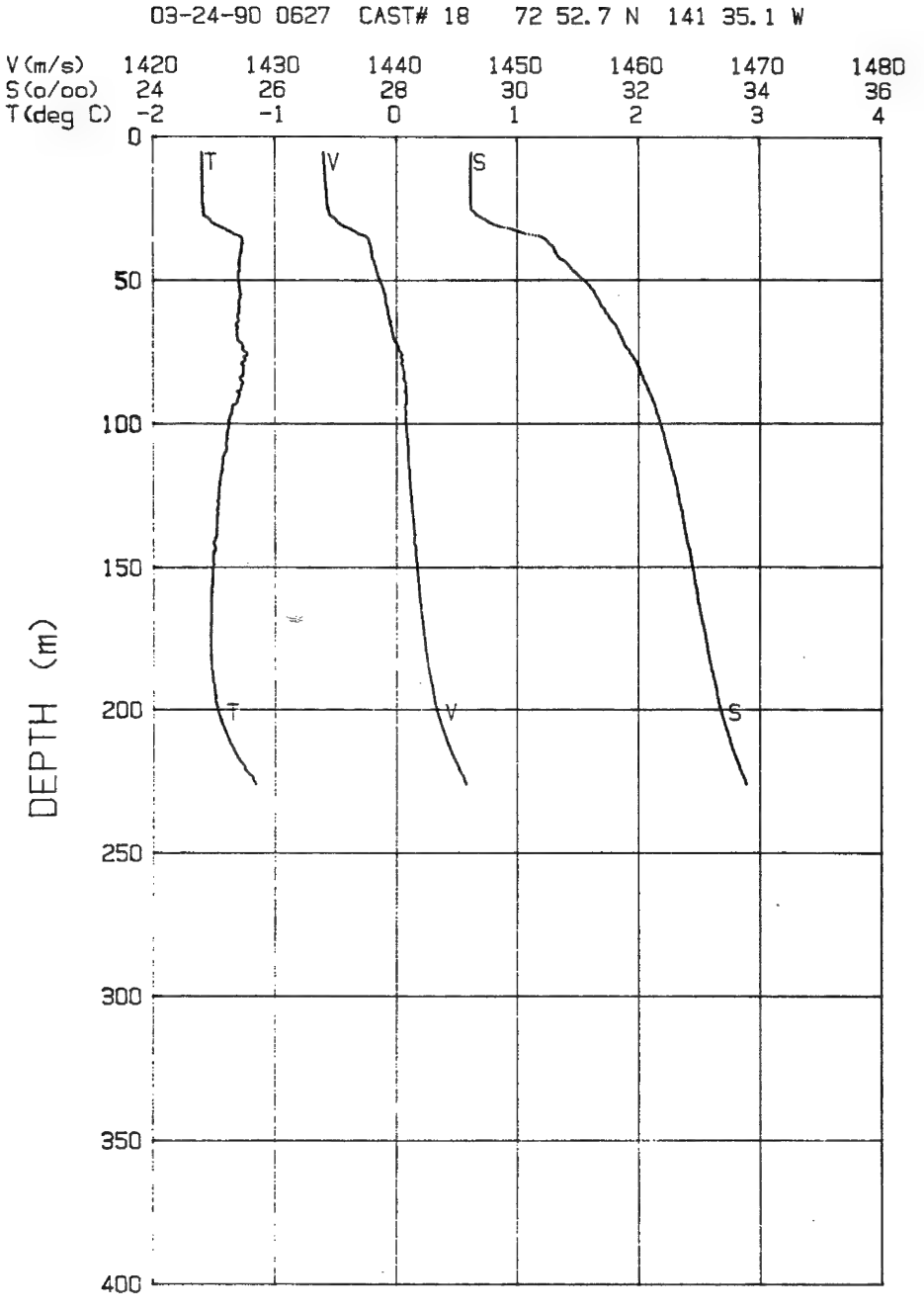
03-24-90 0627 CAST# 18 72 52.7 N 141 35.1 W
V(m/s) 1420 1430 1440 1450 1460 1470 1480
S(o/oo) 24 26 28 30 32 34 36
T(deg C) -2 -1 0 1 2 3 4
DEPTH (m)
0
50
100
150
200
250
300
350
400
T
V
S

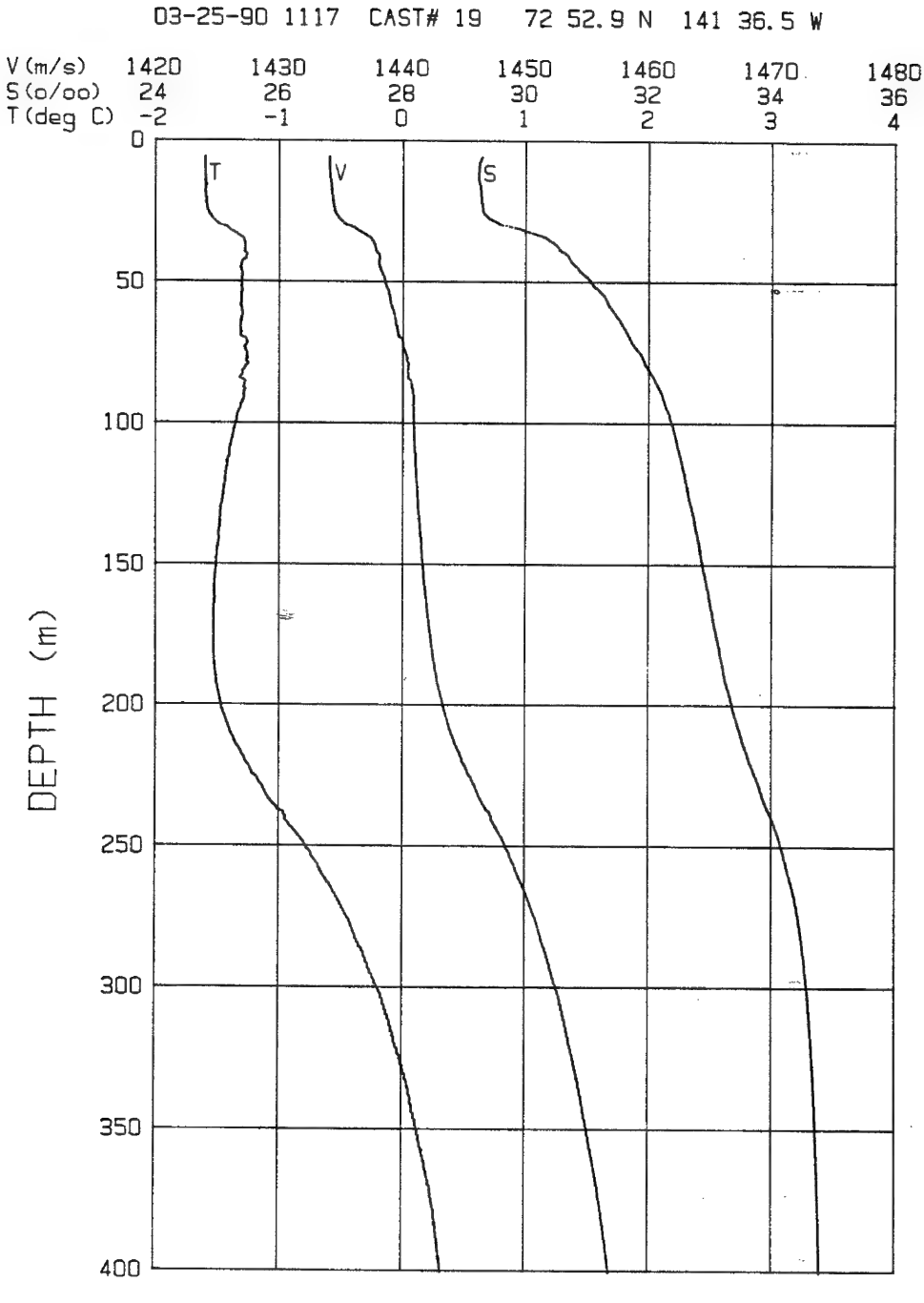
03-25-90 1117 CAST# 19 72 52.9 N 141 36.5 W
V(m/s) 1420 1430 1440 1450 1460 1470 1480
S(o/oo) 24 26 28 30 32 34 36
T(deg C) -2 -1 0 1 2 3 4
T
V
S
DEPTH (m)
0
50
100
150
200
250
300
350
400

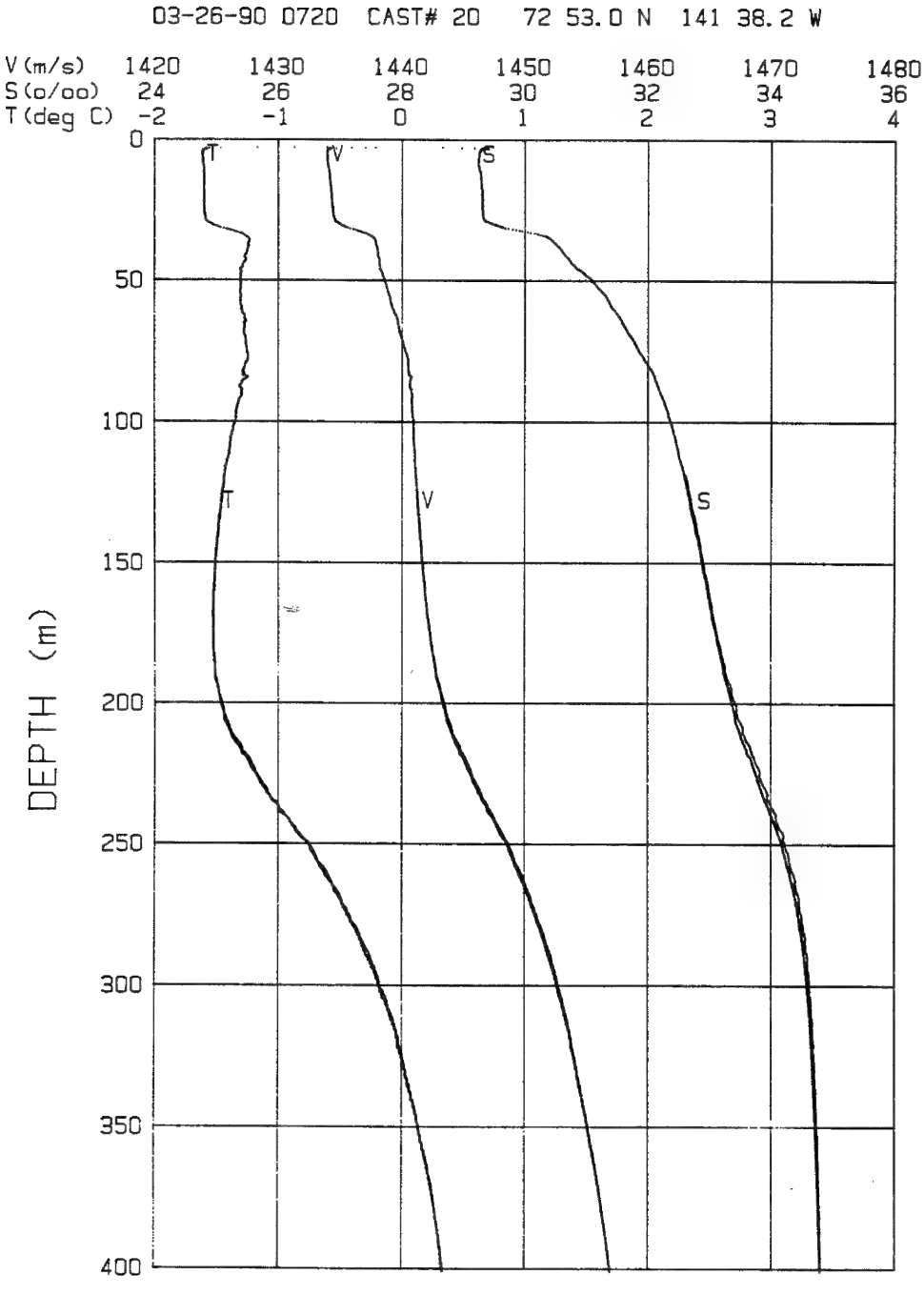
03-26-90 0720 CAST# 20 72 53.0 N 141 38.2 W
V(m/s) 1420 1430 1440 1450 1460 1470 1480
S(o/oo) 24 26 28 30 32 34 36
T(deg C) -2 -1 0 1 2 3 4
0
50
100
150
200
250
300
350
400
DEPTH (m)
T
V
S

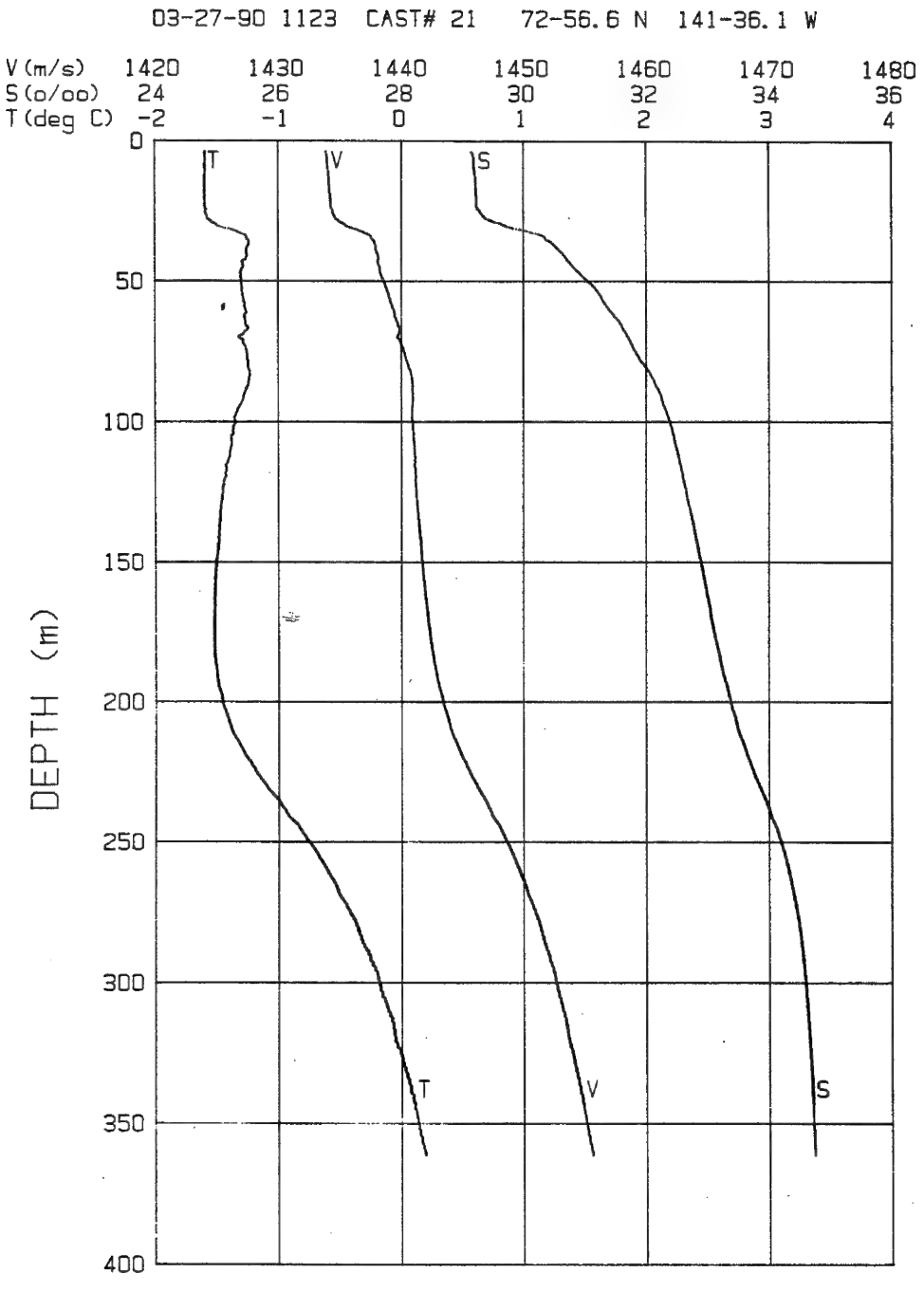
03-27-90 1123 CAST# 21 72-56.6 N 141-36.1 W
V(m/s) 1420 1430 1440 1450 1460 1470 1480
S(o/oo) 24 26 28 30 32 34 36
T(deg C) -2 -1 0 1 2 3 4
0
50
100
150
200
250
300
350
400
DEPTH (m)
T
V
S
T
V
S

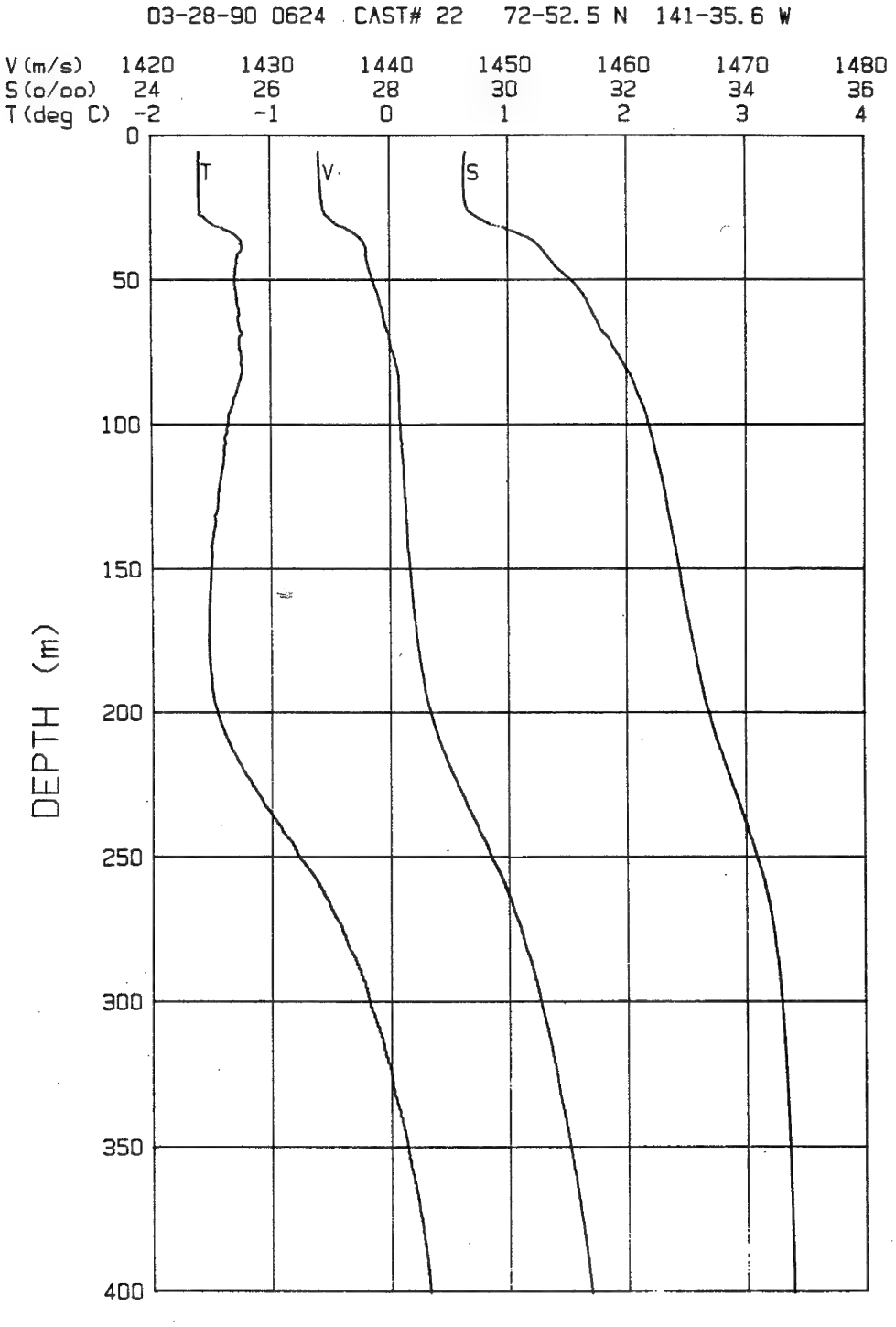
03-28-90 0624 CAST# 22 72-52.5 N 141-35.6 W
V(m/s) 1420 1430 1440 1450 1460 1470 1480
S(o/oo) 24 26 28 30 32 34 36
T(deg C) -2 -1 0 1 2 3 4
T
V
S
DEPTH (m)
0
50
100
150
200
250
300
350
400

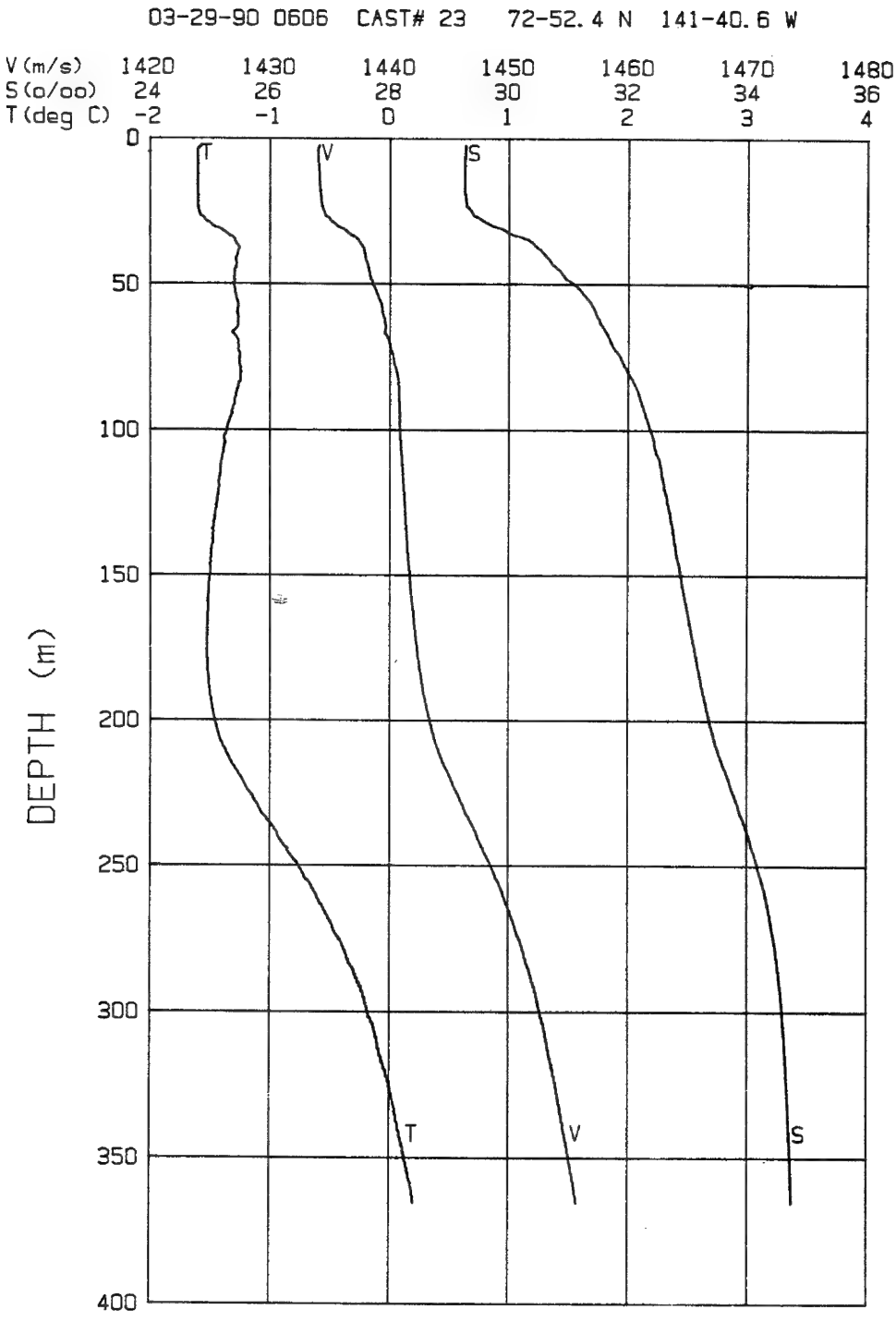
03-29-90 0606 CAST# 23 72-52.4 N 141-40.6 W
V(m/s) 1420 1430 1440 1450 1460 1470 1480
S(o/oo) 24 26 28 30 32 34 36
T(deg C) -2 -1 0 1 2 3 4
DEPTH (m)
0
50
100
150
200
250
300
350
400
T
V
S
T
V
S

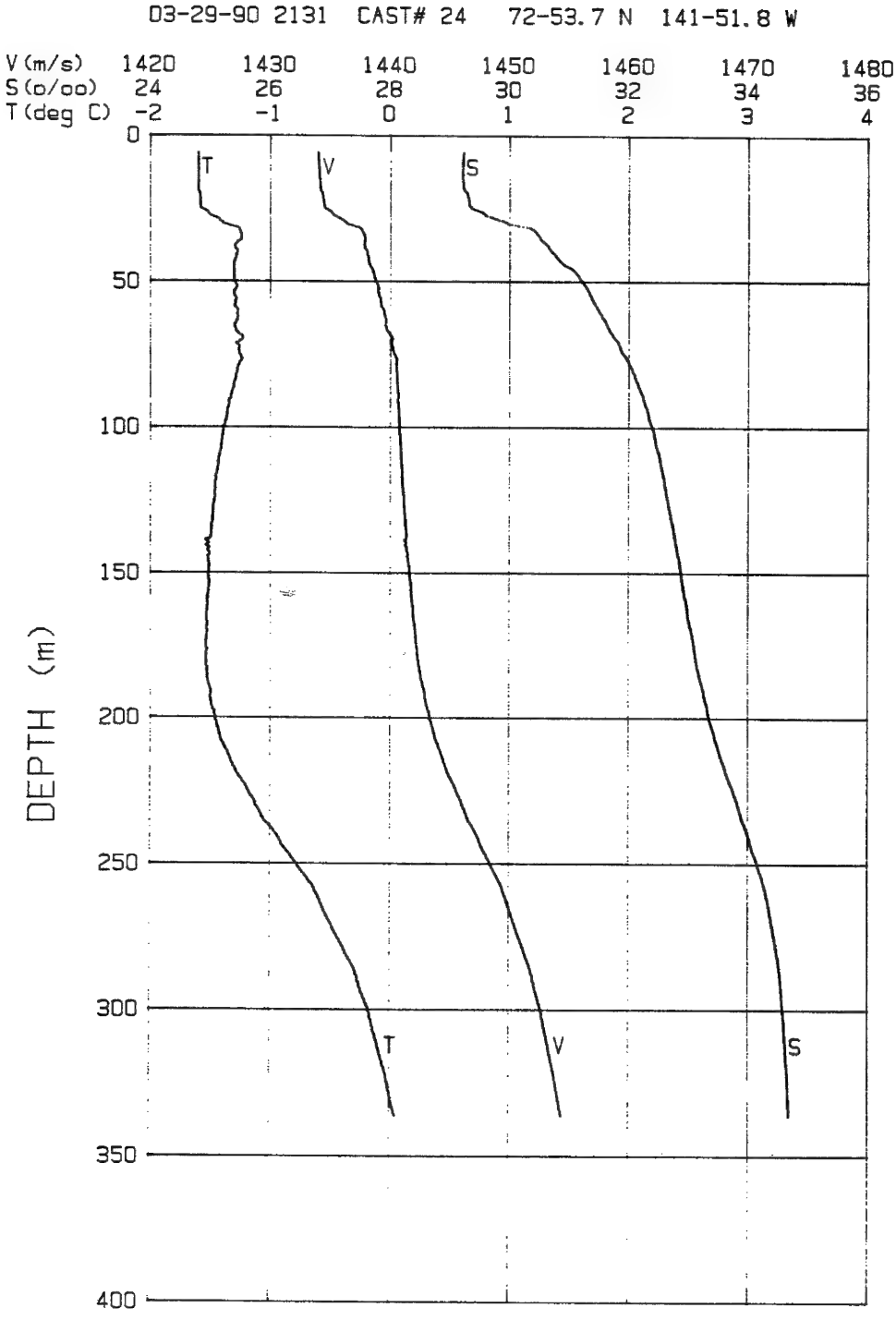
03-29-90 2131 CAST# 24 72-53.7 N 141-51.8 W
V(m/s) 1420 1430 1440 1450 1460 1470 1480
S(o/oo) 24 26 28 30 32 34 36
T(deg C) -2 -1 0 1 2 3 4
0
50
100
150
200
250
300
350
400
DEPTH (m)
T
V
S
T
V
S

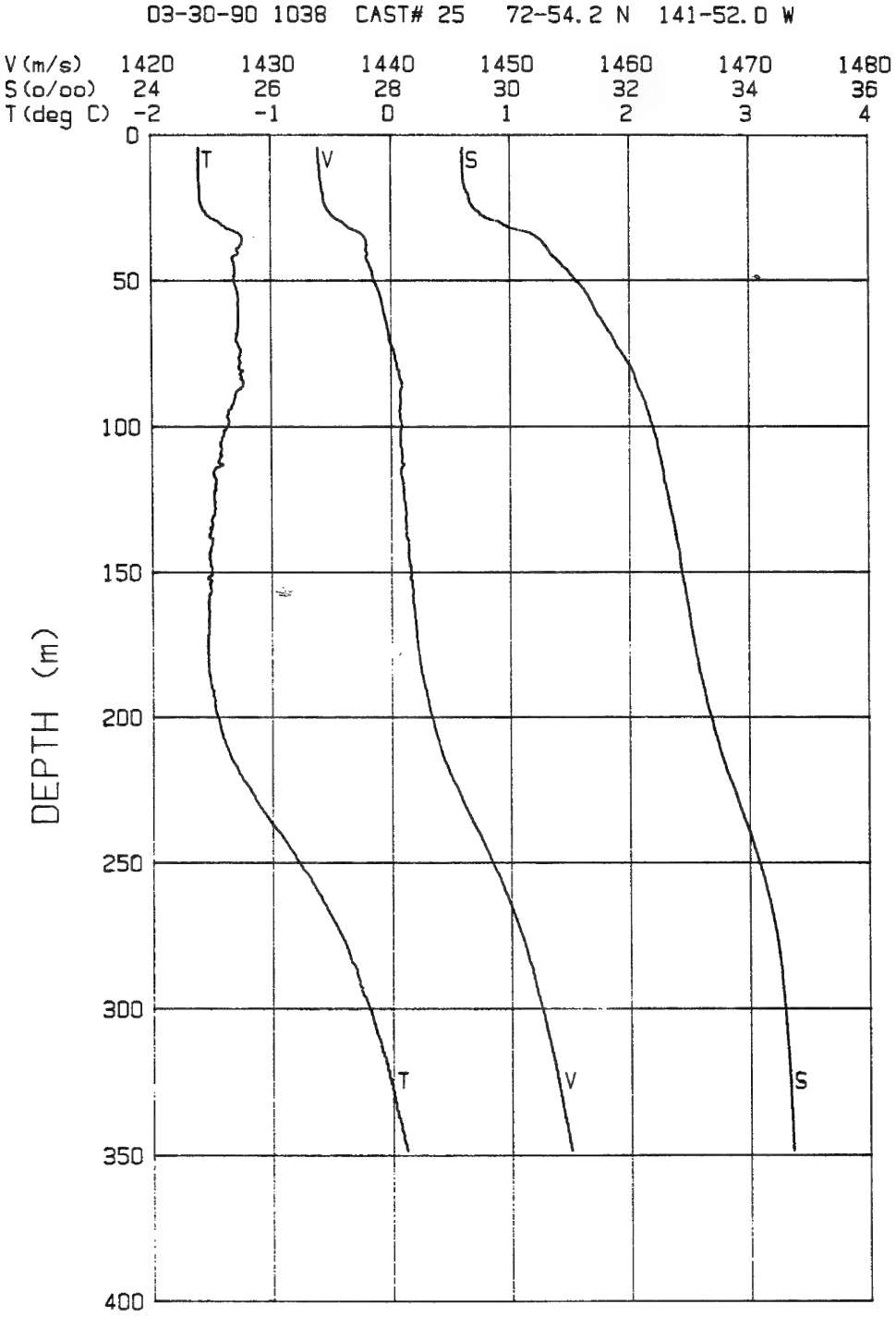
03-30-90 1038 CAST# 25 72-54.2 N 141-52.0 W
V(m/s) 1420 1430 1440 1450 1460 1470 1480
S(o/oo) 24 26 28 30 32 34 36
T(deg C) -2 -1 0 1 2 3 4
DEPTH (m)
0
50
100
150
200
250
300
350
400
T
V
S
T
V
S

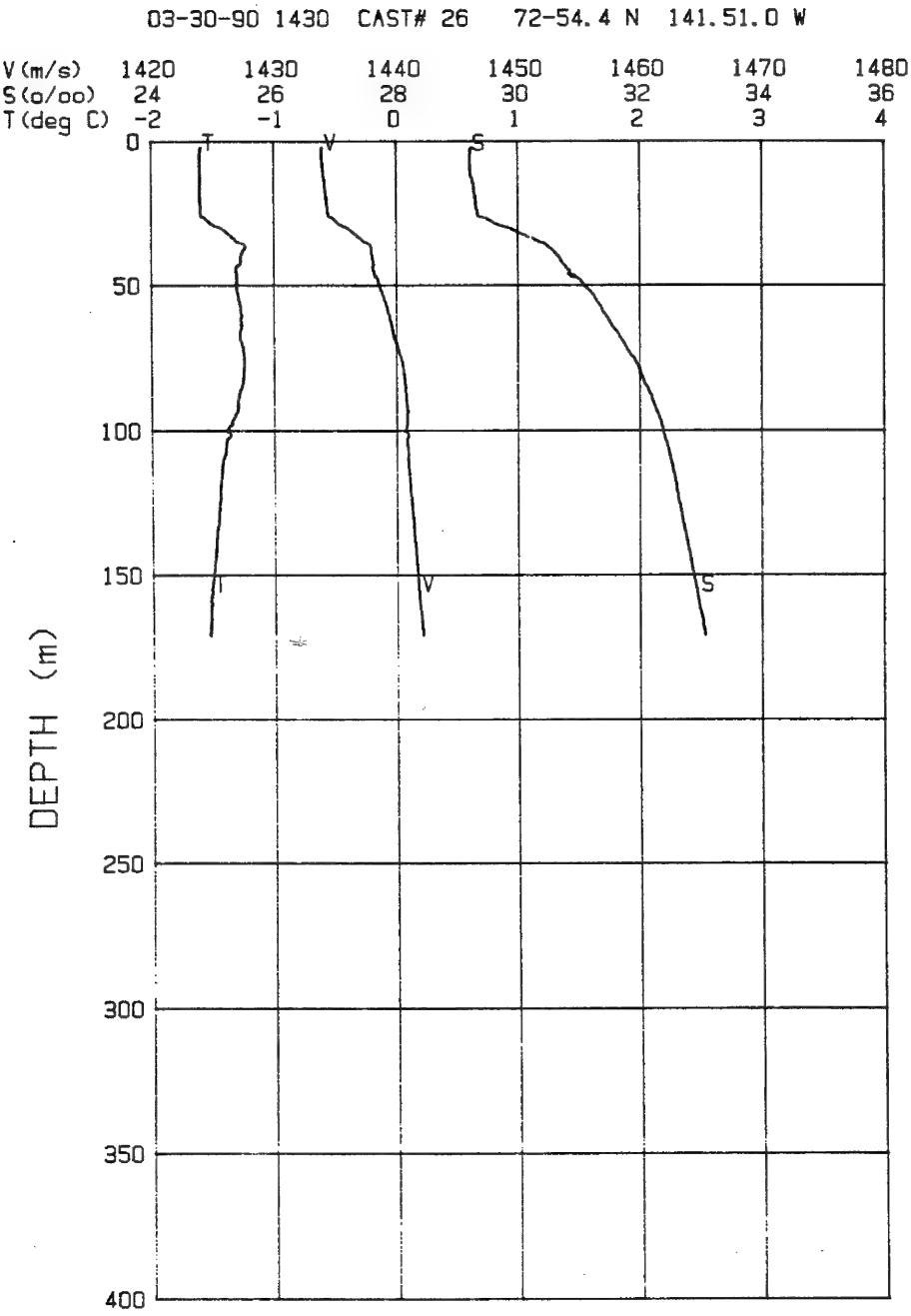
03-30-90 1430 CAST# 26 72-54.4 N 141.51.0 W
V(m/s) 1420 1430 1440 1450 1460 1470 1480
S(o/oo) 24 26 28 30 32 34 36
T(deg C) -2 -1 0 1 2 3 4
DEPTH (m)
0
50
100
150
200
250
300
350
400
T
V
S

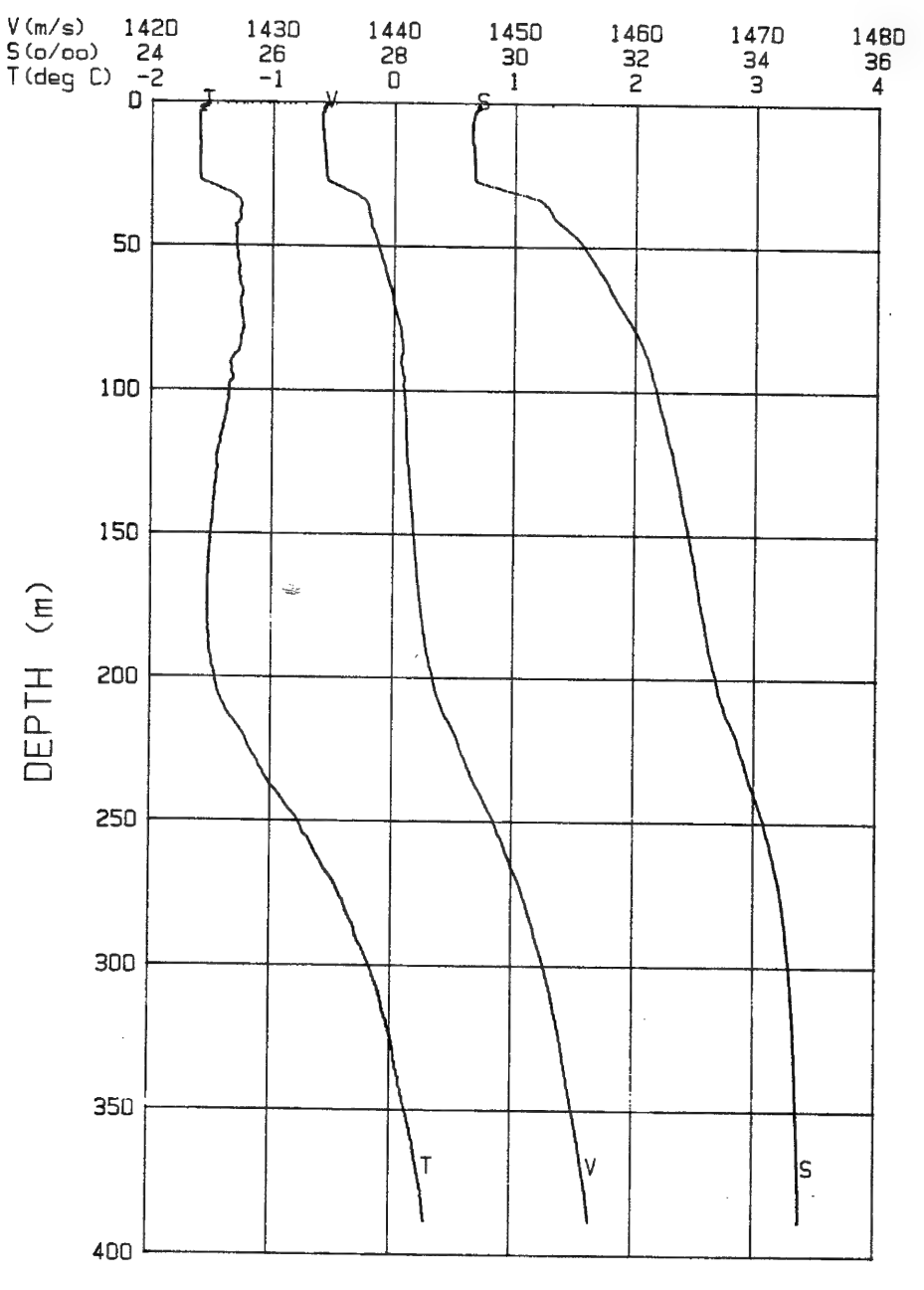
03-30-90 2117 CAST# 27 72-54.3 N 141-51.0 W
V(m/s) 1420 1430 1440 1450 1460 1470 1480
S(o/oo) 24 26 28 30 32 34 36
T(deg C) -2 -1 0 1 2 3 4
T
V
S
0
50
100
150
200
250
300
350
400
DEPTH (m)
T
V
S

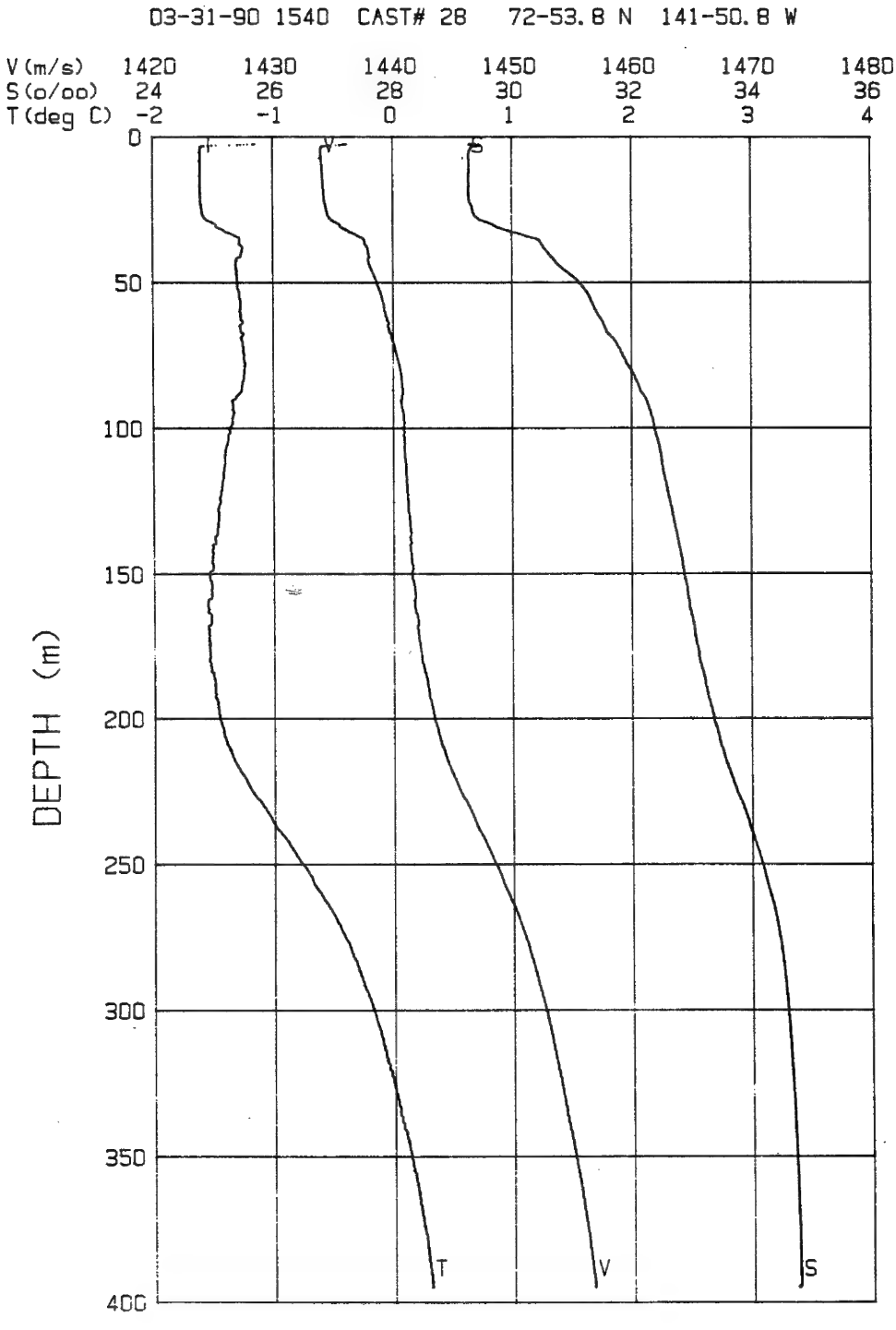
03-31-90 1540 CAST# 28 72-53.8 N 141-50.8 W
V(m/s) 1420 1430 1440 1450 1460 1470 1480
S(o/oo) 24 26 28 30 32 34 36
T(deg C) -2 -1 0 1 2 3 4
DEPTH (m)
0
50
100
150
200
250
300
350
400
T
V
S

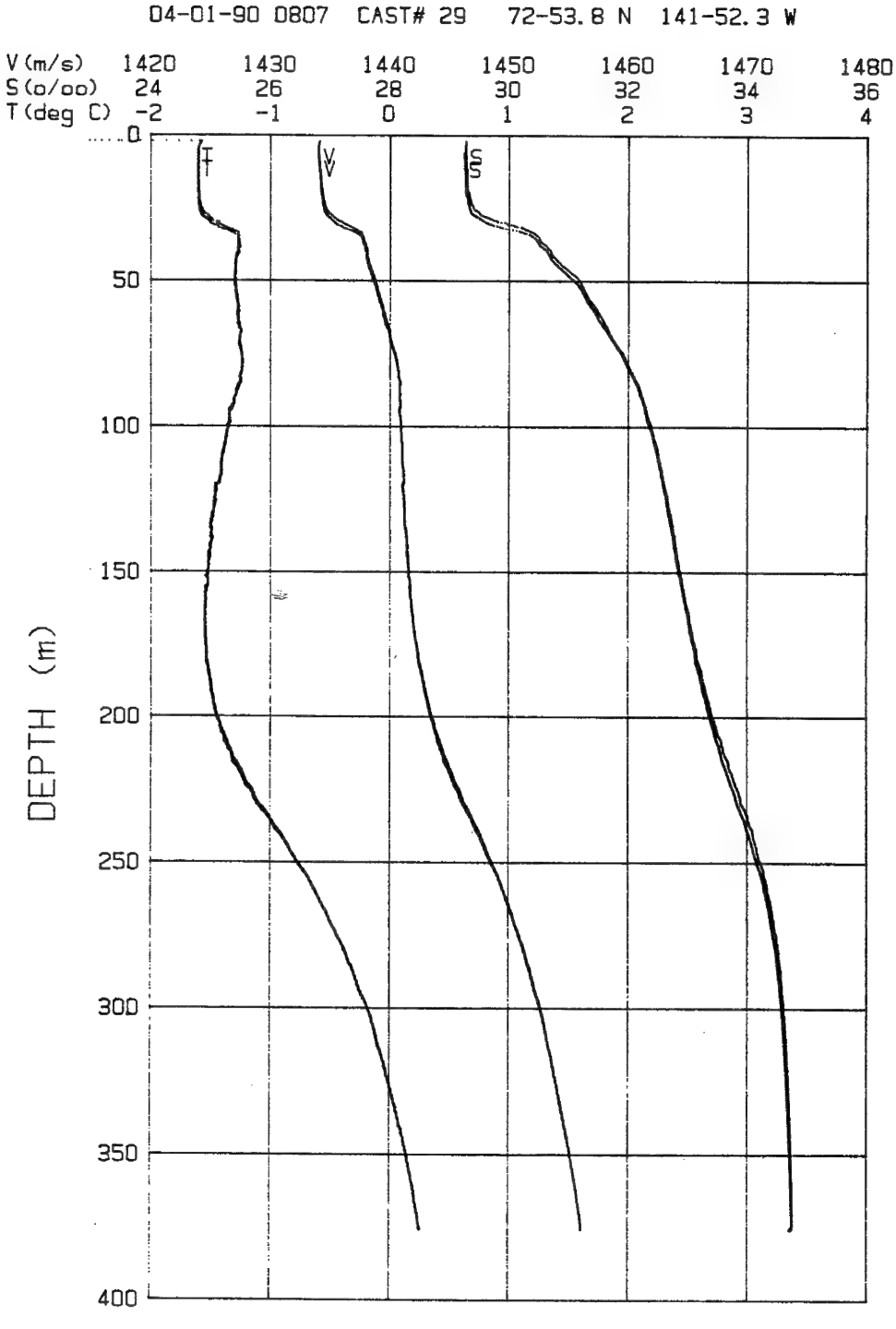
04-01-90 0807 CAST# 29 72-53.8 N 141-52.3 W
V(m/s) 1420 1430 1440 1450 1460 1470 1480
S(o/oo) 24 26 28 30 32 34 36
T(deg C) -2 -1 0 1 2 3 4
T
V
S
0
50
100
150
200
250
300
350
400
DEPTH (m)

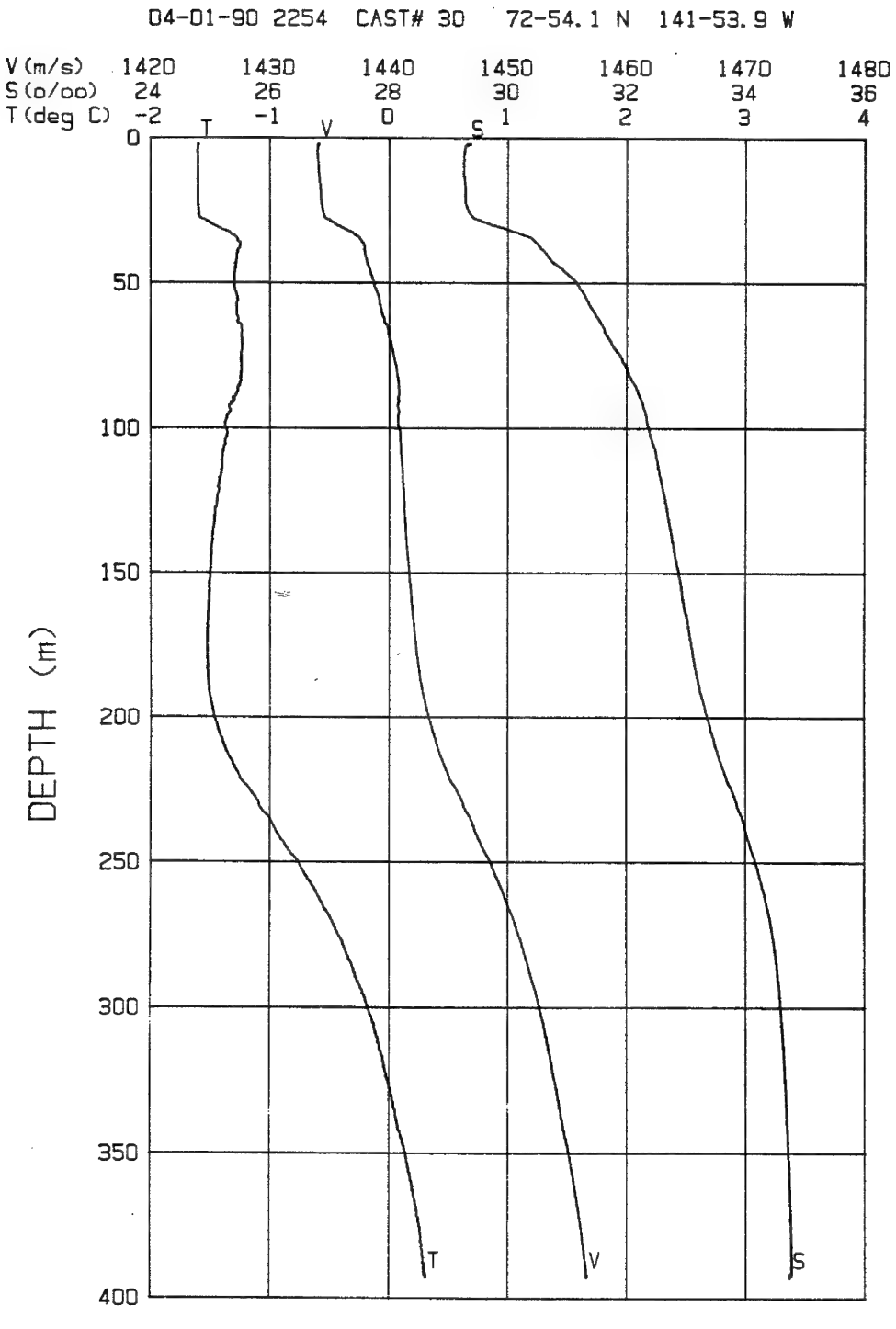
04-01-90 2254 CAST# 30 72-54.1 N 141-53.9 W
V(m/s) 1420 1430 1440 1450 1460 1470 1480
S(o/oo) 24 26 28 30 32 34 36
T(deg C) -2 -1 0 1 2 3 4
T
V
S
0
50
100
150
200
250
300
350
400
DEPTH (m)
T
V
S

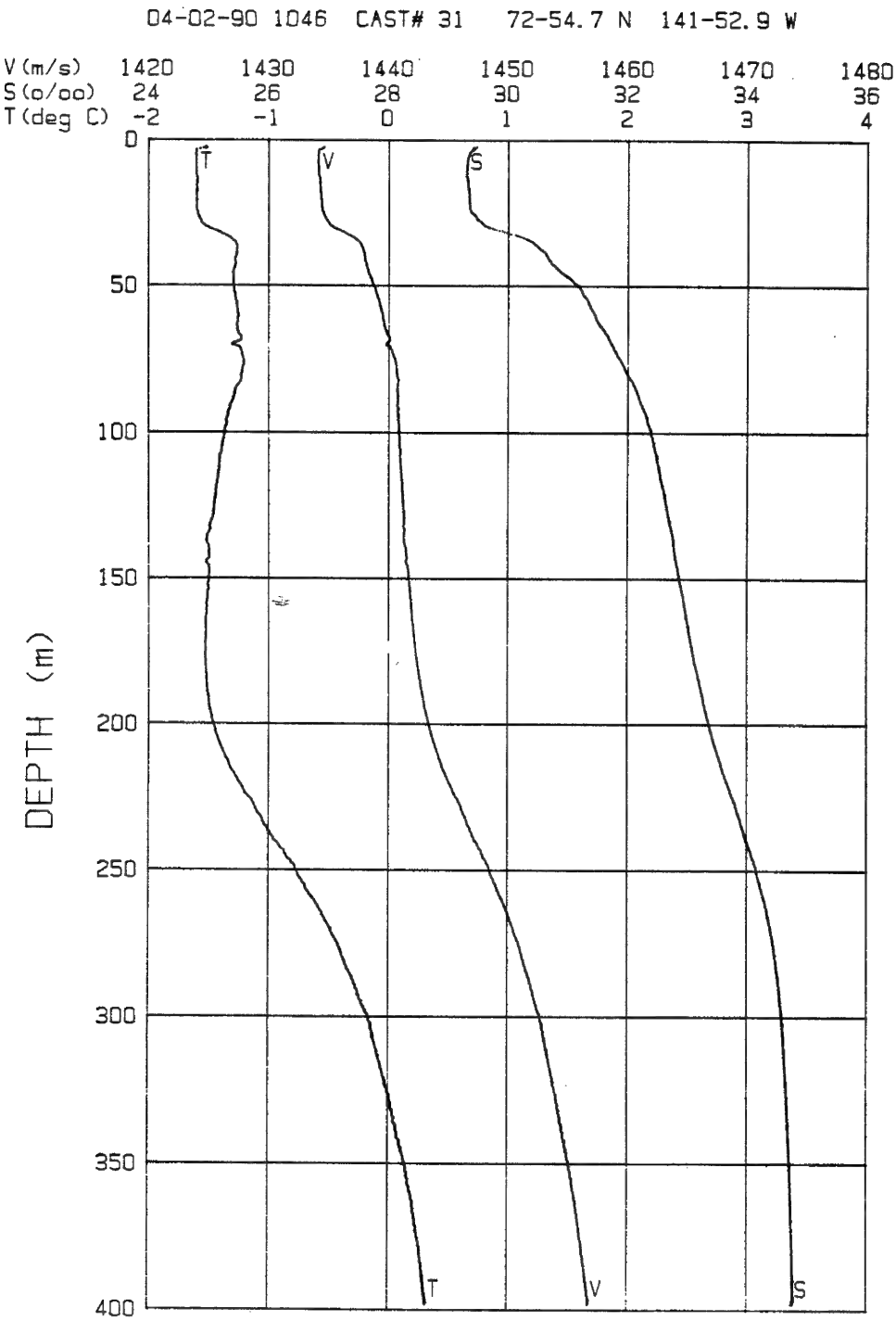
04-02-90 1046 CAST# 31 72-54.7 N 141-52.9 W
V(m/s) 1420 1430 1440 1450 1460 1470 1480
S(o/oo) 24 26 28 30 32 34 36
T(deg C) -2 -1 0 1 2 3 4
DEPTH (m)
0
50
100
150
200
250
300
350
400
T
V
S

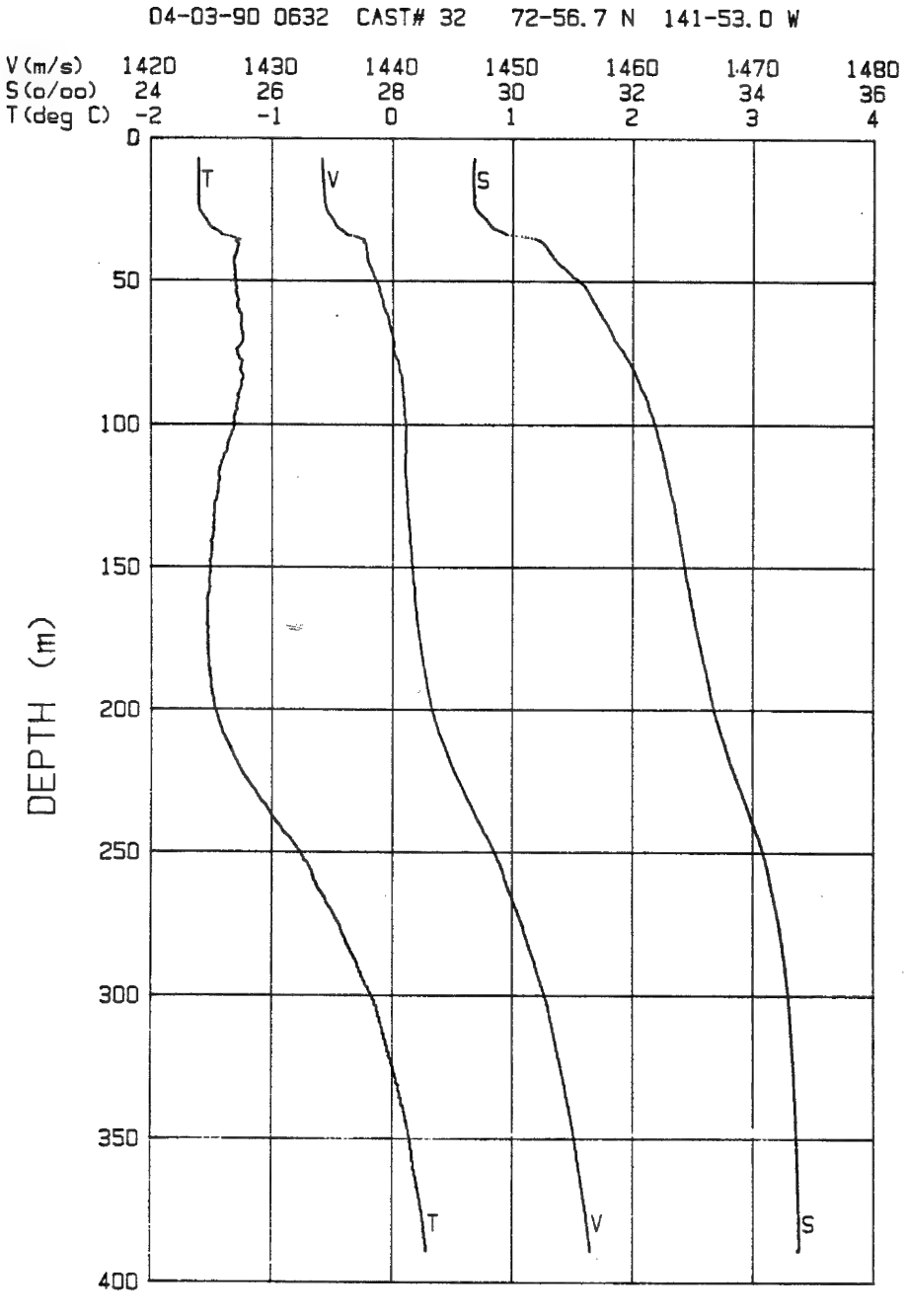
04-03-90 0632 CAST# 32 72-56.7 N 141-53.0 W
V(m/s) 1420 1430 1440 1450 1460 1470 1480
S(o/oo) 24 26 28 30 32 34 36
T(deg C) -2 -1 0 1 2 3 4
DEPTH (m)
0
50
100
150
200
250
300
350
400
T
V
S

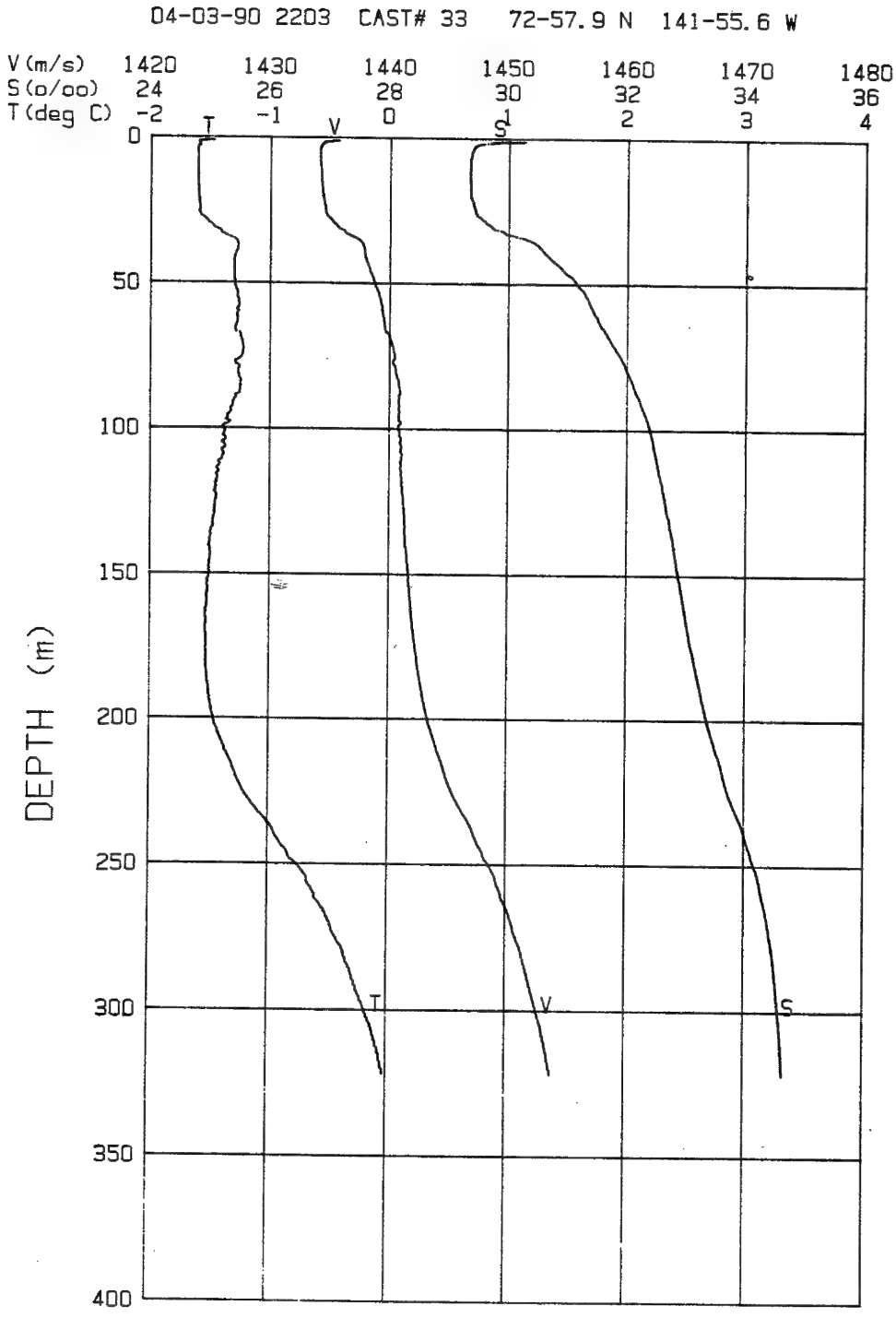
04-03-90 2203 CAST# 33 72-57.9 N 141-55.6 W
V(m/s) 1420 1430 1440 1450 1460 1470 1480
S(o/oo) 24 26 28 30 32 34 36
T(deg C) -2 -1 0 1 2 3 4
T
V
S
DEPTH (m)
0
50
100
150
200
250
300
350
400

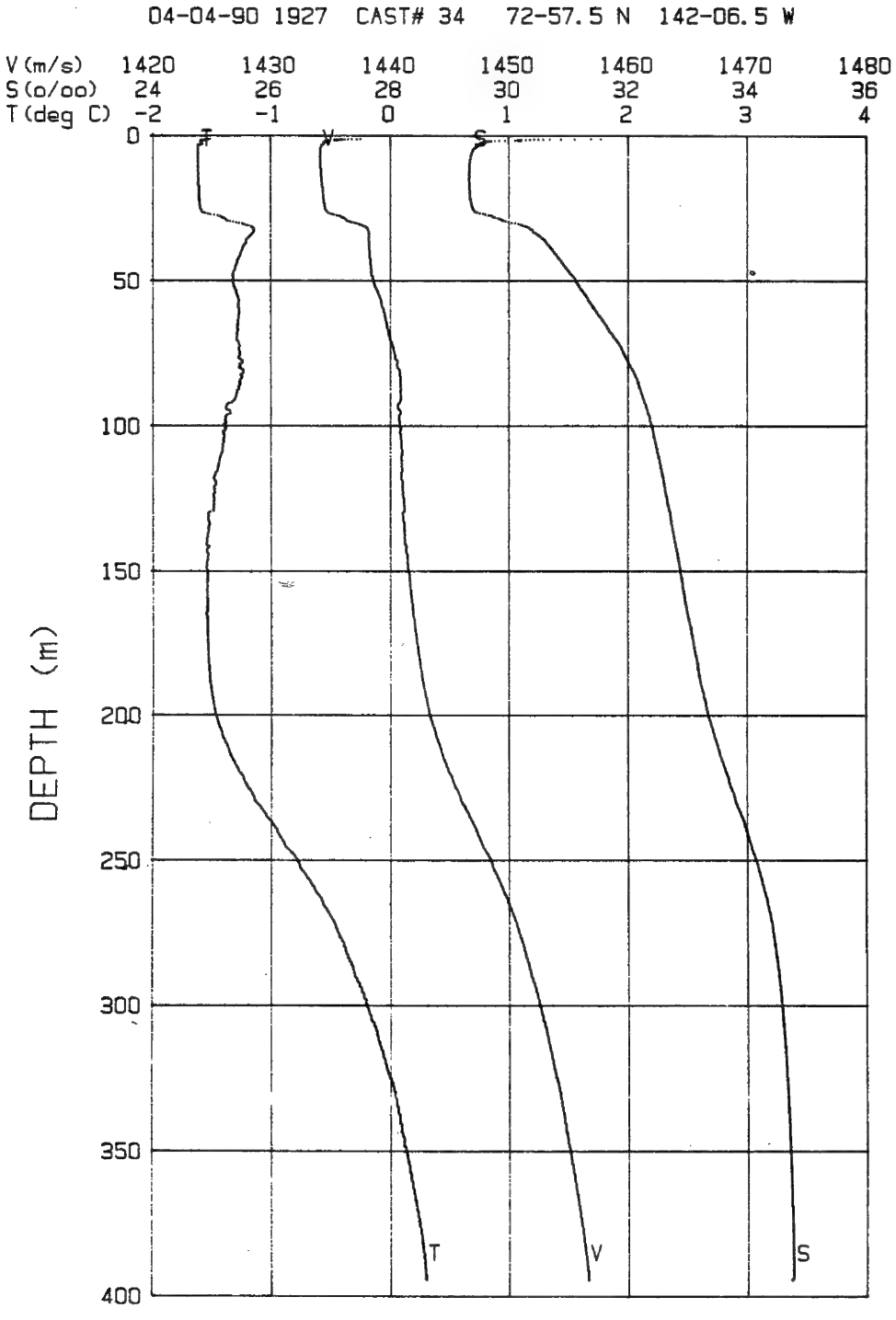
04-04-90 1927 CAST# 34 72-57.5 N 142-06.5 W
V(m/s) 1420 1430 1440 1450 1460 1470 1480
S(o/oo) 24 26 28 30 32 34 36
T(deg C) -2 -1 0 1 2 3 4
T
V
S
0
50
100
150
200
250
300
350
400
DEPTH (m)
T
V
S

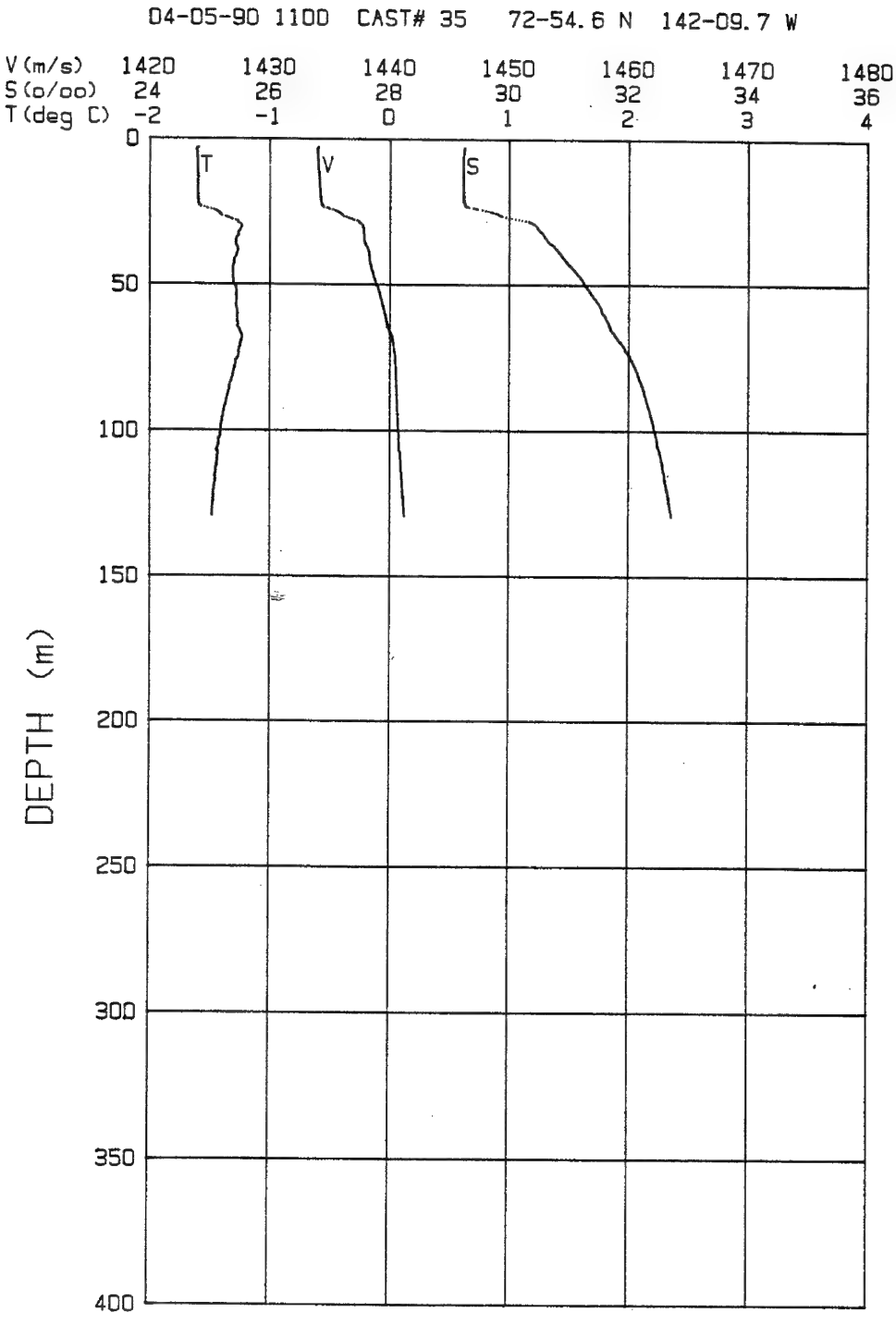
04-05-90 1100 CAST# 35 72-54.6 N 142-09.7 W
V(m/s) 1420 1430 1440 1450 1460 1470 1480
S(o/oo) 24 26 28 30 32 34 36
T(deg C) -2 -1 0 1 2 3 4
T
V
S
DEPTH (m)
0
50
100
150
200
250
300
350
400

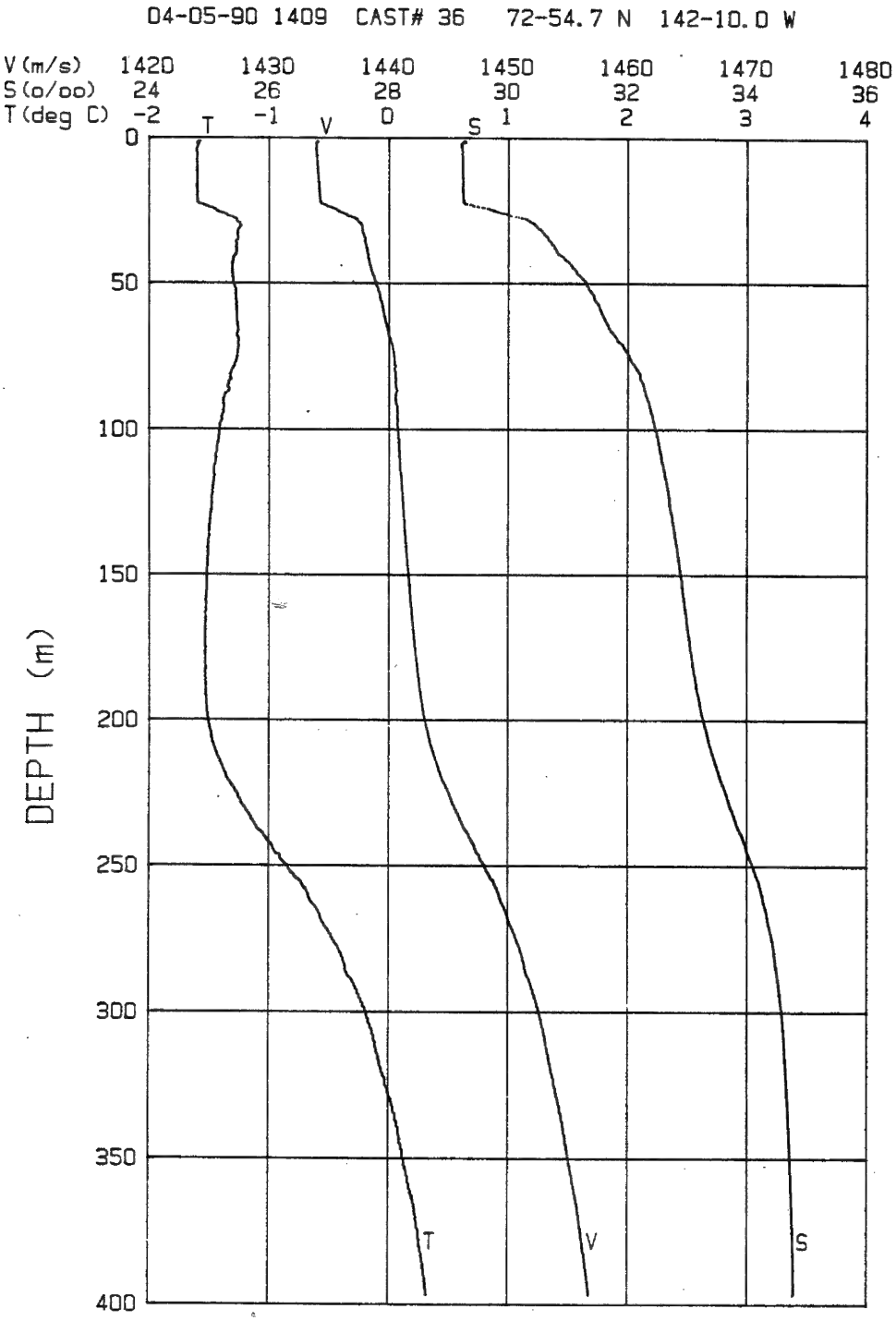
04-05-90 1409 CAST# 36 72-54.7 N 142-10.0 W
V(m/s) 1420 1430 1440 1450 1460 1470 1480
S(o/oo) 24 26 28 30 32 34 36
T(deg C) -2 -1 0 1 2 3 4
T
V
S
DEPTH (m)
0
50
100
150
200
250
300
350
400
T
V
S

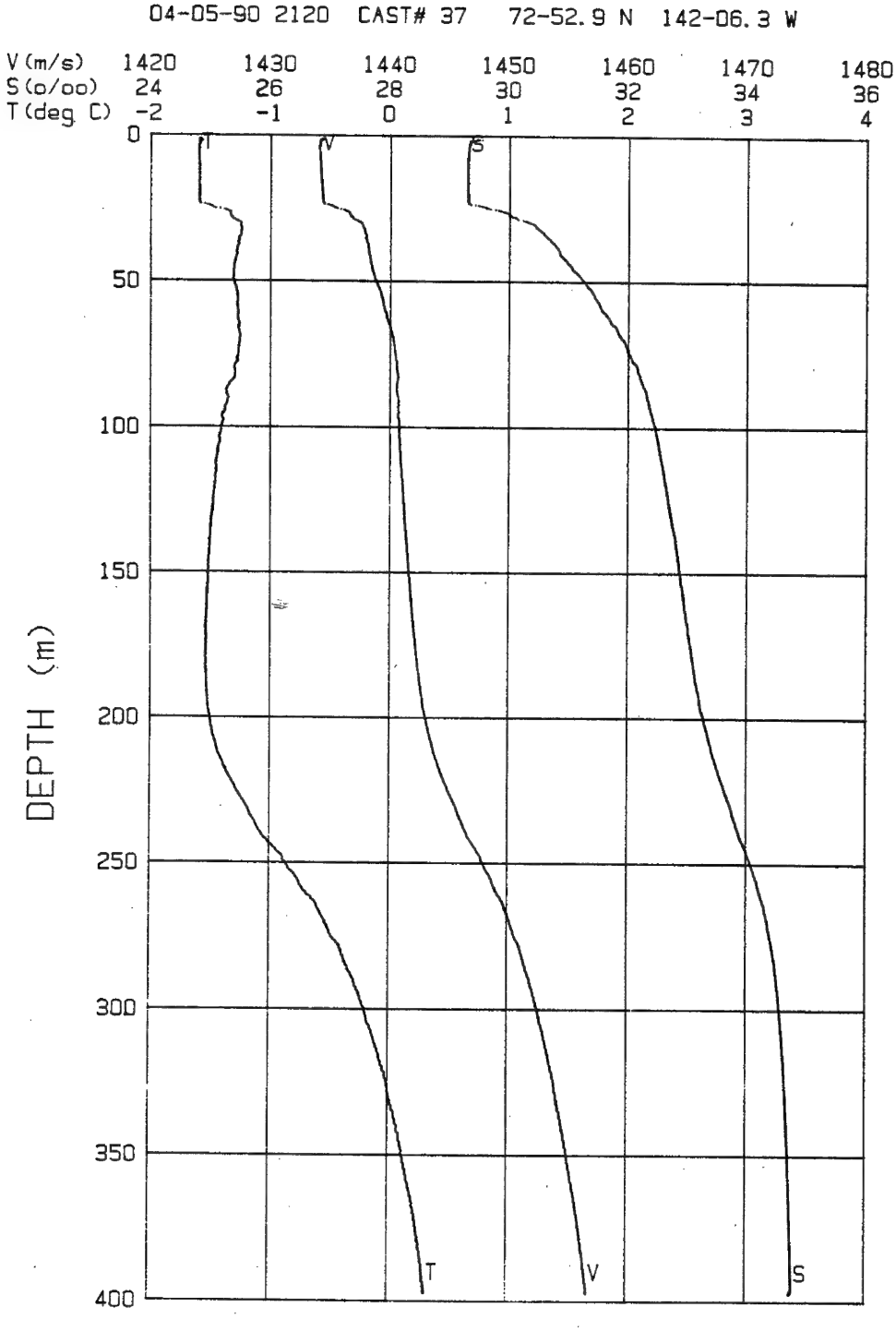
04-05-90 2120 CAST# 37 72-52.9 N 142-06.3 W
V(m/s) 1420 1430 1440 1450 1460 1470 1480
S(o/oo) 24 26 28 30 32 34 36
T(deg C) -2 -1 0 1 2 3 4
0
50
100
150
200
250
300
350
400
DEPTH (m)
T
V
S

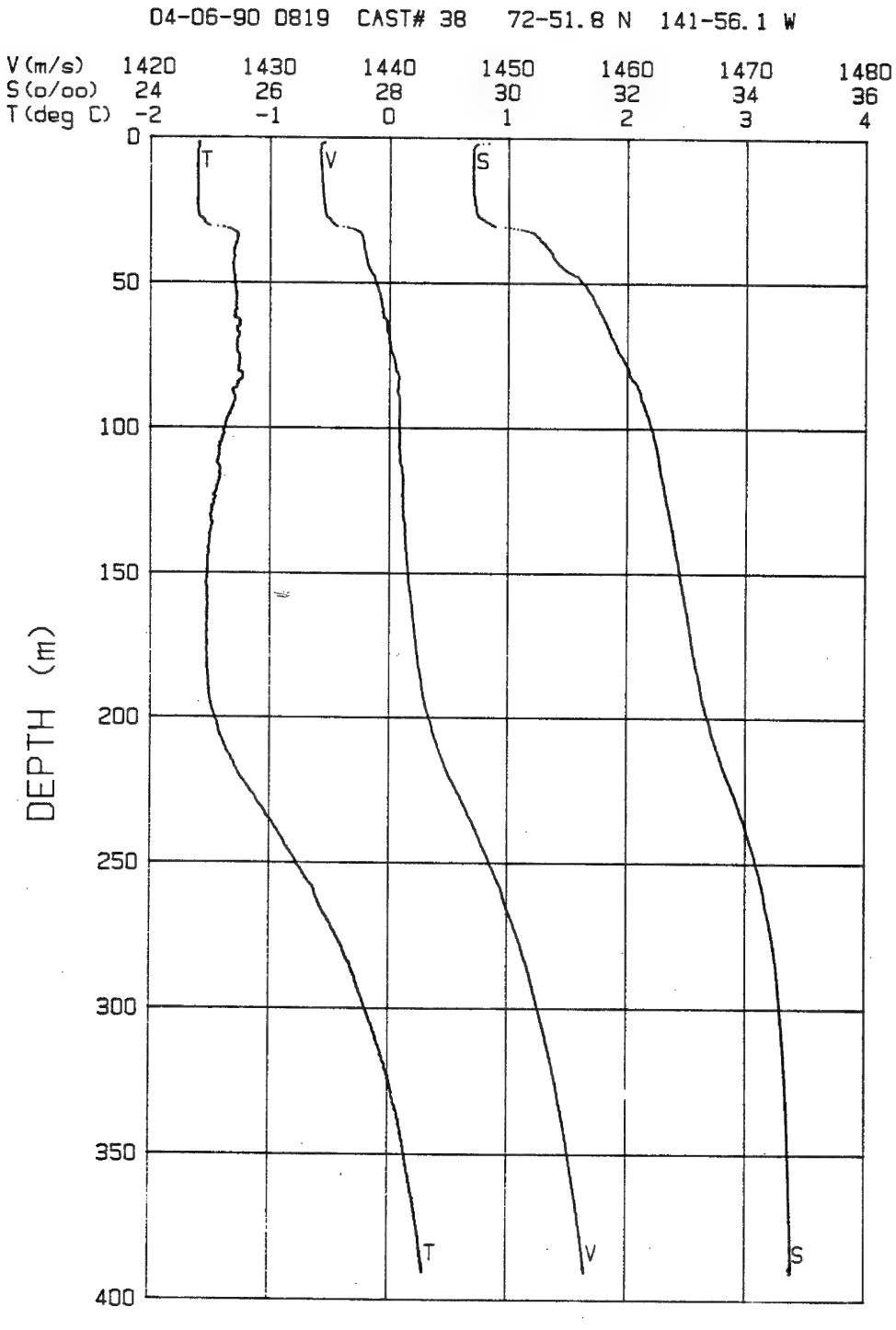
04-06-90 0819 CAST# 38 72-51.8 N 141-56.1 W
V(m/s) 1420 1430 1440 1450 1460 1470 1480
S(o/oo) 24 26 28 30 32 34 36
T(deg C) -2 -1 0 1 2 3 4
0
50
100
150
200
250
300
350
400
DEPTH (m)
T
V
S
T
V
S

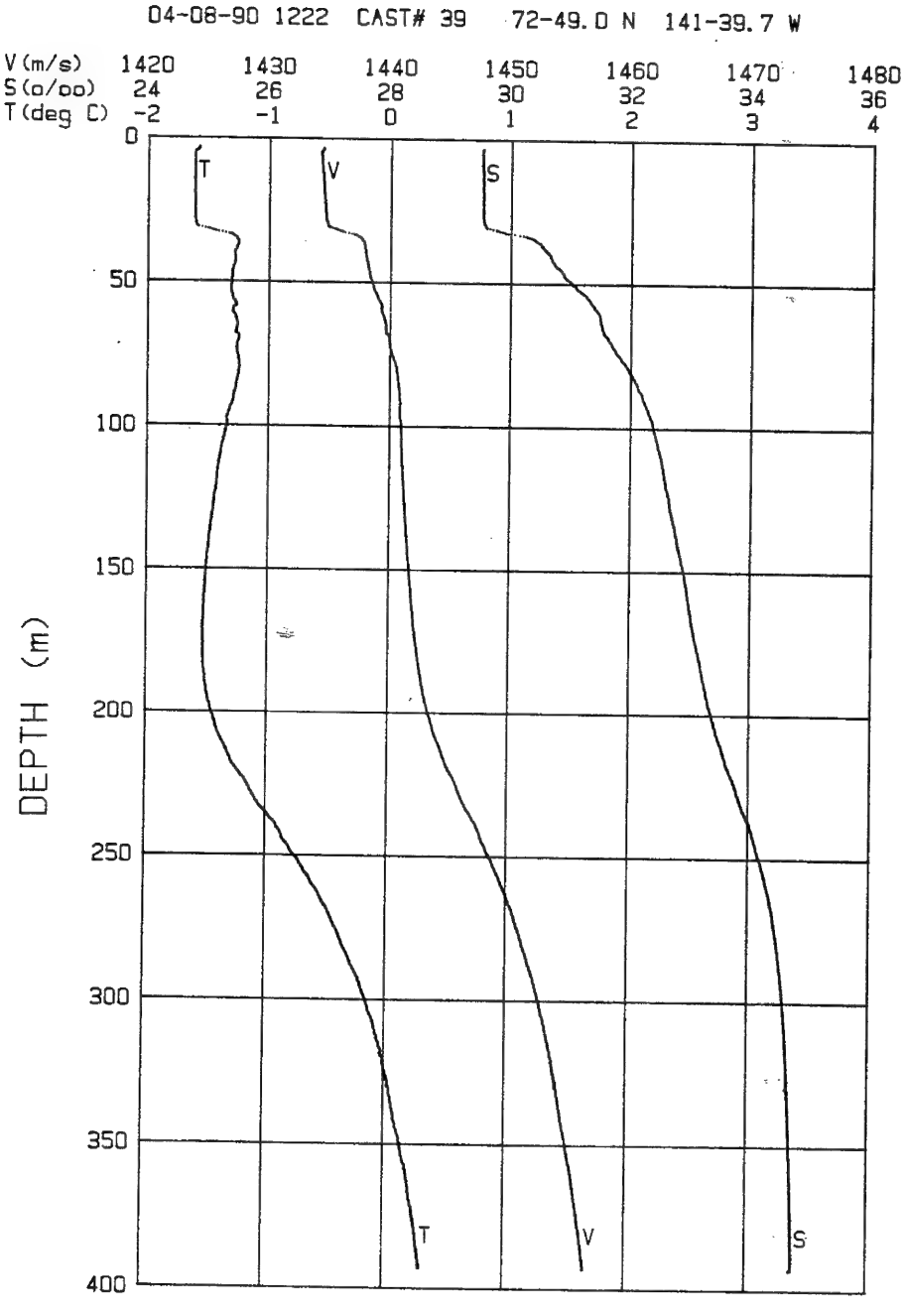
04-08-90 1222 CAST# 39 72-49.0 N 141-39.7 W
V(m/s) 1420 1430 1440 1450 1460 1470 1480
S(o/oo) 24 26 28 30 32 34 36
T(deg C) -2 -1 0 1 2 3 4
0
50
100
150
200
250
300
350
400
DEPTH (m)
T
V
S
T
V
S

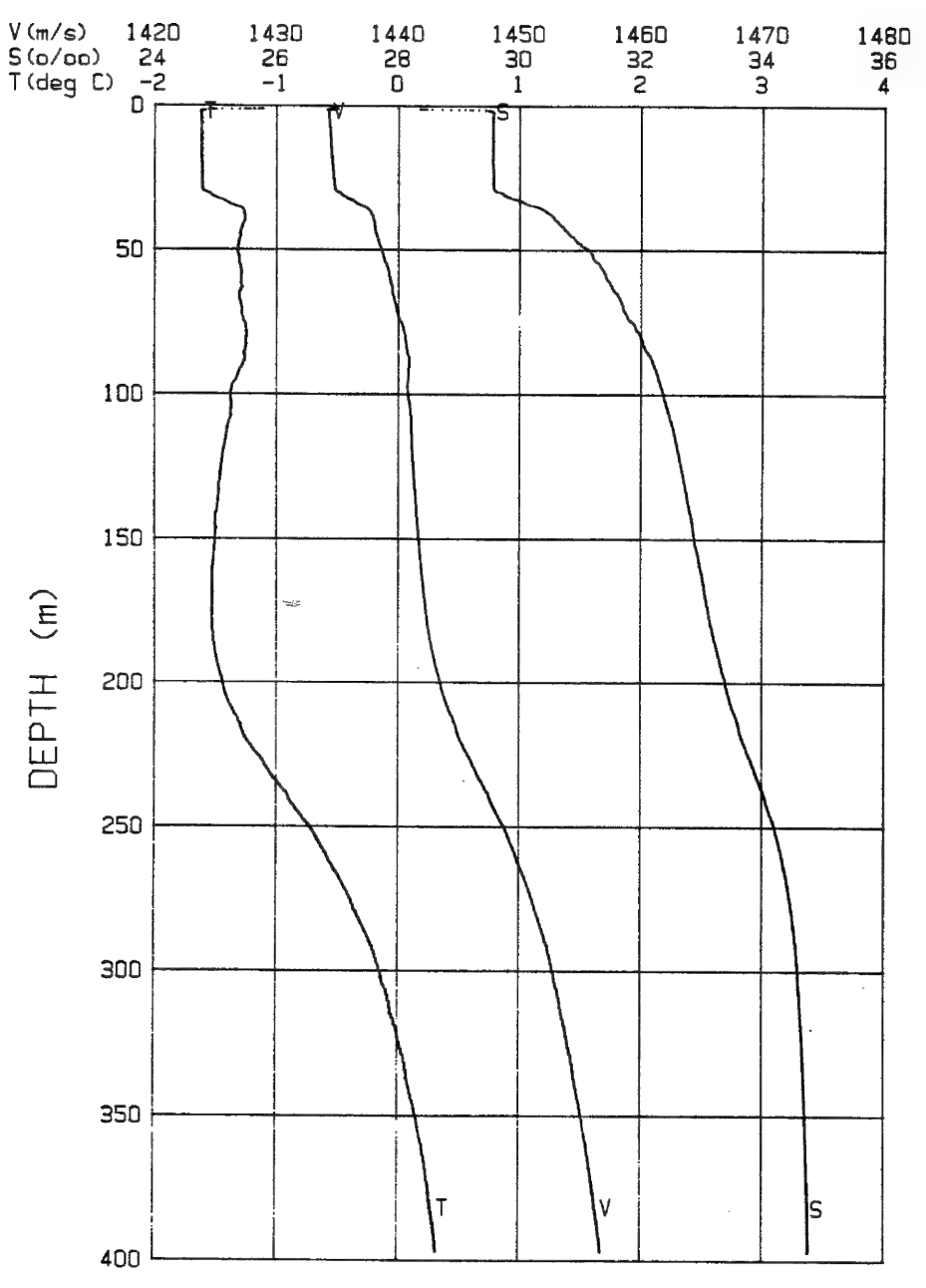
04-09-90 1156 CAST# 41 72-49.4 N 141-38.4 W
V(m/s) 1420 1430 1440 1450 1460 1470 1480
S(o/oo) 24 26 28 30 32 34 36
T(deg C) -2 -1 0 1 2 3 4
DEPTH (m)
0
50
100
150
200
250
300
350
400
T
V
S

APPENDIX C

Measured and Predicted Properties of Ice Cores

Table C1a. Ice core DT-1, APLIS 90.

4/4/90, thickness = 117 cm, snow cover = 7.6 cm.

Depth (cm)	Temp (C)	Salinity (o/oo)	Density (Mg/m^3)	Brine Vol. (o/oo)	Yng Mod ($dynes/cm^2$)	Strength Factor
3.8	-12.0	9.63	0.929	46.8	0.836E+11	0.78
11.4	-11.8	8.90	0.928	43.8	0.846E+11	0.79
19.0	-11.4	7.30	0.926	36.8	0.871E+11	0.81
26.7	-10.8	7.05	0.926	37.0	0.870E+11	0.81
33.8	-10.5	5.62	0.925	30.1	0.895E+11	0.83
40.6	-9.7	5.79	0.925	32.9	0.884E+11	0.82
48.3	-9.1	5.87	0.925	35.1	0.877E+11	0.81
55.9	-8.4	6.10	0.925	38.9	0.863E+11	0.80
63.0	-7.9	5.33	0.925	35.7	0.875E+11	0.81
69.8	-7.1	5.16	0.925	37.8	0.867E+11	0.81
77.5	-6.3	4.67	0.924	37.9	0.867E+11	0.81
85.1	-5.7	4.55	0.924	40.3	0.859E+11	0.80
92.2	-5.3	4.29	0.924	40.5	0.858E+11	0.80

Table C1b. Ice core DT-2, APLIS 90.

4/4/90, thickness = 117 cm, snow cover = 7.6 cm.

Depth (cm)	Temp (C)	Salinity (o/oo)	Density (Mg/m^3)	Brine Vol. (o/oo)	Yng Mod ($dynes/cm^2$)	Strength Factor
3.8	-12.5	9.62	0.929	45.4	0.841E+11	0.79
19.0	-11.6	7.39	0.927	36.7	0.871E+11	0.81
26.7	-10.9	7.31	0.927	38.1	0.866E+11	0.80
44.4	-9.1	5.91	0.925	35.3	0.876E+11	0.81
62.2	-7.5	5.90	0.925	41.3	0.855E+11	0.80
78.2	-6.4	5.42	0.925	43.4	0.848E+11	0.79
85.9	-5.5					
93.5	-4.9	5.45	0.926	55.4	0.806E+11	0.76
105.4	-1.9	5.45	0.933	142.5	0.500E+11	0.62
113.0	-1.8	5.69	0.935	157.9	0.446E+11	0.60

Table C1c. Ice core DT-3, APLIS 90.

4/4/90, thickness = 117 cm, snow cover = 3.5 cm.

Depth (cm)	Temp (C)	Salinity (o/oo)	Density (Mg/m^3)	Brine Vol. (o/oo)	Yng Mod ($dynes/cm^2$)	Strength Factor
3.8	-11.8	10.08	0.929	49.6	0.826E+11	0.78
18.5	-11.3	7.70	0.927	39.1	0.863E+11	0.80
33.8	-10.4	5.74	0.925	30.9	0.891E+11	0.82
49.0	-8.9	5.60	0.925	34.1	0.880E+11	0.82
55.4	-8.4					
63.0	-7.8	5.31	0.925	36.0	0.874E+11	0.81
78.7	-4.4	4.56	0.925	51.1	0.821E+11	0.77
86.4	-3.5					
94.0	-2.5	4.56	0.928	89.0	0.688E+11	0.70
101.6	-1.8	4.68	0.931	129.5	0.546E+11	0.64

Table C1d. Ice core DT-4, APLIS 90.

4/4/90, thickness = 117 cm, snow cover = 7.6 cm.

Depth (cm)	Temp (C)	Salinity (o/oo)	Density (Mg/m^3)	Brine Vol. (o/oo)	Yng Mod ($dynes/cm^2$)	Strength Factor
3.8	-11.5	9.43	0.929	47.3	0.834E+11	0.78
18.5	-11.0	6.72	0.926	34.7	0.878E+11	0.81
26.2	-10.6					
33.8	-10.2	5.65	0.925	30.9	0.892E+11	0.82
42.7	-9.3					
47.8	-8.8	5.48	0.925	33.6	0.882E+11	0.82
55.4	-8.2					
63.0	-7.9	5.04	0.924	33.8	0.882E+11	0.82
75.7	-5.4	5.27	0.925	49.0	0.828E+11	0.78
83.3	-4.7					
90.9	-4.2	5.13	0.926	60.1	0.789E+11	0.75
98.6	-3.6	5.72	0.928	77.7	0.727E+11	0.72
106.2	-2.9	4.41	0.927	74.0	0.740E+11	0.73
113.8	-1.7					

Table C2a. Measured and predicted properties for ice core APL-1.

			MEASUREMENT			BIOT MODEL		HOMOGENEOUS SOLID MODEL	
d (cm)	t(C)	s(o/oo)	longitudinal sv(m/s)	shear sv(m/s)	porosity	longitudinal sv(m/s)	shear sv(m/s)	longitudinal sv(m/s)	shear sv(m/s)
3.8	-14.3	0.21			0.00008	3740	1836	4065	2013
12.2	-14.2	2.87			0.012	3697	1807	3978	1970
20.6	-13.9	3.44	3635	1873	0.015	3688	1800	3959	1959
28.7	-14.0	4.27	3642	1924	0.018	3674	1790	3931	1946
35.8	-13.5	4.90	3481	1671	0.022	3663	1782	3909	1933
42.7	-11.8	4.3	3619	1784	0.021	3666	1784	3930	1935
50.8	-12.3	4.68	3626	1810	0.022	3661	1781	3916	1930
58.9	-11.3	4.94	3626		0.025	3652	1773	3905	1919
67.3	-10.8	4.98	3653	1719	0.026	3648	1771	3902	1914
75.4	-10.6	4.14	3626	1781	0.022	3663	1782	3937	1930
83.8	-9.8	4.34	3559	1778	0.024	3654	1775	3929	1920
92.2	-10.5	4.55	3593		0.024	3654	1775	3920	1921
99.3	-9.8	4.66	3462		0.026	3648	1770	3915	1913
105.9	-8.2	4.75	3578	1771	0.031	3632	1758	3908	1893
113.5	-8.5	5.01	3597	1800	0.032	3629	1756	3895	1890
122.4	-7.6	4.56	3572	1764	0.032	3630	1756	3916	1890
130.6	-6.6	5.01	3568		0.039	3603	1736	3882	1858
138.9	-6.1	4.37	3706	1826	0.036	3613	1743	3919	1868
145.8	-5.7	4.39	3507	1531	0.039	3604	1736	3913	1857
151.6	-5.3	4.13	3505	1744	0.039	3604	1736	3927	1856
158.8	-4.3	3.89	3577	1782	0.044	3585	1721	3926	1832
165.4	-4.2	4.52			0.052	3554	1698	3859	1798
172.0	-3.2	4.2			0.064	3516	1667	3821	1751
180.0	-2.4	4.33	3309		0.088	3427	1598	3653	1647

Table C2b. Measured and predicted properties for ice core APL-2.

			MEASUREMENT			BIOT MODEL		HOMOGENEOUS SOLID MODEL	
d (cm)	t(C)	s(o/oo)	longitudinal sv(m/s)	shear sv(m/s)	porosity	longitudinal sv(m/s)	shear sv(m/s)	longitudinal sv(m/s)	shear sv(m/s)
9.9	-12.4	0.85	3786	1881	0.0039	3727	1829	4057	2001
18.0	-12.6	3.2	3520	1808	0.015	3688	1800	3970	1959
26.2	-12.4	4.49	3695	1711	0.021	3666	1784	3923	1934
33.5	-11.7	4.19	3713	1719	0.021	3668	1785	3935	1936
41.1	-12.2	2.93	3727	1871	0.014	3691	1803	3982	1962
49.3	-11.5	4.62	3600	1772	0.023	3659	1779	3918	1927
57.4	-12.	4.69	3726	1714	0.023	3660	1779	3915	1928
65.5	-11.3	4.76	3736	1743	0.024	3655	1776	3912	1923
73.7	-11.	4.65	3702	1814	0.024	3656	1776	3916	1923
82.0	-10.8	4.14	3728	1827	0.022	3664	1782	3937	1932
90.2	-10.5	4.42	3714	1705	0.024	3657	1777	3926	1924
98.3	-10.5	4.23	3624	1748	0.023	3661	1780	3934	1928
105.0	-9.8	4.09	3604	1700	0.023	3659	1779	3941	1925
115.0	-9.6	3.77	3730	1846	0.022	3665	1782	3956	1931
119.9	-9.3	3.77	3686	1811	0.022	3663	1781	3956	1928
128.0	-8.8	3.81	3692	1797	0.023	3659	1778	3956	1923
136.1	-9.1	3.73	3684	1692	0.022	3663	1781	3959	1928
140.5	-8.9	3.24			0.020	3672	1788	3983	1937
145.0	-8.6	3.18	3707	1867	0.020	3672	1787	3988	1936
153.2	-7.7	3.98			0.027	3645	1768	3949	1907
161.3	-7.5	3.52	3716	1750	0.025	3655	1775	3975	1916
169.4	-7.7	3.63	3739		0.025	3654	1774	3968	1916
177.5	-6.7	3.40	3669		0.026	3650	1771	3984	1909
185.4	-4.7	3.48	3586	1716	0.036	3613	1743	3973	1864

APPENDIX D

Plots of Under-Ice Ambient Noise Spectra

In each plot, time of measurement is given in UTC (year day, hour, minute). The Knudsen noise level at sea state 0 for the open ocean is shown for comparison. The first two spectra were taken in real-time and have a larger bandwidth. The rest were from recorded data with a bandwidth of 20 kHz. Note: The equivalent in-water self-noise of the system is ~17 dBs.

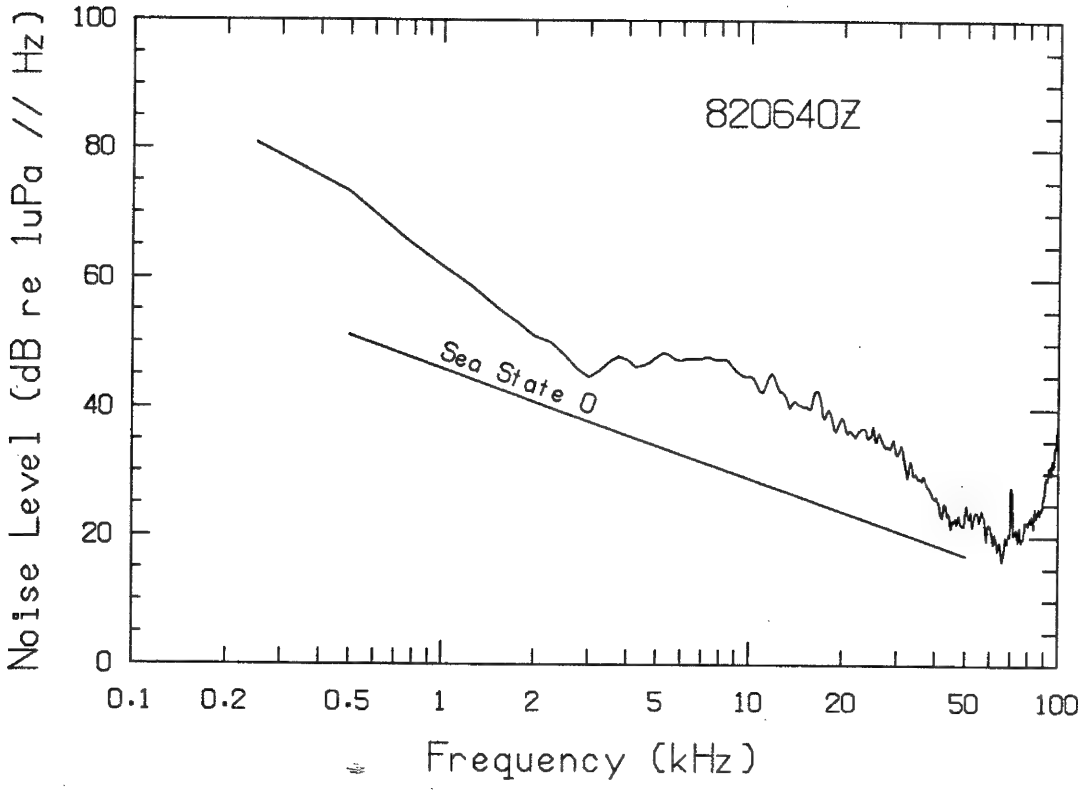
820640Z
Sea State 0
Noise Level (dB re 1uPa // Hz)
Frequency (kHz)
100
80
60
40
20
0
0.1
0.2
0.5
1
2
5
10
20
50
100

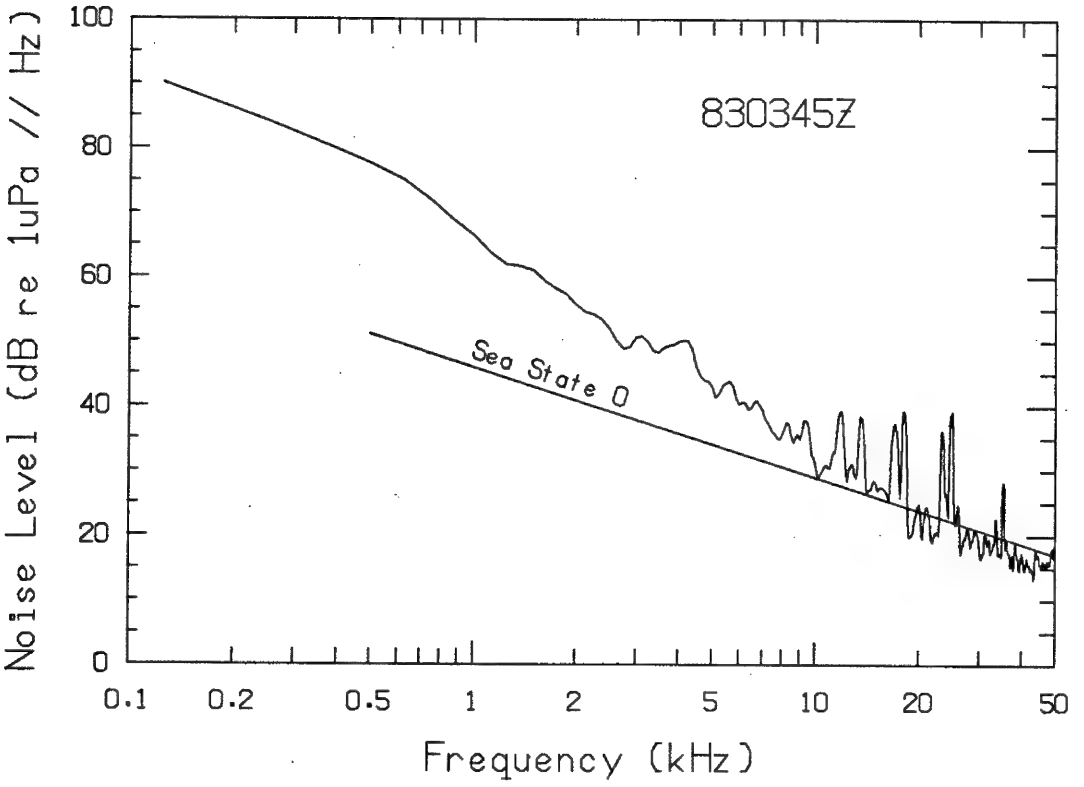
830345Z
Sea State 0
Noise Level (dB re 1uPa // Hz)
Frequency (kHz)
100
80
60
40
20
0
0.1
0.2
0.5
1
2
5
10
20
50

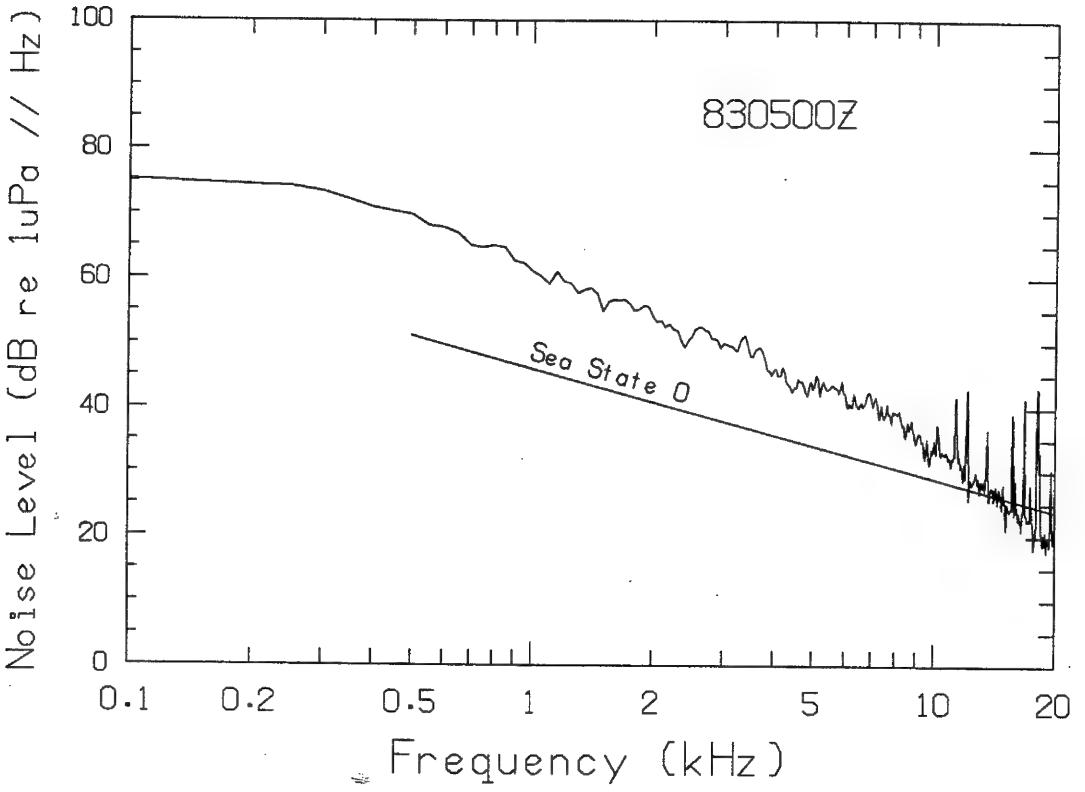
830500Z
Sea State 0
Noise Level (dB re 1uPa // Hz)
100
80
60
40
20
0
0.1
0.2
0.5
1
2
5
10
20
Frequency (kHz)

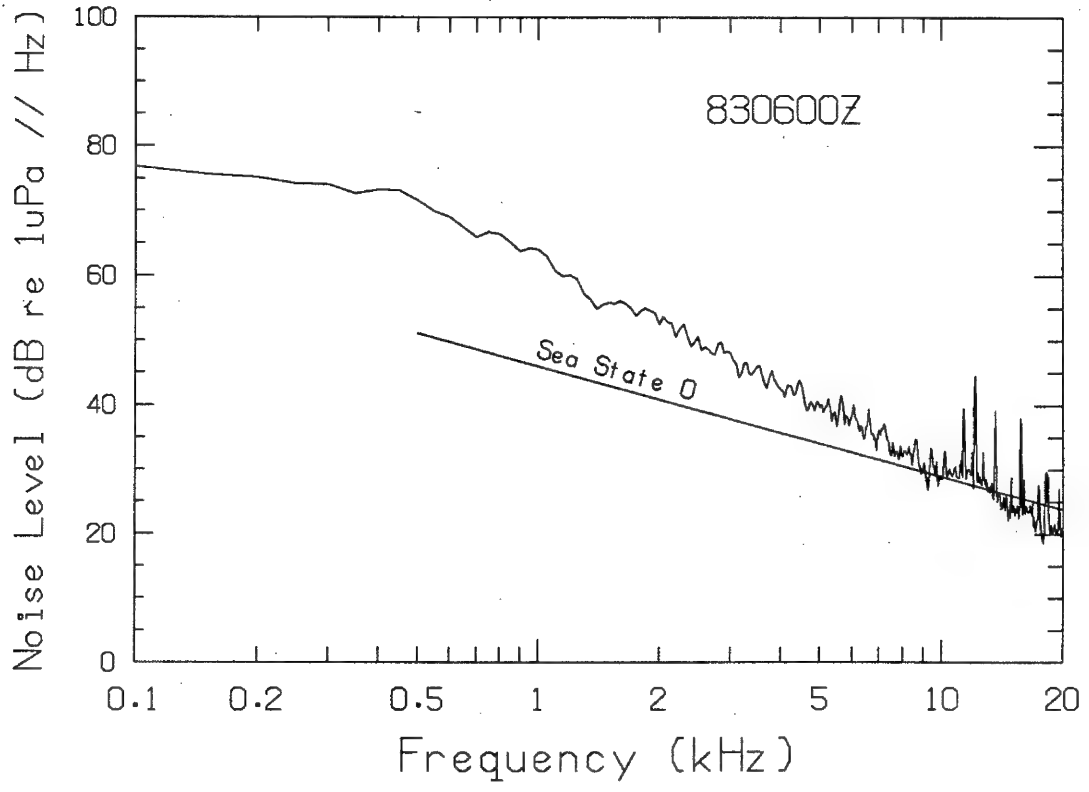
830600Z
Sea State 0
Noise Level (dB re 1uPa // Hz)
100
80
60
40
20
0
0.1
0.2
0.5
1
2
5
10
20
Frequency (kHz)

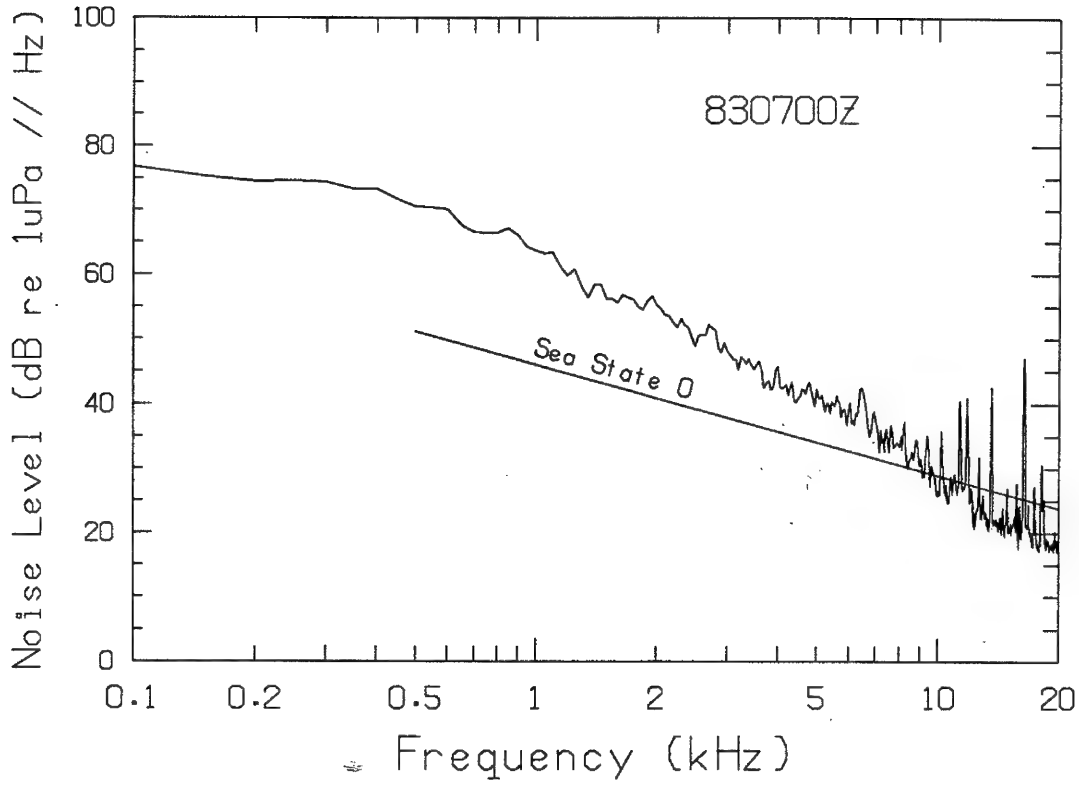
830700Z
Sea State 0
Noise Level (dB re 1uPa // Hz)
Frequency (kHz)
100
80
60
40
20
0
0.1
0.2
0.5
1
2
5
10
20

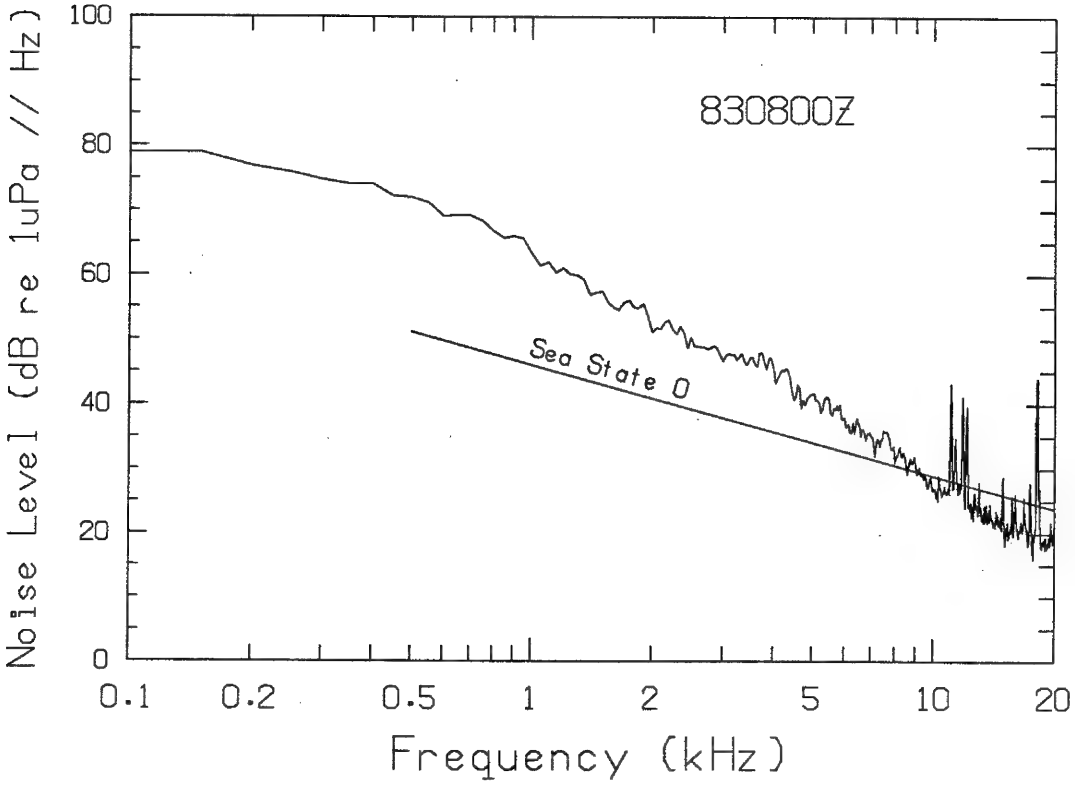
830800Z
Sea State 0
Noise Level (dB re 1uPa // Hz)
Frequency (kHz)
100
80
60
40
20
0
0.1
0.2
0.5
1
2
5
10
20

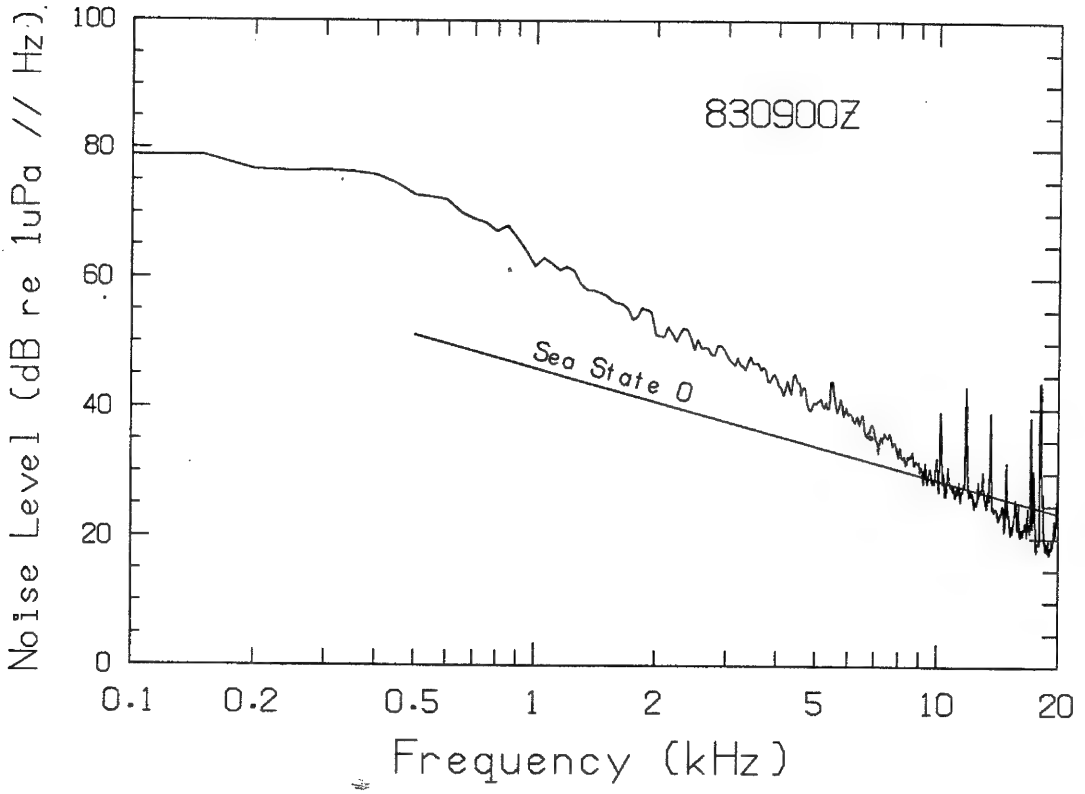
830900Z
Sea State 0
Noise Level (dB re 1uPa // Hz)
Frequency (kHz)
100
80
60
40
20
0
0.1
0.2
0.5
1
2
5
10
20

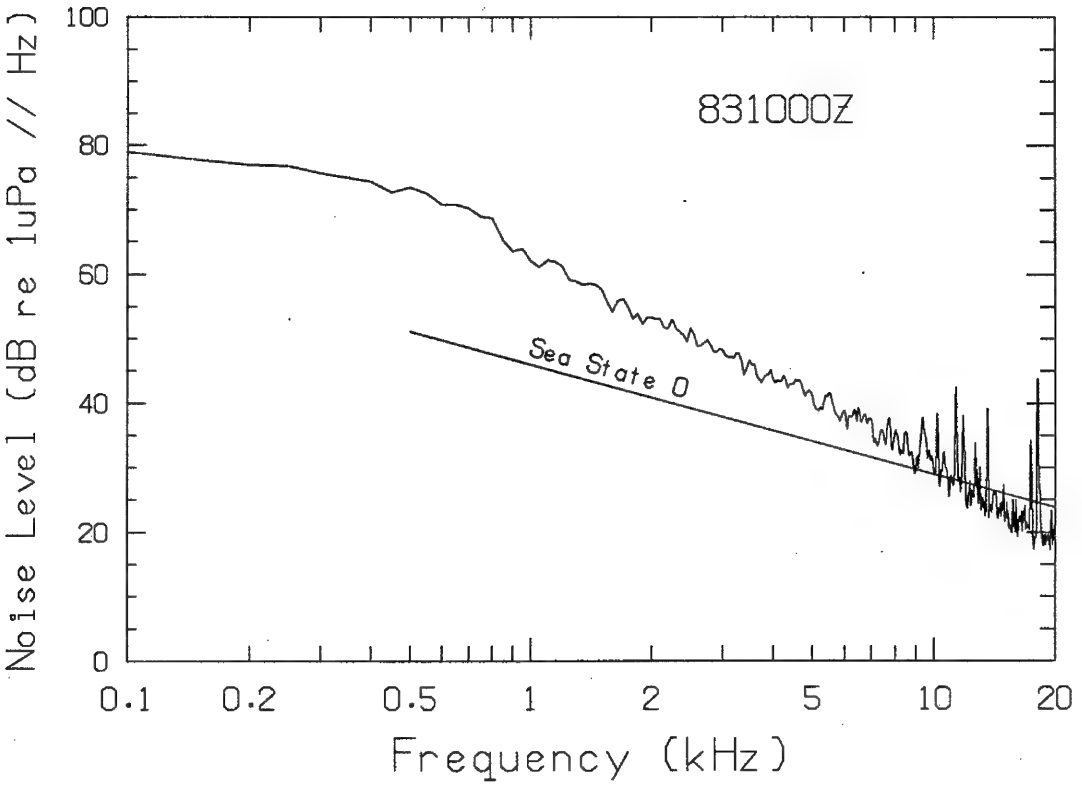
831000Z
Sea State 0
Noise Level (dB re 1uPa // Hz)
Frequency (kHz)
100
80
60
40
20
0
0.1
0.2
0.5
1
2
5
10
20

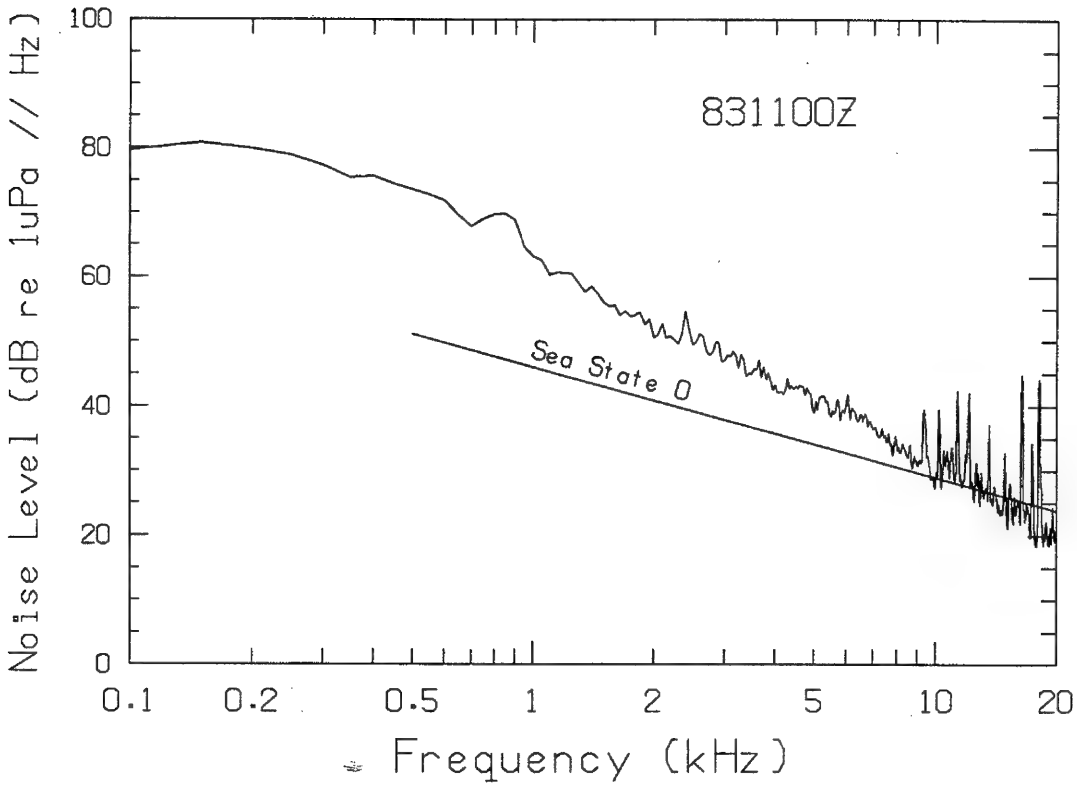
831100Z
Sea State 0
Noise Level (dB re 1uPa // Hz)
100
80
60
40
20
0
0.1
0.2
0.5
1
2
5
10
20
Frequency (kHz)

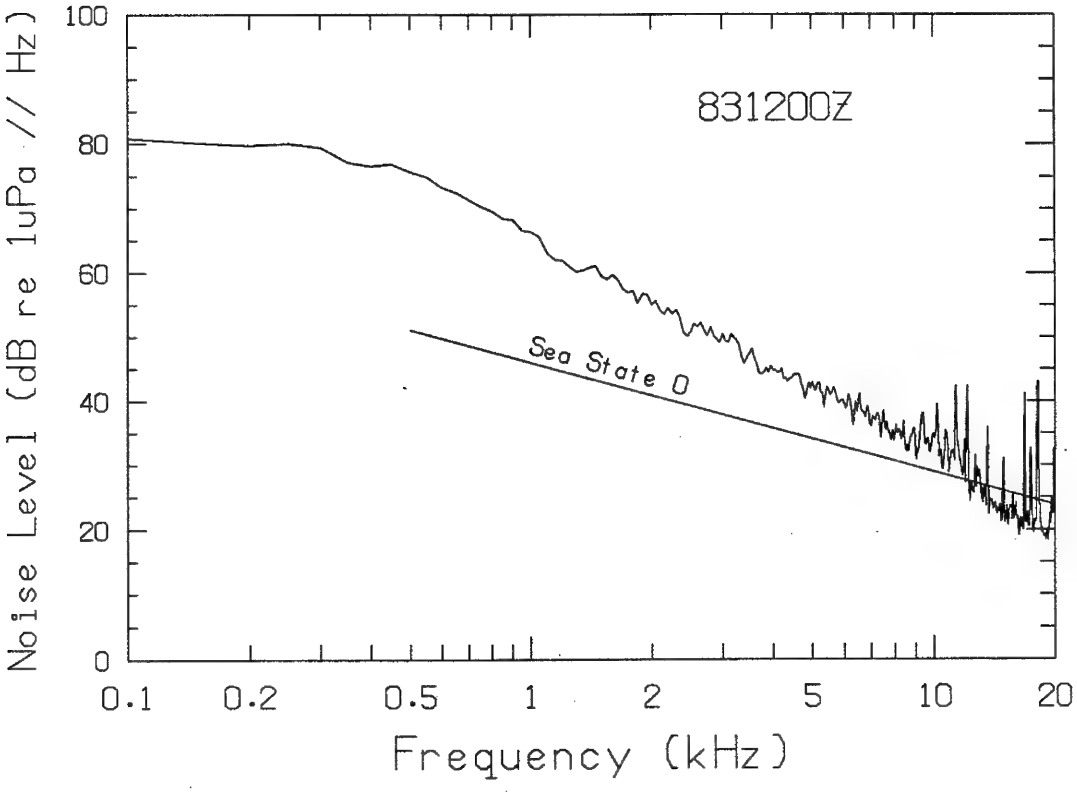
831200Z
Sea State 0
Noise Level (dB re 1uPa // Hz)
100
80
60
40
20
0
0.1
0.2
0.5
1
2
5
10
20
Frequency (kHz)

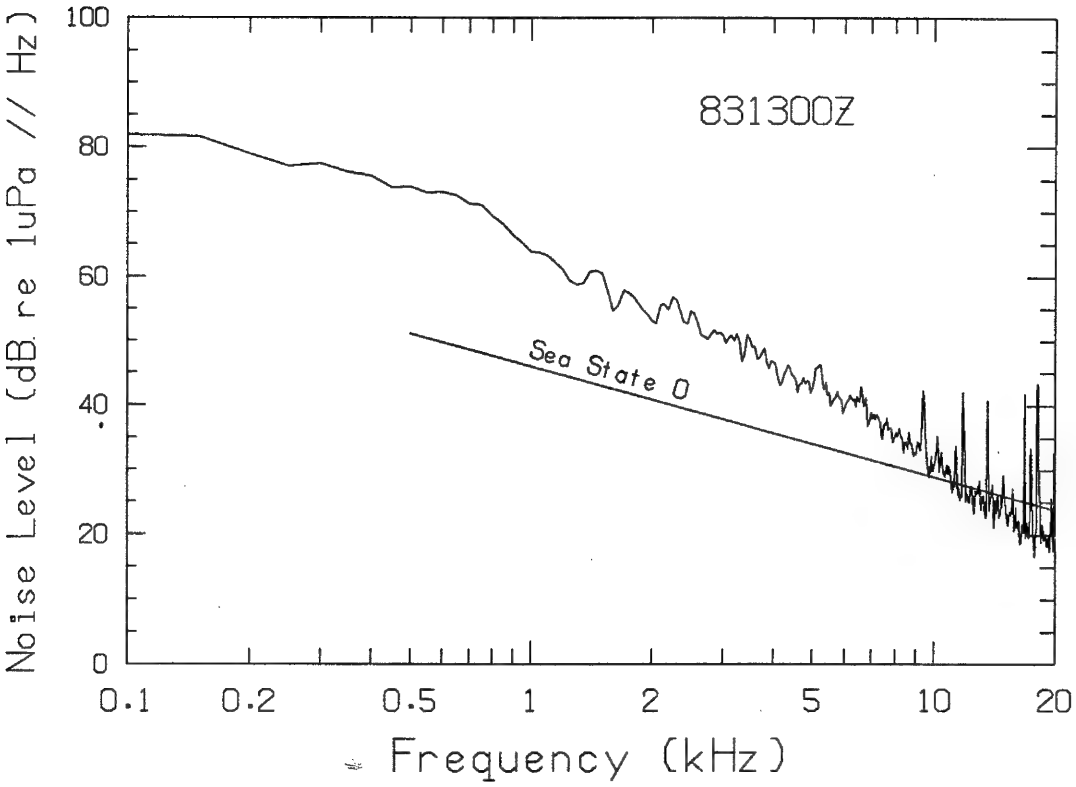
831300Z
Sea State 0
Noise Level (dB re 1uPa // Hz)
100
80
60
40
20
0
0.1
0.2
0.5
1
2
5
10
20
Frequency (kHz)

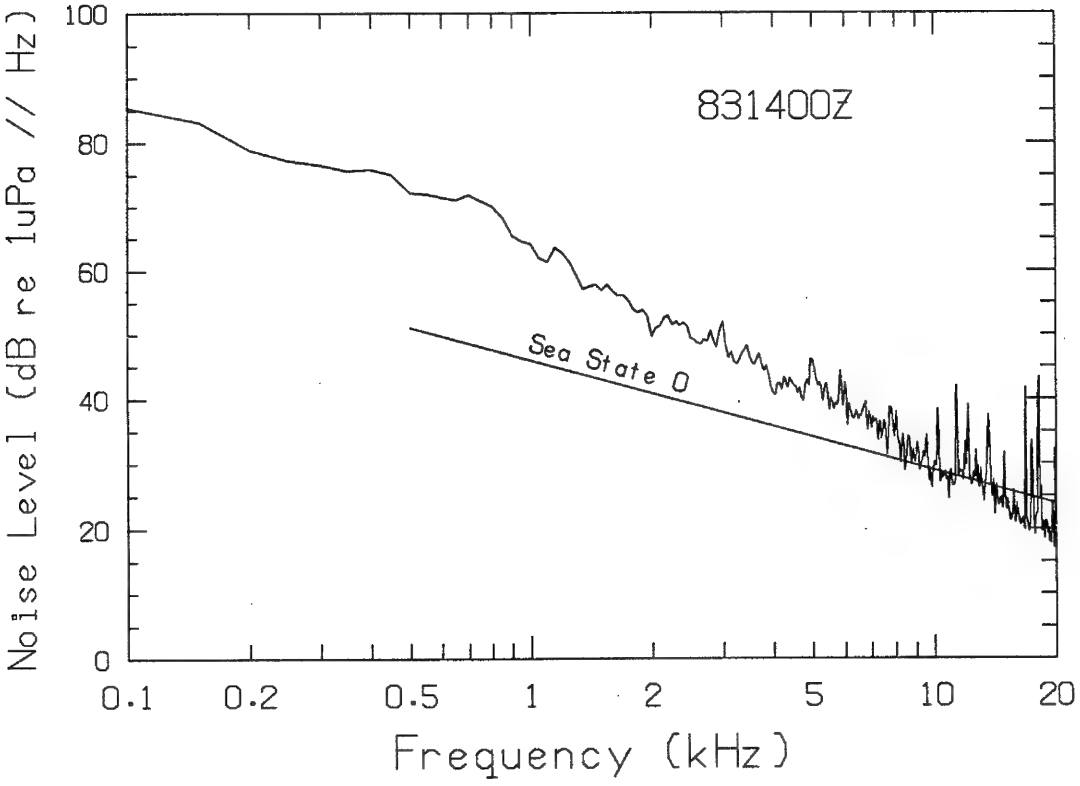
831400Z
Sea State 0
Noise Level (dB re 1uPa // Hz)
100
80
60
40
20
0
0.1
0.2
0.5
1
2
5
10
20
Frequency (kHz)

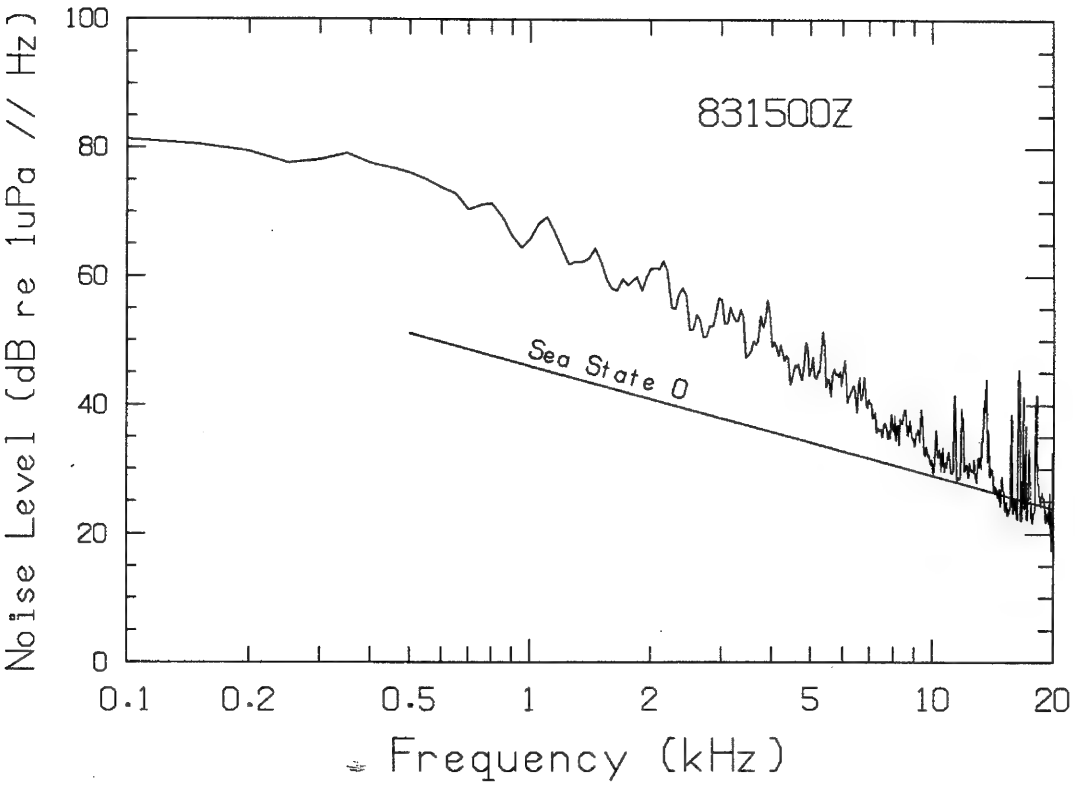
831500Z
Sea State 0
Noise Level (dB re 1uPa // Hz)
100
80
60
40
20
0
0.1
0.2
0.5
1
2
5
10
20
Frequency (kHz)

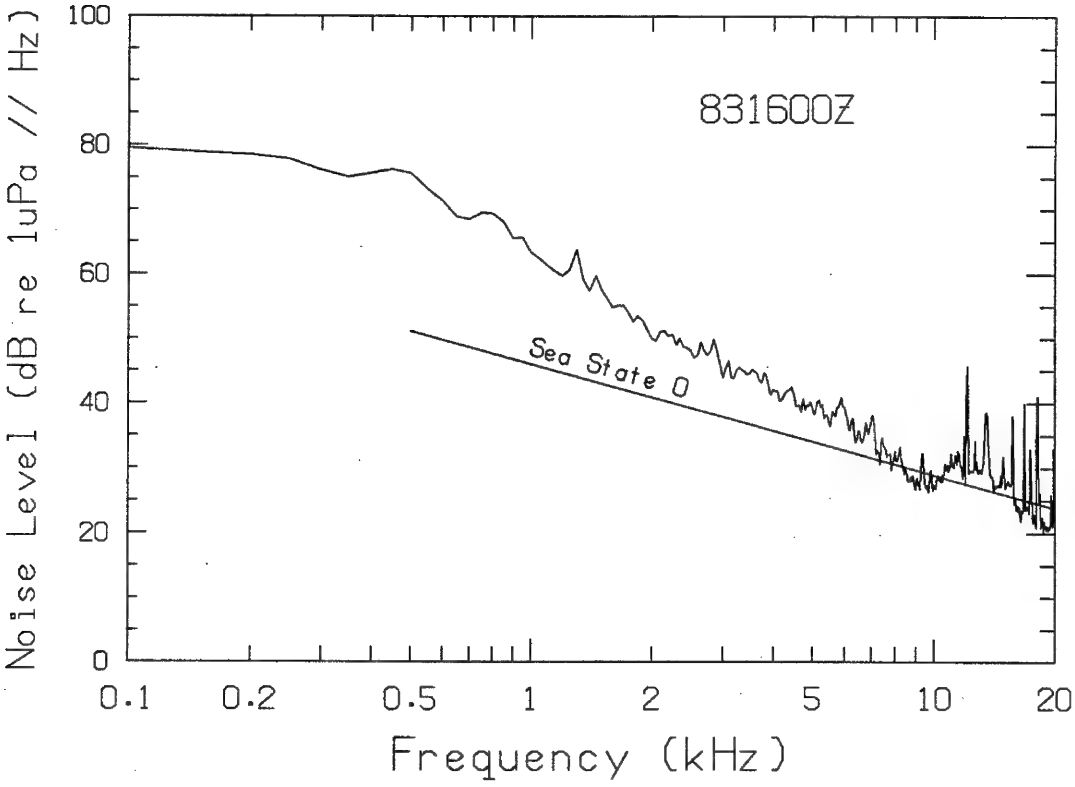
831600Z
Sea State 0
Noise Level (dB re 1uPa // Hz)
100
80
60
40
20
0
0.1
0.2
0.5
1
2
5
10
20
Frequency (kHz)

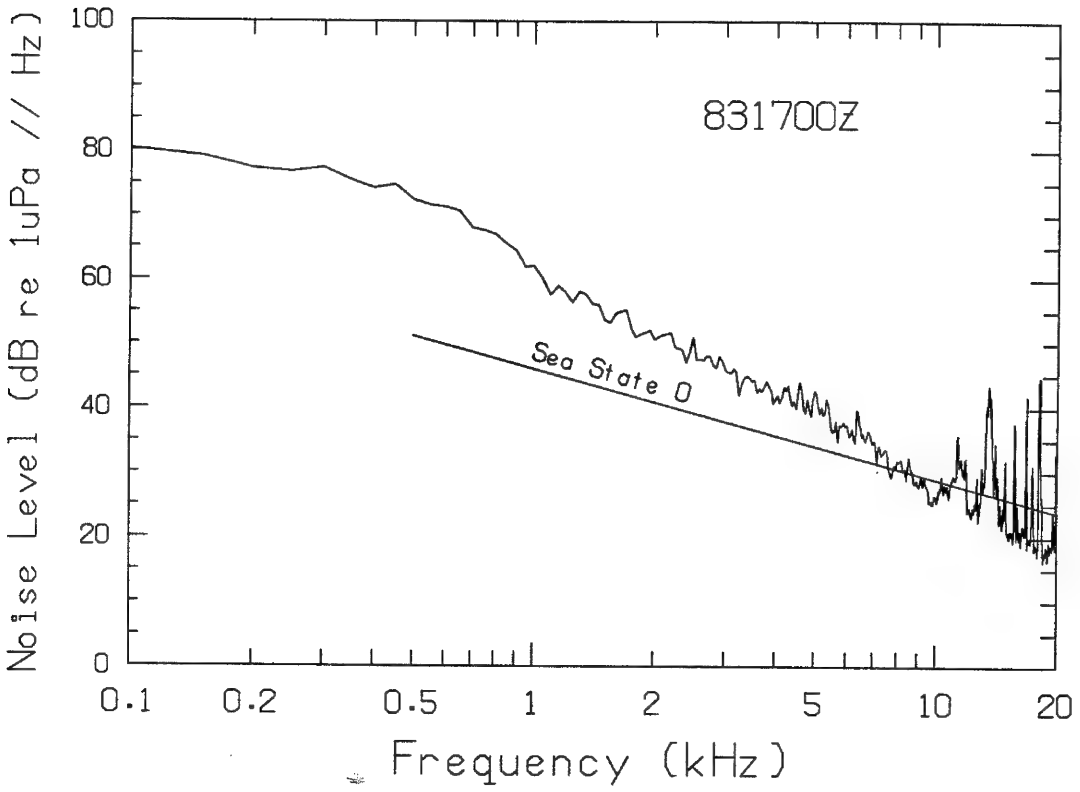
831700Z
Sea State 0
Noise Level (dB re 1uPa // Hz)
Frequency (kHz)
100
80
60
40
20
0
0.1
0.2
0.5
1
2
5
10
20

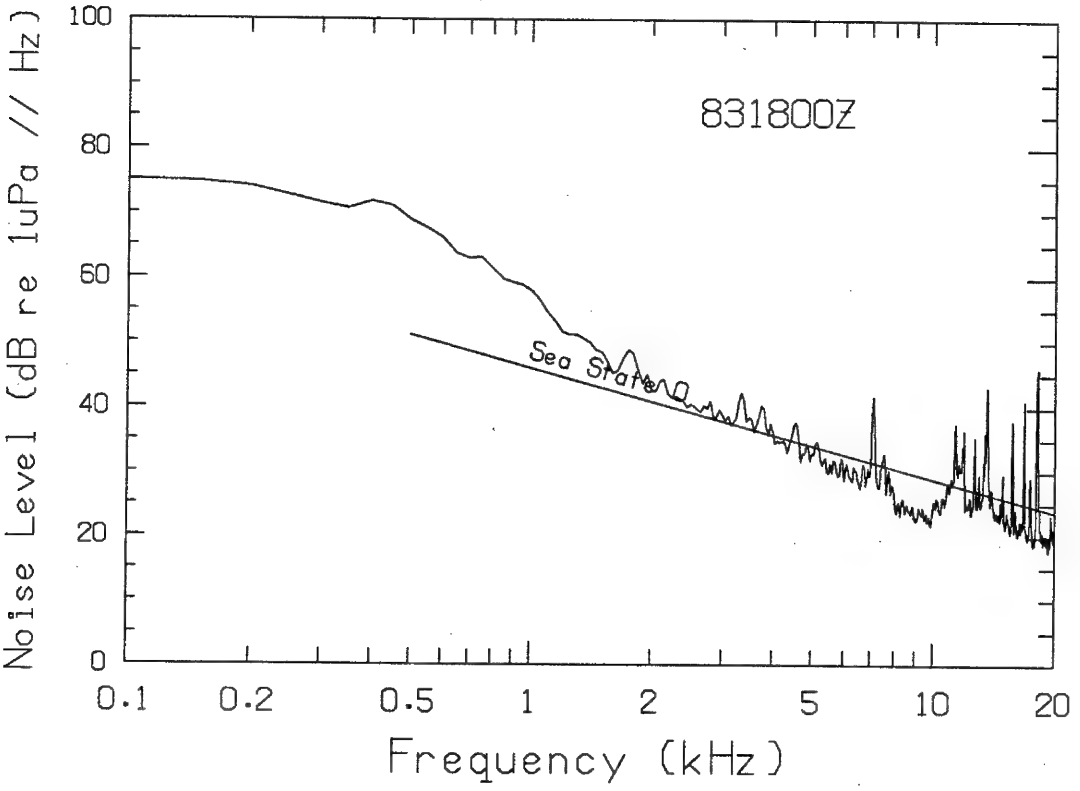
831800Z
Sea State 0
Noise Level (dB re 1uPa // Hz)
Frequency (kHz)
100
80
60
40
20
0
0.1
0.2
0.5
1
2
5
10
20

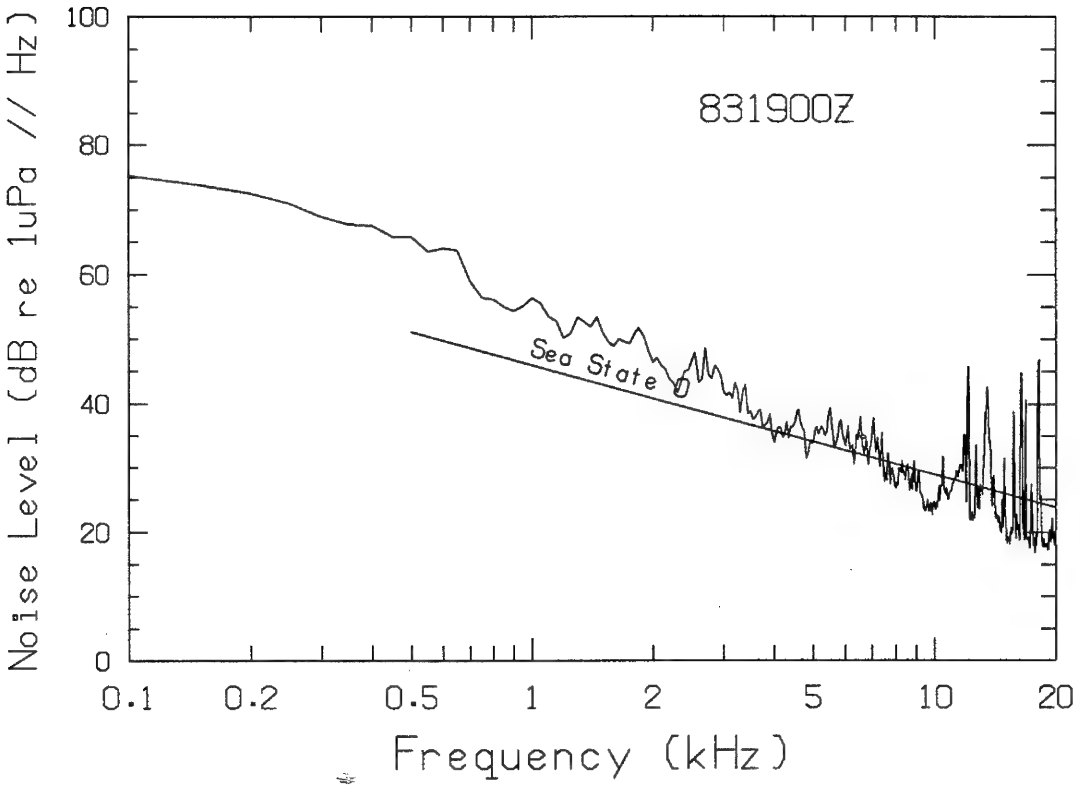
831900Z
Sea State 0
Noise Level (dB re 1uPa // Hz)
Frequency (kHz)
100
80
60
40
20
0
0.1
0.2
0.5
1
2
5
10
20

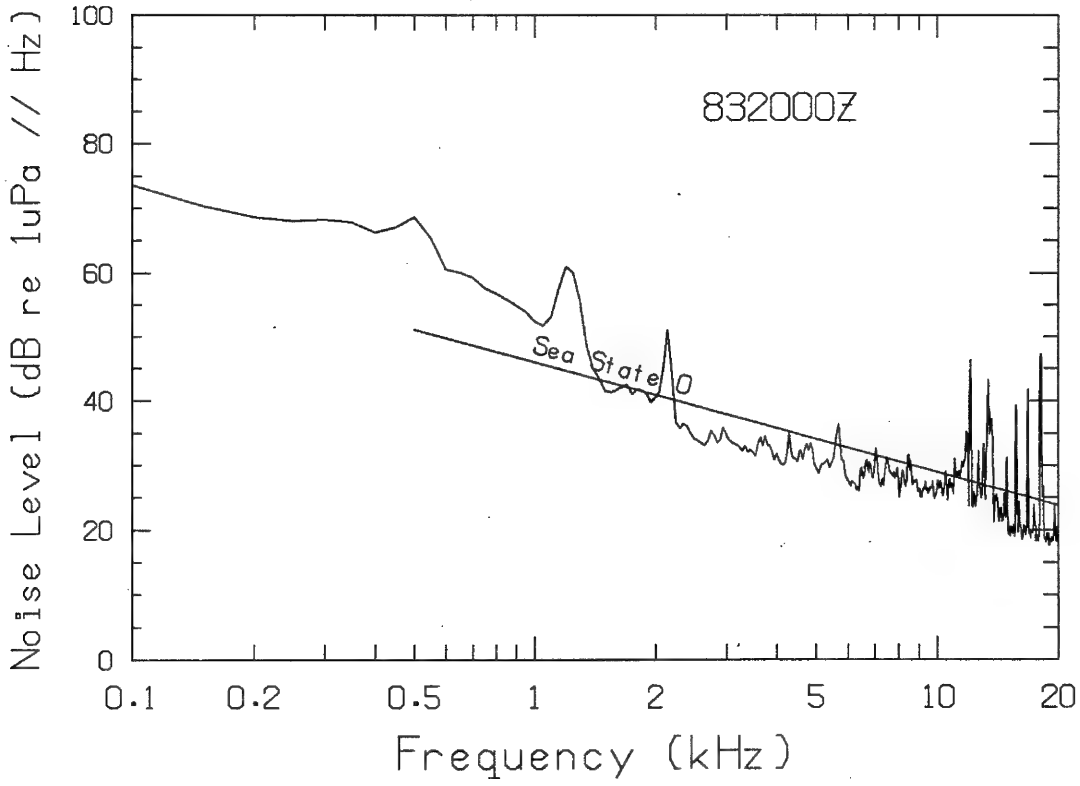
832000Z
Sea State 0
Noise Level (dB re 1uPa // Hz)
Frequency (kHz)
100
80
60
40
20
0
0.1
0.2
0.5
1
2
5
10
20

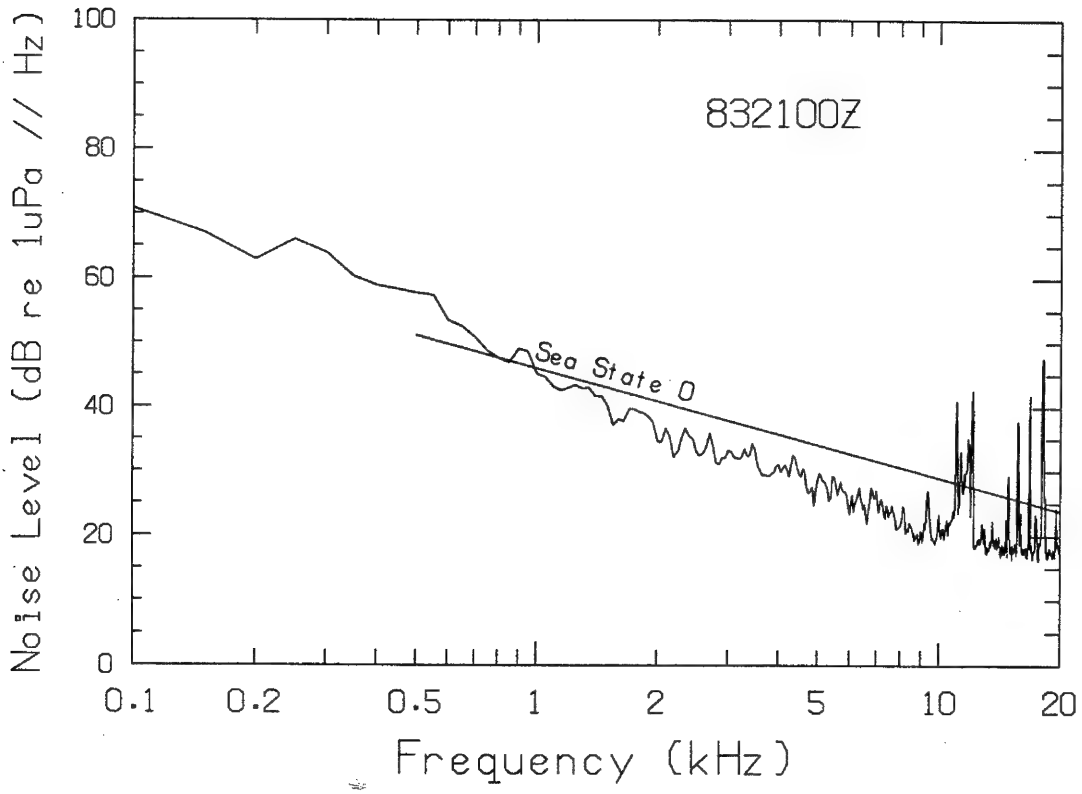
832100Z
Sea State 0
Noise Level (dB re 1uPa // Hz)
Frequency (kHz)
100
80
60
40
20
0
0.1
0.2
0.5
1
2
5
10
20

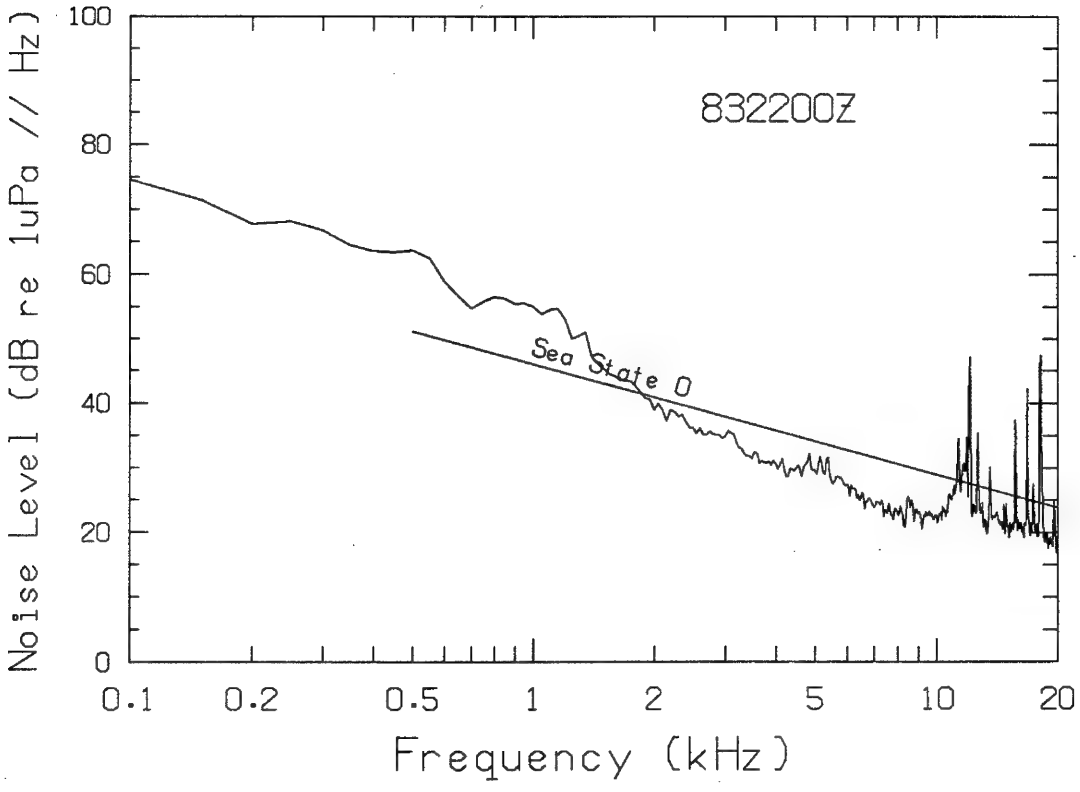
832200Z
Sea State 0
Noise Level (dB re 1uPa // Hz)
Frequency (kHz)
100
80
60
40
20
0
0.1
0.2
0.5
1
2
5
10
20

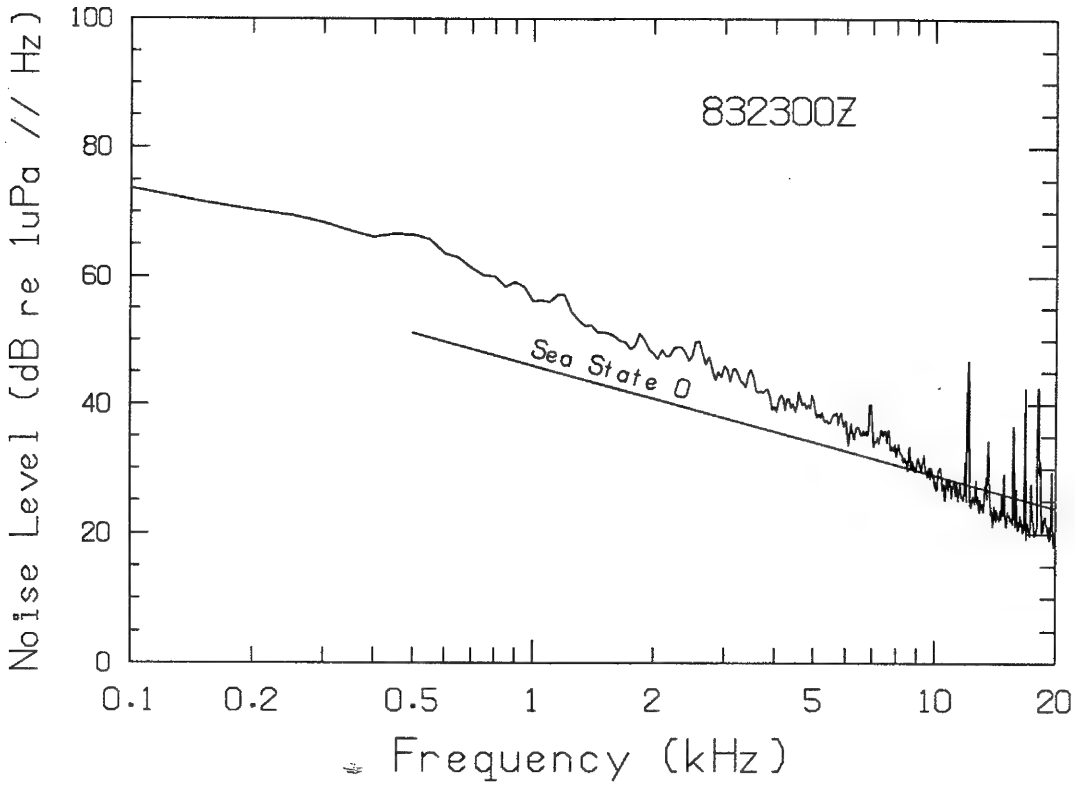
832300Z
Sea State 0
Noise Level (dB re 1uPa // Hz)
Frequency (kHz)
100
80
60
40
20
0
0.1
0.2
0.5
1
2
5
10
20

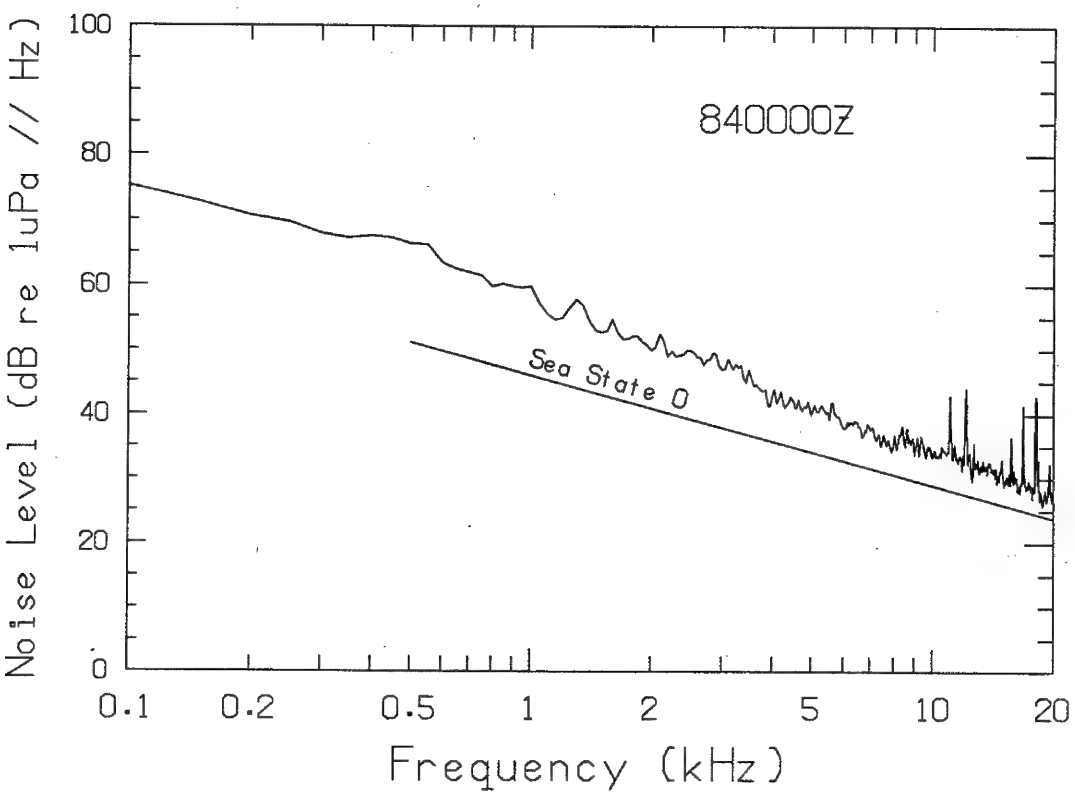
840000Z
Sea State 0
Noise Level (dB re 1uPa // Hz)
Frequency (kHz)
100
80
60
40
20
0
0.1
0.2
0.5
1
2
5
10
20

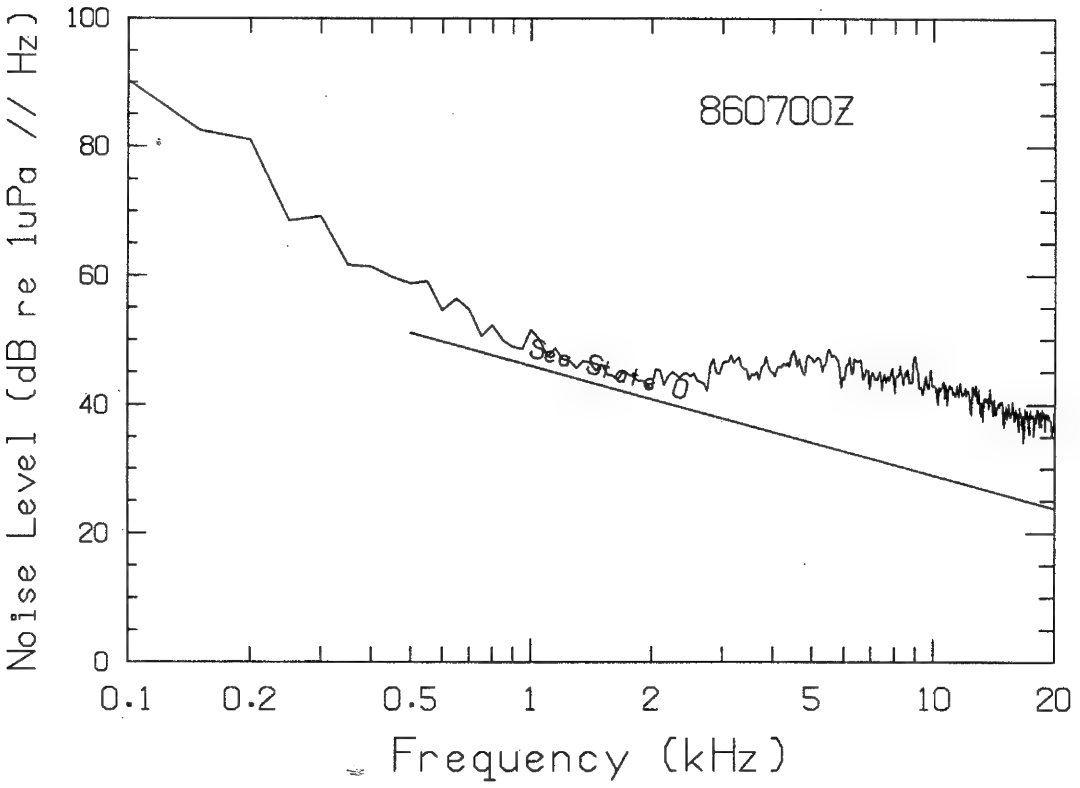
860700Z
Sea State 0
Noise Level (dB re 1uPa // Hz)
Frequency (kHz)
100
80
60
40
20
0
0.1
0.2
0.5
1
2
5
10
20

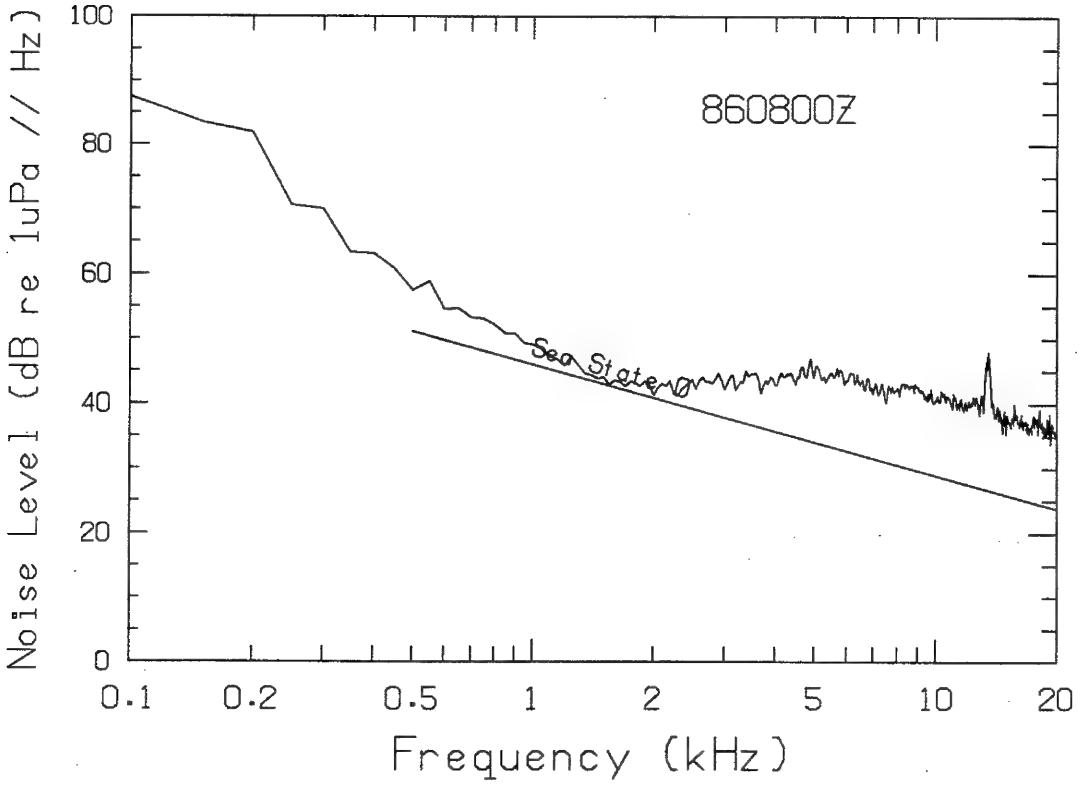
860800Z
Sea State 0
Noise Level (dB re 1uPa // Hz)
Frequency (kHz)
100
80
60
40
20
0
0.1
0.2
0.5
1
2
5
10
20

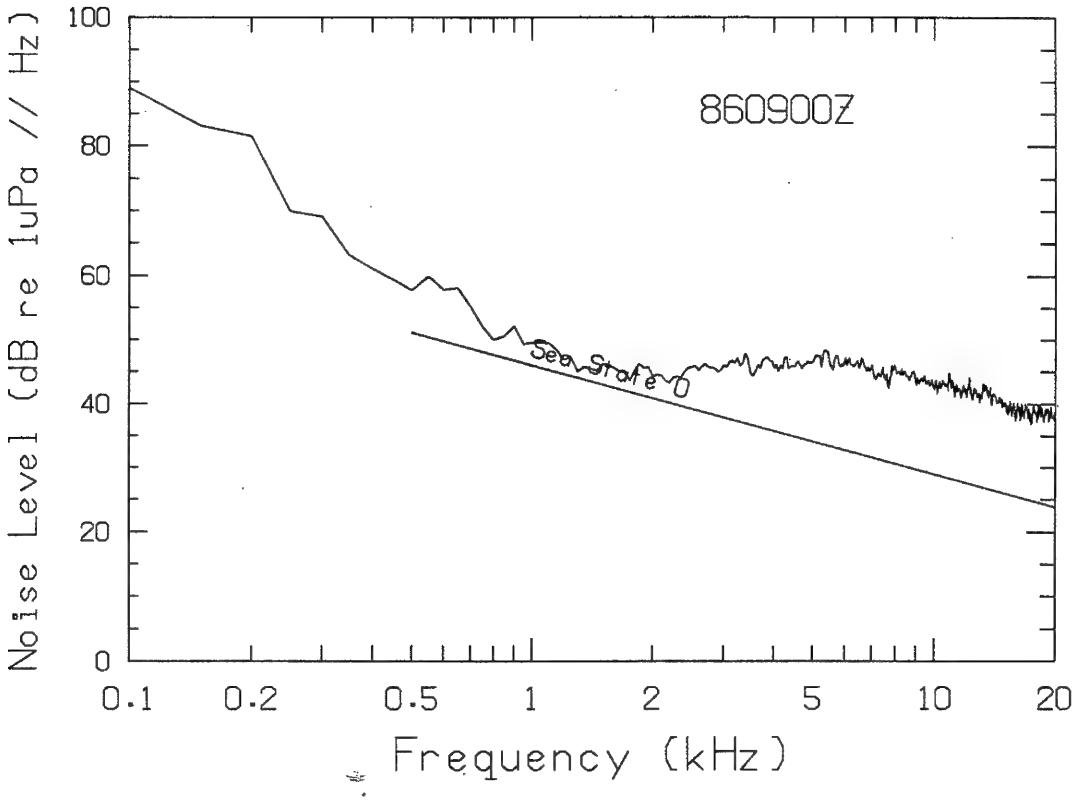
860900Z
Noise Level (dB re 1uPa // Hz)
Frequency (kHz)
See Strafe 0
100
80
60
40
20
0
0.1
0.2
0.5
1
2
5
10
20

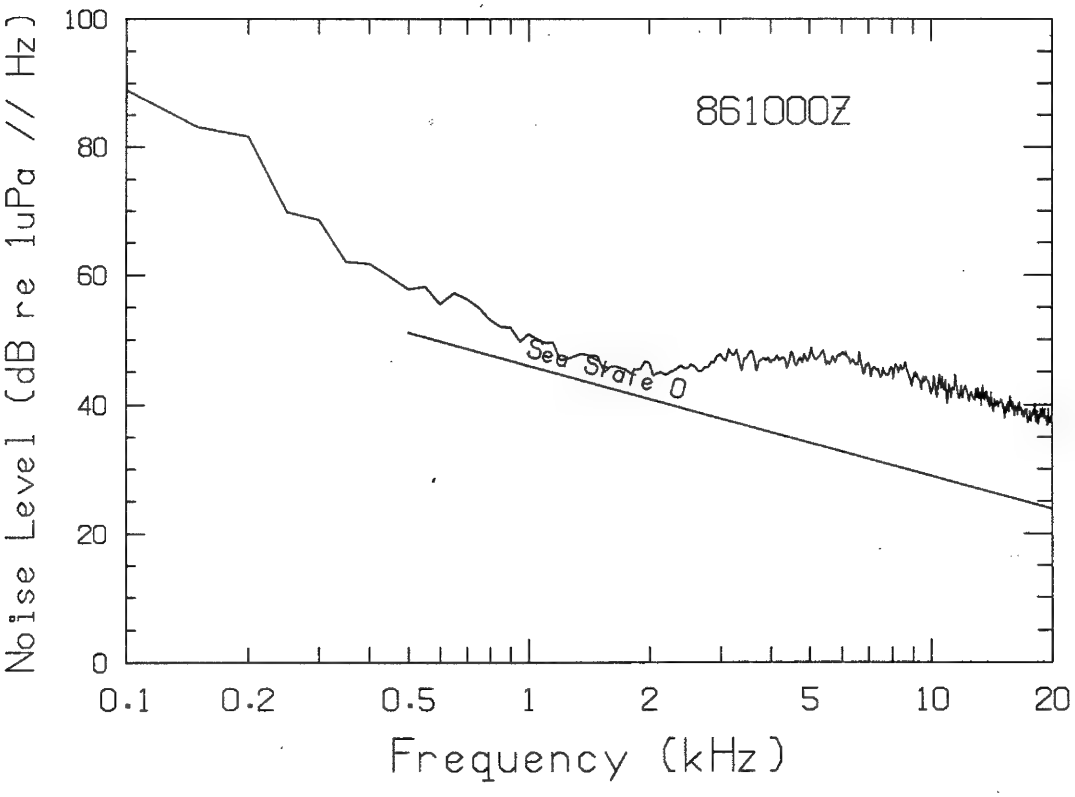
861000Z
Noise Level (dB re 1uPa // Hz)
Frequency (kHz)
See Strafe 0
100
80
60
40
20
0
0.1
0.2
0.5
1
2
5
10
20

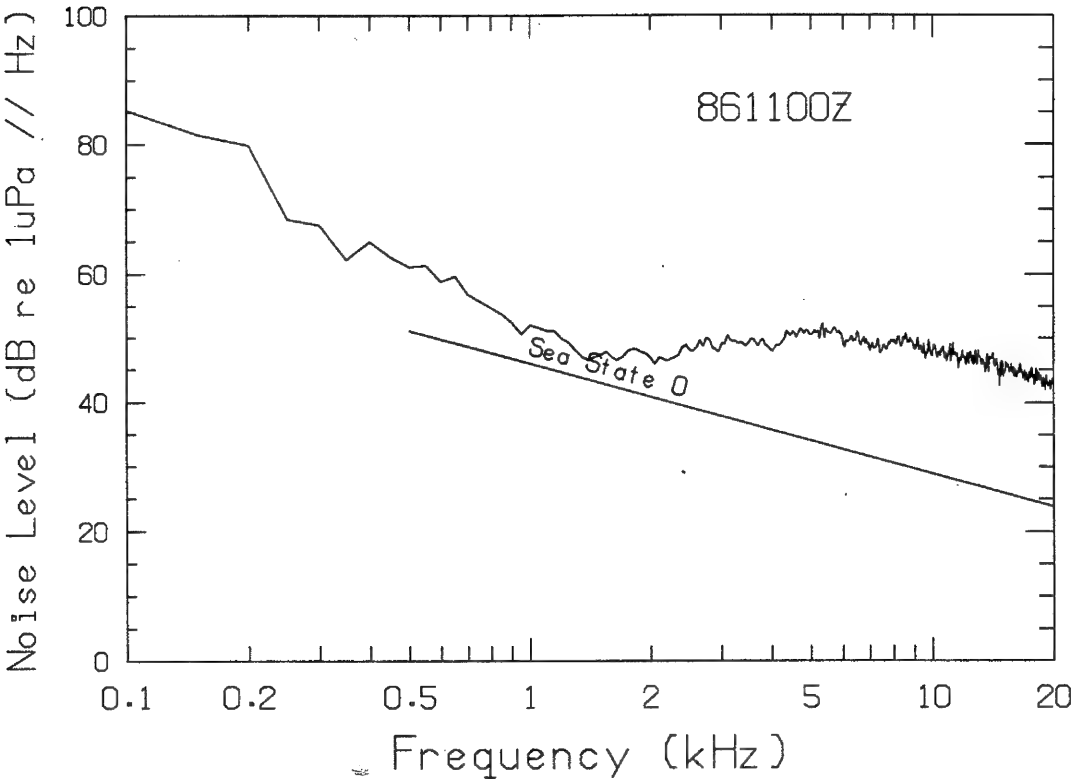
861100Z
Sea State 0
Noise Level (dB re 1uPa // Hz)
100
80
60
40
20
0
0.1
0.2
0.5
1
2
5
10
20
Frequency (kHz)

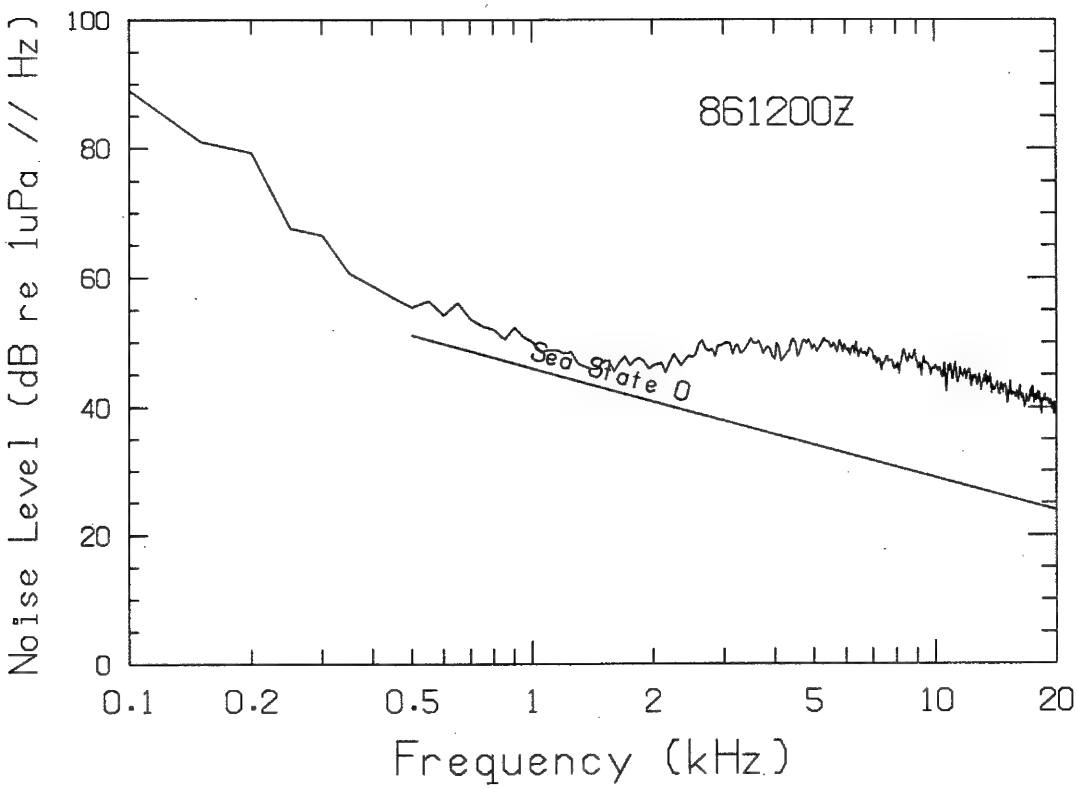
861200Z
Sea State 0
Noise Level (dB re 1uPa // Hz)
100
80
60
40
20
0
0.1
0.2
0.5
1
2
5
10
20
Frequency (kHz)

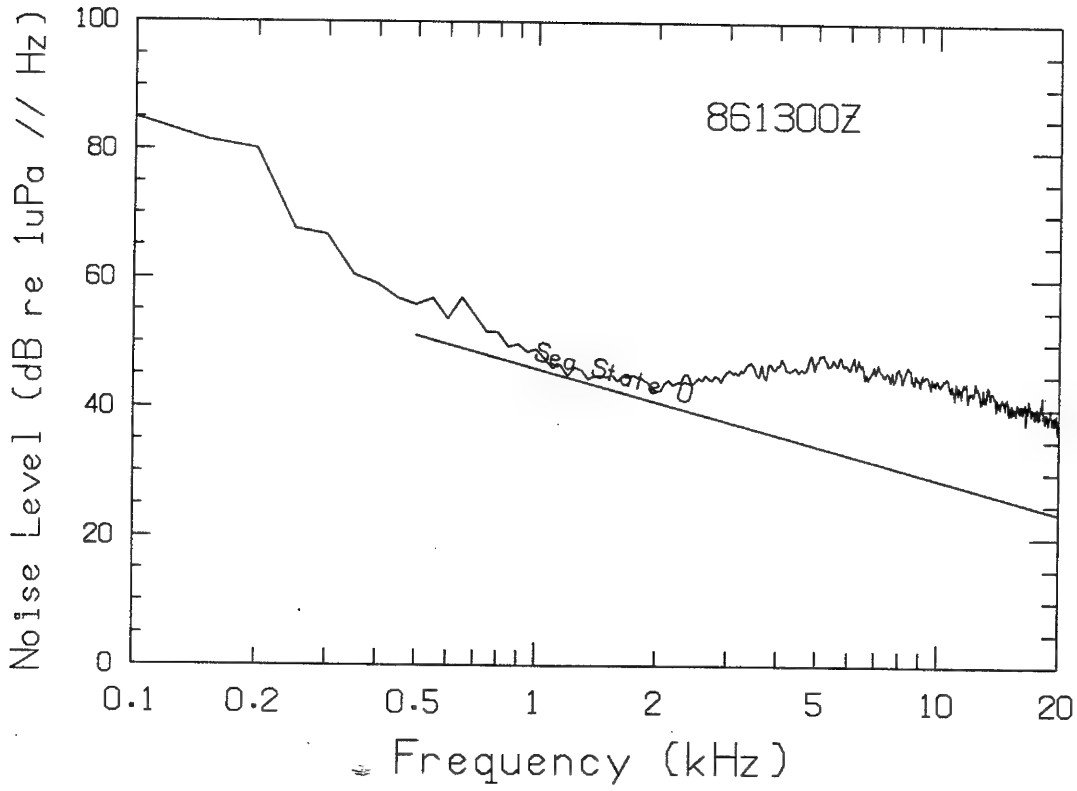
861300Z
Sea State 0
Noise Level (dB re 1uPa // Hz)
100
80
60
40
20
0
0.1
0.2
0.5
1
2
5
10
20
Frequency (kHz)

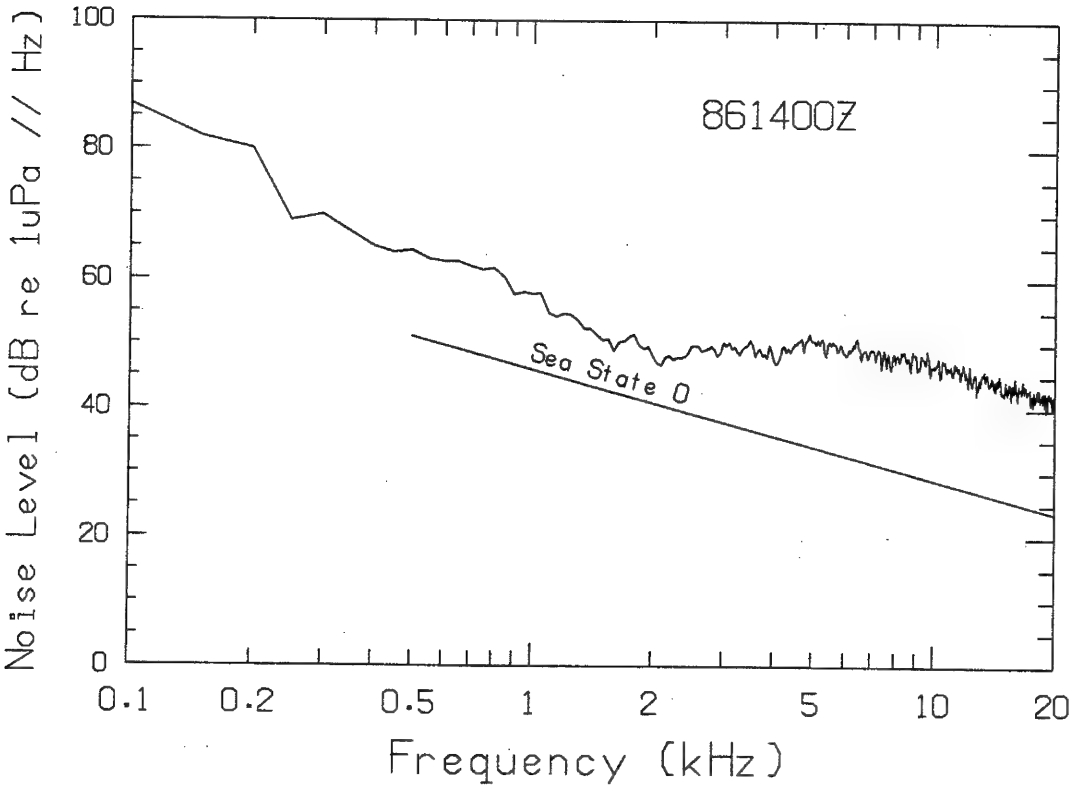
861400Z
Sea State 0
Noise Level (dB re 1uPa // Hz)
100
80
60
40
20
0
0.1
0.2
0.5
1
2
5
10
20
Frequency (kHz)

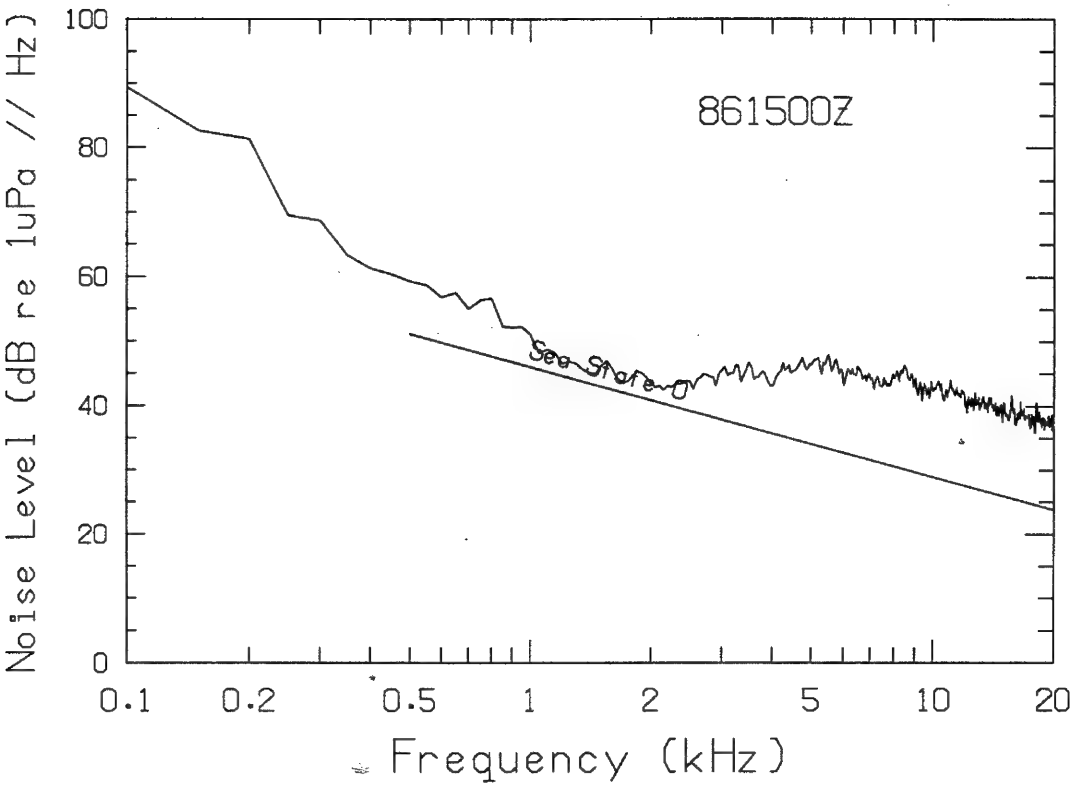
861500Z
Sea State 0
Noise Level (dB re 1uPa // Hz)
Frequency (kHz)
100
80
60
40
20
0
0.1
0.2
0.5
1
2
5
10
20

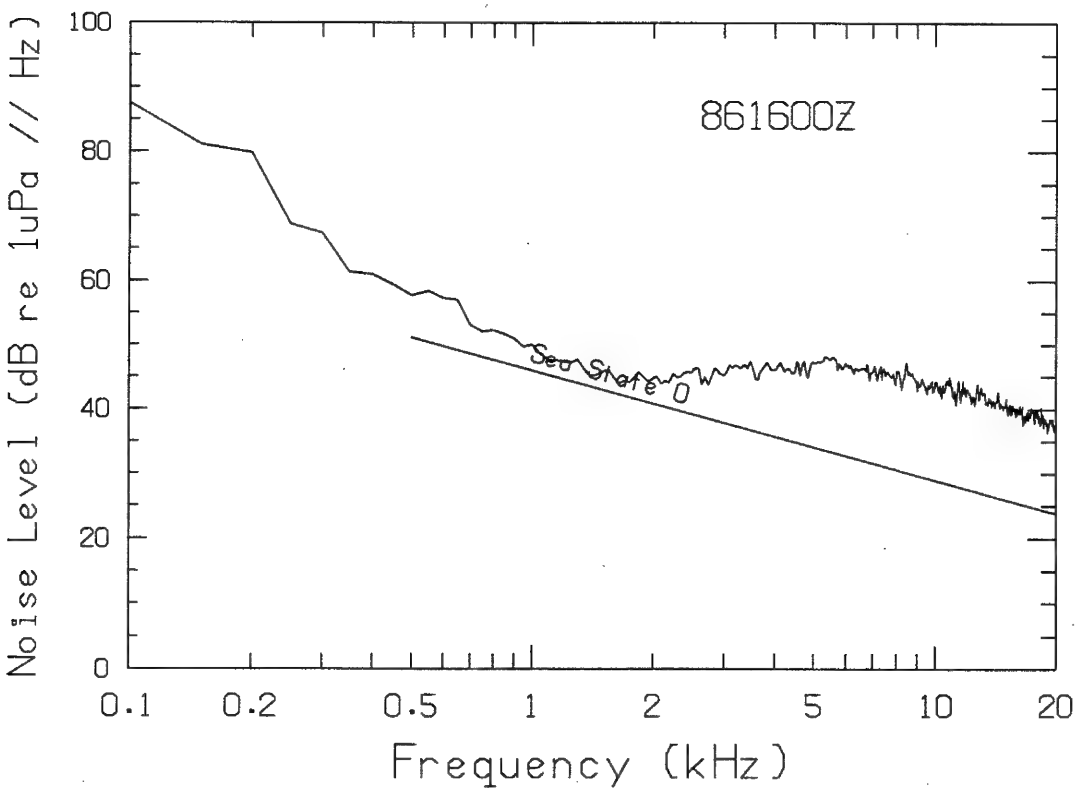
861600Z
Sea State 0
Noise Level (dB re 1uPa // Hz)
Frequency (kHz)
100
80
60
40
20
0
0.1
0.2
0.5
1
2
5
10
20

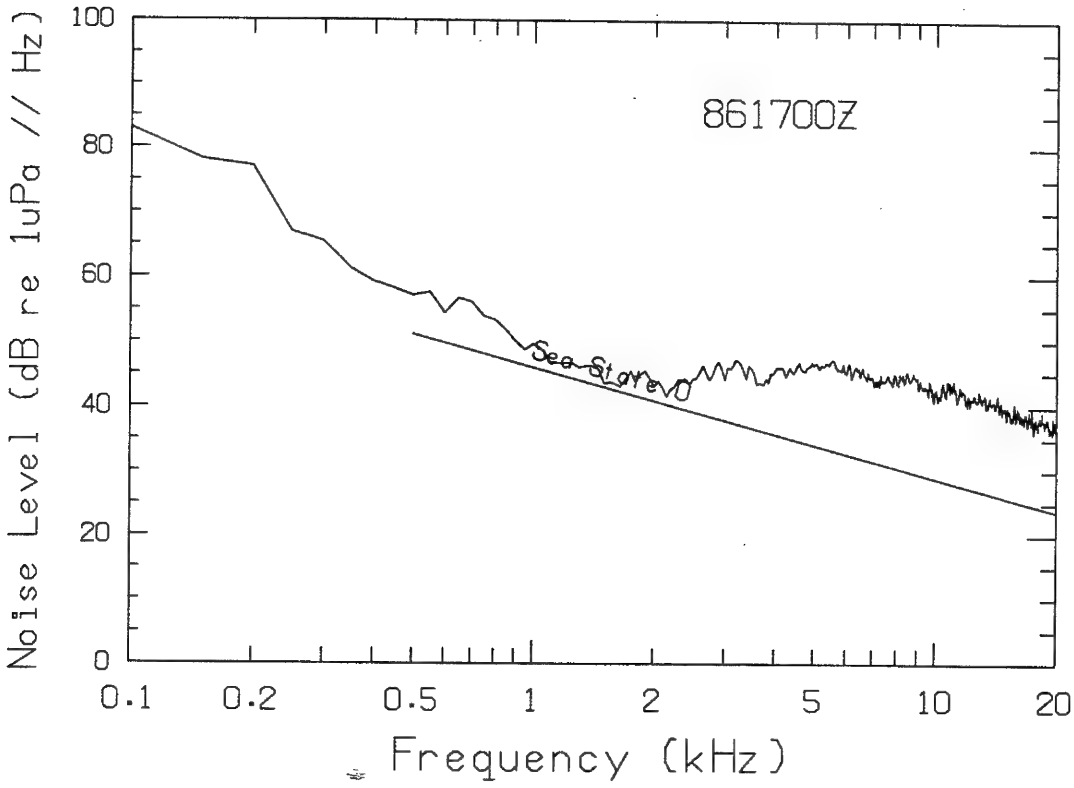
861700Z
Sea State 0
Noise Level (dB re 1uPa // Hz)
Frequency (kHz)
100
80
60
40
20
0
0.1
0.2
0.5
1
2
5
10
20

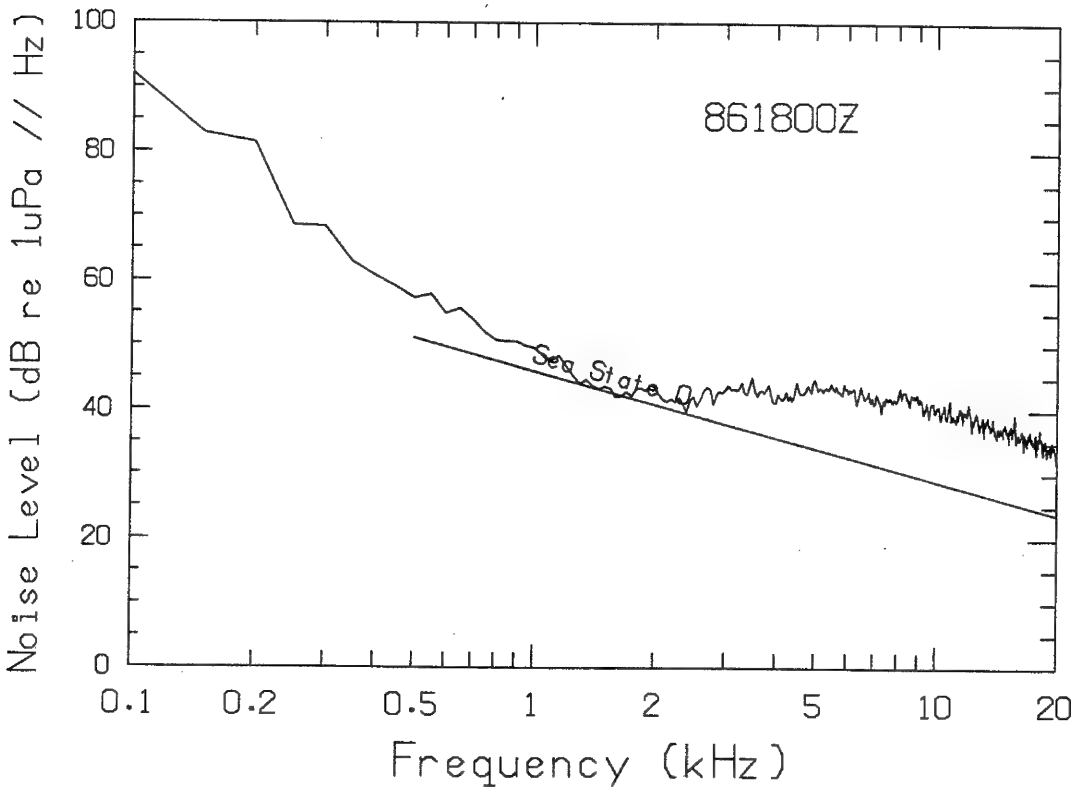
861800Z
Sea State 0
Noise Level (dB re 1uPa // Hz)
Frequency (kHz)
100
80
60
40
20
0
0.1
0.2
0.5
1
2
5
10
20

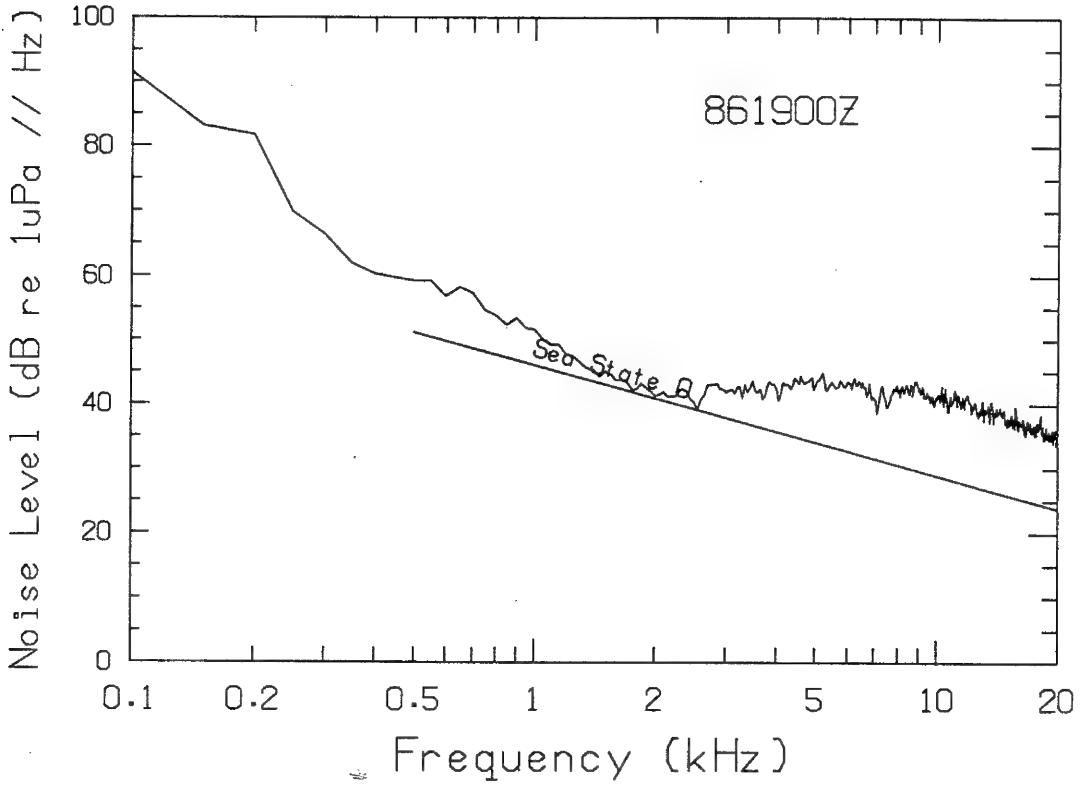
861900Z
Sea State 0
Noise Level (dB re 1uPa // Hz)
Frequency (kHz)
100
80
60
40
20
0
0.1
0.2
0.5
1
2
5
10
20

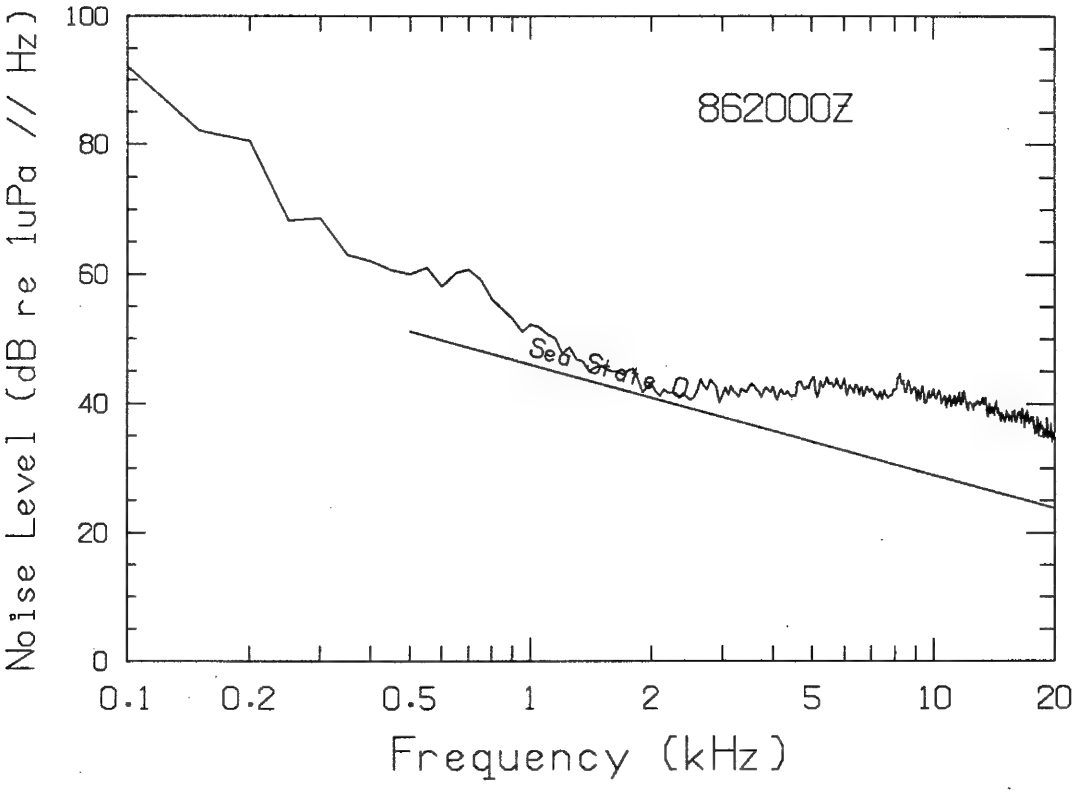
862000Z
Sea State 0
Noise Level (dB re 1uPa // Hz)
Frequency (kHz)
100
80
60
40
20
0
0.1
0.2
0.5
1
2
5
10
20

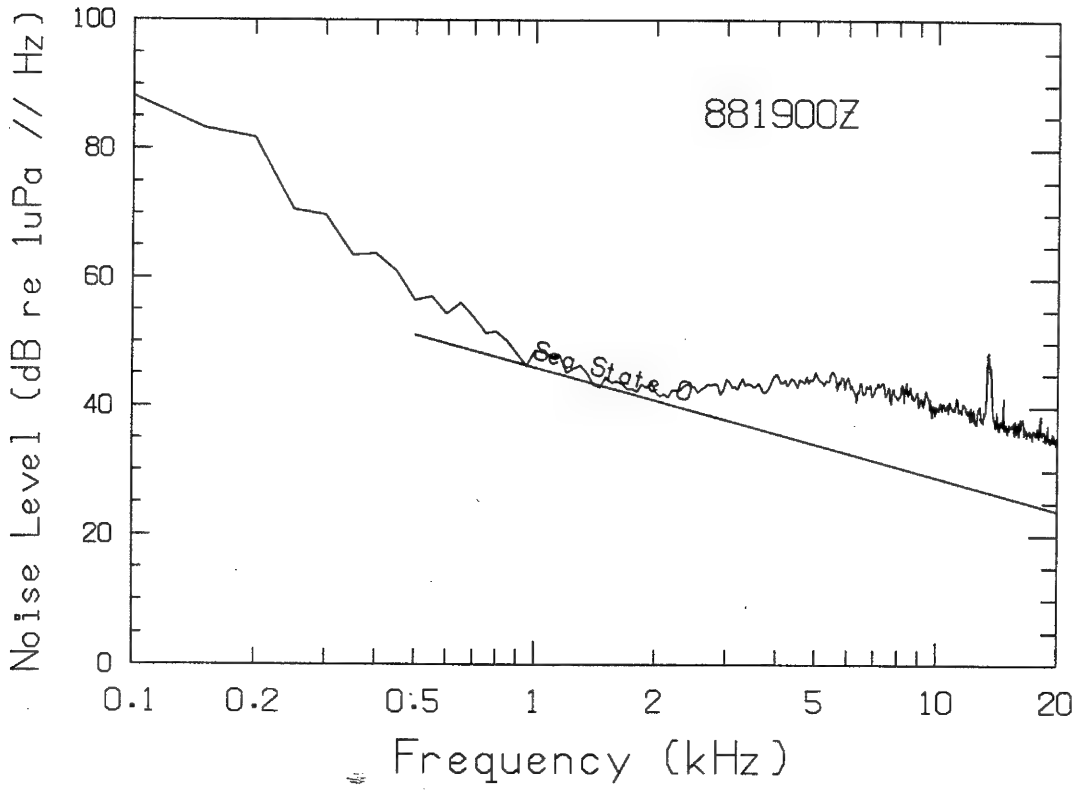
881900Z
Sea State 0
Noise Level (dB re 1uPa // Hz)
100
80
60
40
20
0
0.1
0.2
0.5
1
2
5
10
20
Frequency (kHz)

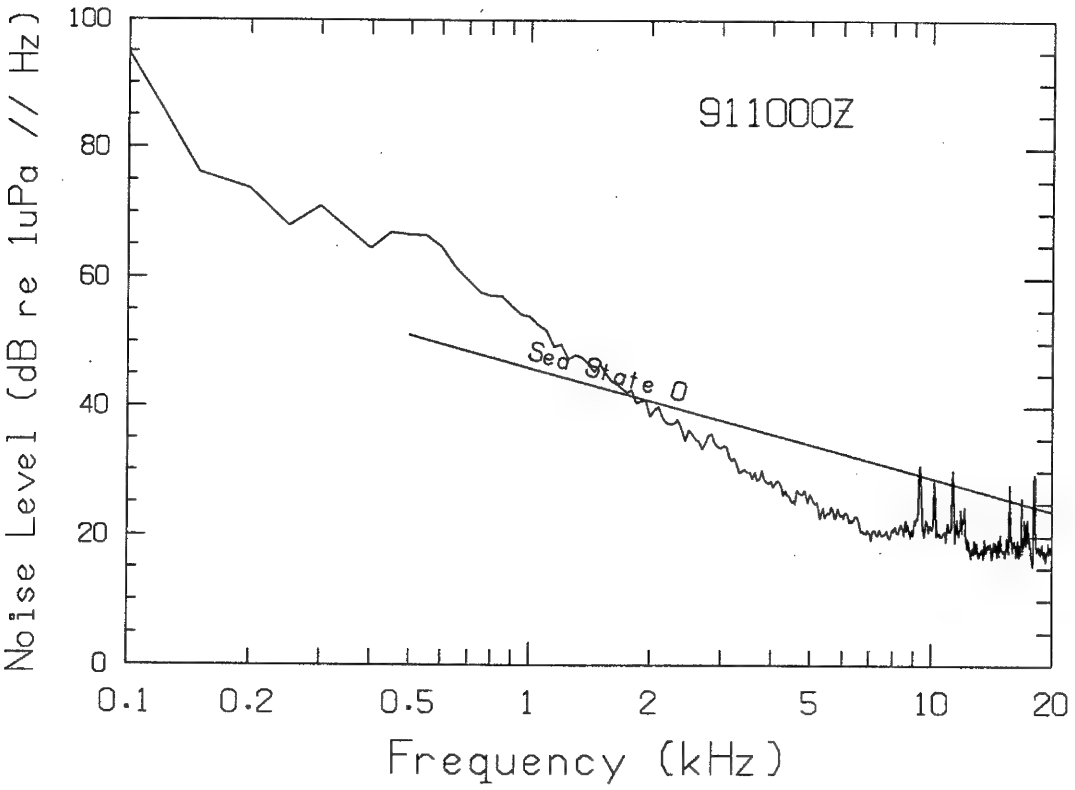
911000Z
Sea State 0
Noise Level (dB re 1uPa // Hz)
100
80
60
40
20
0
0.1
0.2
0.5
1
2
5
10
20
Frequency (kHz)

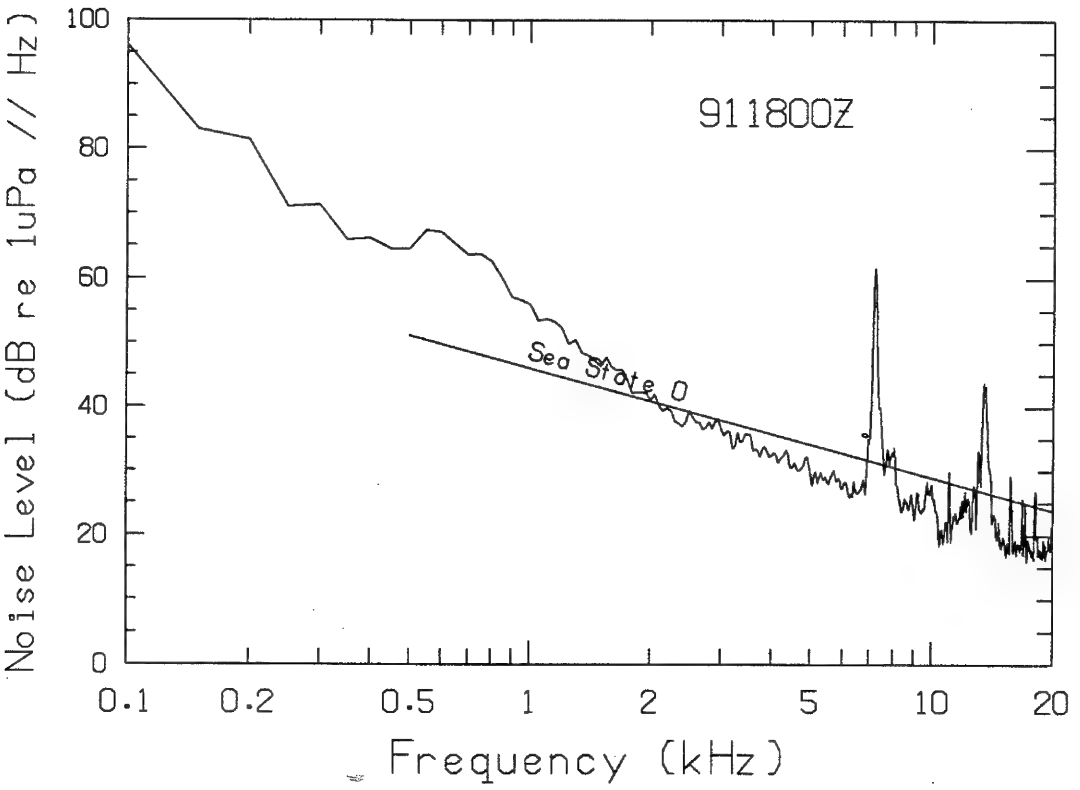
911800Z
Sea State 0
Noise Level (dB re 1uPa // Hz)
100
80
60
40
20
0
0.1
0.2
0.5
1
2
5
10
20
Frequency (kHz)

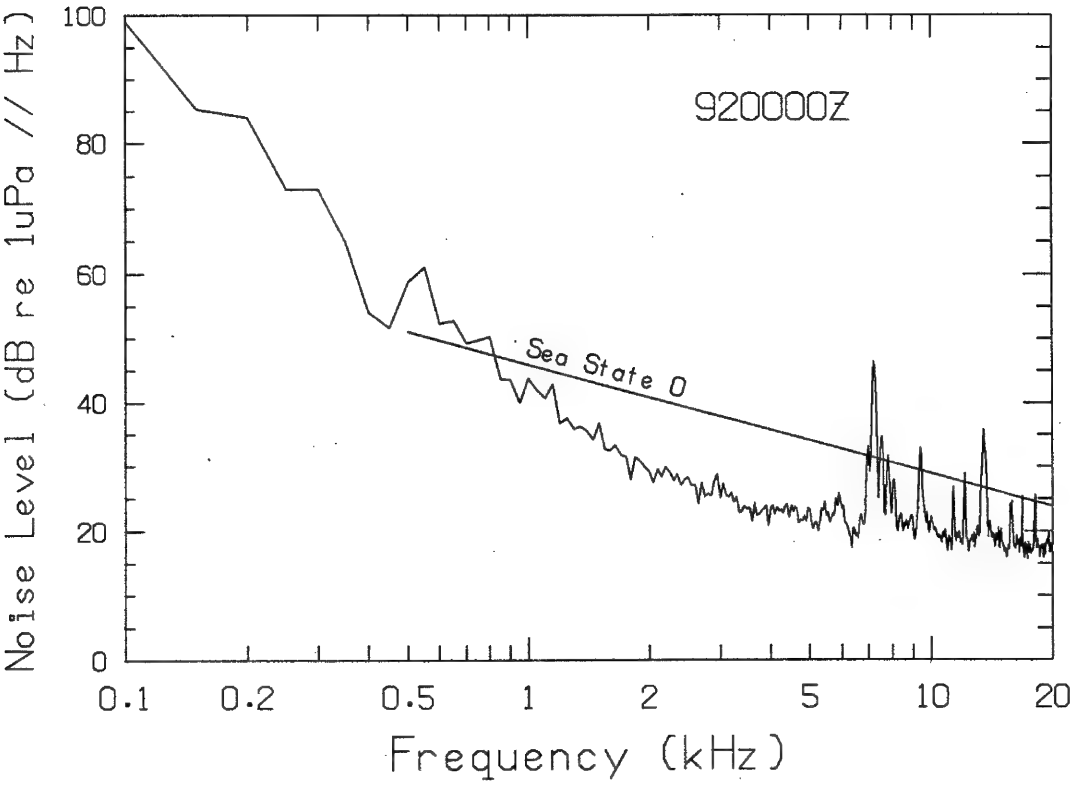
920000Z
Sea State 0
Noise Level (dB re 1uPa // Hz)
100
80
60
40
20
0
0.1
0.2
0.5
1
2
5
10
20
Frequency (kHz)

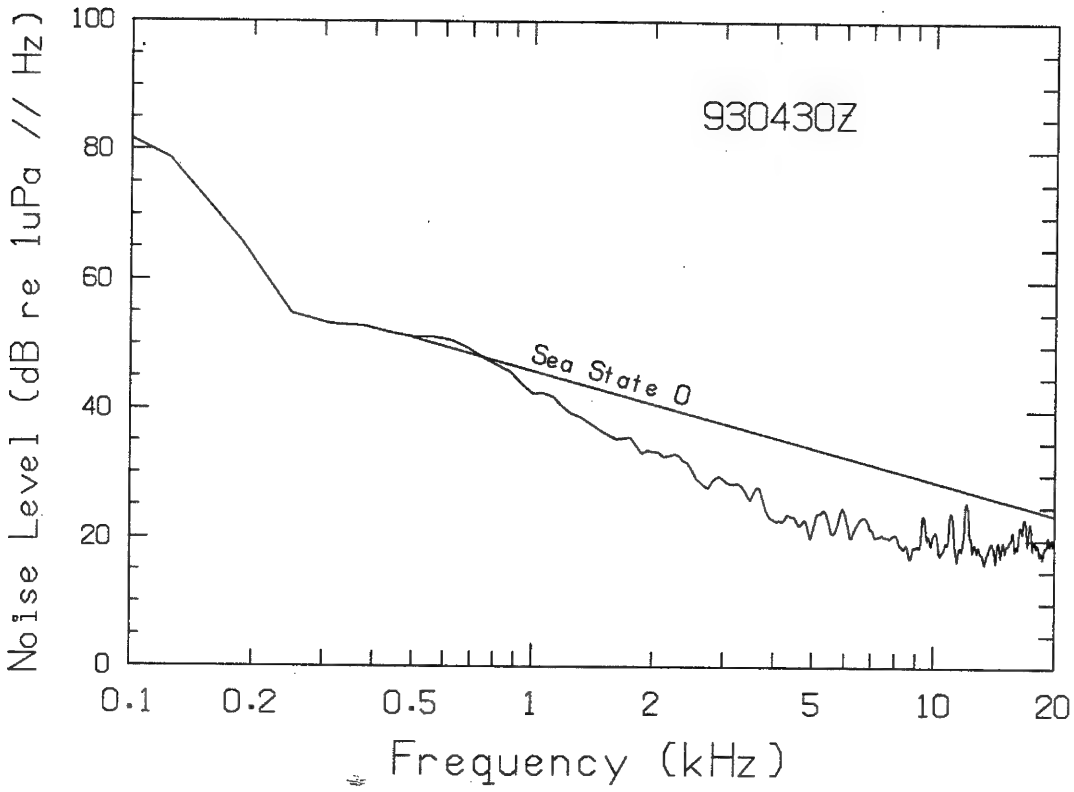
930430Z
Sea State 0
Noise Level (dB re 1uPa // Hz)
Frequency (kHz)
100
80
60
40
20
0
0.1
0.2
0.5
1
2
5
10
20

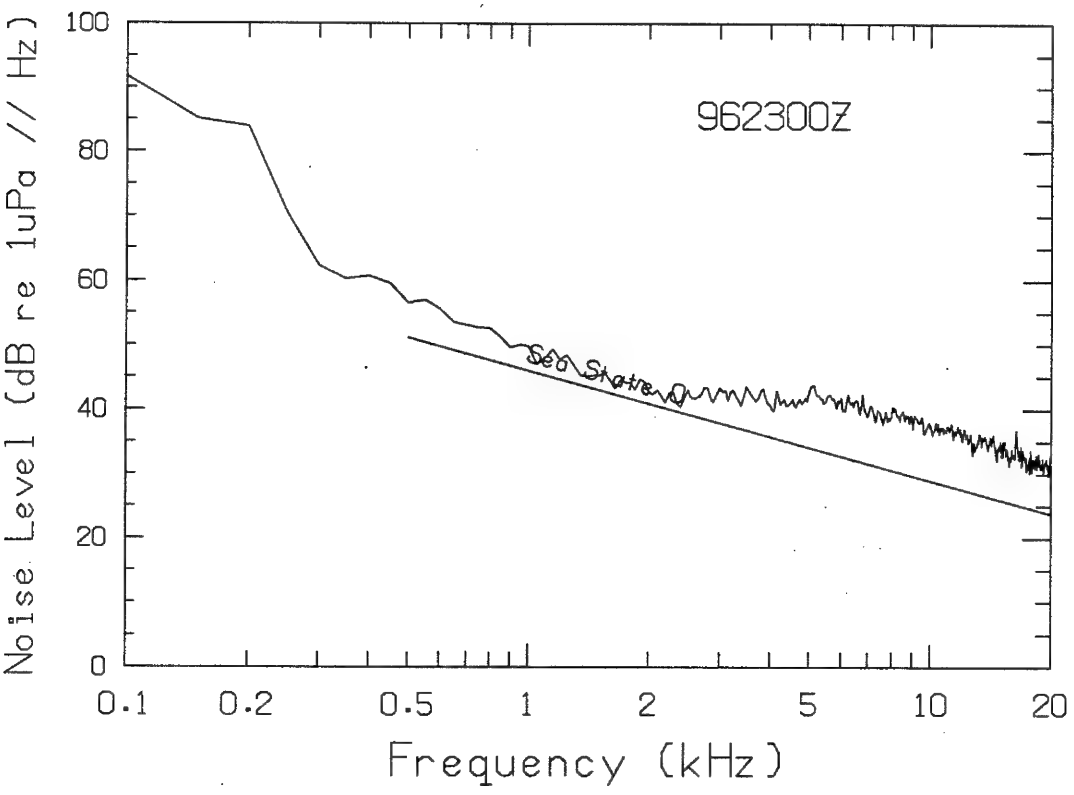
962300Z
Sea State 0
Noise Level (dB re 1uPa // Hz)
Frequency (kHz)
100
80
60
40
20
0
0.1
0.2
0.5
1
2
5
10
20

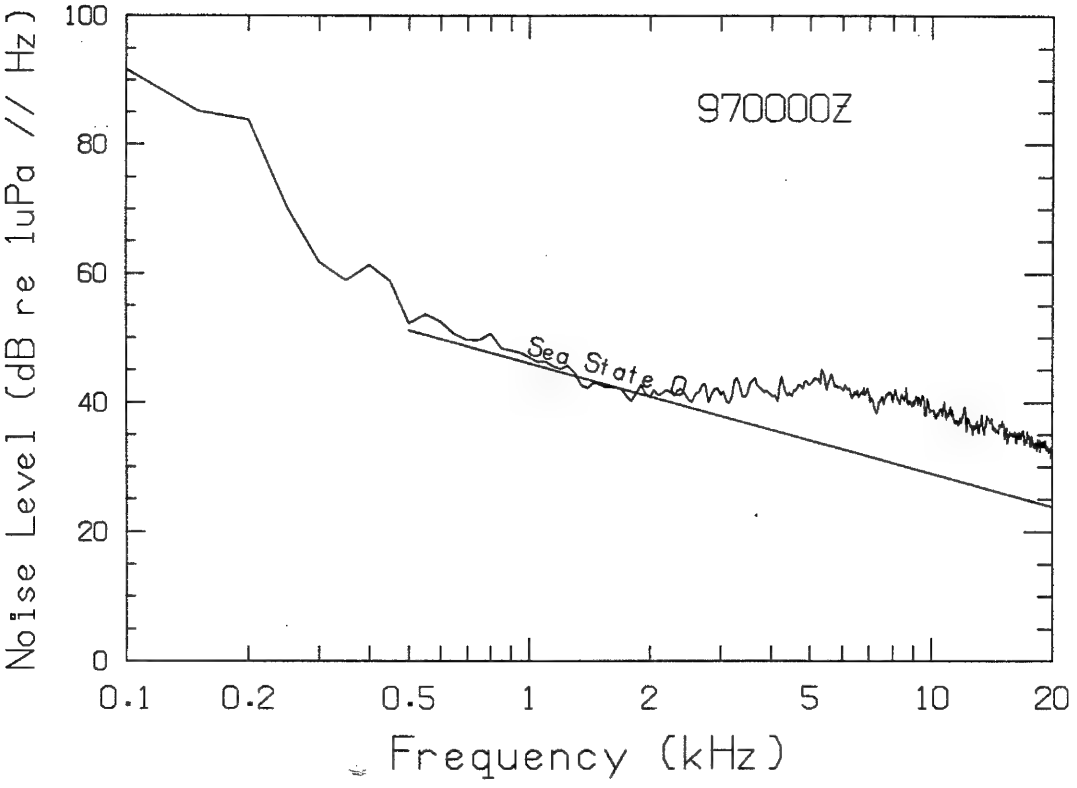
970000Z
Sea State 0
Noise Level (dB re 1uPa // Hz)
Frequency (kHz)
100
80
60
40
20
0
0.1
0.2
0.5
1
2
5
10
20

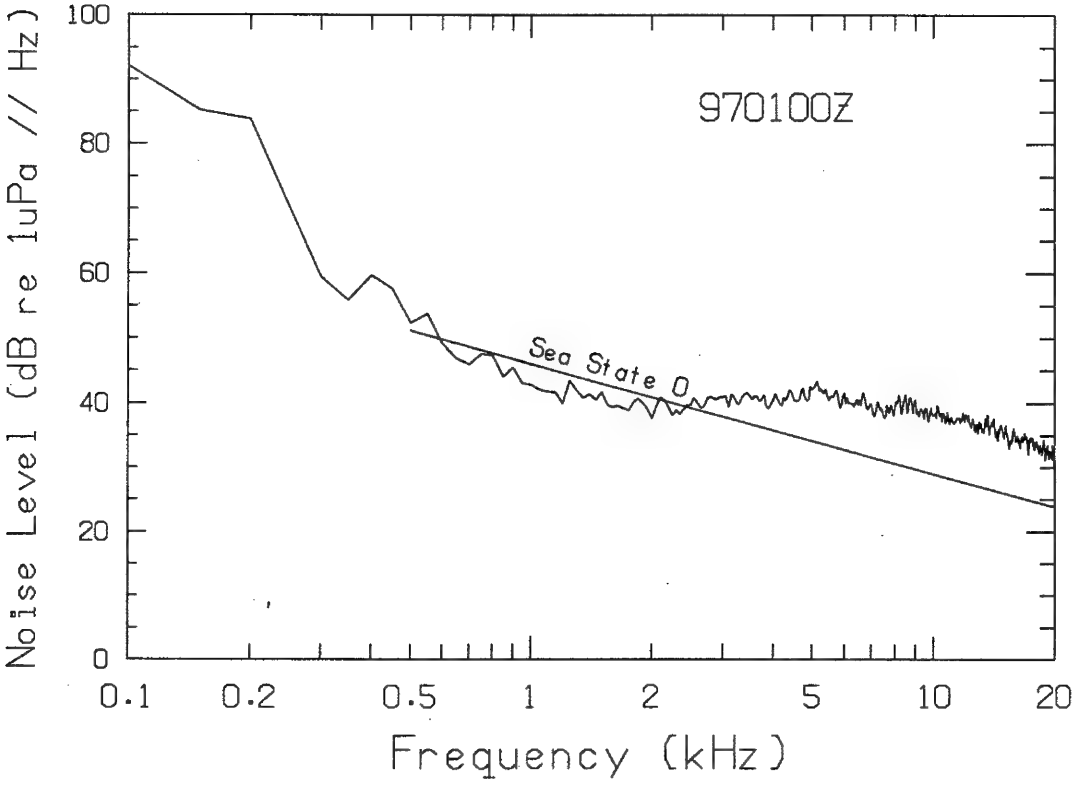
970100Z
Sea State 0
Noise Level (dB re 1uPa // Hz)
Frequency (kHz)
100
80
60
40
20
0
0.1
0.2
0.5
1
2
5
10
20

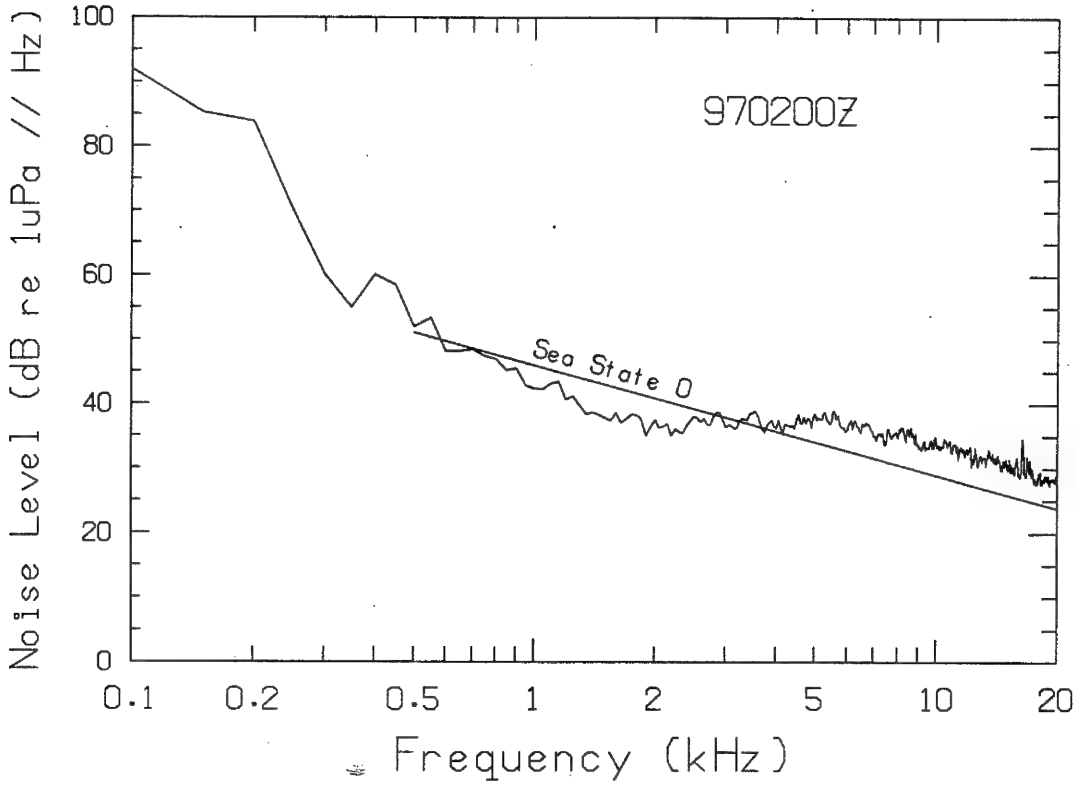
970200Z
Sea State 0
Noise Level (dB re 1uPa // Hz)
Frequency (kHz)
100
80
60
40
20
0
0.1
0.2
0.5
1
2
5
10
20

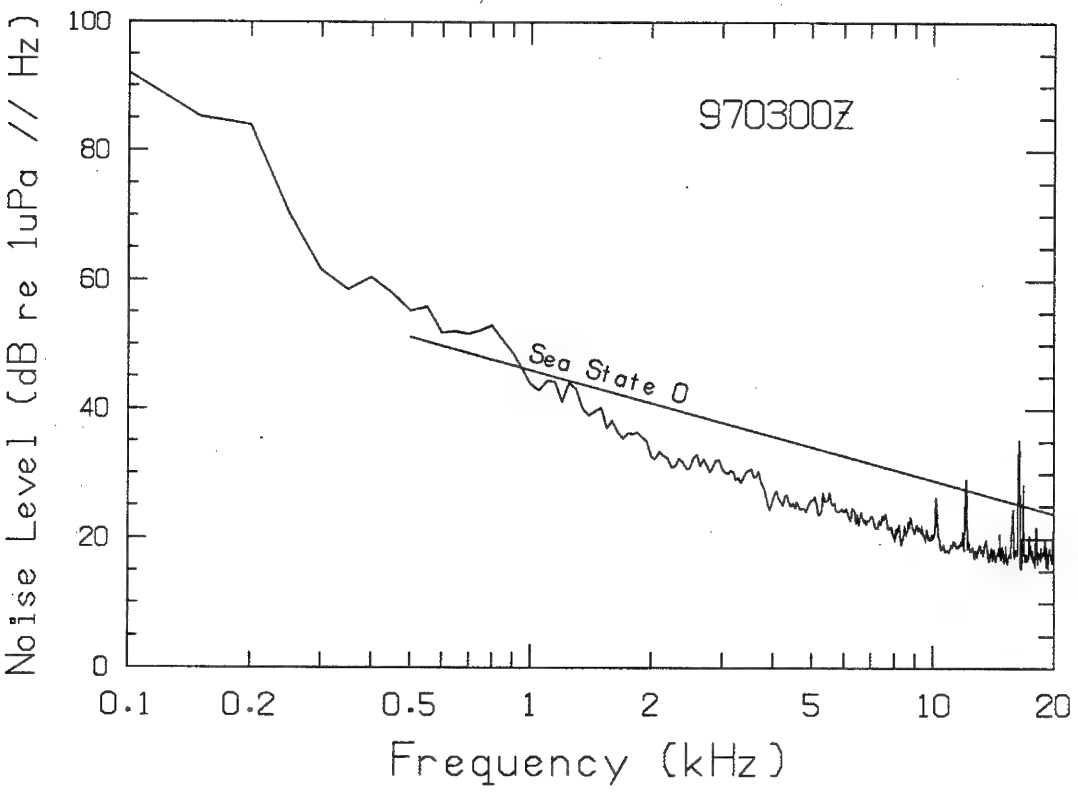
970300Z
Sea State 0
Noise Level (dB re 1uPa // Hz)
Frequency (kHz)
100
80
60
40
20
0
0.1
0.2
0.5
1
2
5
10
20

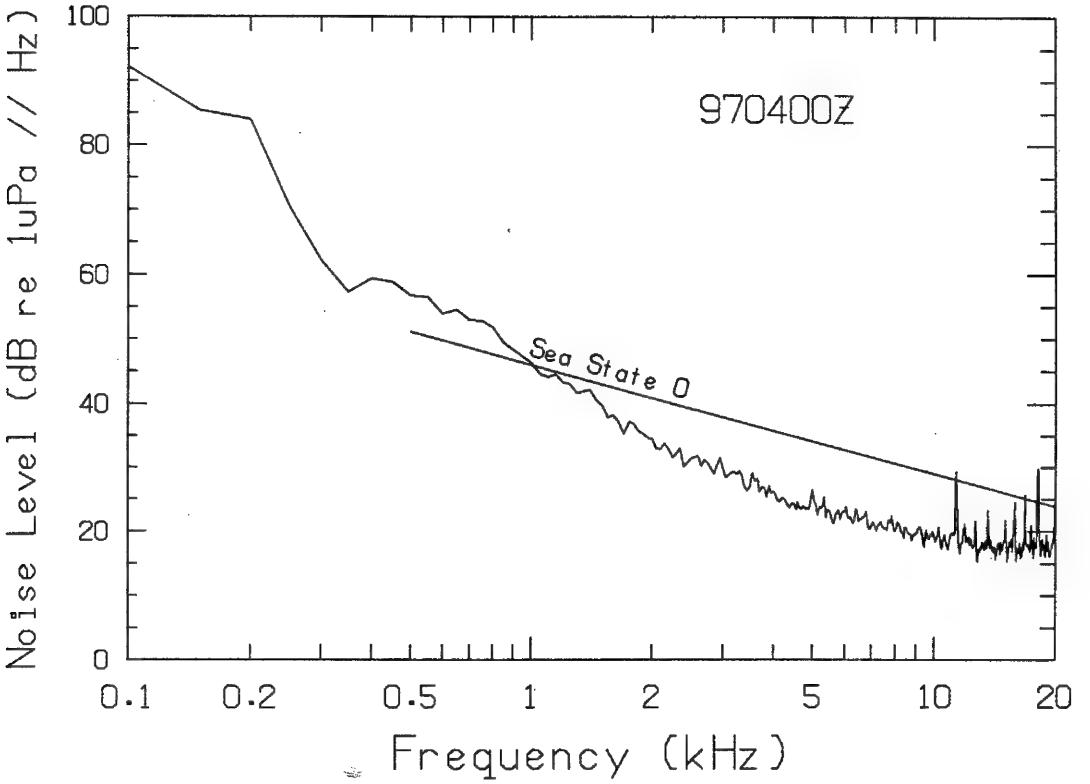
970400Z
Sea State 0
Noise Level (dB re 1uPa // Hz)
Frequency (kHz)
100
80
60
40
20
0
0.1
0.2
0.5
1
2
5
10
20

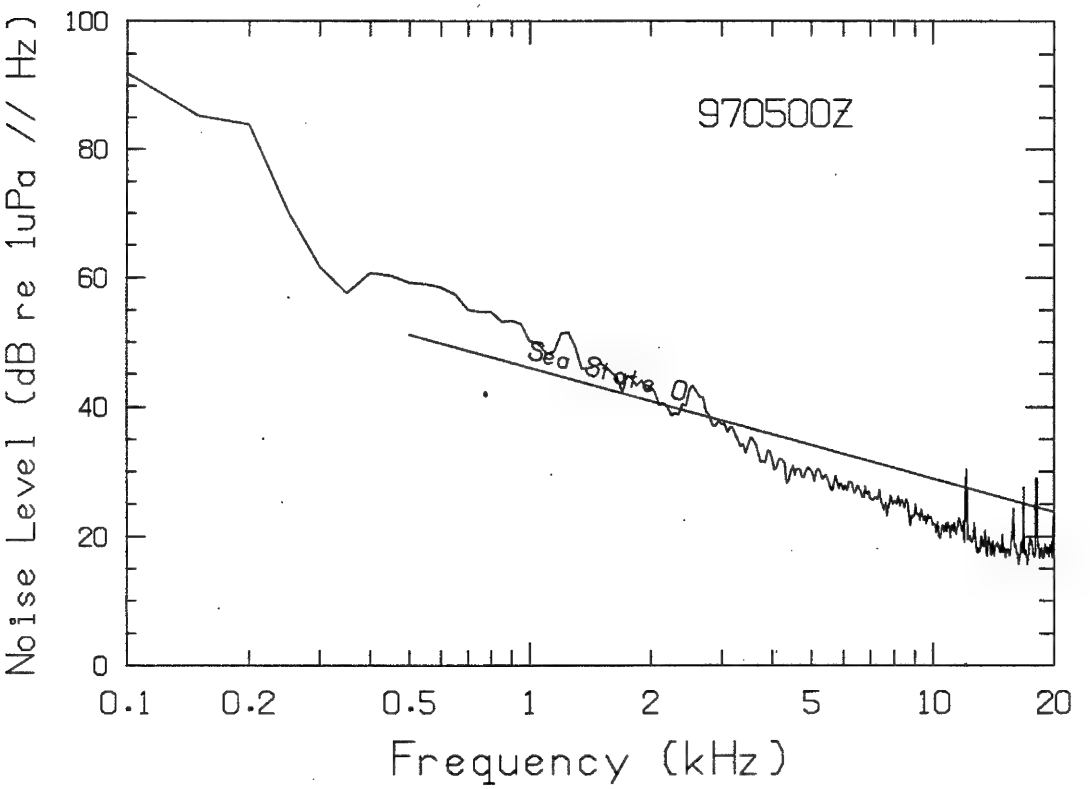
970500Z
Sea State 0
Noise Level (dB re 1uPa // Hz)
Frequency (kHz)
100
80
60
40
20
0
0.1
0.2
0.5
1
2
5
10
20

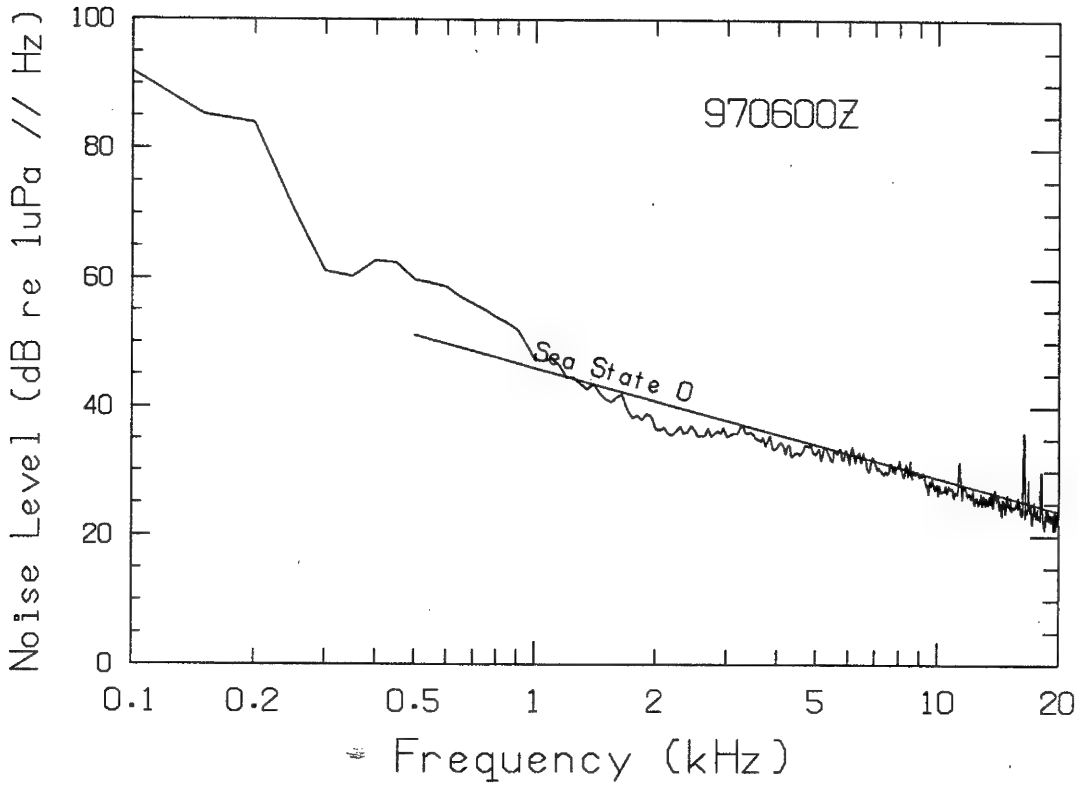
970600Z
Sea State 0
Noise Level (dB re 1uPa // Hz)
100
80
60
40
20
0
0.1
0.2
0.5
1
2
5
10
20
Frequency (kHz)

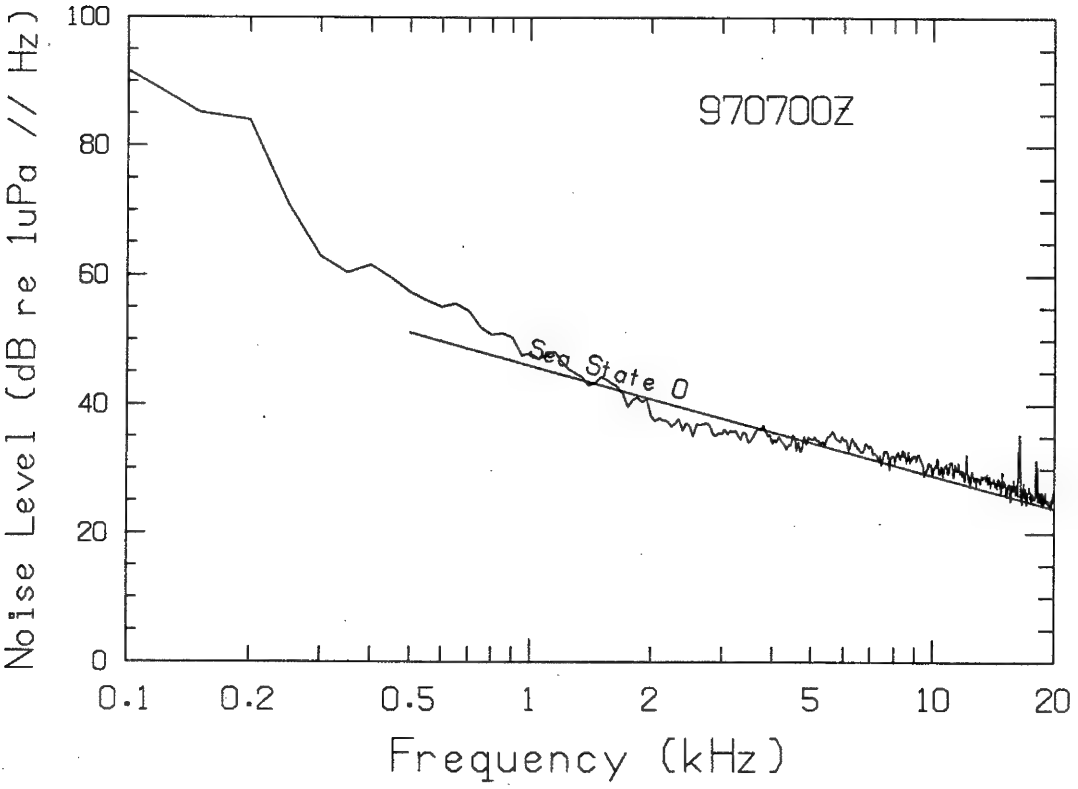
970700Z
Sea State 0
Noise Level (dB re 1uPa // Hz)
100
80
60
40
20
0
0.1
0.2
0.5
1
2
5
10
20
Frequency (kHz)

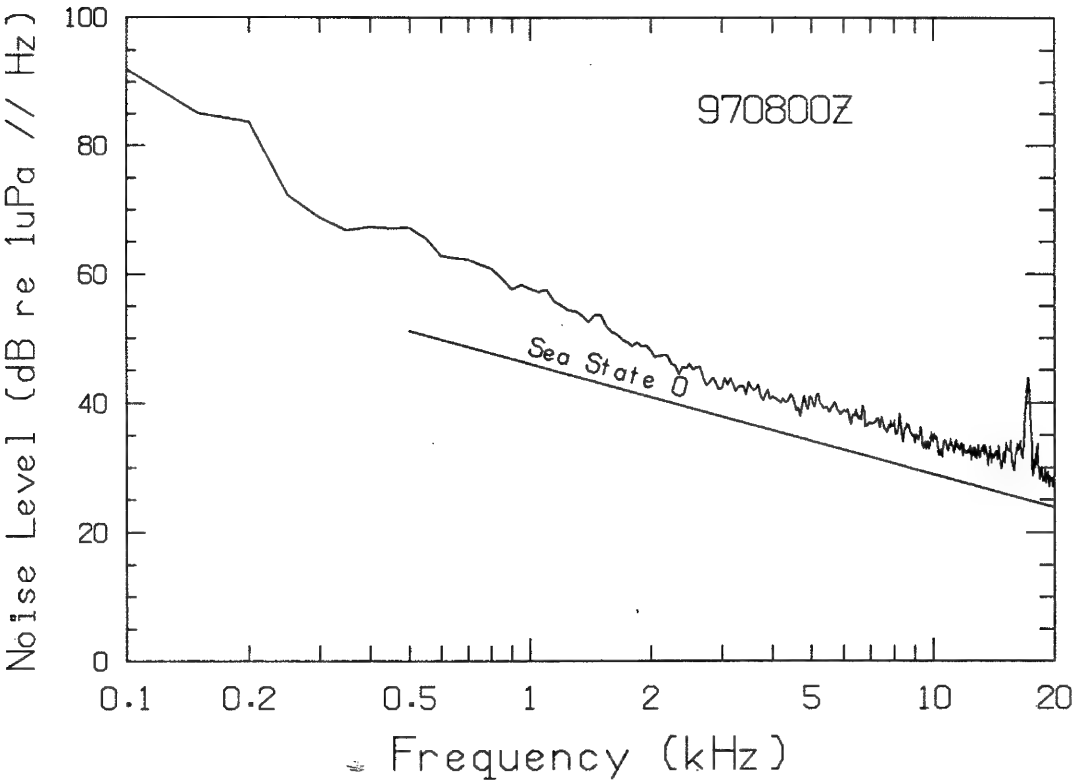
970800Z
Sea State 0
Noise Level (dB re 1uPa // Hz)
100
80
60
40
20
0
0.1
0.2
0.5
1
2
5
10
20
Frequency (kHz)

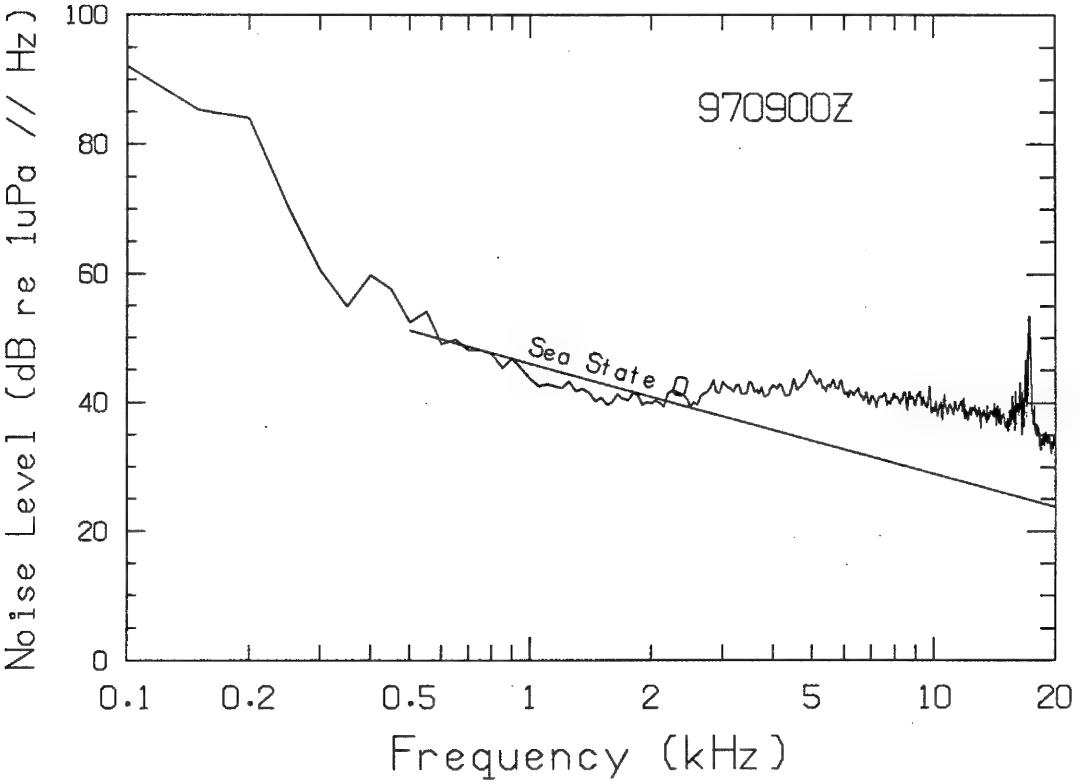
970900Z
Sea State 0
Noise Level (dB re 1uPa // Hz)
100
80
60
40
20
0
0.1
0.2
0.5
1
2
5
10
20
Frequency (kHz)

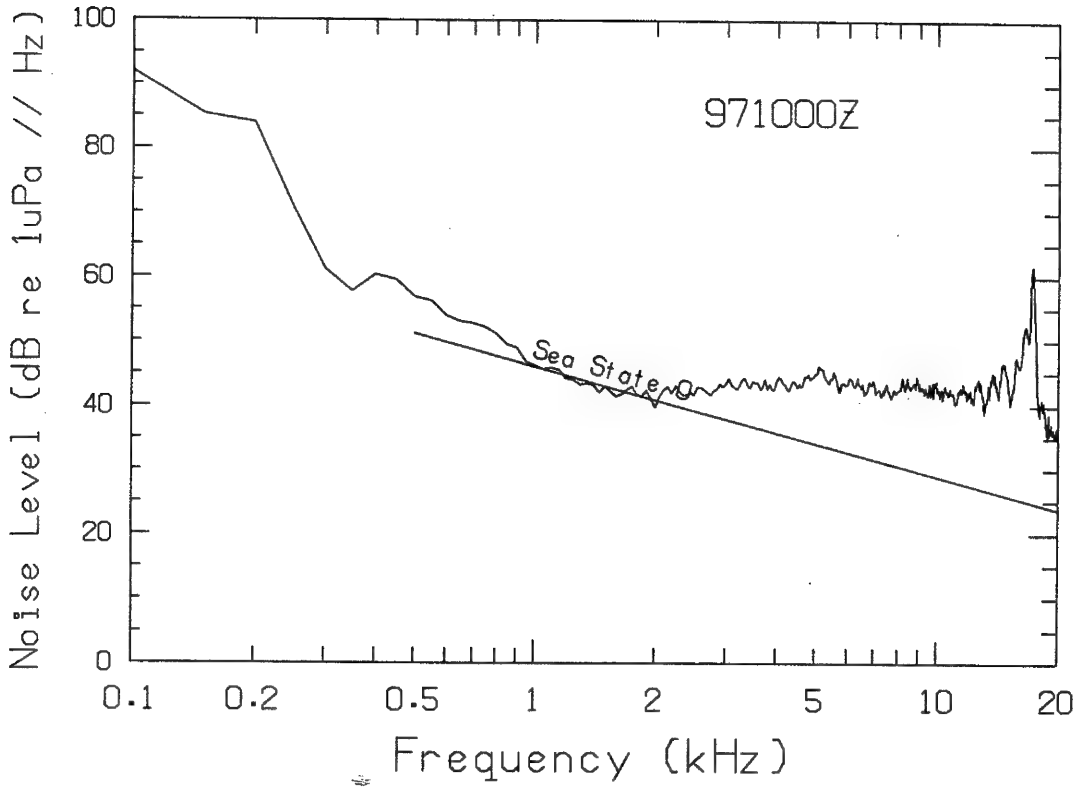
971000Z
Sea State 0
Noise Level (dB re 1uPa // Hz)
100
80
60
40
20
0
0.1
0.2
0.5
1
2
5
10
20
Frequency (kHz)

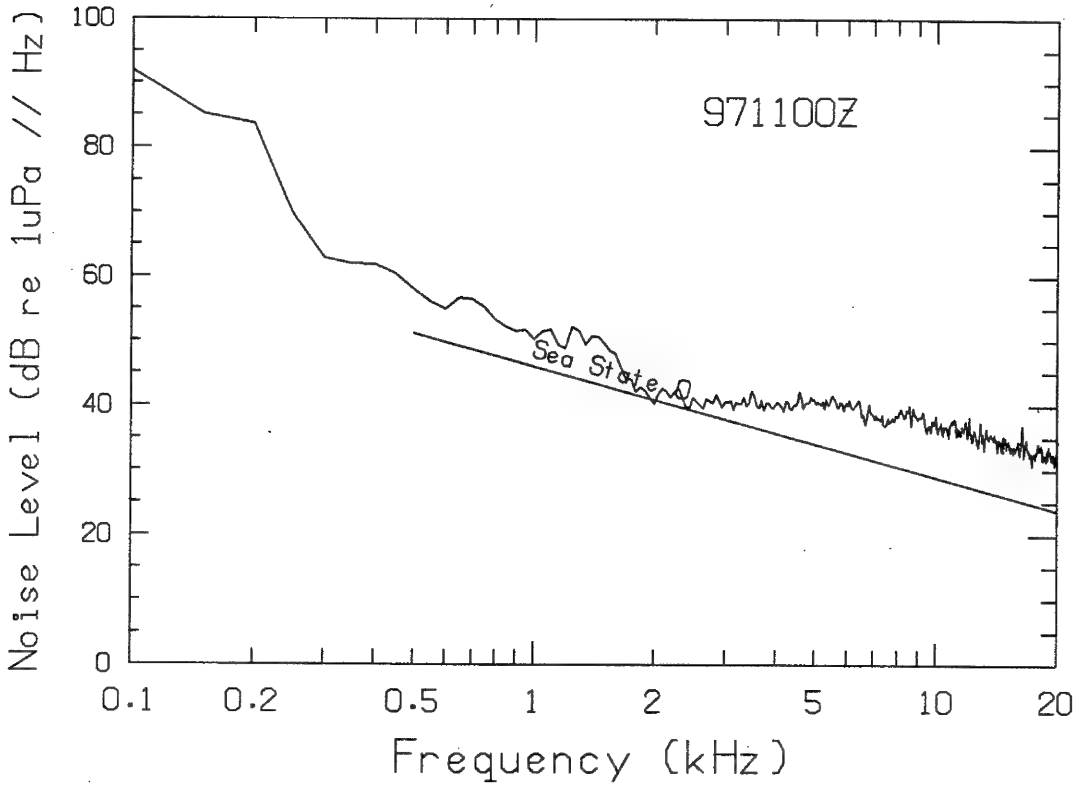
971100Z
Sea State 0
Noise Level (dB re 1uPa // Hz)
100
80
60
40
20
0
0.1
0.2
0.5
1
2
5
10
20
Frequency (kHz)

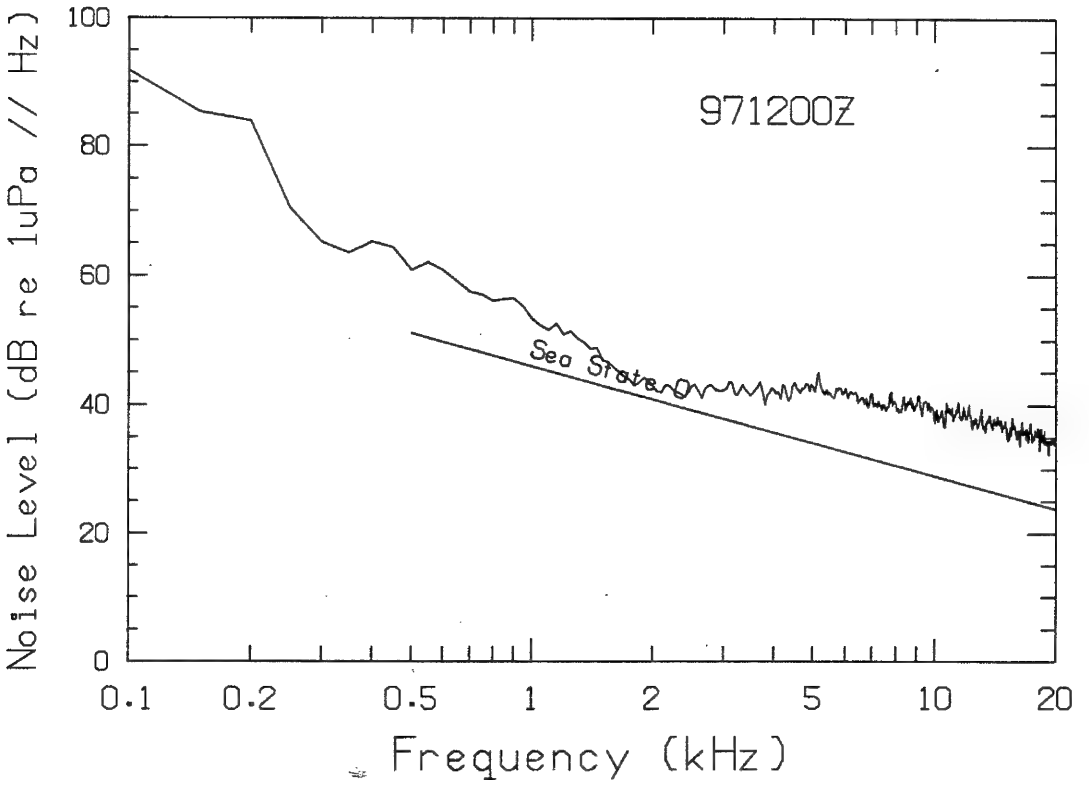
971200Z
Sea State 0
Noise Level (dB re 1uPa // Hz)
Frequency (kHz)
100
80
60
40
20
0
0.1
0.2
0.5
1
2
5
10
20

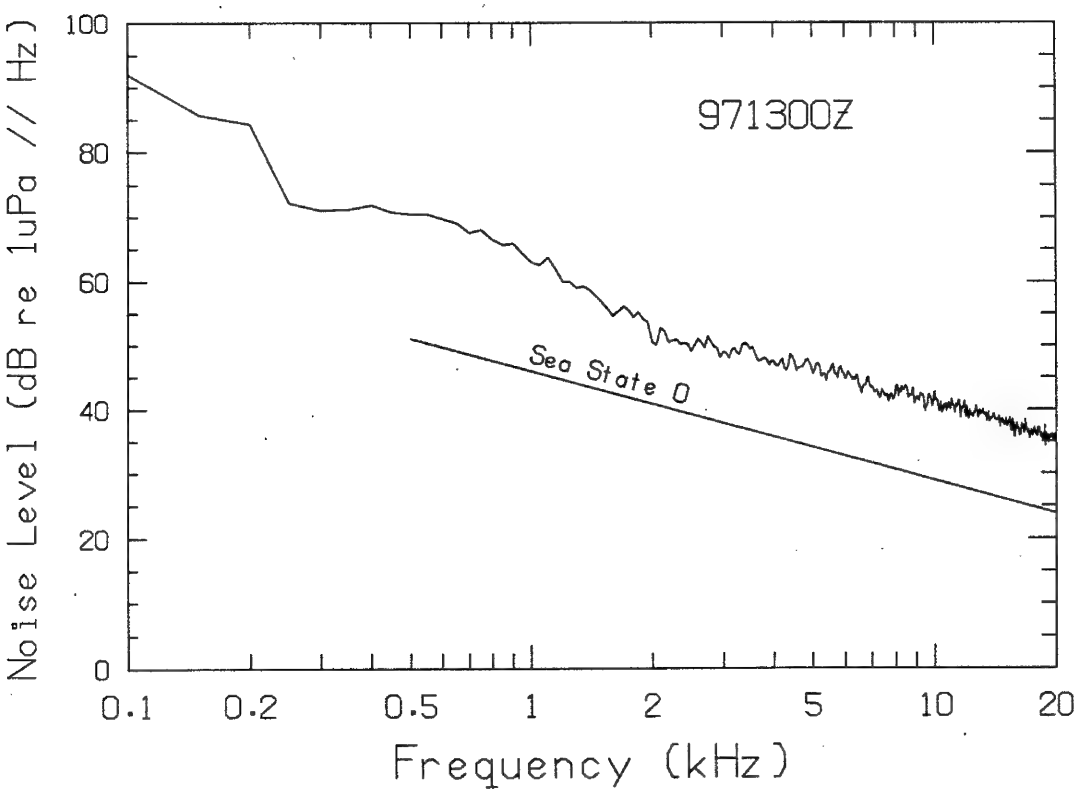
971300Z
Sea State 0
Noise Level (dB re 1uPa // Hz)
Frequency (kHz)
100
80
60
40
20
0
0.1
0.2
0.5
1
2
5
10
20

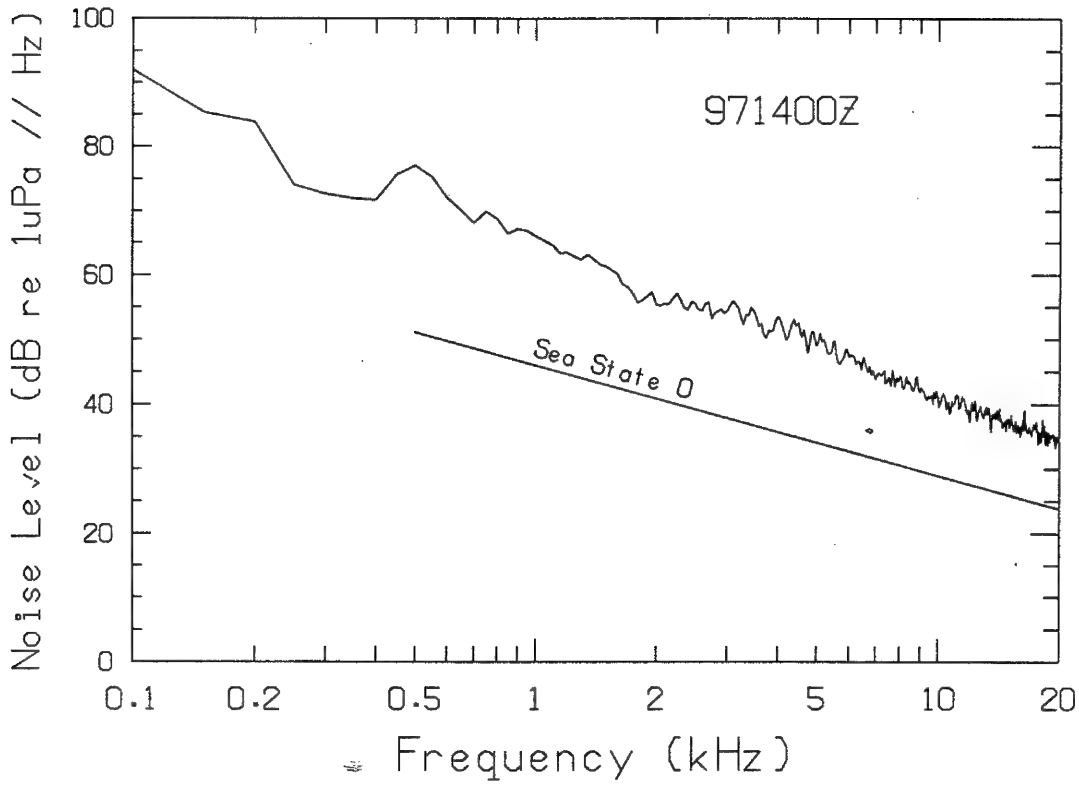
971400Z
Sea State 0
Noise Level (dB re 1uPa // Hz)
100
80
60
40
20
0
0.1
0.2
0.5
1
2
5
10
20
Frequency (kHz)

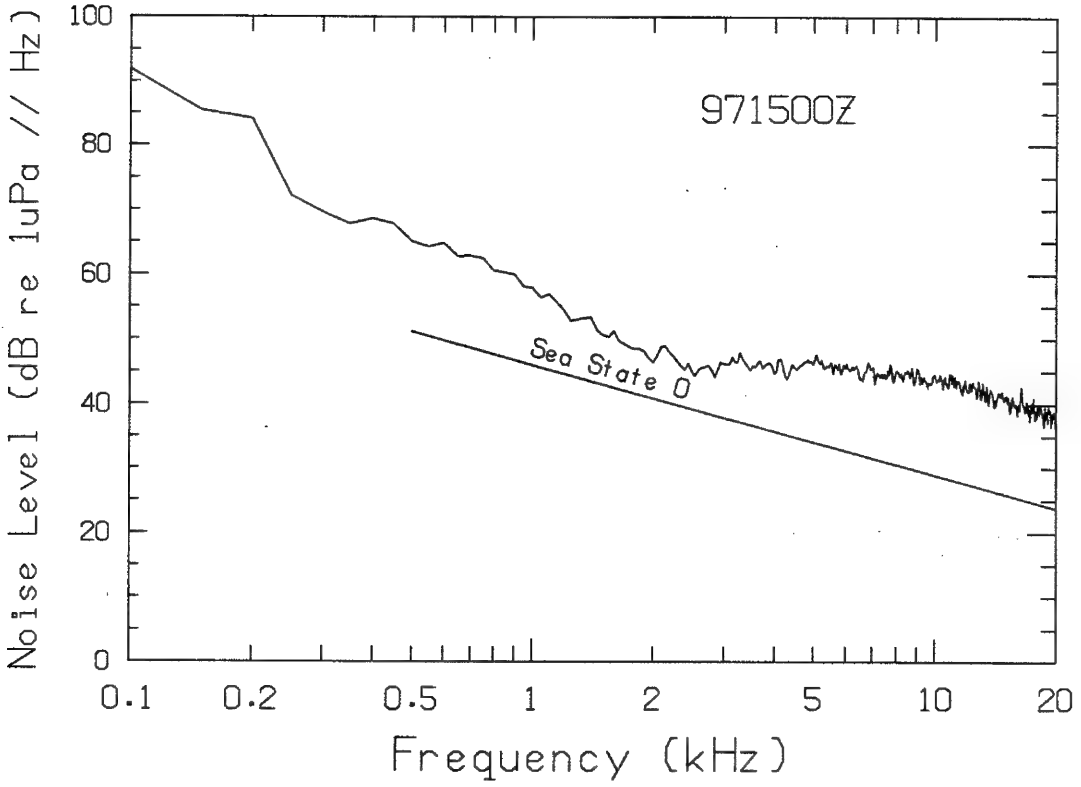
971500Z
Sea State 0
Noise Level (dB re 1uPa // Hz)
100
80
60
40
20
0
0.1
0.2
0.5
1
2
5
10
20
Frequency (kHz)

UNCLASSIFIED
SECURITY CLASSIFICATION OF THIS PAGE

REPORT DOCUMENTATION PAGE

Form Approved
OMB No. 0704-0188

1a. REPORT SECURITY CLASSIFICATION
Unclassified

1b. RESTRICTIVE MARKINGS

2a. SECURITY CLASSIFICATION AUTHORITY
NAVINST S5513.5A, Encl. 73

2b. DECLASSIFICATION / DOWNGRADING SCHEDULE

3. DISTRIBUTION / AVAILABILITY OF REPORT
Approved for Public Release
Distribution is unlimited

4. PERFORMING ORGANIZATION REPORT NUMBER(S)
APL-UW TR9105

5. MONITORING ORGANIZATION REPORT NUMBER(S)

6a. NAME OF PERFORMING ORGANIZATION
Applied Physics Laboratory
University of Washington

6b. OFFICE SYMBOL (If applicable)

7a. NAME OF MONITORING ORGANIZATION
Arctic Submarine Laboratory
Naval Ocean Systems Center

6c. ADDRESS (City, State, and ZIP Code)
1013 N.E. 40th Street
Seattle, WA 98105-6698

7b. ADDRESS (City, State, and ZIP Code)
San Diego, CA 92152-5000

8a. NAME OF FUNDING / SPONSORING ORGANIZATION
NAVSEA and ONT

8b. OFFICE SYMBOL (If applicable)

9. PROCUREMENT INSTRUMENT IDENTIFICATION NUMBER
SPAWAR Contract N00039-88-C-0054

8c. ADDRESS (City, State, and ZIP Code)

10 SOURCE OF FUNDING NUMBERS

PROGRAM ELEMENT NO.	PROJECT NO.	TASK NO.	WORK UNIT ACCESSION NO.

11. TITLE (Include Security Classification)
Environmental Measurements in the Beaufort Sea, Spring 1990

12. PERSONAL AUTHOR(S)
T. Wen, F.W. Karig, W.J. Felton, J.C. Luby, K.L. Williams

13a. TYPE OF REPORT	13b TIME COVERED	14. DATE OF REPORT (Year, Month, Day)	15. PAGE COUNT
Technical	FROM 3/1/90 TO 4/20/90	December 1990	132

16. SUPPLEMENTARY NOTATION

17. COSATI CODES		
FIELD	GROUP	SUB-GROUP
68	03	
20	01	

18. SUBJECT TERMS (Continue on reverse if necessary and identify by block number)
arctic Beaufort Sea currents ice penetrating
floe drift CTD casts weather

19. ABSTRACT (Continue on reverse if necessary and identify by block number)

This report summarizes environmental data obtained in March and April 1990 at an ice camp in the Beaufort Sea 375 km north of Prudhoe Bay, Alaska. The measurements include weather, floe drift, CTD profiles, ice properties, currents, and underwater noise.

20. DISTRIBUTION / AVAILABILITY OF ABSTRACT
☐ UNCLASSIFIED/UNLIMITED ☒ SAME AS RPT. ☐ DTIC USERS

21 ABSTRACT SECURITY CLASSIFICATION
Unclassified

22a. NAME OF RESPONSIBLE INDIVIDUAL
CAPT Charles E. Armitage

22b TELEPHONE (Include Area Code)
(619) 553-7441

22c. OFFICE SYMBOL
NOSC, 19

DD Form 1473, JUN 86 Previous editions are obsolete.
S/N 0102-LF-014-6603

SECURITY CLASSIFICATION OF THIS PAGE
UNCLASSIFIED

Distribution List

Assistant Secretary of the Navy
(Research, Engineering and Systems)
Department of the Navy
Washington, DC 20350 [2 cp]

Chief of Naval Operations
Department of the Navy
Washington, DC 20350-2000

OP 02
OP 22
OP 223
OP 225
OP 07
OP 071
OP 095
OP 96T
OP 0962E
OP 0962X
OP 098

Director of Defense Research
Office of Assistant Director (Ocean Control)
The Pentagon
Washington, DC 20301-5000

Defense Technical Information Center
Cameron Building #5
Alexandria, VA 22304-6145

Office Chief of Naval Research
Department of the Navy
800 N. Quincy Street
Arlington, VA 22217-5000

OCNR 00
OCNR 000A
OCNR 112
OCNR 1125
OCNR 1125AR
OCNR 1125OA
OCNR 1222T
OCNR 124
OCNR 125 [2 cp]

Office of Naval Research
R. Silverman, Resident Representative
315 University District Bldg., JD-16
1107 N.E. 45th Street
Seattle, WA 98195

Office of Naval Technology
Department of the Navy
Ballston Center Tower #1
800 N. Quincy Street
Arlington, VA 22217-5000

Code 22
Code 23
Code 23D
Code 232
Code 234

Director
Defense Advanced Research Project Agency
1400 Wilson Boulevard
Arlington, VA 22209

Commanding Officer
Naval Intelligence Support Center
4301 Suitland Road
Washington, DC 20390

Commanding Officer
Naval Polar Oceanographic Center
4301 Suitland Road
Washington, DC 20390-5140

Library

Center for Naval Analyses
4401 Ford Avenue
P.O. Box 16268
Alexandria, VA 22302-0268

Attn: Technical Information Center

Commander
Naval Air Systems Command Hq.
Department of the Navy
Washington, DC 20361

AIR 340L

Commander
Space and Naval Warfare Systems Command (NC1)
(SPAWAR)
Department of the Navy
Washington, DC 20363-5100

SPAWAR 005
PMW-180
PMW-181
PMW-182
PMW-182-2

Commander
Naval Sea Systems Command
Department of the Navy
Washington, DC 20362

NSEA 05R
NSEA 06
NSEA 06U2
NSEA 06UR
NSEA 06UR-45
NSEA 06URB
Code PM0-402
Code PM0-406
Code PM0-407

Commanding Officer
Naval Underwater Systems Center
Newport, RI 02840

Library [2 cp]
Code 00
Code 22201
Code 382
Code 3824
Code 801
Code 81
Code 8211 [2 cp]
Code 8212
Code 8231
Code 82391 [2 cp]

Officer-in-Charge
New London Laboratory
Naval Underwater Systems Center
New London, CT 06320

Library
Code 01Y [2 cp]
Code 341
Code 2111
Code 2113
Code 3423

Commander
Naval Weapons Center
China Lake, CA 93555

Library

Commander
Naval Surface Warfare Center
White Oak
Silver Spring, MD 20903-5000

Library [2 cp]
Code R-01
Code R-43 [2 cp]
Code U-04
Code U-06
Code U-42 [2 cp]

Commander
Naval Ocean Systems Center
San Diego, CA 92152-5000

Library
Code 00
Code 19 [3 cp]
Code 541
Code 844 [3 cp]

Commanding Officer
Naval Civil Engineering Laboratory
Port Hueneme, CA 93043-5003

Library
Code L1B
Code L14
Code L43 [2 cp]

Director
Naval Research Laboratory
Washington, DC 20375

Library
Code 5100
Code 5550
Code 5123
Code 6090

Commanding Officer
Naval Coastal Systems Center
Panama City, FL 32407

Library
Code 2120

Commanding Officer
Naval Ocean Research and
Development Activity
Stennis Space Center, MS 39529-5004

Library [2 cp]
Code 113
Code 200
Code 240
Code 242 [3 cp]
Code 252

Commanding Officer
Naval Oceanographic Office
Stennis Space Center, MS 39522-5001

Code OA
Code OAR
Code OARU

Commander
Naval Air Development Center
Warminster, PA 18974

Library
Code 3031 (A. Horbach)

Commander
David Taylor Research Center
Bethesda, MD 20084

Library
Code 1720 [2 cp]
Code 1908

Commanding Officer
Naval Submarine School
Box 70
Naval Submarine Base -- New London
Groton, CT 06340

Superintendent
Naval Postgraduate School
Monterey, CA 93943-5100

Library [2 cp]
Code 68

Commander, SECOND Fleet
Fleet Post Office
New York, NY 09501

Commander, THIRD Fleet
Fleet Post Office
San Francisco, CA 96601

Commander Submarine Force
U.S. Atlantic Fleet
Norfolk, VA 23511

Code 00
Code 019
Code 22
Code N311

Commander Submarine Force
U.S. Pacific Fleet
Pearl Harbor, HI 96860

Code 00
Code N2
Code N21

Commander
Submarine Squadron THREE
Fleet Station Post Office
San Diego, CA 92132

Commander
Submarine Group FIVE
Fleet Station Post Office
San Diego, CA 92132

Commander
Submarine Development Squadron TWELVE
Box 70
Naval Submarine Base - New London
Groton, CT 06340

Code N20

Knut Aagaard
Pacific Marine Environmental Laboratory
NOAA
7600 Sand Point Way NE, Building 3
Bin C15700
Seattle, WA 98115-0070

Director
Applied Research Laboratories
The University of Texas at Austin
P.O. Box 8029
Austin, TX 78713-8029

Library
Dr. J. Huckaby

Director
Applied Research Laboratory
The Pennsylvania State University
State College, PA 16801

C. Ackerman
R. Ingram [2 cp]
E. Liszka
S. McDaniel
F. Symons, Jr.
J. Kisenwether

Sandia National Laboratories
Kirtland Air Force Base
P.O. Box 5800
Albuquerque, NM 87185

CBNS
P.O. Box 4855
Washington, D.C. 20008
Attn: CDR A.M. Poulter [2 copies]

Library

APL-UW
R. Francois
E. Gough
F. Karig
J. Luby
R. Stein
T. Wen
K. Williams

University of Washington
Oceanography Dept. [2 cp]